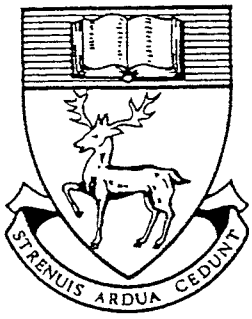

UNIVERSITY OF SOUTHAMPTON

FACULTY OF MATHEMATICAL STUDIES

Statistical Mechanics of Vesicles, Membranes and Interfaces

by

Robert Ellis Norman

A thesis submitted for the degree of Doctor of Philosophy

April 1993

UNIVERSITY OF SOUTHAMPTON

ABSTRACT

FACULTY OF MATHEMATICAL STUDIES

MATHEMATICS

Doctor of Philosophy

STATISTICAL MECHANICS OF VESICLES, MEMBRANES AND INTERFACES

by Robert Ellis Norman

A variety of theoretical and numerical methods are used to investigate the statistical mechanical properties of vesicles, membranes and interfaces. The study of vesicles, membranes and interfaces is a small part of the more general study of exotic structures. Understanding the structure and properties of these exotic phases has important applications in many diverse fields, from food stabilization and improvement to enhanced oil recovery.

Several models of vesicles in two dimensions are briefly discussed. A continuum model of vesicles due to Ostrowsky and Peyraud is investigated further. The model is extended and a detailed scaling analysis of the effects of osmotic pressure and curvature on the shape polydispersity is presented. These results are compared and contrasted with results from an altenative model. The vesicle is subjected to a nematic ordering field to simulate the effect of a shear flow field.

A model of membranes and interfaces confined between hard parallel walls is discussed. Analytical extensions to the current state of the literature are discussed. The models are studied numerically by Monte Carlo simulation and the results are analysed to establish the consistency of the new analytical arguements.

Twisted and helical lipid membrane stuctures have been observed to form from lipid membranes whose molecules are chiral. Recent attempts to explain these structures have relied on mean field theory. A statistical mechanical simulation model is devised that should be a useful tool for studying these chiral membranes. The model is investigated for long thin membranes and diamond shaped membranes. The results are analysed systematically and typical membrane configurations are presented.

CONTENTS

Chapter 6

MEMBRANES AND INTERFACES CONFINED BETWEEN PARALLEL WALLS

PREFACE

This dissertation contains original work which has been, or which is envisaged will be, published in the scientific literature:

- Chapter 5 section 3 is the result of collaboration with Dr G.C. Barker of the Agricultural and Food Research Council (AFRC) Institute of Food Research, Colney Lane, Norwich NR4 7UA, UK. Most of the work has appeared in "Statistical mechanics of two dimensional vesicles", by R.E.Norman, G.C.Barker and T.J.Sluckin, *J. Phys. (France)* **2** (1992) 1362.
- Chapter 6 is the result of collaboration with Dr A.O.Parry of the H.H.Wills Physics Laboratory, University of Bristol, Bristol BS8 1TL, UK. In particular the arguments detailed in section 6.5 and section 6.7 are due to Dr Parry. The work is the subject of a paper, not quite finished, which we intend to send to *J. Chem. Phys.* for publication; "Universality for confined membranes and interfaces" by R.E.Norman, A.O.Parry and T.J.Sluckin.
- Chapter 7 is the result of collaboration with Dr A.C.Maggs of the Groupe de Physico-Chimie Théorique, ESPCI Laboratoire associé au Centre National de Récherche Scientifique (CNRS), Paris Cedex 05, France. It is envisaged that this work will be published at a later date but the details of this have yet to be finalised.

ACKNOWLEGEMENTS

I am grateful for the supervision and guidance of my project supervisor, Tim Sluckin. In particular his knack for meeting the right people for fruitful collaboration was invaluable throughout the course of this project. Thus I would like to thank Gary Barker, Anthony Maggs and Andrew Parry for their stimulating discussions and efforts during our collaboration. I would also like to thank my Mother who despite, at times, difficult circumstances never failed to encourage me in my schooling. My thanks to all the teachers who fostered and encouraged my interest in science throughout the years, in particular the teachers of Wing County Secondary School, many of whom did far more to help me than I had the right to expect. Let me also mention my Fiancèe, Miss Tina Banh, who has been so patient with me. Thanks also to my friend Ayad Al-Khoury who helped me practically and whose encouragment was invaluable when problems seemed insurmountable. Thanks also to Paulo Teixeira for his help in proof reading this thesis. Thanks to the lads in the office for putting up with my sometimes unbearable humour and general rantings. Also I am grateful to SERC and the AFRC Food Research Institute, Norwich, U.K. for a CASE award which supported me during the course of this work.

CHAPTER ONE

INTRODUCTION

1.1 States And Structure Of Matter

From the earliest ages men have striven to understand the structure and constitution of matter. The ancient Greeks entertained many theories about the structure and constitution of matter and of how it interacted to form the everyday objects and motions we are all familiar with (Hall 1969). The idea that underlying the apparent diversity of matter and form there was a simpler but hidden substructure permeated throughout their work. Elemental theories, where there were a small set of pure elements which when mixed in varying proportions gave the less fundamental manifestations of matter, were popular. For instance a popular theory held that earth, air, fire and water were the elements and any other matter could be reduced to them or constructed out of them,if only one knew how. In China a similar theory of elements is known to have been well subscribed to, as well as a simple theory of interactions (Needham 1956). We know nowadays, thanks to the accumulated work of many centuries of science, that although these theories give insight in certain restricted contexts, they are seriously incomplete and inadequate when considered as models for the properties of matter.

The *atomic theory* of matter, rediscovered (an atomic theory was postulated by the Greeks - Hall 1969) and experimentally proven by Dalton (Dampier 1942), was the first substantially successful scientific theory of the constitution of matter. In fact it is now well known that atoms are not the most basic indivisible species as postulated in the atomic theory. Nevertheless the atomic theory of matter is still an important theory and explains well certain phenomena.

The search for the most basic, elemental and indivisible particles goes on and much progress is currently being made. However, although understanding of the constitution of matter is now well advanced and *grand unified theories* of everything are claimed to be on the horizon, there remain many unanswered questions about the

structure of matter; that is how atoms and molecules interact, en-masse, to form the everyday matter that surrounds us.

We are all aware that the same substance can occur in more than one form, or *state*, with each state having very different physical properties. For instance we are aware that water occurs as ice, liquid-water and steam depending on the physical conditions (temperature and pressure). The physical state of a substance is called its *phase* (Atkins 1982). The three most basic phases of matter are solid, liquid and gas. We all know intuitively what solid, liquid and gaseous phases are like but specifically defining what they are is more tricky.

One can take an empirical viewpoint and define the phases by their observed physical properties. For instance the definition of a gas could be - that phase in which the substance expands to fill its entire container. A liquid could be defined as - that phase which adapts to the shape of its container but for which a meniscus is observable. In the same fashion a solid could be defined as a rigid object resistant to shape deformations.

On the other hand one can look at the microscopic organisation of the phases and see on this level if there are characteristic differences between them. It turns out that this is a more objective method of categorisation, and hence preferable for scientific purposes.

Along these lines it is well known that on the microscopic scale solids are characterised by rigid crystal lattices. The constituent molecules of the lattice are fixed into an ordered matrix, free only to vibrate about their lattice sites (Ashcroft and Mermin 1976, Kittel 1986). Liquids, however, are characterised by the ability of their constituent molecules to flow freely around. Short range regions of crystalline order constantly fluctuate in and out of existence (Hansen and McDonald 1986). By contrast, gases are characterised by the almost total lack of order of their constituent molecules, which move in a Brownian (random) motion (Golden 1964).

It is possible to make precise mathematical statements that correspond to these observations. Hence one can set objective tests that enable one to classify the phase of a particular piece of matter by observing it through the microscope or by using diffraction techniques. Moreover it can be seen that the physical properties of a phase are due to its microscopic organisation.

However there exist phases that cannot be classified as solid, liquid or gas, called *exotic phases*. When one looks at the molecules on a microscopic-scale one finds that there are subtle differences between the order of the exotic phase and each of the simpler phases. Often the difference is a matter of scales. For instance, when one looks on a particular length scale one may find the phase has the behaviour of one phase (e.g. liquid), whilst if one looks on a different scale one finds that a substance has the characteristics of a different phase (e.g. solid)! Alternatively, one may find that a substance is solid-like when observed over a short time scale, but liquid like when observed over longer times; and so on.

By determining the structure of exotic phases it is possible to explain the observed properties of the phase. It is also possible to predict, as yet, unforeseen properties that may (or may not) be of much use. One class of exotic structures are the structures formed by *amphiphilic* molecules which I intend to discuss in this thesis. The structures formed by amphiphilic molecules are intermediate in structure between solid and liquid; which explains why collectively they are referred to as *liquid crystalline (lc)* phases.

1.2 Organisation Of This Thesis

In chapter two I explain the basic properties of amphiphilic molecules. I present a detailed, but by no means complete, catalogue of liquid crystalline structures that amphiphilic molecules assemble into, with schematic illustrations. Then I present some generic phase diagrams for amphiphilic systems. Finally the liquid crystalline nature of biological membranes is briefly discussed.

In chapter three I discuss general aspects of *shape polydispersity in fluid vesicles*. A brief discussion of modelling and the classification of vesicle models is given. Then the fundamental geometrical ideas of curvature in two and three dimensions are presented as a prelude to the Helfrich Free Energy. Using a simple spring model of a membrane the Helfrich Hamiltonian for a surface in two and three dimensions is motivated.

For an analysis of the shape polydispersity of vesicles certain concepts and analytical tools are required. In chapter four the concepts of Scaling, Fractality and

Universality are discussed in the context of polymer chains. The similarity between the study of polymers and vesicles, as well as the key differences, are pointed out.

In chapter five some models of 2D or quasi-2D fluid vesicles are discussed. The models of Helfrich and Leibler, Singh and Fisher are briefly outlined. The Ostrowsky-Peyraud method of studying the Helfrich curvature model of vesicles is treated to a thorough investigation. I present a detailed scaling analysis and universal curves obtained from my implementation of the Ostrowsky-Peyraud model. I define a nematic scaling field to simulate shear flow conditions and systematically analyze the effects on shape polydispersity.

In chapter six I discuss a rather different model of membranes and interfaces in two and three dimensions. I study the interfaces confined between parallel walls. I discuss well known and novel analytical arguments yielding the probability distribution functions of the membranes and interfaces. The results of extensive Metropolis Monte-Carlo simulations are presented and analyzed. I demonstrate that the novel analytical arguments are in good agreement with the observed results.

Finally in chapter seven I discuss a model of membranes suitable for investigating tilted chiral lipid membranes in three dimensions. The chemical properties of the constituent molecules of this type of membrane turns out to be important in the mesoscopic structures that the membrane forms. By extending and adapting a common model of lipid membranes some of the important structural features are reproduced in the simulations. I present and analyze the results for a number of membrane geometries. The model represents a significant tool for investigating the statistical mechanics, albeit numerically, of this important class of structurally exotic membranes. There is scope for development of the model to other interesting membrane geometries.

CHAPTER TWO

COMPLEX FLUID STRUCTURES

2.1 Amphiphiles

An *amphiphile* (amphiphilic molecule) as the Greek root suggests (*amphi*: on both sides, *philos*:love), has two attractions. In practice, by this one means that part of the molecule is *hydrophillic* (likes water) and the other part is *oleophilic* (likes oil) or *hydrophobic* (dislikes water), although from the definition the solvents need not necessarily be water and oil; more generally they will be polar and non-polar solvents respectively. Amphiphilic molecules are generally organic polymers with attached ionic groups. The ionic group forms a hydrophillic 'head' whilst the organic chain forms the oleophilic, hydrophobic 'tail'.

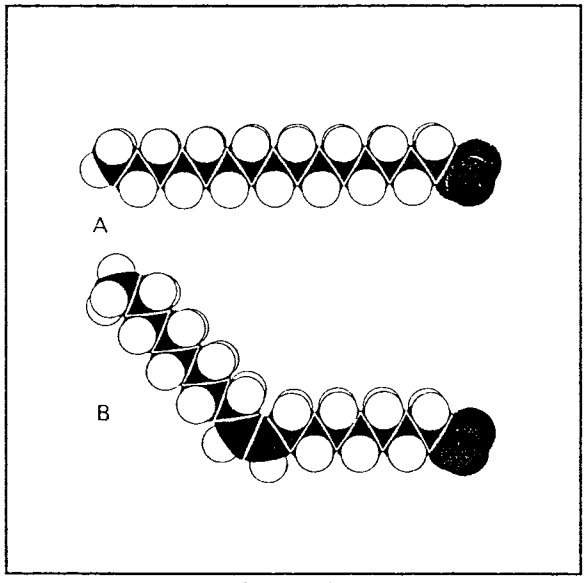

Figure 2.1
Space filling models of a) oleate
and b) palmitate ions.

Well known examples of amphiphiles are sodium palmitate, sodium stearate (soap) and potassium oleate (detergent) (Cevc and Marsh 1987). In figure 2.1 space filling models of oleate and palmitate ions are illustrated. Note that the molecules are

rod-like (the chains are relatively stiff due to their short length - oleate C_{16} and palmitate C_{18}) with a relatively large negative charge centre at one end. The palmitate molecule has a bend in it due to an unsaturated bond.

These amphiphiles are also called *surfactants* (*surf*ace *act*ive re-agents), because when added to immiscible oil-water mixtures they reside at the oil-water interface. The interface is stabilised and the interfacial tension greatly reduced by the presence of the surfactants, thus allowing the oil and water to mix more freely, albeit separated by the surfactant layer. It is the amphiphilic nature of the molecules which is responsible for this surfactant property - the action from which soaps and detergents derive their cleansing properties.

Amphiphiles, in the form of *phospho-lipids* (lipid=fat=polymer chain), are the main building blocks, of biological cell membranes and cell *organelles* (intra-cellular structures). The lipids fall into two main chemical classes; sphingosine and glycosine based. The difference is in the chemical structure of the head group only and is not a significant differentiating factor for the phase behaviour of lipid systems. In figure 2.2 a space filling model of a typical (sphingosine) lipid molecule is illustrated. Note that the molecule is "double tailed", which is characteristic of lipids, but it is still rather rod-like with a negative charge centre at one end.

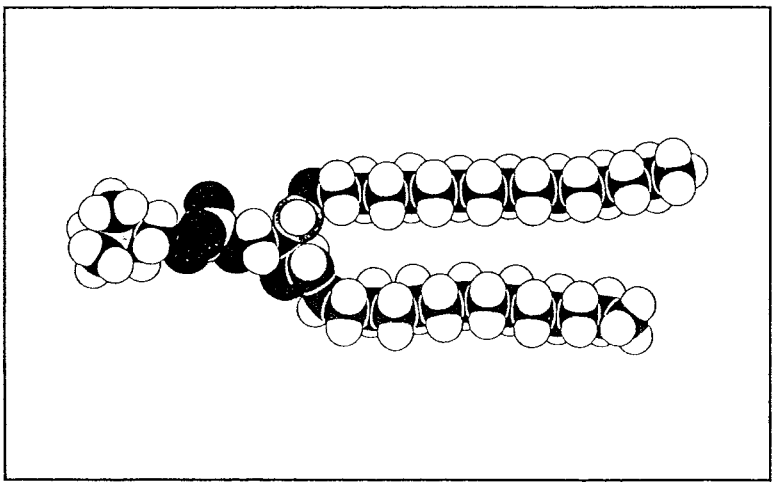

Figure 2.2
Space filling model of (sphingosine) lipid molecule sphingomyelin.

In aqueous solution pure lipids behave in the same way as other amphiphiles and form the same types of structures and membranes. Cell membranes, on the other hand

are rather more complex than surfactant stabilised oil-water interfaces; they contain significant percentages of proteins which complicate the structure somewhat, although the lipid, amphiphilic, character of the membrane is still important.

In figure 2.3 a schematic representation of one and two tailed amphiphiles is illustrated. The purpose of such a representation is to embody the main features of the molecule without worrying about its exact geometry, so that when one uses the schematic representation in illustrations of the conformation of the supermolecular structures formed by the cooperative interaction of such molecules one is not distracted, unduly, by microscopic details.

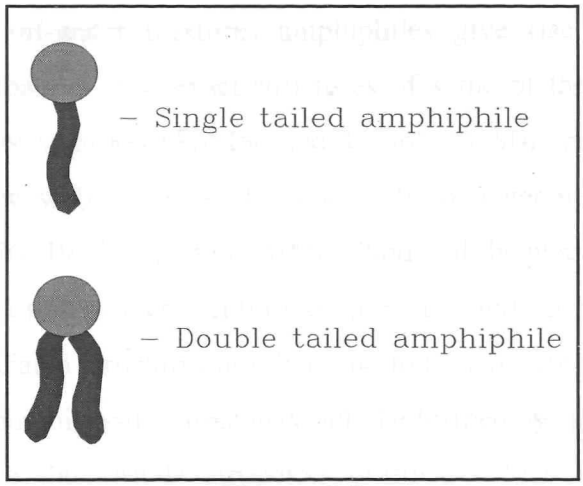

Figure 2.3
Schematic representation of one and two tailed amphiphilic molecules.

Cell membranes, oil-water-surfactant and water surfactant systems are structurally exotic. They cannot be classified as being solid or liquid in the conventional sense. They lie somewhere in between and as such are termed liquid crystalline. In studying such systems, from a theoretical point of view one hopes to extend the classification of substances. From a practical point of view one hopes to discover new, exciting, and potentially useful properties.

2.2 Applications

It is evident that an understanding of amphiphiles and the structures they form will be of interest and application in a variety of fields of study. More specifically the understanding of amphiphilic systems is, at least, of direct relevance to the detergent

industry (increased cleansing properties, new more ecologically friendly detergents) (Langevin *et al* 1985), oil industry (surfactant enhanced oil recovery) (Bansal and Shah 1976, Shah 1981, Dake 1982), pollution control (dispersants for accidental oil spillage), pharmaceutical industry (e.g. methods of drug delivery) (Poste and Papahadjopolous 1979), food industry (e.g stabilisers/emulsifiers) (Dickinson 1987, 1991), and liquid crystal research (e.g. display device technology) (Meier *et al* 1975, Shanks 1982, Kahn 1982, Schadt 1989).

2.3 A Catalogue Of Amphiphilic Structures

In water and oil-water mixtures amphiphiles give rise to, or stabilise, an abundance of exotic phases. The exact structures of some of these phases is still the subject of intensive investigation (Seddon and Templar 1990), but many of the more basic features are now well understood, at least from a geometrical point of view (Israelachvilli *et al* 1976, 1977, Lipowsky 1991). Some of the phases form spontaneously under suitable conditions of concentration, pressure and temperature for a given amphiphile. The associated structures are then said to be *self-assembling*. Other phases and the associated amphiphilic structures may only be formed by special treatment of the mixture - for instance the vesicle structures outlined below are often formed by sonification, although they form spontaneously for some amphiphiles. Below, I detail some of these peculiar phases and the associated structure of matter in them.

2.3.1 Type-I (Normal) And Type-II (Inverted) Micelles

In water-amphiphile mixtures the simplest structures formed by amphiphiles are called *micelles*. A schematic illustration of the structure of a micelle is shown below in figure 2.4.

Micellisation is the process of aggregation of amphiphiles into micelles. Experimentally it is found that micellisation is spontaneous, occurs at extremely low amphiphilic concentrations and the onset is characterised by a *critical micellar concentration* (cmc) (Mittal and Mukerjee 1976). Below the cmc the amphiphiles are to be found at the fluids interfaces.

The formation of the micelles is clearly driven by the hydrophobic character of the tail. The early onset of micellisation is an indication of the relative cost of hydrating

industry (increased cleansing properties, new more ecologically friendly detergents) (Langevin *et al* 1985), oil industry (surfactant enhanced oil recovery) (Bansal and Shah 1976, Shah 1981, Dake 1982), pollution control (dispersants for accidental oil spillage), pharmaceutical industry (e.g. methods of drug delivery) (Poste and Papahadjopolous 1979), food industry (e.g stabilisers/emulsifiers) (Dickinson 1987, 1991), and liquid crystal research (e.g. display device technology) (Meier *et al* 1975, Shanks 1982, Kahn 1982, Schadt 1989).

2.3 A Catalogue Of Amphiphilic Structures

In water and oil-water mixtures amphiphiles give rise to, or stabilise, an abundance of exotic phases. The exact structures of some of these phases is still the subject of intensive investigation (Seddon and Templar 1990), but many of the more basic features are now well understood, at least from a geometrical point of view (Israelachvilli *et al* 1976, 1977, Lipowsky 1991). Some of the phases form spontaneously under suitable conditions of concentration, pressure and temperature for a given amphiphile. The associated structures are then said to be *self-assembling*. Other phases and the associated amphiphilic structures may only be formed by special treatment of the mixture - for instance the vesicle structures outlined below are often formed by sonification, although they form spontaneously for some amphiphiles. Below, I detail some of these peculiar phases and the associated structure of matter in them.

2.3.1 Type-I (Normal) And Type-II (Inverted) Micelles

In water-amphiphile mixtures the simplest structures formed by amphiphiles are called *micelles*. A schematic illustration of the structure of a micelle is shown below in figure 2.4.

Micellisation is the process of aggregation of amphiphiles into micelles. Experimentally it is found that micellisation is spontaneous, occurs at extremely low amphiphilic concentrations and the onset is characterised by a *critical micellar concentration* (cmc) (Mittal and Mukerjee 1976). Below the cmc the amphiphiles are to be found at the fluids interfaces.

The formation of the micelles is clearly driven by the hydrophobic character of the tail. The early onset of micellisation is an indication of the relative cost of hydrating

this chain as compared with the loss of entropy caused by the assembly of the amphiphiles into more ordered systems.

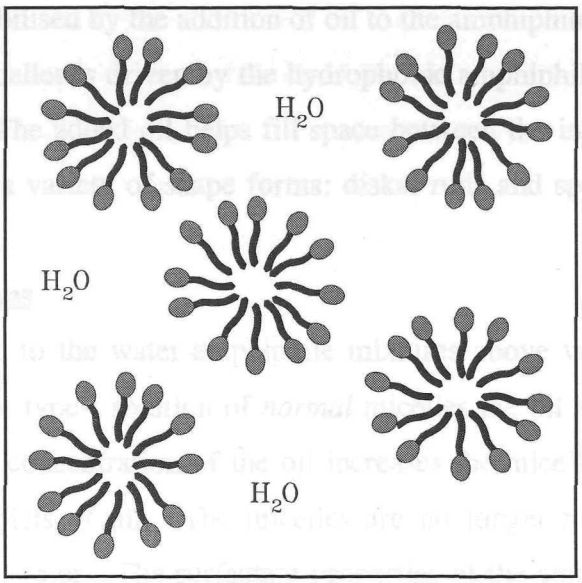

Figure 2.4
Type-I (Normal) micelle.

The micelles illustrated in figure 2.4 are called a *type*-I (or *normal*) micelle. In figure 2.5 *type*-II (or *inverted*) micelles are illustrated. The phases associated with type-I and type-II phases are designated L_I and L_{II} respectively.

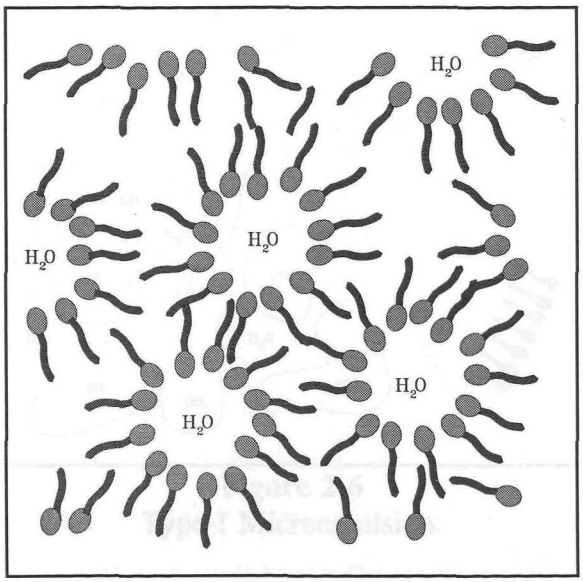

Figure 2.5
Type-II (Inverted) micelles.

It is evident that a type-II micelle is an inverted type-I micelle. Clearly type-II micelles occur when the concentration of amphiphile is very large. The formation of type-II micelles is stabilised by the addition of oil to the amphiphile-water solution. The formation of such micelles is driven by the hydrophobic amphiphile tails rather than the hydrophillic heads. The added oil helps fill space between the inverted micelles.

Micelles take a variety of shape forms: disks, rods and spheres.

2.3.2 Microemulsions

If oil is added to the water-amphiphile mixtures above very similar structures form. When added to type-I solution of *normal* micelles the oil is initially held within the micelles. As the concentration of the oil increases the micelles expand, absorbing and surrounding droplets of oil. The micelles are no longer micelles but rather oil droplets suspended in water. The surfactant properties of the amphiphiles are revealed as they now form an amphiphilic surface monolayer dividing the oil droplets from the water. The associated phase is called the type-I microemulsion (Hoar and Schulman 1943, Prince 1977, Langevin *et al* 1985, Kahlweit 1988, Meunier *et al* 1987).

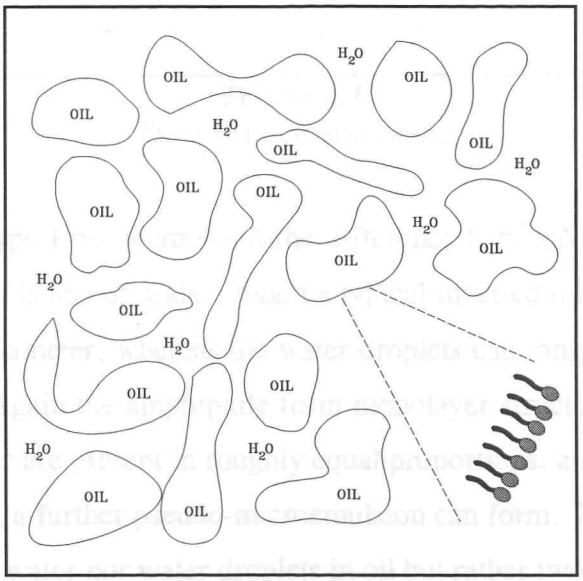

Figure 2.6
Type-I Microemulsion.

Apart from the presence of oil in the interior of the oil droplets the difference between a type-I micelle and type-I microemulsion is one of scale. A typical normal micelle is a microscopic object of molecular diameter, whereas oil droplets can range

from mesoscopic to macroscopic sizes. Oil droplets are characterised by the formation of an amphiphilic monolayer.

When oil is added to type-II solution of micelles it is initially held within the interstices between the water centres. Initially the oil stabilises the microscopic micellar structure; in fact inverted micelles sometimes only occur when stabilised by an oil component. However, as further oil (and water) is added the micelles become water droplets suspended in oil. This droplet phase is called the type-II microemulsion.

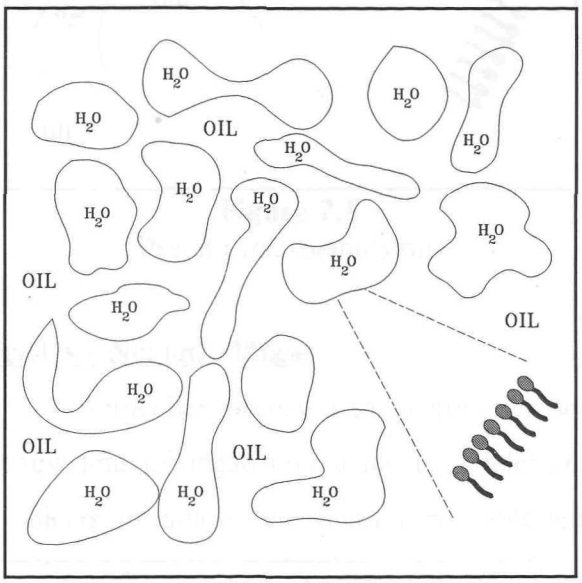

Figure 2.7
Type-II microemulsion.

As with the type-I microemulsion the difference between a type-II micelle and type-II microemulsion is one of scale. Again a typical inverted micelle is a microscopic object of molecular diameter, whereas the water droplets can range from mesoscopic to macroscopic sizes. Again the amphiphile form monolayer structures.

If oil and water are present in roughly equal proportions, and there is an adequate supply of amphiphile, a further pseudo-microemulsion can form. In this phase there are neither oil droplets in water nor water droplets in oil but rather two random bicontinuous percolation regions, one of oil, one of water; separated by an amphiphilic monolayer. In figure 2.8 one such bicontinuous pseudo microemulsions is illustrated schematically.

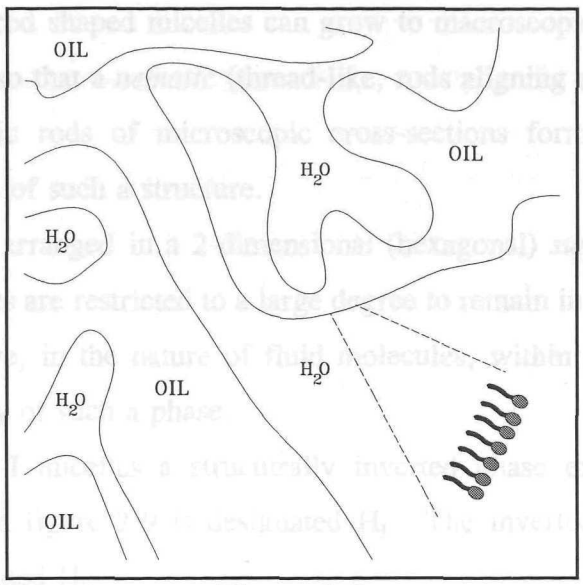

Figure 2.8
Pseudo-microemulsion.

2.3.3 Long Rod Micelles - Nematic Phase

The type-I and type-II micelles discussed above are microscopic objects of typical size of the order of a few tens of angstroms at most. Under certain conditions these microscopically sized objects are able to grow to macroscopic lengths.

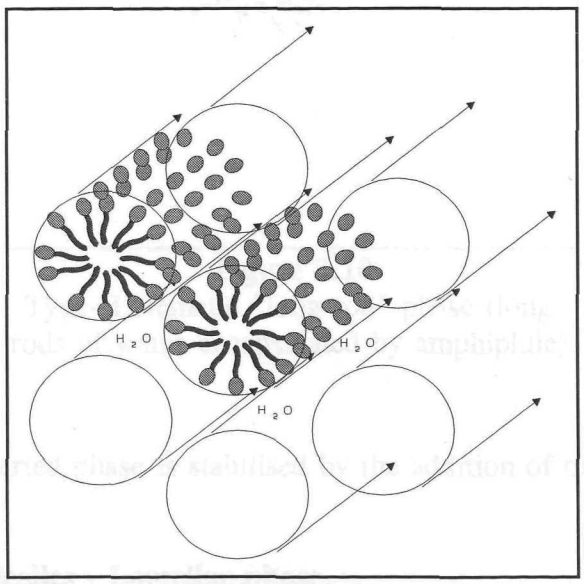

Figure 2.9
Type-I Nematic "long rod" phase (long amphiphilic rods in water).

In particular rod shaped micelles can grow to macroscopic lengths. Such rods exclude one another so that a *nematic* (thread-like, rods aligning along a common axis) phase of macroscopic rods of microscopic cross-sections forms. Figure 2.9 is a schematic illustration of such a structure.

The rods are arranged in a 2-dimensional (hexagonal) *super-lattice;* whilst the individual amphiphiles are restricted to a large degree to remain in their respective rods, they are free to move, in the nature of fluid molecules, within the rods. Hence the liquid-solid ambiguity of such a phase.

As with type-I micelles a structurally inverted phase exists. The phase of micelles illustrated in figure 2.9 is designated H_I. The inverted phase illustrated in figure 2.10 is designated H_{II}.

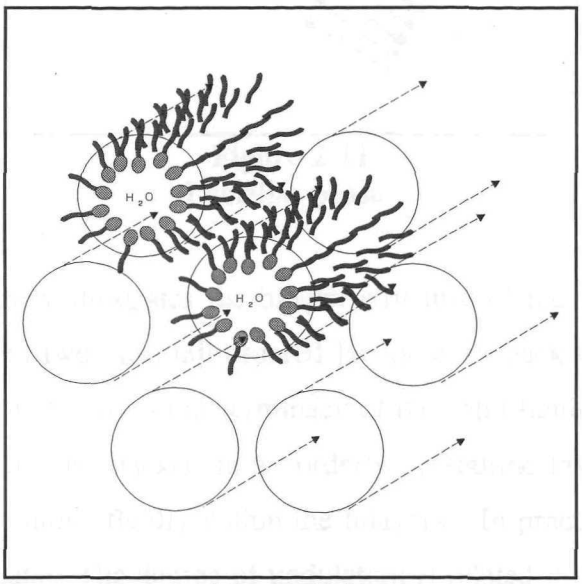

Figure 2.10
Type-II Nematic "long rod" phase (long rods of water encapsulated by amphiphile).

Again the inverted phase is stabilised by the addition of oil to the mixture.

2.3.4 Sheet-like Micelles - Lamellar phase

Long rods are not the only way in which micelles may grow. Disk shaped micelles may grow into progressively larger and larger sheets, eventually extending to macroscopic scales throughout the mixture. Sheets like rods exclude one another (viz two sheets cannot freely interpenetrate just as, for instance, two sheets of paper cannot).

Hence the mixture forms a layer structure - one sheet lying over the next. Such layered phases are called *lamellar* and are designated L_{α}. In figure 2.11 there is a schematic illustration of the lamellar a phase.

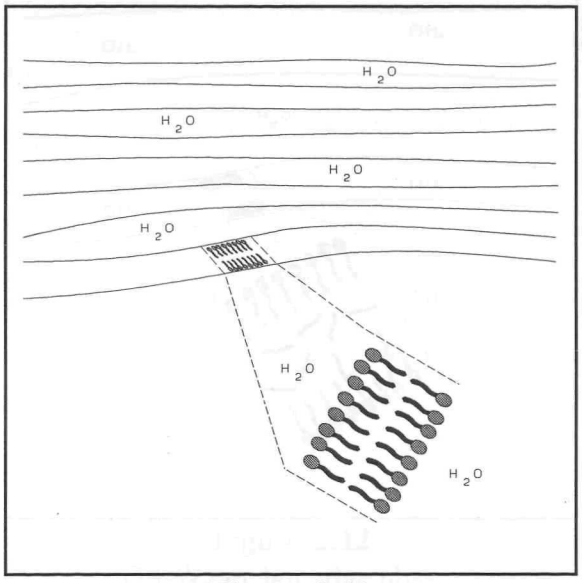

Figure 2.11
Lamellar phase.

The figure clearly illustrates the bilayer structure of the sheets; the sheets are seemingly formed from two head-tail ordered layers stuck back to back. As with the long rod phases there is a certain indeterminacy of the solid liquid nature of the phase, for while the layers may be stacked in an orderly crystalline fashion the amphiphiles themselves are free to move fluidly within the bilayers. In practice the layers are not flat; rather they undulate. The degree of undulation is related to layer-layer separation through the effect of the layer-layer exclusion. Once the phase has formed more water can be added or removed increasing or reducing the layer-layer separation respectively. The stability of the phase is thus strongly influenced by the concentration of water. Such a phase is termed *lyotropic*.

In oil-water-amphiphile mixtures similar but not quite inverted structures can form. The oil resides in the bilayer; if there is a surfeit of oil the bilayer splits into separate fluctuating mono-layers. In figure 2.12 there is a schematic illustration of the lyotropic lamellar phase. In the illustration there is a surfeit of oil which has separated the bilayer as described. The result as the figure illustrates is a multi-layered sandwich

of oil and water. In practice the layers can be rather more convoluted than the illustration shows.

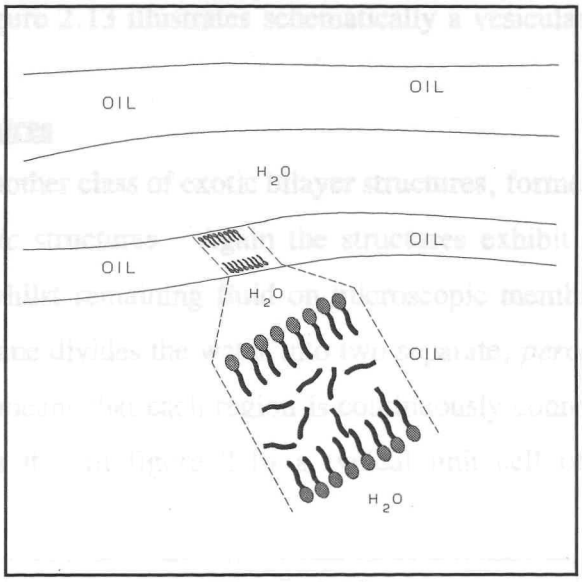

Figure 2.12
Oil-Water lamellar phase.

2.3.5 Vesicles

When disk shaped micelles grow into bilayer sheets, instead of growing to macroscopic lengths as above they may turn around, curling back on themselves to form closed surfaces like bubbles. Closed bilayer surfaces such as this are called *vesicles*.

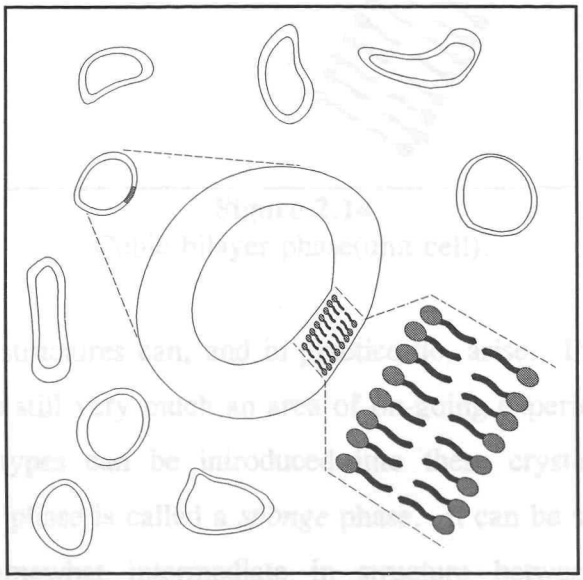

Figure 2.13
Vesicular phase.

Unlike bubbles vesicles exhibit a wide range of non-spherical shapes, which as I shall further elucidate later, is due to the fact that vesicles are subject to only vanishing surface tensions. Figure 2.13 illustrates schematically a vesicular amphiphilic phase.

2.3.6 Cubic Structures

There is yet another class of exotic bilayer structures, formed in amphiphile-water solutions, called *cubic* structures. Again the structures exhibit super-crystallinity on macroscopic scales whilst remaining fluid on microscopic membrane scales. In these structures the membrane divides the water into two separate, *percolating*, regions. The percolation property means that each region is continuously connected and the water is free to flow through it. In figure 2.14 a typical unit cell of the super-crystal is illustrated.

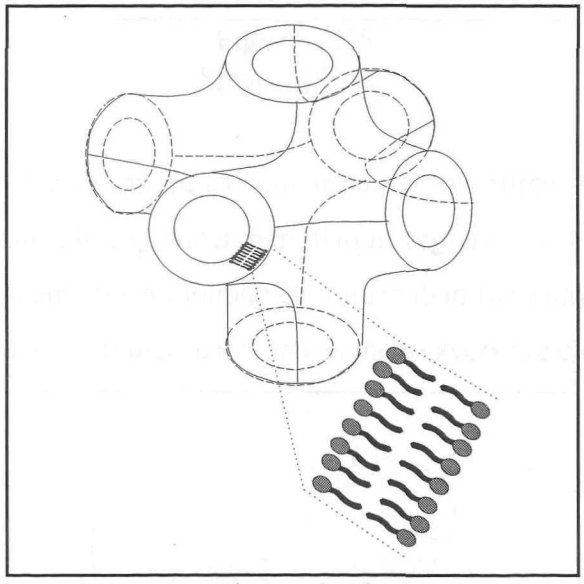

Figure 2.14
Cubic bilayer phase(unit cell).

Other crystal structures can, and in practice do, arise. In fact the structure of such super-crystals is still very much an area of on-going experimental investigations. Defects of various types can be introduced into these crystals. If such defects predominate then the phase is called a *sponge* phase. It can be seen therefore that the sponge phase is somewhat intermediate in structure between the fully random bicontinuous microemulsion phase and the rather more ordered three dimensional

crystalline structure of the cubic phase. In figure 2.15 one such type of defect is illustrated.

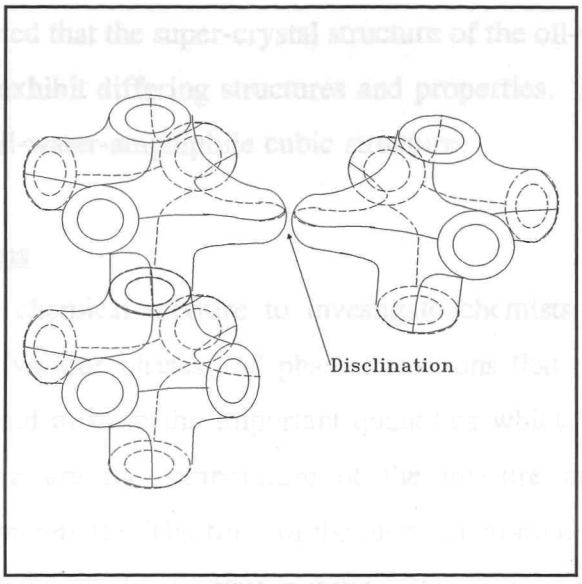

Figure 2.15
Sponge phase.

In oil-water-surfactant mixtures similar super-crystalline structures arise, but in these structures separate oil and water percolation regions are formed. Moreover the surfactants in these systems form monolayers rather than the bilayers illustrated above. The bilayers illustrated are symmetrical whereas monolayers are clearly not. One might

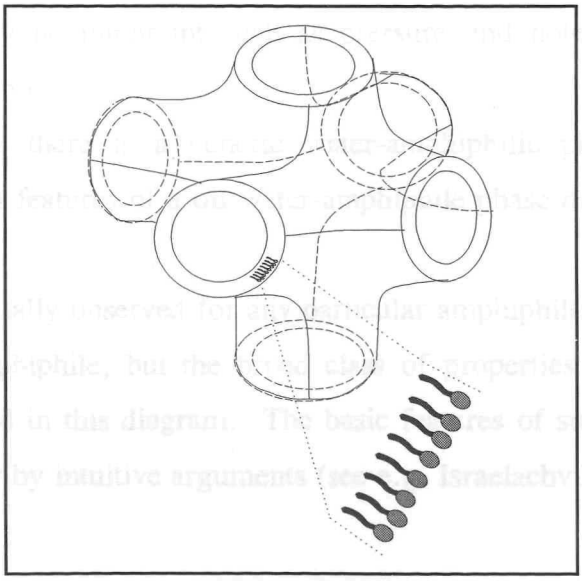

Figure 2.16
Oil-water cubic phase.

expect, therefore, that monolayers might possess an intrinsic curvature; that is they may prefer when in equilibrium to curve around towards one side rather than being flat. Hence it is to be expected that the super-crystal structure of the oil-water-amphiphile and the amphiphile-water exhibit differing structures and properties. Below is a schematic representation of an oil-water-amphiphile cubic structure.

2.4 Phase Diagrams

When given a chemical mixture to investigate chemists use *phase diagrams* (Atkins 1982) to map various phases and phase transitions that occur in the mixture. Typically, given a liquid mixture the important quantities which determine the phases present in the mixture are the temperature of the mixture and the mixture-wide concentration of its *components*. The form of the phase diagram depends on the number of components of the mixture. Let us first investigate two-component water-amphiphile phase diagrams before moving on to the more complex three-component oil-water-amphiphile phase diagrams.

2.4.1 Water-Amphiphile Phase Diagrams

In a two component phase diagram we plot component concentration along the horizontal and mixture temperature up the vertical. We hold constant any other parameters which may be important such as pressure and note their value for the particular phase diagram.

In figure 2.17 there is a generic water-amphiphilic phase diagram which illustrates the standard features of a oil-water-amphiphile phase diagram(Meunier *et al* 1987).

The phases actually observed for any particular amphiphile in solution will vary depending on the amphiphile, but the broad class of properties of amphiphile-water mixtures is represented in this diagram. The basic features of such a diagram can be explained qualitatively by intuitive arguments (see e.g. Israelachvilli *et al* 1976, 1977).

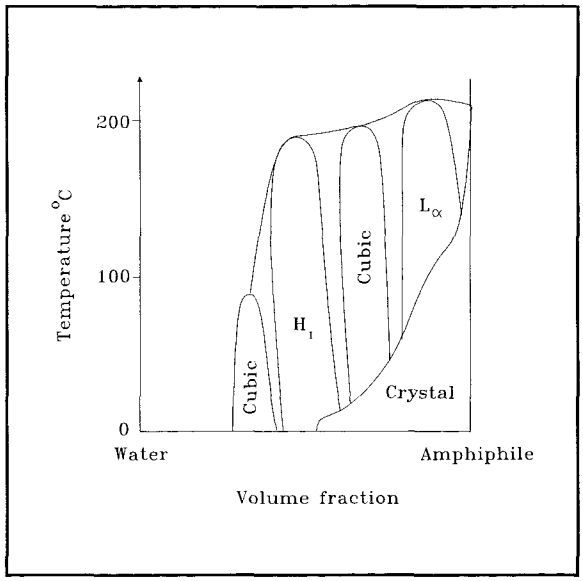

Figure 2.17
Generic water-amphiphile phase diagram.

2.4.2 Oil-Water-Amphiphile Phase Diagrams

A three component phase diagram is plotted within a triangle. Any mixture is unambiguously described by its component mixture-wide concentrations. From these concentrations one can map to the relevant position within the triangle and vice versa, as illustrated in figure 2.18.

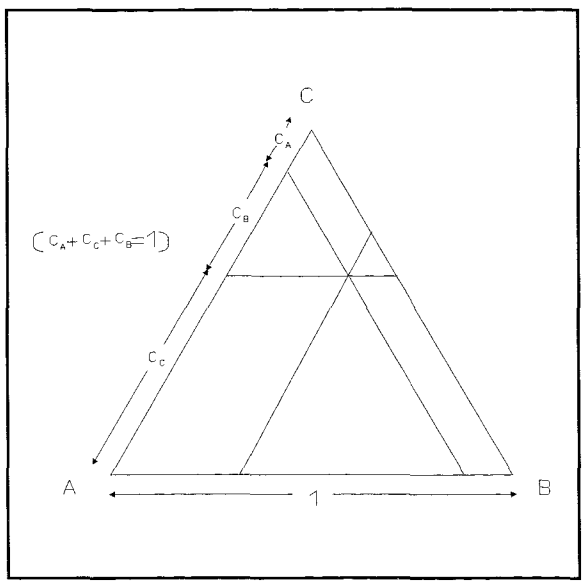

Figure 2.18
Three component phase diagram concentrations.

One should note that temperature and other relevant parameters cannot be included (in 2-dimensions) and are held constant within the diagram. To discern the temperature dependence of the diagrams one looks at a series of diagrams (temperature contours) or plots the diagrams in 3-dimensions the vertical dimension representing temperature. In figure 2.19 a generic three component oil-water-amphiphile diagram is illustrated which exhibits some of the general features of such systems.

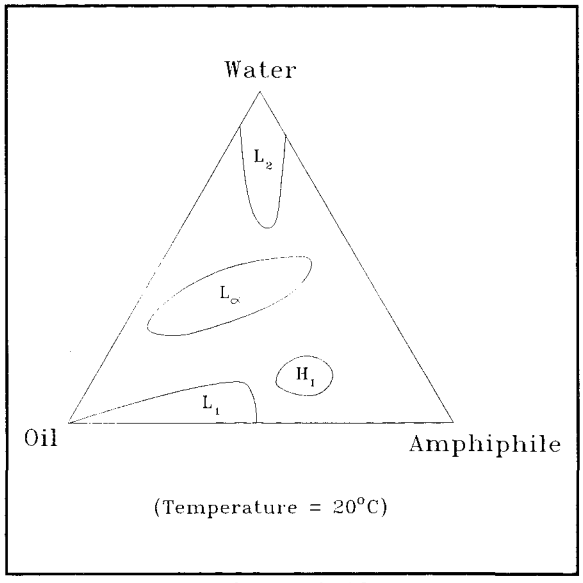

Figure 2.19
Generic oil-water-amphiphile
phase diagram.

2.5 Biological Membranes

So far I have discussed two and three component, that is water-amphiphile and oil-water-amphiphile, systems only. Cellular systems have many components. In fact it is not possible at present to specify all of the components present, in situ, in a living cell. Nevertheless, biologists have been able, over the last fifty years or so, to identify at least some of the essential components that make life possible.

Great strides have been made in the understanding of how cells use DNA to synthesise the compounds they need. Also the catalysis of the metabolic process by enzymes is now much better understood. At the forefront of these advances have been geometrical concepts of shape and form.

The cell membrane is a fundamental unit in cellular systems. It marks the boundary between the cell and the outside world. Cell membranes are not impermeable,

permeable or even semi-permeable barriers between the cell and the outside world. Rather they are *selectively* permeable allowing, as far as possible, desirable chemicals to enter and nourish the cell and interdicting undesirable or poisonous chemicals. Hence it is to be expected that cell membranes are not the simple structures dealt with so far.

In fact biologists have been able, using a variety of techniques, to determine the geometrical structure of cell membranes quite well. They have discovered that the structure of a cell membrane closely resembles the structure of a vesicle membrane; cell membranes are amphiphilic bilayers. The selective permeability of the membrane is achieved by adding proteins to the membrane which act as molecular pumps. Thus the sophistication of the membrane is built by adding sophisticated equipment to a basically simple amphiphilic bilayer. This model of a biological membrane is called the *fluid mosaic* model (Singer and Nicolson 1972). Below in figure 2.20 is a schematic illustration of the fluid mosaic model of a membrane.

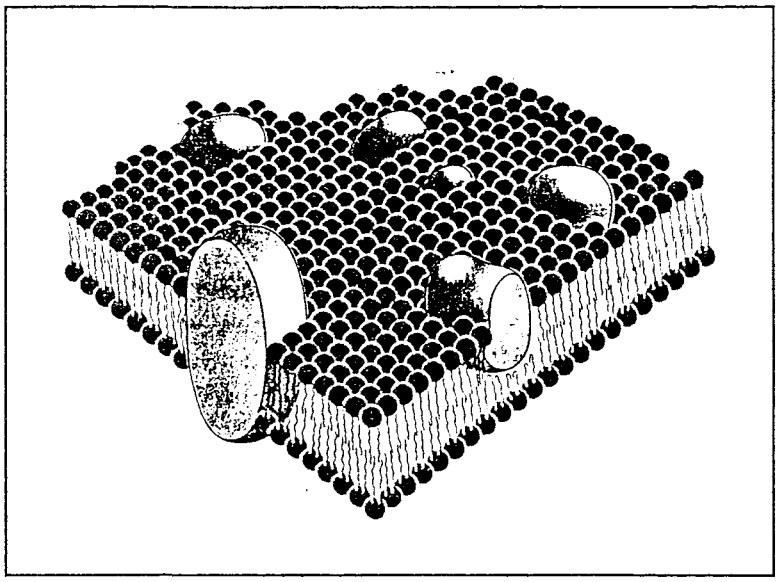

Figure 2.20
Fluid mosaic model of a cell membrane.

The amphiphilic building blocks are phospho-lipids. Within a cell membrane the lipid chains vary in length from molecule to molecule. Generally there is an asymmetry of lipid length across the bilayer, i.e. the average chain length of lipids on one side of the bilayer is often significantly different from the other side. Typical lipid chain lengths are 10-100 carbon units.

CHAPTER THREE

MICROSCOPIC MODELS OF MEMBRANES

3.1 Introduction

In the context of this work *modelling* is the process of describing a real physical system in a mathematical way. It is a process of *reduction* in which the system is successively reduced from its initial complexity and diversity by discarding irrelevant, redundant and negligible terms. Relevant terms and features are reduced to their simplest, most basic, identities. Sometimes relevant features have to be omitted for the sake of reducing the model to a simpler form; one solves the simpler model and tries to take account of the omission later by looking at the results.

The success of a model is measured in several ways. Clearly the fewer relevant terms that have to be omitted the better. The degree to which the equations that the model generates can be solved is of importance, as is the proximity of the results so obtained to available experimental data; quantitatively or, at least, qualitatively. Some models can be solved using analytical methods whilst others require the use of numerical methods. Analytical methods are to be preferred over numerical methods and numerical methods over none. However, in general if one wants to model a more faithful (to the physical reality), and thus more complex, representation then only numerical methods provide a reasonable means of obtaining results.

3.2 Shape Polydispersity In Fluid Vesicles

In order to model the complex fluid structures outlined in chapter one considerable reduction of the problem is necessary. This thesis is concerned with the effect of *shape polydispersity* in vesicle systems. So one can see that already the problem of studying the complex fluid structures has been narrowed to studying just one aspect of such structures.

In fact further reduction of the problem has proved necessary in many vesicle models. A common method of reducing the complexity of a problem is to reduce the

dimension of the space. Vesicles are closed two dimensional surfaces in three dimensional space. The generalisation of a membrane is a closed *hypersurface*. A hypersurface is an (d-1)-dimensional object embedded in a (d)-dimensional space. In particular, a *one-surface* is a one dimensional object sitting in a two dimensional space. A one-surface corresponds to a curve in 2-dimensional space. It is considerably easier, both theoretically and numerically, to study closed curves in two dimensions than it is to study closed surfaces in three dimensions. As a result much work in the study of vesicle shape is on two dimensional vesicle models. Ideally one would prefer not to have to make the simplification but in practice it is often necessary.

3.3 Classification Of Membrane Models

In the literature models of membranes fall into two main categories; microscopic and mesoscopic. Microscopic models of membranes treat membranes on the molecular scale of the constituent amphiphiles whereas mesoscopic models treat membranes on the scale of the membrane *persistence length*. The persistence length is the length scale below which the membrane can essentially be considered flat (or rigid). Typically the persistence length ranges from hundreds to thousands of times the molecular length.

Within the class of mesoscopic models there is a subdivision into continuum and continuum limit models. In continuum models the membrane is smooth and continuous everywhere. In continuum limit models the membrane is continuous, but strictly only smooth on scales below the persistence length. A true continuum model takes the Helfrich Hamiltonian whereas continuum limit models only have the Helfrich Hamiltonian approximately in the limit of a low curvature.

3.4 Mathematical Description Of Curvature

The ancient Greeks studied the relationships of lines, shapes and angles, a branch of mathematical study now called *geometry*. The study of curvature falls into the same category. Hence, one should not be surprised to learn that there is already a wealth of knowledge accumulated in the mathematics literature about curvature. One naturally has intuitive notions about the geometrical property called curvature, just as intuitively one has notions about length or weight. In fact curvature is a well defined, unambiguous, mathematical entity whose properties are already well understood.

3.4.1 Curvature Of A One-surface (Curve)

It is easier to consider first the curvature properties of a one-surface. Below one such membrane is illustrated. In the illustration one particular point of the curve has been chosen and the *circle of curvature* of that point is shown.

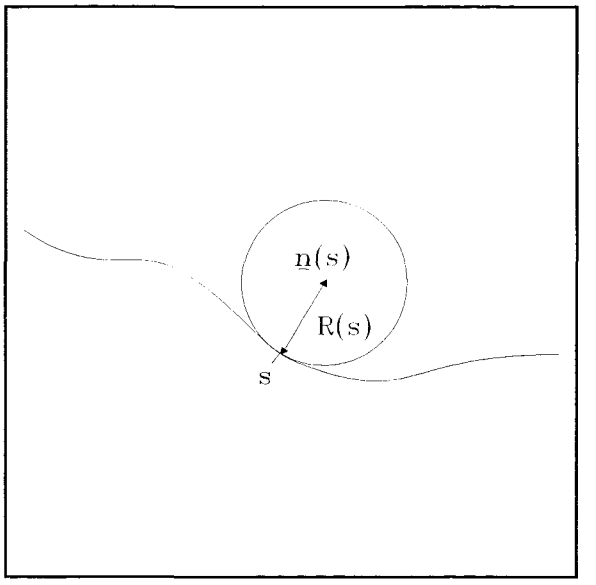

Figure 3.1
Circle of curvature.

The circle of curvature at any point, s, on the curve is defined to be the circle that touches the curve at, s, and whose gradient and rate of change of gradient is same as the curve at s. The radius of the circle, R, is the *radius of curvature*. The sign of R is fixed arbitrarily by convention. For example, for a closed curve, R can be chosen to be positive if the *centre of curvature* is inside the curve and negative if it is outside. The *curvature*, c, of the curve is defined by $c = R^{-1}$. Note that for a straight line $R = \pm\infty$ so that $c = 0$, i.e. a straight line has zero curvature, and the intuitive idea that a straight line is not curved has not been lost in the definition.

There are several ways in which one can parameterise a curve. A common and often useful way is as a height function, z(x), above a given axis, x; i.e. z=z(x). A more general (since curves need not be single valued in general) way of parameterising curves is in terms of the curve-length, s; i.e. x=x(s) and z=z(s).

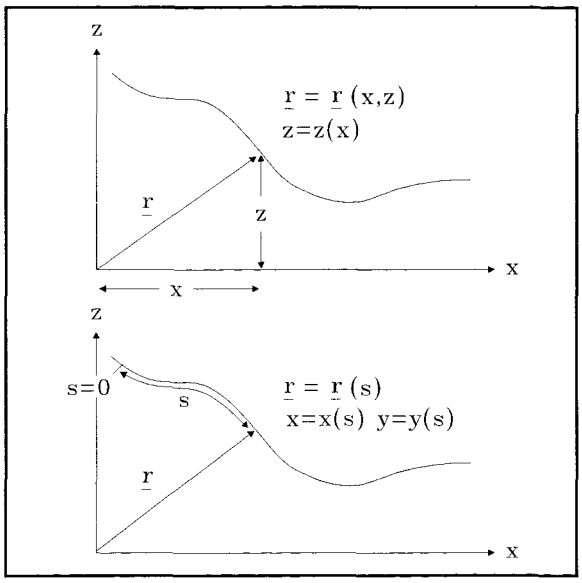

Figure 3.2.
Parameterisations of a curve.

Thus one should not be surprised to find that there are several ways of expressing the curvature of a curve depending on the mathematical description of the curve. Consider a small element of the curve of radius curvature R; illustrated below.

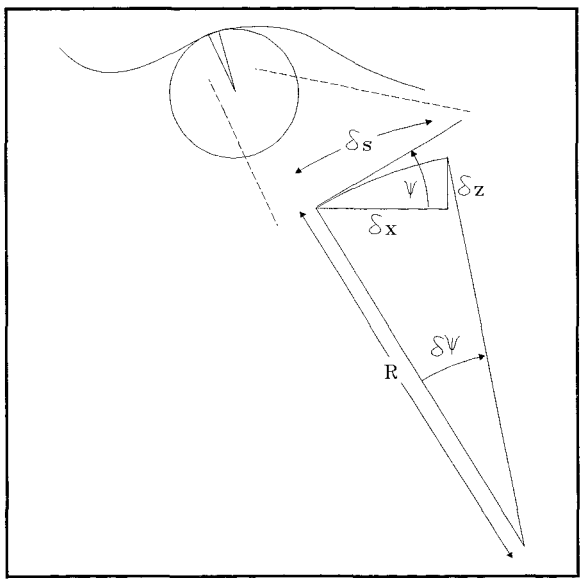

Figure 3.3
"Infinitesimal" curvature segment.

Now $R\delta\psi = \delta s$ (3.4.1;1)

so $c = R^{-1} = d\psi/ds.$ (3.4.1;2)

Also $\delta s^2 = \delta x^2 + \delta z^2 = \delta x^2[1 + (dz/dx)^2]$. (3.4.1;3)

If curve is nearly flat (i.e parallel to x-axis) then $dz/dx \ll 1$.

$\therefore$ $\delta s \approx \delta x$ (3.4.1;4)

and $R\delta\psi \approx \delta x$. (3.4.1;5)

So $c = R^{-1} \approx d\psi/dx$. (3.4.1;6)

But $\tan(\psi) = dz/dx$ (3.4.1;7)

and $\tan(\psi) \approx \psi$ for $\psi \ll 1$. (3.4.1;8)

So $\psi \approx dz/dx$ for $dz/dx \ll 1$ (3.4.1;9)

and $c = R^{-1} \approx d\psi/dx \approx d^2z/dx^2$ for $dz/dx \ll 1$. (3.4.1;10)

Note then that for a curve parameterised in terms of its curve-length, s, we have an exact expression for the curvature, $c = d\psi/dx$. In contrast, for a curve described by a height function, z(x), we have an expression for the curvature, $c = d^2z/dx^2$, only approximately correct in the nearly flat limit, $dz/dx \ll 1$.

3.4.2 Curvature Of A Two-surface (Surface)

Now we are in a position to consider the curvature properties of a two-surface. In figure 3.4 one such membrane is illustrated. The first point to note when considering the curvature of a surface in three dimensions is that there is an extra degree of freedom over and above that available to a curve in two dimensions; for any given point on the surface there are an infinite number of curves lying in the surface and passing through that point. Each curve through the point, generally, has a different circle of curvature at the point to the others.

The problem of defining the curvature of a surface at a point is analogous to the problem of defining the tangent of a surface at a point, since the tangent angle of the surface at the point depends on the direction of the curve through the point too. Therefore, not surprisingly, the solution to the problems is similar.

Before considering expressions for curvature let us consider how a surface may be parameterised. First note that there is no unique procedure for doing this. There are two widely used methods whose two dimensional space curve analogues were described

earlier. On the one hand one can define a surface as a height function, Z(x,y), above a flat surface, defined arbitrarily to be the xy-plane. On the other hand, one can parameterise the surface in terms of curve length parameters, s and t, for a set of orthogonal curves embedded in the surface; i.e. $x=x(s,t)$, $y=y(s,t)$ and $z=z(s,t)$. The second method is more general because surfaces, like curves, can fold back on themselves so that Z(x,y) is not necessarily single-valued.

In order to solve the problem of defining the tangent of a surface the *directional derivative*, D_θ, was introduced. *Partial derivatives* are a special case of directional derivatives; they are the directional derivatives in the x and y axial directions. Using a vector of partial derivatives, of the surface function, one is able to determine the tangent angle in any particular direction at any point on the curve.

In fact the directional derivative of Z(x,y) in the direction θ is given by

$$D_\theta Z = \cos(\theta)\frac{\partial Z}{\partial x} + \sin(\theta)\frac{\partial Z}{\partial y} \qquad (3.4.2;1)$$

Which in vector notation can be written

$$D_\theta Z = [\cos(\theta),\sin(\theta)]\begin{bmatrix}\frac{\partial Z}{\partial x}\\ \frac{\partial Z}{\partial y}\end{bmatrix} \qquad (3.4.2;2)$$

So one can see that given the vector of first partial derivatives of the surface, $[\partial Z/\partial x\,,\,\partial Z/\partial y]$, and using the direction vector, $[\cos(\theta),\sin(\theta)]$, one can obtain the slope in any given direction.

The curvature of a surface in three dimensions is also a directional quantity. In order to specify the curvature in any particular direction at a given point on the surface one needs a matrix of partial derivatives, called the *curvature tensor* (Spivac 1979). A tensor is a multi-dimensional generalisation of a matrix; in this case however the curvature need only be considered to be a matrix. It can be shown, in an argument based on that in section 3.4.1, that in the nearly flat limit, ($Z_x \ll 1$, $Z_y \ll 1$), the curvature tensor can be written

$$\Omega \simeq \begin{bmatrix}Z_{xx} & Z_{xy}\\ Z_{yx} & Z_{yy}\end{bmatrix} \qquad (3.4.2;3)$$

The curvature at a given point in a given direction, c_θ, can then be determined from the following expression

$$c_\theta = [\cos(\theta),\sin(\theta)]\begin{bmatrix} Z_{xx} & Z_{xy} \\ Z_{yx} & Z_{yy} \end{bmatrix}\begin{bmatrix} \cos(\theta) \\ \sin(\theta) \end{bmatrix} \qquad (3.4.2;4)$$

The maximal and minimal circles of curvature at a point are called the *principal circles of curvature* of that point. The eigenvalues, c_1 and c_2, of the curvature tensor at the point correspond to the *principal curvatures* (i.e. maximal and minimal curvature) at the point. The corresponding eigenvectors indicate the *principal directions of curvature* at the point. Since the curvature tensor is real and symmetric ($Z_{xy} = Z_{yx}$).

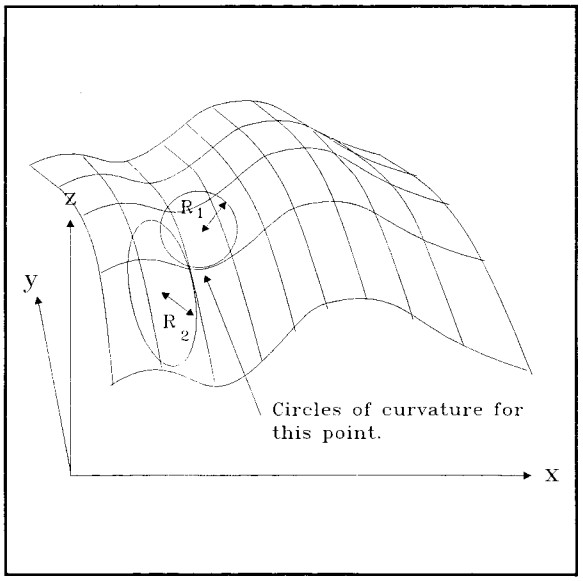

Figure 3.4
Principal circles of curvature.

then the principal curvatures always exist and the eigenvectors are *orthogonal* (at right angles). Also since the curvature matrix is 2×2 then there are only two principal circles of curvature. In figure 3.4 one particular point of the surface has been chosen and the two principal circles of curvature for that point are shown.

3.5 Microscopic Membrane Models

Microscopic models are used, principally, to investigate the nature of the membrane *Hamiltonian* (The Hamiltonian is the energy function of a system; in this case

the system being a unit area of membrane). In the Hamiltonian there is a set of elasticity constants associated with the various possible types of deformations (stretch, shear and bend) possible for the membrane. Using microscopic models one is able to make some progress in the evaluation of dependencies of these constants in terms of the geometrical quantities embodied by the membrane.

3.5.1 Microscopic Spring Model Of One-surface Bilayer

In microscopic spring models of vesicles the bilayer is imagined to be made up of a series of connected springs. Figure 5, below, illustrates one such arrangement for a one-surface.

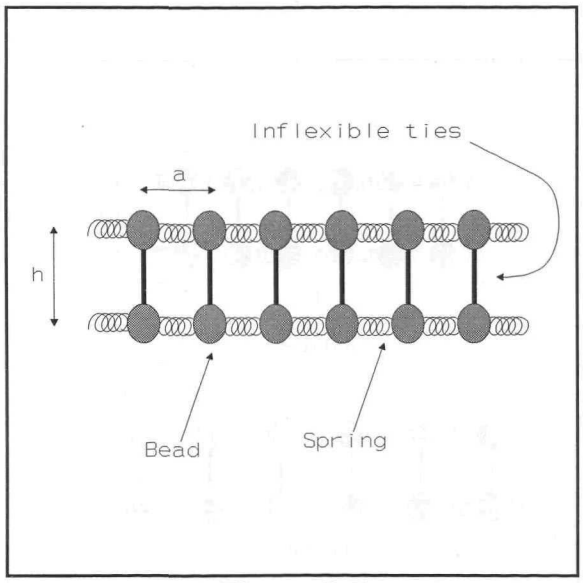

Figure 3.5
Microscopic spring model of a one-brane bilayer.

Define:

a_0 = equilibrium spring length

a = actual spring length

h = membrane thickness

k = spring constant

So that:

single spring energy $\epsilon = k(a-a_0)^2/2$ (3.5.1;1)

number of particles / per unit length $n = a^{-1}$ (3.5.1;2)

This simple model of a membrane is able to provide the basic features of the Hamiltonian upon which more complex models are dependant. There are two types of deformations such a membrane can experience - *stretch* and *curvature* (i.e. bend). Associated with each of these deformations is an energy, that arises, in this model, from the extension or compression of the springs induced by the deformation.

Let us first consider the contribution to the Hamiltonian arising from stretching deformations of the membrane. A stretching deformation of the membrane is illustrated in figure 3.6.

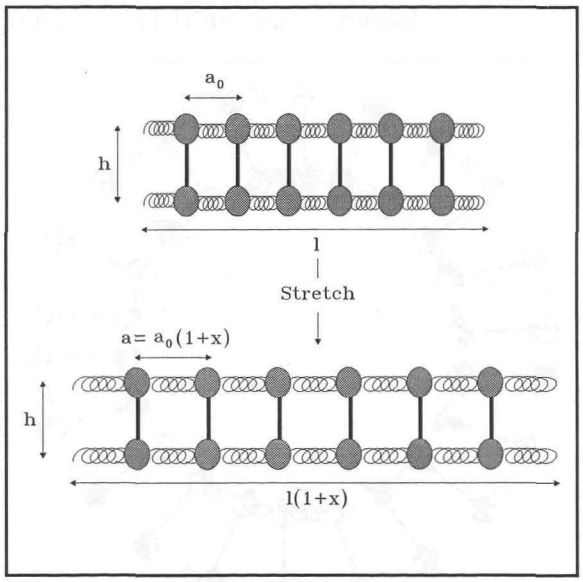

Figure 3.6
Stretch deformation.

Suppose such a membrane, of length l, is stretched uniformly. Then

unit length $\rightarrow (1+x)$ (3.5.1;3)

length l $\rightarrow l(1+x)$ i.e. $\delta l = lx$. (3.5.1;4)

where x is the extension per unit length of the membrane due to the stretching.

Each spring is equally stretched so that a spring

length a_0 $\rightarrow a_0(1+x)$ i.e. $\delta a = a_0 x$. (3.5.1;5)

Hence, each spring stores elastic energy

$$\epsilon = ka_0^2x^2/2. \qquad (3.5.1;6)$$

Number of springs in length l of membrane is

$$2(l/a). \qquad (3.5.1;7)$$

Therefore total elastic energy change due to stretch is

$$2(l/a).(ka_0^2x^2/2) \approx kla_0x^2. \qquad (3.5.1;8)$$

So the stretch energy per unit length is

$$H_s=ka_0x^2. \qquad (3.5.1;9)$$

If we write this in the form $H_S=\sigma x^2/2$ then we get an expression for the stretch elasticity or *line tension* $\sigma=2ka_0$. This tells us that the membrane stores energy proportional to the extension squared; which is how a spring stores energy and is, on reflection, what we would expect from such a model.

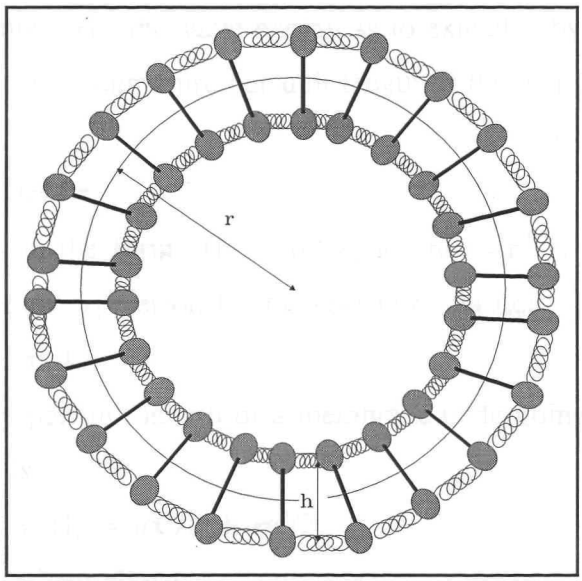

Figure 3.7
Curvature deformation.

Let us now consider a uniform curvature deformation and the contribution it makes to the membrane Hamiltonian. Suppose one such membrane, of length l, is bent around so that it forms a circle, of radius r (such a deformation is illustrated in figure 3.7). Then the curvature, $c=1/r$, is uniform and if the membrane is not stretched (no net extension of the membrane) there is no energy due stretching and $r=l/2\pi$. However, as the figure shows, springs on the outside of the circle are extended whilst springs on the inside are compressed and so a bending force is required to put the membrane into

the circular configuration. The energy associated with this force is the curvature energy of the configuration.

Now the outer ring of springs has radius r+h/2. So the circumference of the outer ring of springs is $2\pi(r+h/2)$. Consequently the outer ring of spring experiences a uniform extension of πh. The extension per unit length of the outer ring is approximately (h small) $\pi h/2\pi r = h/2r$. The energy associated with this energy is just half the energy required to extend a bilayer by the same amount, $ka_0h^2/8r^2$.

Now the inner ring of springs has radius r-h/2. So the circumference of the inner ring of springs is $2\pi(r-h/2)$. Consequently the inner ring of spring experiences a uniform compression of πh. The compression per unit length of the outer ring is approximately (h small) $\pi h/2\pi r = h/2r$. The energy required for this compression is the same as the energy required to extend the outer ring (since compressing a (Hookean) spring by a given amount takes the same energy as to extend it by that same amount).

So the total energy of curvature per unit length of the membrane curved around a circle of radius r is

$$H_c = ka_0h^2/4r^2. \qquad (3.5.1;10)$$

If we write this in the form $H_c = \kappa c^2/2$, where $c=r^{-1}$ is the curvature of the membrane, then we get an expression for the curvature elasticity:

$$\kappa = ka_0h^2/2 = \sigma h^2/4. \qquad (3.5.1;11)$$

The total energy per unit length of a membrane undergoing a stretch and being curved around a circle is

$$H = H_s + H_c = \sigma x^2/2 + \kappa c^2/2, \qquad (3.5.1;12)$$

with σ and κ constants, given above.

In fact, this Hamiltonian is more generally applicable. In general membranes experience position, s, dependent stretch and curvature deformations; $x \rightarrow x(s)$ and $c \rightarrow c(s)$. However, locally around a small element of the curve of length δs the curvature and stretch can be considered uniform. So locally the Hamiltonian can be considered to be the Hamiltonian just derived; i.e.

$$H \rightarrow H(s) = \sigma x(s)^2/2 + \kappa c(s)^2/2. \qquad (3.5.1;12)$$

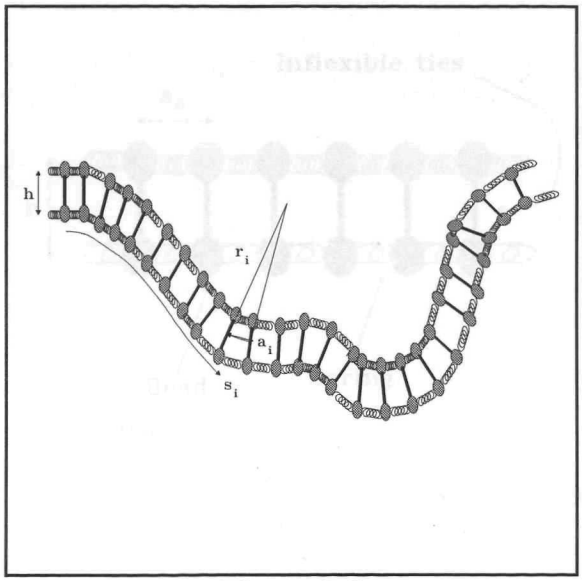

Figure 3.8
Instantaneous stretch and curvature.

Clearly to get the total Hamiltonian of the membrane one has to sum, viz integrate, over the local elements, so that in fact:

$$H = \int_0^1 \tilde{H}(s)ds = \int_0^1 \left(\frac{\sigma}{2} x(s)^2 + \frac{\kappa}{2} c(s)^2 \right) ds \qquad (3.5.1;13)$$

The Hamiltonian in (3.5.1;13) is the basic Hamiltonian used in mesoscopic models of membranes in two dimensions. It is called the *Helfrich model* of a membrane. Later the generalisation to three dimensions shall be motivated.

Intuitively one can see that allowing a one-surface to have position dependent stretch and curvature deformations is the most general deformation possible. In fact there are well known theorems of geometry which can prove this intuitive idea.

3.5.2 Microscopic Spring Model Of An Asymmetric One-surface Bilayer

The spring model can easily be adapted to model a monolayer or an asymmetric bilayer. The key point about these membranes is that they prefer to curve towards one side than the other, because of the internal asymmetry of the membrane. The asymmetry of the membrane can be introduced by making the spring coupling constants and equilibrium spring lengths for the top and bottom side of the membrane different.

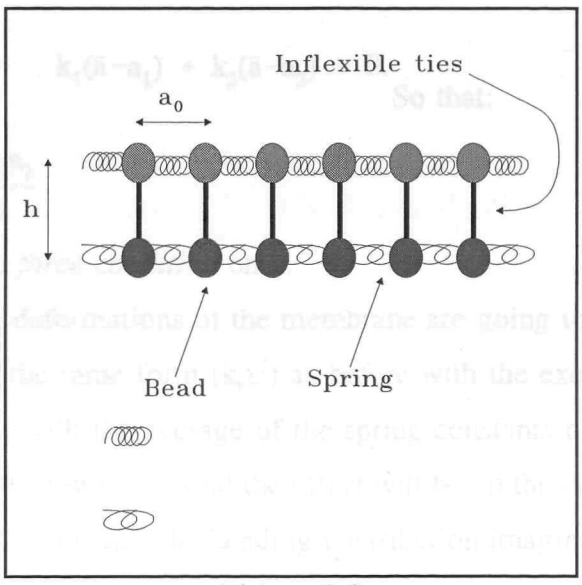

Figure 3.9
Microscopic spring model of a one-brane monolayer.

Define:

a_1, a_2 = equilibrium spring lengths

a = actual spring length

h = membrane thickness

k_1, k_2 = spring constants

So that now:

energy top springs	$\epsilon_1 = k_1(a-a_1)^2/2$	(3.5.2;1)
energy bottom springs	$\epsilon_2 = k_2(a-a_2)^2/2$	(3.5.2;2)
no of particles per unit length	$n = a^{-1}$	(3.5.2;3)

The flat state of the membrane is now no longer the freely adopted position, in general. In the flat state the energy per unit length is given by:

$$\frac{1}{2}n[k_1(\tilde{a}-a_1)^2 + k_2(\tilde{a}-a_2)^2] \qquad (3.5.2;4)$$

where, $\tilde{a}$, is mean length of springs.

The energy contribution of one set of springs is just $\epsilon = \epsilon_1 + \epsilon_2$. For equilibrium we should minimise ϵ. Hence for equilibrium in flat state:

$$\frac{\partial \epsilon}{\partial \tilde{a}} = 0 \quad \Rightarrow \quad k_1(\tilde{a}-a_1) + k_2(\tilde{a}-a_2) = 0. \qquad (3.5.2;5)$$

So that:

$$\tilde{a} = \frac{k_1 a_1 + k_2 a_2}{(k_1+k_2)} \qquad (3.5.2;6)$$

This is called the *zero force condition* on $\tilde{a}$.

Clearly stretch deformations of the membrane are going to lead to contributions to the Hamiltonian of the same form ($k_s x^2$) as before with the exception that the spring constant for the bilayer will the average of the spring constants of top and bottom.

It is not so clear, however, what the effect will be on the curvature contributions to the Hamiltonian. To calculate the bending contribution imagine taking a length $2\pi r$ of the flat state membrane and bending it round into a circle. The resulting circular membrane in equilibrium would have a radius r+x (not r!), where x is small but not necessarily zero as we shall see. The membrane now has uniform curvature $c \approx r^{-1}$.

The outer radius is now R+h/2+x and inner radius is R-h/2+x. Hence separation of particles in outer circle is $a_{out}=\tilde{a}[1+h/(2r)+x/r]$ and separation of particles in inner circle is $a_{in}=\tilde{a}[1-h/(2r)+x/r]$. Therefore the energy per unit length of such a configuration is:

$$H_c = \frac{1}{2}n\left[k_1\left(\tilde{a}-a_1+\frac{\tilde{a}h}{2r}+\frac{\tilde{a}x}{r}\right)^2 + k_2\left(\tilde{a}-a_2-\frac{\tilde{a}h}{2r}+\frac{\tilde{a}x}{r}\right)^2\right] \qquad (3.5.2;7)$$

Expanding this expression:

$$H_c = \frac{1}{2}n\left[[k_1(\tilde{r}-a_1)^2+k_2(\tilde{r}-a_2)^2] + \frac{h\tilde{a}}{r}[k_1(\tilde{a}-a_1)-k_2(\tilde{a}-a_2)] + \frac{hx}{r}[k_1(\tilde{a}-a_1)+k_2(\tilde{r}-a_2)] + \frac{1}{4}\frac{h^2\tilde{a}^2}{r^2}(k_1+k_2) + \frac{\tilde{a}^2x^2}{r^2}(k_1+k_2) + \frac{h\tilde{a}^2x}{2r^2}(k_1-k_2)\right] \qquad (3.5.2;8)$$

The first term is just the flat state energy, H_f say. From the definition of $\tilde{a}$ the first order term in x cancels. The expression can be minimised for x yielding:

$$\tilde{x} = \frac{h}{2}\frac{(k_2-k_1)}{(k_1+k_2)} \qquad (3.5.2;9)$$

The most important point to note in this equation is its dependence on the curvature, c. There are now linear and quadratic terms in c. The linear term was not

present in the case of the symmetric membrane. As a consequence the energy is minimised for $c \neq 0$, in general. In fact,

$$c_0 \propto h[k_1(\tilde{a}-a_1) + k_2(\tilde{a}-a_2)] \qquad (3.5.2;10)$$

is the minimizing value of curvature. So only if c_0 as above $=0$ is a flat state possibly the preferred state.

So we can write the curvature energy per unit length:

$$H_c = H_f + \frac{1}{2}\kappa(c-c_0)^2 \qquad (3.5.2;11)$$

where,

$$\kappa = \frac{1}{4}n(k_1+k_2)\tilde{a}^2h^2 \qquad (3.5.2;12)$$

As with the symmetric membrane case this Hamiltonian is more generally valid for position dependent stretches and bends. Then we write the Hamiltonian as

$$H = \int_0^s \tilde{H}(s)ds = \int_0^s \left(\frac{\sigma}{2}x(s)^2 + \frac{\kappa}{2}(c(s)-c_o(s))^2\right)ds \qquad (3.5.2;13)$$

where $c_0(s)$ is the only new term over the symmetric membrane expression (3.5.1;13).

3.5.3 Microscopic Spring Model Of Two-surface Bilayer

The spring model of a two-surface bilayer is no more complicated, conceptually, than the spring model of a one-surface. One can arrange sets of beads and springs into a bilayer structure quite easily. One such arrangement is illustrated in figure 3.10. In these illustrations the amphiphiles are structured hexagonally in the membrane. In fact the beads could be joined up into any arbitrary structure, but once linked they are fixed. Since experimental studies show that the amphiphiles are free to diffuse through the membrane in a fluid fashion then clearly the spring two-surface does not model physical reality accurately in this respect.

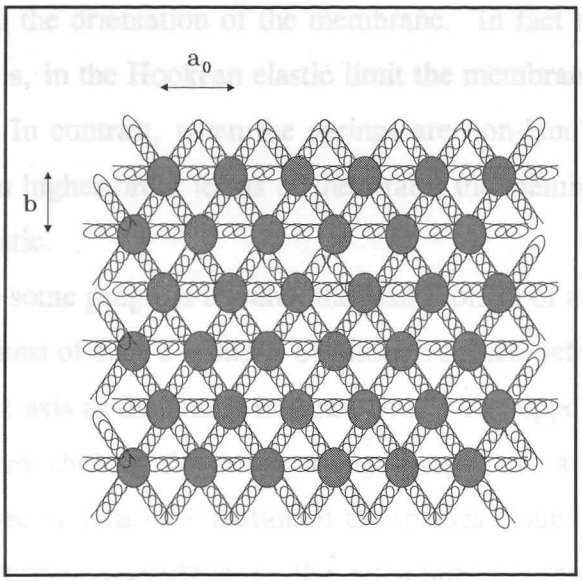

Figure 3.10
Plan view of spring model of a bilayer two-brane.

True to its solid like structure this spring model of a membrane supports *shear* deformations as illustrated in figure 3.11; viz it has a non-zero *shear elasticity* constant.

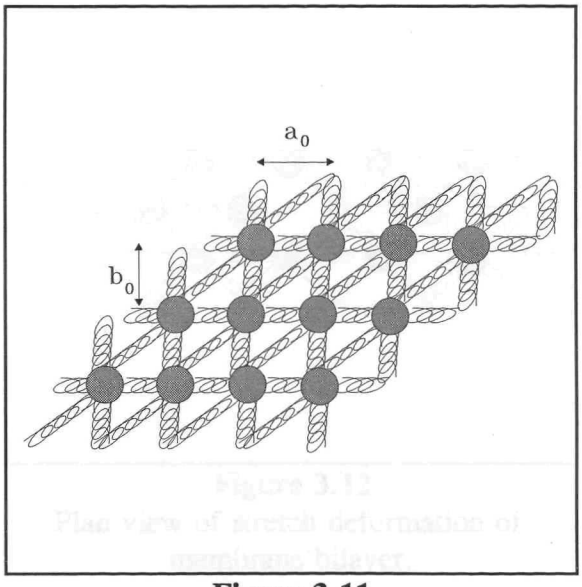

Figure 3.11
Plan view of a shear deformation of membrane bilayer.

At first appearance one might expect the membrane to be *anisotropically* elastic; viz the deformations produced by applying forces to the membrane depend not only on

the forces but also on the orientation of the membrane. In fact this can be shown not to be the case. That is, in the Hookean elastic limit the membrane can be shown to be *isotropically* elastic. In contrast, when the springs are non-Hookean (i.e have elastic energies dependent on higher order terms of the strain) the membrane can be shown to be anisotropically elastic.

One can make some progress towards the Hamiltonian of an isotropic membrane considering deformations of such a model. Consider a stretch deformation along one of the crystal axes, e.g. x axis as illustrated in figure 3.12. The opposite sides are clamped so that there is no net shift of the beads along the y axis, and that strain field is negligible. One can see that the contribution of the springs along the x axis is Hookean. But the transverse springs contribute to the stretching energy too. In fact their contribution is also Hookean. So the membrane responds to stretch deformations like a single spring albeit with a modified spring constant. One can impose a strain field in any direction, the response is always the same.

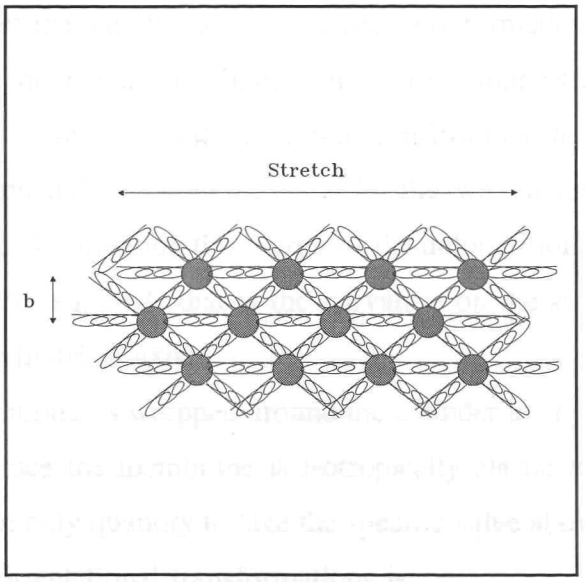

Figure 3.12
Plan view of stretch deformation of membrane bilayer.

Now consider simultaneously applying a stretch deformation in the transverse (y-axial) direction. If the deformation is small so that the springs continue to respond in a Hookean fashion then the energy due to each deformation will be independent. Moreover if the membrane is isotropic then the elastic constant for each deformation will

be identical, σ say. So the total energy due to the stretch is the sum of the two independent stretches, i.e.

$$H_s = \frac{\sigma}{2}\left(x_x^2 + x_y^2\right) \qquad (3.5.3;1)$$

where x_x and x_y are the strain components in the x and y directions respectively.

Further one can decompose any general global stretch deformation locally into a pair of orthogonal stretches and so more generally one can write

$$H_s = \frac{\sigma}{2}\int\int\left(x_s^2(s,t) + x_t^2(s,t)\right)dsdt \qquad (3.5.3;2)$$

where s and t parameterise the membrane and x_s and x_t are the corresponding local strain components.

Now consider the simplest curvature deformation of the membrane; imagine it rolled into a cylinder. As for the membrane in two dimensions considered in section 3.5.1 one should expect the membrane to resist such a deformation. As previously, the reason being that the inner and outer membranes are compressed and stretched with respect to each other. A short consideration will confirm that the nature of the stretch and compression are uniaxial. As such the result for the two dimensional system follows through, so that for this deformation the energy of the deformation is proportional to the curvature of the cylinder squared (that is the curvature on the surface in the direction perpendicular to the cylindrical axis).

Now if the membrane is wrapped around the cylinder in any other orientation the same result applies, since the membrane is isotropically elastic to such deformations. It can be shown that the only quantity to take the specific value above and which remains invariant under these orientational transformations is

$$H_c = \frac{\kappa}{2}\left(c_x + c_y\right)^2 \qquad (3.5.3;3)$$

where c_x and c_y are the x and y components of the curvature; which is uniform for the cylindrical deformation (The quantity (c_x+c_y) is the trace of the curvature tensor which is why it remains invariant under rotational transformations).

In fact (3.5.3;3) remains valid locally for all other curvature deformations. So that one can write

$$H_c = \frac{\kappa}{2}\int\int (c_s(s,t) + c_t(s,t))^2 ds dt \qquad (3.5.3;4)$$

where s and t parameterise the membrane and c_s and c_t are the corresponding curvatures. Equivalently one can write

$$H_c = \frac{\kappa}{2}\int\int (c_1(s,t) + c_2(s,t))^2 ds dt \qquad (3.5.3;5)$$

where c_1 and c_2 are the principal curvatures.

Hence the final form of the Hamiltonian for a membrane (of fixed topology) in three dimensions is

$$H = \int\int (\kappa(c_1(s,t)+c_2(s,t)-c_0(s,t))^2+\sigma(x_s^2+x_t^2))ds dt \qquad (3.5.3;6)$$

where I have included the asymmetry term, c_0, from (3.5.2;13) for completeness. This Hamiltonian represents the full Hamiltonian for membrane systems experiencing stretch and curvature stresses. There is no shear term, so that the membrane it models is supposed to be fluid. The expression in (3.5.2;3) is exact. The first term is the Helfrich curvature term. The second is a surface tension term.

3.5.4 Molecular Models Of Membranes

The spring models discussed above do not truly model membranes on a molecular scale, despite their success in providing the Helfrich Model for use in mesoscopic models. There are models which attempt to model more faithfully the molecular reality of membrane systems (Israelachvilli 1976). These models calculate the free energy associated with any particular configuration of the membrane in order to determine energy dependence of stretches, and more particularly bends. There are many such models using different numerical or analytical techniques, but the basic flavour is the same. Figure 3.13 illustrates a possible representation of a membrane in such a model.

Here the membrane is modelled as a collection of chain molecules whose heads are packed into a particular surface configuration. The chains of molecules are self avoiding, i.e. no two molecular units can occupy the same place. One can introduce a deformation to the membrane and ask what is the free energy of the deformed membrane compared to the original. One can alter the sizes of chains and so on to investigate the

effect on the free energy. If one imagines the chains on a lattice one can make some headway in finding analytical expressions for the free energy of configurations.

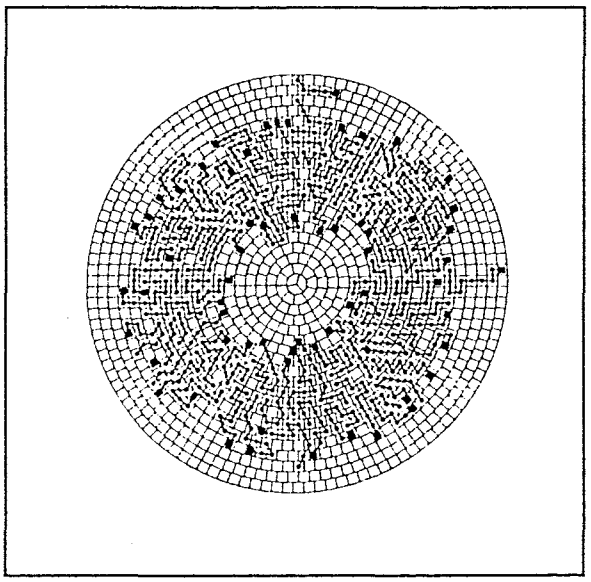

Figure 3.13
Molecular model of an amphiphilic bilayer.

CHAPTER FOUR

SCALING THEORY IN POLYMER CHAINS

4.1 Introduction

When one initiates a study into some new or unexplained phenomenon one looks to see if there are any analogous phenomena from which one can adapt the analyses to apply in explaining the new phenomenon. This cross-fertilisation of ideas makes progress much easier and faster, even facilitating progress where it was not previously possible.

The study of membranes is closely related to the study of polymers. Indeed in the two dimensional case membranes and ring polymers are indistinguishable from a modelling point of view. In higher dimensions, and in particular three dimensions, this is of course not the case. Nevertheless one should not be too surprised to learn that the analytical techniques used and developed to study polymers are directly relevant to the study of membranes, and in particular vesicles.

Recent advances in the field of shape polydispersity in vesicles have stemmed from the use of *scaling analysis* to interpret results generated by numerical models and simulations. These scaling analyses were motivated by the successes of scaling analysis in the theory of polymers and the direct analogy between polymers and membranes.

Hence in this chapter I shall discuss the scaling theory of polymers and related topics such as *fractality* (Mandelbrot 1983), which is currently an area of intense research and discussion, and the *renormalisation group method* (Ma 1985, Huang 1987).

4.2 The Free-flight Chain

The *free-flight chain* is probably the simplest model of a polymer. From an analytical point of view it is essentially identical to the *random walk* (also called *drunkard's walk*) model of the diffusion of gas molecules. In the free flight chain model of a polymer the polymer is imagined to be constructed from a series of smaller, rigid,

and essentially linear segments, called links, joined together by freely flexible joints, sometimes called spacers.

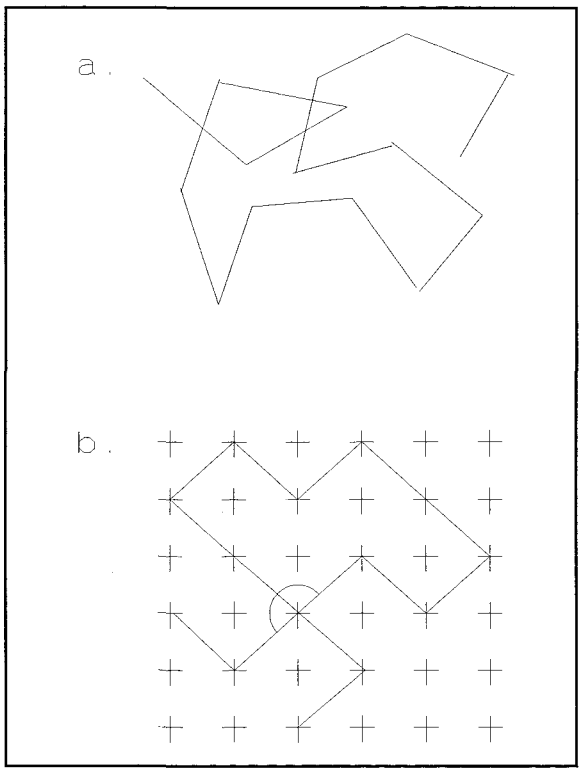

Figure 4.1
Free-flight chain model.

In the free-flight model there are no restrictions on the orientation of the links except, of course, that they must all remain joined together. It is assumed *a priori* that each configuration is equally likely. In the simplest case the links are all assumed of equal length, *a* say (c.f. in random walks a corresponds to the mean free path λ). Any given chain has a fixed number of links, N say. The total length of the polymer chain is therefore Na.

If one was studying an ensemble of free-flight chains one would be interested in how the properties of the chain depend upon N, a and d, the dimensionality of the space. One might expect that the *end-to-end displacement* $\underline{R}$ of the polymer chain would be an interesting property to study and this is in fact the case. However the average displacement is identically zero, i.e. $<\underline{R}> \equiv 0$ (i.e $=0$ $\forall a,N,d$), since for every configuration, $\underline{R}=\underline{R}_1$ say, there is a "conjugate" configuration, $\underline{R}=-\underline{R}_1$, that is equally likely and which therefore cancels with the former term in the averaging.

A more interesting quantity is the *end-to-end distance* of the chain defined by, $R_F = <\underline{R}^2>^{1/2}$. In some sense the end-to-end distance tells us how large the polymer is on average; it tells us how "strung out" the chain is. One can derive an analytical expression for the end-to-end distance in terms of the ensemble parameters, N and a, in the case of the free flight chain (Chandrasekhar 1943).

If the i'th link is $\underline{r}_i$ then by definition a molecule in this model is the *ordered* set $\{\underline{r}_1, \underline{r}_2, \ldots, \underline{r}_N\}$. The set is ordered since changing the order of any of the links generally changes the configuration of the molecule.

By definition:

$$|\underline{r}_i| = a \quad \text{and} \quad \underline{R} = \sum_i \underline{r}_i. \tag{4.2;1}$$

Moreover

$$\underline{R}^2 = \sum_{i,j} \underline{r}_i.\underline{r}_j \quad \Rightarrow \quad <\underline{R}^2> = \sum_{i,j} <\underline{r}_i.\underline{r}_j>. \tag{4.2;2}$$

But

$$<\underline{r}_i.\underline{r}_j> = \begin{cases} i=j : & <\underline{r}_i.\underline{r}_i> = <|\underline{r}_i|^2> = a^2 \\ i\neq j : & <\underline{r}_i>.<\underline{r}_j> = 0 \end{cases} \tag{4.2;3}$$

because i'th and j'th steps are independent for $i \neq j$ (c.f. in probabilities P(A.B) = P(A)-P(B) for A and B independent events), and $<\underline{r}_i> = 0$.

Hence $R_F^2 = <\underline{R}^2> = Na^2$. (4.2;4)

So $R_F = aN^{1/2}$. (4.2;5)

This argument is valid independently of the number of dimensions, d, in which the polymer is embedded. So the end-to-end distance is independent of the dimensionality of the space - something we may not have expected a priori. One can show that this is a result of the idealised nature of free flight chains, and is not true for real polymers. Most important is the N dependence of the relation, since experimentally it is easy to vary N but difficult or impossible to vary a without changing the polymer chemically. We shall see that in general the end to end distance varies according to $R_F \sim N^{\nu}$, where ν is known as the *chain exponent* and $\nu = 1/2$ is the *ideal* chain exponent.

A related quantity of interest is the *radius of gyration*, R_G, defined by the relation $R_G = \sqrt{\langle\langle r^2\rangle - \langle r\rangle^2\rangle}$.. An analogous argument shows that $R_G \cong aN^{\nu}$, with $\nu = 1/2$ once again. The end-to-end distance turns out to be useful in studying rubber elasticity whereas the radius of gyration is well suited to explanations and descriptions of the rheological properties of polymer fluids and solutions (de Gennes 1979).

One can go further and ask more searching questions about the end to end displacement, $\underline{R}$, of a free flight chain than simply its mean and mean-square values. In particular one can ask if there is an analytical expression for the *probability density function* $p_N(\underline{R})$ (Chandrasekhar 1943). Note that this is a natural progression of the investigation since the mean and mean-square end to end displacements are expectation values of $\underline{R}$ and $\underline{R}^2$ for the distribution and as such are clearly subordinate to it.

When one says $p_N(\underline{R})$ is the probability density function of $\underline{R}$ what one means is that the probability of a polymer chain having an end to end displacement in the ("infinitesimal") region $[\underline{R},\underline{R}+d\underline{R}]$ is $p_N(\underline{R})d^dR$ (in this notation $d^dR = dR_1dR_2...dR_d$, where dR_i is the i'th component of $\underline{R}$).

From this definition and basic probability theory it should be clear that:

$$\int_{\mathbb{R}^d} p_N(\underline{R})d^dR = 1 \qquad (4.2;6)$$

since displacement must be somewhere in $\mathbb{R}^d$ and

$$\langle\underline{R}\rangle = \int_{\mathbb{R}^d} \underline{R}p_N(\underline{R}).d^dR = 0 \qquad (4.2;7)$$

$$\langle\underline{R}^2\rangle = \int_{\mathbb{R}^d} \underline{R}^2p_N(\underline{R})d^dR = R_F^2 = Na^2. \qquad (4.2;8)$$

by definition of the expectation operator $\langle\ \rangle$.

Now in this notation a chain of only one link has a probability density function p_1 for its displacement. But each link can itself be considered as a chain of just one link. So the displacement $\underline{r}_i$ of the i'th link also has a probability density $p_1(\underline{r}_i)$; that is to say there is a probability $p_1(\underline{r})d^dr$ of the link displacement, $\underline{r}_i$, being in the region $[\underline{r},\underline{r}+d\underline{r}]$.

It is possible to relate $p_N(\underline{R})$ to $\{p_1(\underline{r}_i)\}$. Given that a molecular configuration has been reduced to an ordered set of links $\{\underline{r}_i\}$ it is possible to find $\underline{R}$ through the relation:

$$\underline{R} = \sum_i \underline{r}_i. \tag{4.2;9}$$

On the other hand given $\underline{R}$ there is no single (ordered) set $\{\underline{r}_i\}$ which uniquely yields $\underline{R}$ as its total displacement. Rather there are many sets of $\{\underline{r}_i\}$ which yield $\underline{R}$ as their total displacement (N.B. it is easy to see for instance that $\underline{R}$ does not depend on the ordering of the links because of the transitivity of vector addition). The probability of any particular set in the interval $[\{\underline{r}_i\},\{\underline{r}_i+d\underline{r}_i\}]$ arising is:

$$p(\{\underline{r}_i\}) = p_1(\underline{r}_1)d^d r_1 p_1(\underline{r}_2)d^d r_2 \ldots\ldots p_1(\underline{r}_N)d^d r_N. \tag{4.2;10}$$

where we use the fact that each link is independent of all the others (so that P(A.B)=P(A).P(B)).

Consequently it is clear that:

$$p_N(\underline{R}) = \int\ldots\int p_1(\underline{r}_1)p_1(\underline{r}_2)\ldots p_1(\underline{r}_N)\delta(\underline{r}_1+\underline{r}_2+\ldots+\underline{r}_N-\underline{R})d^d\underline{r}_1 d^d\underline{r}_2\ldots d^d\underline{r}_N \tag{4.2;11}$$

It is clear from the rotational symmetry of the distribution function, which was responsible for $<\underline{R}>=\underline{0}$, that the distribution function must be a function of the rotational invariants of $\underline{R}$. A vector $\underline{R}$ has only one rotational invariant, its magnitude, R. So $p_N(\underline{R})$ can be written as a function of R, i.e. $p_N(\underline{R})\rightarrow p_N(R)$. For such a symmetry one can also transform the volume element so that:

$$d^dR = C_d R^{d-1} dR \tag{4.2;12}$$

where C_d is a constant depending on d. In particular, for three dimensions:

$$d^3R = 4\pi R^2 dR \tag{4.2;13}$$

Now the *Central Limit Theorem* of Statistics (see Kreyszig 1983) tells us that the probability distribution of a sum of, N, independent variables with the same probability distribution is the Gaussian distribution, in the limit $N\rightarrow\infty$. Applying the Central limit theorem to (4.2;11), tells us that $p_N(\underline{R})$ is the normal distribution in the limit of large N, i.e. $N\gg 1$. So, in three dimensions:

$$p_N(R) \propto \exp\left(-\frac{3R^2}{2R_F^2}\right) \sim \exp\left(-\frac{3(x^2+y^2+z^2)}{2R_F^2}\right) \tag{4.2;14}$$

The constant of proportionality is determined through the normalisation requirement. After normalising we get:

$$p_N(R) = \frac{R^2}{(2\pi)^{3/2}R_F^3}\exp\left(-\frac{3R^2}{2R_F^2}\right) = \frac{R^2}{(2\pi N)^{3/2}a^3}\exp\left(-\frac{3R^2}{2Na^2}\right) \qquad (4.2;15)$$

These are *Gaussian* statistics and so the free flight chain is sometimes called a *Gaussian chain*. The free-flight chain is also known as the *ideal chain*. The chain is only truly Gaussian in the large N limit. Some headway can be made towards the lower N regions but the analysis becomes extremely involved (Flory 1969).

4.3 The Biased-flight Chain

In the free flight chain the displacement probability distribution of each link is uncorrelated, i.e. independent of, the displacements of all of the other links. This property stemmed from the fact that all orientations of the links were allowed and were equally likely as the links were assumed to be joined by freely flexible spacers. Of course, in practice this assumption is not usually true, usually the orientation of a link will be influenced by, and hence correlated to, the orientations of its neighbouring links. In biased-flight chain models one tries to take account of these correlations.

There is more than one way of introducing correlations into the free-flight chain model. The effect of biasing on the chain's scaling relations is to change the prefactor only. The characteristic scaling exponent, ν, is unchanged, $=1/2$. Thus we see why the scaling exponent is considered a more fundamental property of ideal polymers than the prefactor. Underlying this result is a re-scaling argument that is more fundamental than the result itself (de Gennes 1979, Flory 1969, Mandelbrot 1983). The ideas of rescaling are embodied in the so called *Renormalisation Group Theory* (Ma 1985, Huang 1987). The name of this theory is rather misleading in the context in which we use it since there is no "group theory" involved. Renormalisation is the keyword. It points to the concept of having an invariant scaling law, but with a prefactor determined by normalisation; that is re-normalisation on the appropriate length scale.

The important idea in the renormalisation of the biased chain is that there is a correlation length, ξ, along the chain beyond which memory, i.e. correlations to, the original link displacement is forgotten. For chain lengths $L \leq \xi$ correlations cannot be

neglected. But for $L \gg \xi$ the chain can be thought of as an unbiased free-flight chain with $a \sim \xi$, and with $N \sim (L/\xi)$ links. So it is not surprising that $R_G \sim L^{\nu}$ with $\nu = \frac{1}{2}$ unchanged. A biassed chain with its correlation length is illustrated in figure 4.2.

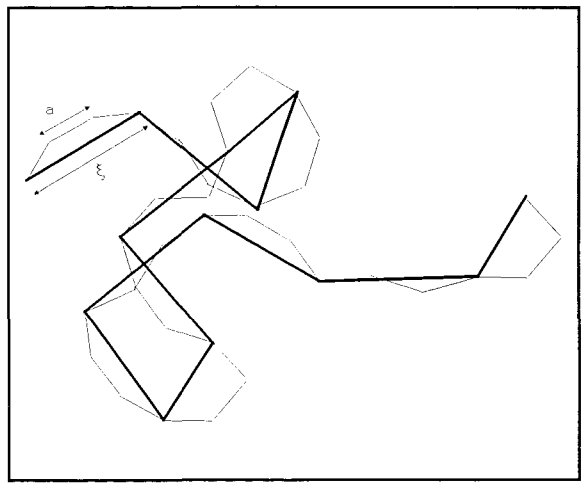

Figure 4.2
Biassed chain model.

4.4 Self-avoiding Chain

The biased-flight chain discussed in the previous section introduced the concept of local correlations between chain links. In fact significant global correlations between the links do exist in real polymers. The principal source of correlations is from *exclusion*. In real molecules no two atoms or molecules can occupy the same point in space. As a consequence in our model of a polymer the links should not be permitted to intersect. A random walk in which the path never intersects with itself is called a *self-avoiding walk* (Chandrasekar 1943). A self-avoiding random walk on the lattice is illustrated in figure 4.3.

Other sources of global correlations exist to a lesser extent; examples are van der Waals bonding, hydrogen bonding and in the extreme case zwitter-ionic attractions.

The effect of including the global self-exclusion correlation into the free-flight chain model turns out to be more profound than including the local correlations. It is clear that the re-scaling argument used there cannot be applied analogously for this self-exclusion property. To make any progress analytically we have to approach the problem from an entirely new direction. We shall find that the self-exclusion effect causes the value of the scaling exponent, ν, to change. In fact the value of ν is characteristic of the

type of model we look at; we can determine whether an ensemble of chains is ideal or self-excluding by looking at the chain exponent.

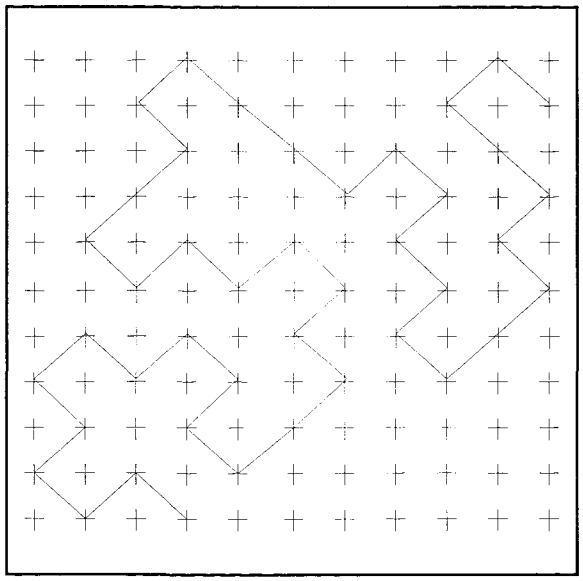

Figure 4.3
Self-avoiding chain model.

First let us re-derive the scaling relation for an ideal chain using Flory's argument. From the definition of $p_N(R)$ it is clear that $p_N(R) \propto$ number of ways of arranging a random walk starting at $\underline{0}$ and finishing near $\underline{R}$. The *entropy* S associated with such a walk $\sim k_B \ln(p_N)$. So that:

$$\frac{S(R)}{k_B} = -\frac{3R^2}{2Na^2} + \ln\left(\frac{R^2}{N^{3/2}}\right) + \text{const} \qquad (4.4;1)$$

where (4.2;10) has been substituted.

In equilibrium the *Helmholtz free energy*, A, is minimised. Now

$$A = U_T - TS \; . \qquad (4.4;2)$$

But for an ideal chain $U_T=0$. So that, in this case, minimising A is equivalent to maximising S. Maximising S will give us the most favourable value of R, R_F. For the ideal chain

$$\frac{1}{k_B}\frac{\partial S}{\partial R} = -\frac{3R}{Na^2} + \frac{2}{R} \qquad (4.4;3)$$

so that

$$\frac{1}{k_B}\frac{\partial S}{\partial R}\bigg|_{R=R_F} = 0 \quad \Rightarrow \quad R_F = \sqrt{\frac{2a^2N}{3}} \; . \qquad (4.4;4)$$

Examining (4.2;14) we see that $R_F \sim N^{(1/2)}$, as before (c.f. (4.2;5)), but now the prefactor has changed. So Flory's argument appears to get the form of the equation correctly, with the correct value for the scaling exponent, 1/2, but fails to compute the prefactor correctly. In any case we have already said that the prefactor is of less significance than the exponent.

Now let us use the Flory argument to investigate the self-avoiding chain. Now some of the walks between 0 and R that were previously allowed are forbidden in this case, so that $p_N(R) \rightarrow \tilde{p}_N(R)$. Consequently the entropy S is changed. The change in entropy is called the *correlation entropy*.

We make a guess of the approximate correlation entropy by introducing an *effective* exclusion energy. Suppose that each link has a volume v, and that there are c links per unit volume. Then the associated effective exclusion energy per unit volume U is

$$U \approx \frac{1}{2} k_B T v c^2 \tag{4.4;5}$$

if we think of the links as "freely-floating" throughout the volume in which the chain is effectively confined. We arrive at this form using the same approximations as for *virial expansion* (Golden 1964).

The chain has N links which are effectively confined to a volume $\propto R^d$ so that

$$c \cong NR^{-d} \qquad U_T = \frac{1}{2} k_B T v N^2 R^{-d} = R^d U \tag{4.4;6}$$

Hence

$$\frac{A}{T} \cong \frac{vN^2}{R^d} + \frac{3R^2}{2Na^2} - \ln\left(\frac{R^d}{N^{d/2}}\right). \tag{4.4;7}$$

Note that the dimensionality of the space d is a key parameter in this expression. For $d < 4$ the logarithmic term is unimportant for the limit $N \gg 1$.

Again minimising the free energy, A, gives the most probable value of R, R_F. For the excluded chain

$$\frac{\partial}{\partial R}\left(\frac{A}{T}\right) = -\frac{dvN^2}{R^{d+1}} + \frac{3R}{Na^2} \qquad (d<4). \tag{4.4;8}$$

So that

$$\left.\frac{\partial S}{\partial R}\right|_{R=R_F} = 0 \quad \Rightarrow \quad R_F = \sqrt[d+2]{\frac{dva^2N^3}{3}} \,. \tag{4.4;9}$$

Most importantly

$$R_F \sim N^{\nu_d} \sim N^{3/(d+2)} \quad \Rightarrow \quad \nu_d = \frac{3}{d+2} \tag{4.4;10}$$

and more specifically

$$\nu_1 = 1, \quad \nu_2 = \tfrac{3}{4}, \quad \nu_3 = \tfrac{3}{5} \quad \text{and} \quad \nu_4 = \tfrac{1}{2}. \tag{4.4;11}$$

where the index denotes the dimensionality of the space. These exponents are the so called *Flory exponents*. The argument was initially presented by Flory for 3-dimensions only; the d-dimensional generalisation being attributable to Fisher.

So for self-avoiding chains the exponent depends on d for $d<4$. Note that the value of the scaling exponent for $d=4$ is the same as for the ideal chain. Below $d=4$ the scaling exponent of the self avoiding chain is larger than the scaling exponent of the corresponding ideal chain. Note that intuitively we expect self avoiding chains to be expanded compared with their ideal counterparts; the self avoidance acting effectively as a repelling force. The chains are sometimes said to be *swollen* (with respect to their ideal analogues).

Careful examination would show that the logarithmic term in (4.4;7) becomes important at $d=4$.

This method can be thought of as a *Mean-field theory*, because when we derived the effective energy due to self-avoidance we imagined that the action of the self avoidance of the whole set of links on each individual link could be thought of as an average and uniform field. This is a standard approximation often made which often turns out not to matter in the final result, for the appropriate limit.

Despite the fact that this is a mean field theory one gets "non-mean field" exponents. In statistical mechanics many situations arise where mean field theories get correct results except in the low dimensional limit $d<4$ (Ma 1985, Huang 1987).

The Flory theory is a *self-consistent* theory. In the Flory theory the entropy of the chain is drastically over estimated. The self-avoidance pseudo-potential is also over

estimated. The over estimations appear to cancel against one another in a consistent fashion, since the results of the Flory theory are remarkably consistent with experimental observations and results obtained from simulations.

4.5 Fractality And Self Similarity

Recall the scaling law for a self avoiding chain in three dimensions:

$$R_G \sim N^{\frac{3}{5}} = \left(\frac{L}{a}\right)^{\frac{3}{5}} \qquad (4.5;1)$$

This scaling law tells us how the radius of gyration scales as compared to the ratio of the total chain length, L, to stiffness length a.

Imagine taking a particular polymer then a is fixed, but L can be varied. Then the scaling law tells us that $R_G=L^{3/5}$. How does this compare with the scaling of ordinary objects? Scaling a circle, triangle, square or any fixed polygon or curve causes the radius of gyration to scale according to $R_G=L$. So clearly scaling the polymer is subtly different.

The reason that the polymer does not scale like an ordinary object is that as its perimeter length L is increased then the degrees of freedom of the chain to twist and turn are increased; this corresponds to introducing new vertices into the polygons. In fact if one could examine a given polymer as one drew away from the initially rigid length scale, a, one would observe that the polymer twisted and turned on all subsequent length scales. In fact at large length scales on could not determine the stiffness length of a polymer by observing the character of its twists and turns. The polymer is said to be *self-similar.*

Objects which scale with a fractional scaling exponent such as the self avoiding chains / polymers are said to be *fractal.* Fractals are characteristically self-similar. For instance it is the twists and turns on all length scales that cause the length of the polymer to be soaked up causing the fractality of the radius of gyration and it is the same twists and turns on all length scales which make the polymer self-similar.

4.6 Universality

Often when carrying out physical observations the observed quantity at first instance appears to depend on a large set of independent variables. However it is usually possible to identify that the quantity actually depends upon a reduced set of independent variables. One transforms to the reduced variables from the originals by a specified transformation. A classic example where this occurs is in Wiens law in the Rayleigh-Jeans theory of blackbody radiation (Gasiorowicz 1966). It turns out that this universality behaviour is important in the interpretation of observations on vesicle systems. Here I discuss the analogous case for two-dimensional polymers.

4.6.1 Universality Of Polymers With Finite Rigidity

Consider the two dimensional case, for simplicity, of a chain with rigidity κ. Such a chain has the Helfrich Hamiltonian:

$$H = \frac{\kappa}{2}\int_0^L (c(s))^2 ds + \text{Self-avoidance.} \qquad (4.6.1;1)$$

where s is the length moved along the chain and c(s) is the curvature of the chain at s.

Now clearly $\kappa \sim \xi$ and $R_G = R_G(L,\xi)$.

There are also two scaling forms valid in asymptotia:

$$R_G \sim \left(\frac{L}{\xi}\right)^{\nu} \qquad L\to\infty,\ \kappa\to 0 \qquad (4.6.1;2)$$

$$R_G \sim L \qquad L\to 0,\ \kappa\to\infty \qquad (4.6.1;3)$$

The former is valid as the rigidity is just an example of a local correlation force and the latter is valid since a rigid polymer is just a rod.

One can postulate a *universal scaling form* for R_G:

$$R_G \sim Lf\left(\frac{L}{\xi}\right) \sim Lf\left(\frac{L}{\kappa}\right) \qquad (4.6.1;4)$$

Here f is a *universal function*. That is it is the same function for all polymers and chains. The scaling form should hold for all L,κ. One can see that if the universal scaling form holds then there is, in a sense, one less variable - the ratio L/κ is the independent variable.

One can illustrate a particular case where this holds, the case of the two dimensional free-flight polymer with rigidity.

4.6.2 Universality Of 2D Free-flight Polymer With Rigidity

A polymer of length L can be modelled as a smooth curve of length L. Then the ensemble of all polymer configurations becomes the ensemble of all curve functions of length L. I have already discussed the parameterisation of a curve in terms of its own curve-length, s. The curve itself is synonymous with the normal angle function, $\psi(s)$, since from that function all properties of the curve can be derived. For instance the trajectory (x(s),y(s)) can be evaluated from $\psi(s)$ using:

$$x_{\psi}(s) = \int_0^s \cos\psi(t)dt \qquad (4.6.2;1)$$

$$y_{\psi}(s) = \int_0^s \sin\psi(t)dt \qquad (4.6.2;2)$$

Thus the curve function is the normal angle function $\psi(s)$. The curve function parameterises the ensemble space $\Psi=C^{\infty}$. Hence the *partition function* (Huang 1987), Z, of the ensemble of free flight curve configurations will be a *functional integral.* In fact using statistical mechanics it can be shown that:

$$Z = \int \exp\left(-\kappa\int_0^L\left(\frac{d\psi}{ds}\right)^2 ds\right) D\psi \qquad (4.6.2;3)$$

where I have nominally set $k_BT=1$ so that $\kappa/(k_BT)\rightarrow\kappa$. In effect the temperature dependence is to absorbed into the rigidity constant, κ. $D\psi$ is the volume element in the function space of the ensemble and can be written in the form

$$D\psi = \prod_{s=0}^{1} d\psi(s) \qquad (4.6.2;4)$$

whereupon it becomes clear that a functional integral is equivalent to an infinite dimensional parametric (standard) integral since we are performing the product over a continuous parameter, s. Finally $d\psi/ds$ is the curvature of the polymer as derived in (3.4.1;2).

Now one can make the scaling transformation $s \rightarrow \tilde{s}/L$ so that $s = L\tilde{s}$ and $ds = Ld\tilde{s}$. This transforms a polymer of length L to a polymer of unit length. Under this transformation the partition function, Z, becomes:

$$Z = C\int \Pi d\psi(\tilde{s}) \exp\left(-\frac{\kappa}{2L}\int_0^1 \left(\frac{d\psi}{d\tilde{s}}\right)^2 d\tilde{s}\right) \qquad (4.6.2;5)$$

So one can see that for a system of unit length $\tilde{Z}=\tilde{Z}(\kappa/L)$ and consequently $\tilde{R}_F=\tilde{R}_F(\kappa/L)$ (the tildes indicate the quantity is for the unit length polymer). Now the effect on the average end-to-end length of translating from the unit length polymer to the polymer of length L is just to scale it by a factor L so that

$$R_F = L\tilde{R}_F\left(\frac{\kappa}{L}\right) \qquad (4.6.2;6)$$

This confirms the result (4.6.1;4) motivated in section 4.6.1 for the two dimensional free flight polymer with rigidity; where the association $f \sim \tilde{R}_F$ is made.

CHAPTER FIVE

MESOSCOPIC MODELS OF VESICLES IN TWO DIMENSIONS

5.1. Introduction

The principal use of mesoscopic models is the determination of the natures of membrane shape and size behaviour. For instance, one can determine how the *radius of gyration* of a vesicle varies with the various elastic constants. The membrane Hamiltonian is treated *phenomenologically* (physically determined) in such models; although hypothetical Hamiltonian forms can be tested and the results compared with the real world membranes for rejection or confirmation of the form. Thus microscopic models provide the input data, the Hamiltonian, for mesoscopic models.

5.2. The Helfrich (Mean Field) Model

Helfrich introduced a continuum model of vesicles, the Helfrich model (Helfrich 1973, 1974, 1976, 1990). In this section I intend to briefly outline the method used by Helfrich and to discuss the successes of the model in predicting observed membrane shapes (Berndl *et al* 1990). The method uses a quasi-three dimensional model of a vesicle; that is it models vesicles as volumes of revolution so that although the vesicles are three dimensional one of the dimensions is proscribed and so does no represent a true degree of freedom of the system. The parameterisation is illustrated in figure 5.1.

The method of Lagrangian multipliers (Arfken 1985) is used to minimise the free energy. For this minimisation the vesicle can be parameterised in terms of the tangent function, $\psi(s)$, or the trajectory, $r(s)$. In practise one chooses the parameterisation according to the type of minimisation analysis that one wishes to perform. The tangent function parameterisation is useful for shape analysis of the minimisation, whilst the trajectory parameterisation is more useful for stability analyses.

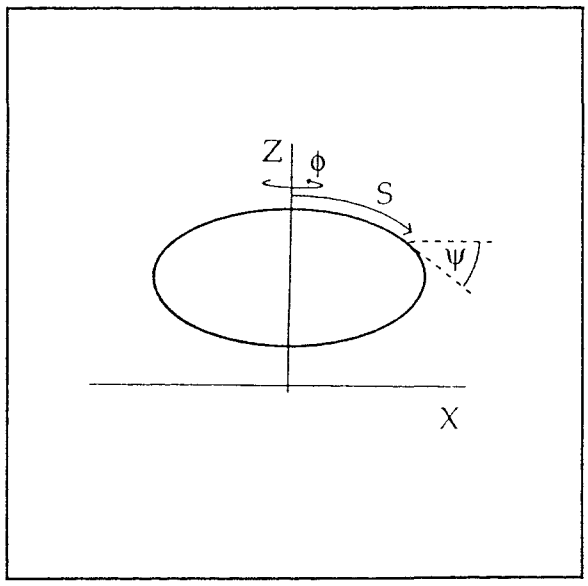

Figure 5.1
Helfrich model of a vesicle.

In the original model of Helfrich, sometimes called the *spontaneous curvature model*, the vesicle shape was minimised for the free energy

$$F = \frac{\kappa}{2}\int_0^L (c(s) - c_o)^2 ds + PA \qquad (5.2;1)$$

where the first term is clearly the curvature energy and the second couples the area of the vesicle, A, to an osmotic pressure differential, P, between the inside and outside of the vesicle.

The osmotic pressure term in the free energy is important because without it the minimisation leads only to the trivial circular geometry. The effect of the pressure is to cause the vesicle to deflate. Observed shapes include elliptical and bilobular geometries (Figure 5.2). In fact a catalog of the deflated vesicle shapes has been produced by Helfrich (Helfrich 1976).

This initial model has been developed further to study the adhesion of vesicles for a variety of potentials; including a contact potential, long and short ranged potentials (Seifert 1991).

A second exciting and more fundamental development of the model has been the introduction of the so called *bilayer coupling model* (Svetina and Zeks 1983, 1989). This model explicitly takes into account that vesicles are made of bilayers. It considers

the bilayer to be a pair of coupled monolayers and assumes that lipid transfer between the monolayers does not occur. The net effect of this is that the differing thermal expansivities of the coupled monolayers renders the monolayer asymmetric and leads to a large number of exotic new vesicle shapes. The asymmetry of the monolayer is reflected in the solutions of the model. Investigations of the phase space have shown it to be particularly rich in vesicle geometries (Svetina and Zeks 1983, Seifert *et al* 1991). Moreover many of these geometries have been observed and identified experimentally in optical micrograph experiments (Berndl *et al* 1990). In figure 5.2 some of these optical micrographs with the associated model vesicles are presented courtesy of Berndl *et al* (1990).

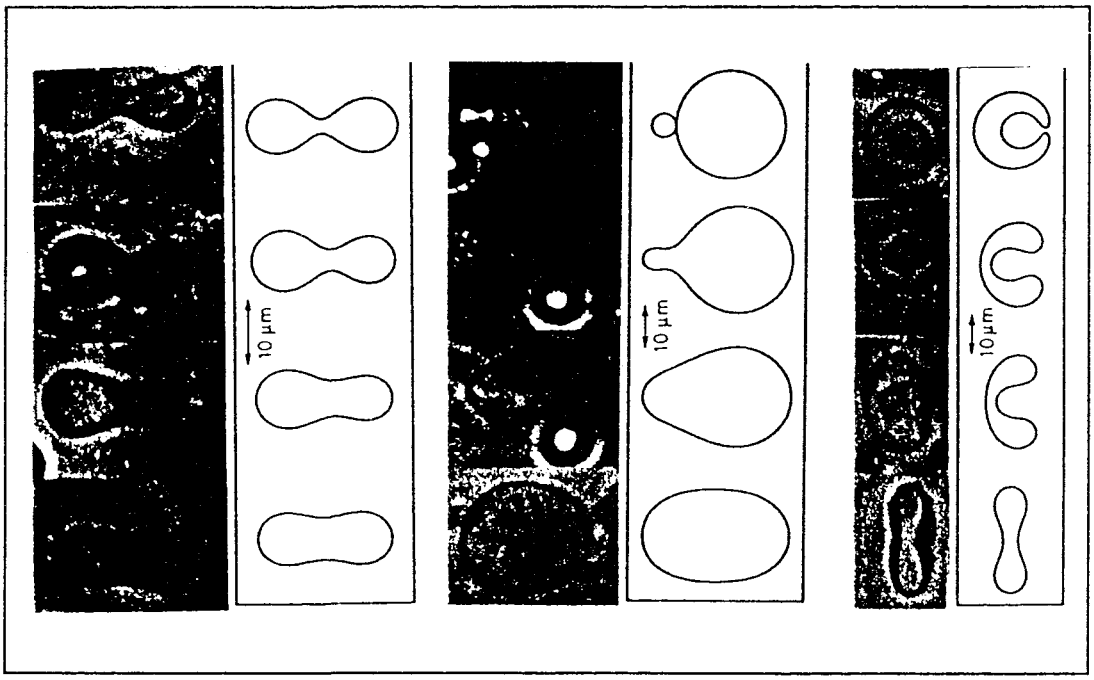

Figure 5.2
Some observed vesicles with corresponding bilayer coupling model shapes, courtesy of Berndl *et al* (1990).

There are some problems and limitations on this model of vesicles. Firstly the Helfrich model looks at most probable vesicle shapes by minimising a free energy. This is in the spirit of the Landau theory of phase transitions. Fluctuations around the most probable shape are neglected. Strictly a more correct approach should take these fluctuations into account. Such fluctuations are accounted for if a full evaluation of the partition function is made.

Intuitively it can be seen that the model does not easily allow convoluted shapes of the type that is to be expected to occur in the partition function.

5.3. The Leibler-Singh-Fisher (Bead Chain) Model

The Leibler-Singh-Fisher model (Leibler *et al* 1987, Fisher 1989) of vesicles is the so called bead chain model. It is a two dimensional model, although it easily extends to three dimensions. The vesicle is modelled as a series of hard (impenetrable) beads joined together by flexible but inextensible strings. The Hamiltonian imposed on this bead chain arrangement has been constructed so that in the limit of the number of beads becoming infinite it is indistinguishable from the Helfrich model; that is, the model is a continuum limit model evaluated in real space. Figure 5.3 is an illustration of one such vesicle.

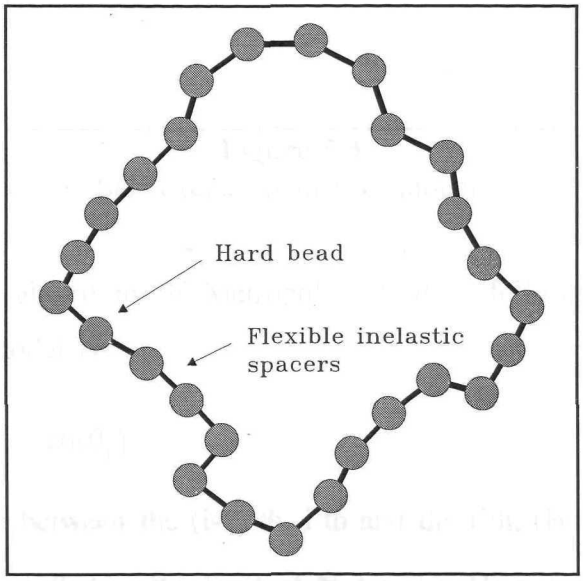

Figure 5.3
LSF model of a vesicle.

The Leibler *et al* model uses the method of Monte-Carlo Simulation. The beads are made to jump randomly in a Brownian fashion subject only to the constraint that the separation of any two neighbouring beads is not greater than a, the maximum bead-bead separation. This constraint taken together with the hard bead property ensures that the vesicle walls are self-excluding as illustrated in figure 5.4.

The hard bead property requires that no bead impinge upon another. This is ensured by checking any bead move and rejecting it if the moved bead impinges on

any other. The simplest way to check this is to check the distance between the moved bead and all the other beads. This is a very time consuming process and with some consideration a significantly better method can be devised. In Appendix such a method is discussed.

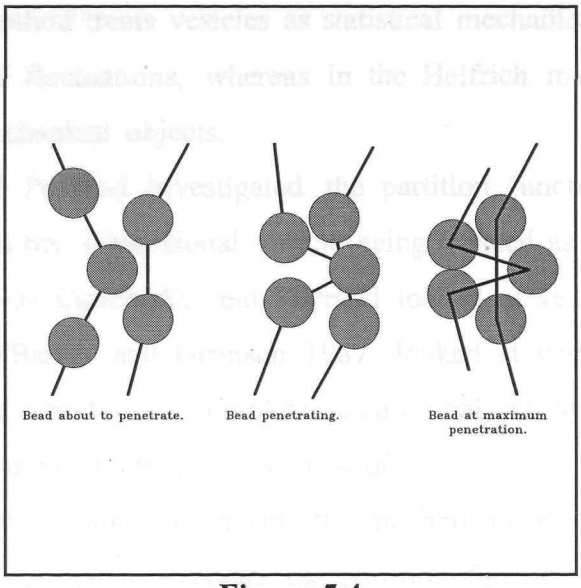

Figure 5.4
Self exclusion in LSF model.

The standard algorithm of Metropolis *et al* is followed (Ma 1985). The Hamiltonian of the model is

$$H = \frac{\kappa}{a} \sum_{i=1}^{N} (1 - \cos\theta_i) \qquad (5.3;1)$$

where θ_i is the angle between the (i-1)'th, i'th and the i'th, (i+1)'th beads.

It can be shown that in the limit of $N \to \infty$ this Hamiltonian and the Helfrich model Hamiltonian are identical. In such a scheme it is possible, by keeping records, to work out various average parameters such as $\langle A \rangle$, $\langle A^2 \rangle$, $\langle R_g^2 \rangle$, $\langle E \rangle$, $\langle E^2 \rangle$ and so on. In fact one can ask any question one can imagine about the statistics of the ensemble and expect an answer. In order to analyze the results of such a procedure one uses scaling theory arguments to postulate analytically what kind of behaviour one expects from such an ensemble and compares these with the actual results for confirmation.

5.4. The Ostrowsky-Peyraud (Continuum) Method

The Ostrowsky-Peyraud method (Ostrowsky and Peyraud 1982) is a method of evaluating the partition function of the Helfrich model; as opposed to the free energy minimisation method due to Helfrich, discussed in section 5.2. This means that the Ostrowsky-Peyraud method treats vesicles as statistical mechanical objects, subject to the associated thermal fluctuations, whereas in the Helfrich method they are being treated as ordinary mechanical objects.

Ostrowsky and Peyraud investigated the partition function for isolated two dimensional vesicles, a two dimensional vesicle being defined as a differentiable self-avoiding loop. Whereas Ostrowsky and Peyraud looked at vesicles of a fixed size Barker and Grimson (Barker and Grimson 1987) looked at vesicles of a variety of sizes. In contrast here I perform a complete scaling analysis, systematically looking at vesicles of various sizes, following Leibler *et al.*

Ostrowsky and Peyraud introduced the method of parameterising the two dimensional vesicles required to evaluate the partition function and other ensemble parameters of interest. The parameterisation they introduced is a q-space method and has the advantage that the entropy of the vesicles is correctly accounted for provided the vesicles are chosen from the ensemble in the correct manner. So far it has not proved possible to generalise the method to three dimensions due to the difficulty of parameterising differentiable closed surfaces with well defined entropic character.

In the following subsections I outline the method of Ostrowsky and Peyraud detailing some of the modifications and extensions made to it by Barker and Grimson and myself. Then in the next section I present an analysis of the results obtained.

5.4.1 The Partition Function

Since the vesicle ensemble is an ensemble of curves then the various properties of interest such as the Partition Function Z depend on a functional integration; that is to say we have to integrate/sum over functions (curves) as opposed to summing over variables. In fact it can be shown that summing over curves is equivalent to summing over an infinite set of variables. In practice we sum only over a finite range of variables; that is, the functional integral is reduced to a finite dimensional integral.

Nevertheless strictly one can write

$$Z = \int_{\Psi} e^{-\frac{E[\psi]}{k_B T}} D\psi \qquad (5.4.1;1)$$

where Ψ is the ensemble of all differentiable self-avoiding vesicles, ψ is a function identifying any particular curve and the D in the $D\psi$ emphasises the functional nature of the integration. $E[\psi]$ is the energy of the vesicle and the square brackets emphasise again that the energy is a functional, i.e. it depends on the curve function ψ.

Also ensemble average parameters such as the ensemble average area, <A>, are given by expressions such as

$$\langle A[\psi] \rangle = \frac{1}{Z} \int_{\Psi} A[\psi] e^{-\frac{E[\psi]}{k_B T}} D\psi \qquad (5.4.1;2)$$

Further one can write down the probability distribution function of ensemble parameters such as the loop area, A, as

$$P(A) = \frac{1}{Z} \int_{\Psi} \delta(A[\psi] - A) e^{\frac{-E[\psi]}{k_B T}} D\psi \qquad (5.4.1;3)$$

5.4.2. Parameterisation Of The Vesicle Ensemble

I have already indicated, in chapter three, that a curve can be parameterised in terms of its curve-length, s. The normal angle, ψ, of such a curve is therefore a function of the curve-length, i.e. $\psi=\psi(s)$. In fact $\psi(s)$ is all we need to know in order to calculate any property of the curve; that is to say $\psi(s)$ defines the curve. For instance the trajectory $(x_\psi(s), y_\psi(s))$ of a curve ψ can be calculated using

$$x_\psi(s) = \int_0^s \cos(\psi(t))dt \qquad (5.4.2;1)$$

and

$$y_\psi(s) = \int_0^s \sin(\psi(t))dt. \qquad (5.4.2;2)$$

The subscripts denote the functional dependence of x and y on ψ. Also the local curvature is just

$$c_\psi(s) = \left.\frac{\partial\psi}{\partial s}\right|_s . \qquad (5.4.2;3)$$

This expression is not an approximation; it is the exact expression for the curvature of the vesicle.

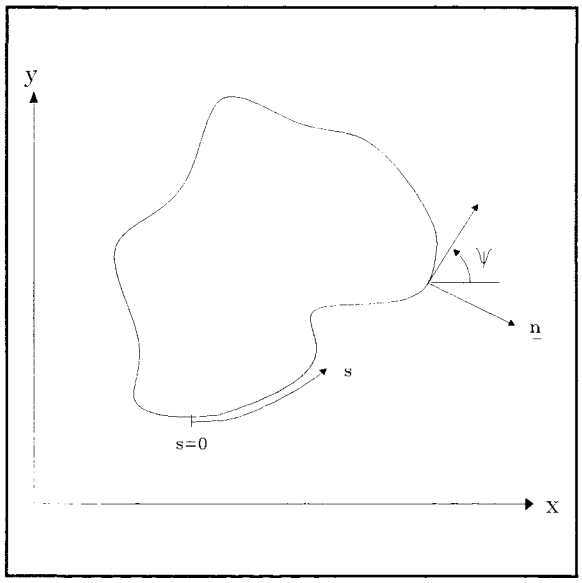

Figure 5.5
Ostrowsky-Peyraud parameterisation of a vesicle.

We can write $\psi(s)$ the normal angle function in terms of a Fourier series plus a linear term. i.e.

$$\psi(s)=\frac{2\pi s}{L} + A_0 + \sum_{n=1}^{\infty} A_n\cos\left(\frac{2\pi ns}{L}\right)+B_n\sin\left(\frac{2\pi ns}{L}\right) \qquad (5.4.2;4)$$

The linear term on the right hand side is incorporated because for a vesicle $\psi(s+L)=\psi(s)+2\pi$. So it is $\psi(s)-2\pi s/L$ which is periodic and as such can be represented as a Fourier series.

5.4.3. Restrictions On The Parameterisation

Clearly it is impossible in any numerical scheme using this representation for $\psi(s)$ to perform such a sum to the limit. In practice there has to be an upper bound to the summation. This corresponds physically to a high frequency/short wavelength

cutoff in the representation. If the upper bound to the summation is M then the shortest wavelength for variation of the tangent of the curve is then $a = L/M$ and

$$\psi(s)=\frac{2\pi s}{L} + A_0 + \sum_{n=1}^{M} A_n\cos\left(\frac{2\pi ns}{L}\right) + B_n\sin\left(\frac{2\pi ns}{L}\right) \qquad (5.4.3;1)$$

We follow Ostrowsky and Peyraud and arbitrarily set $a = 2\pi/5$ so that $L = 2\pi M/5$. In other words a vesicle of length 2π has 5 associated fourier amplitudes, a vesicle of length 4π has 10 and so on. It can be seen that this short wavelength cutoff, a, represents a microscopic cutoff length scale. However when $l_k=\kappa$, the rigidity length scale, is greater than a then it is l_k and not a which is the effective cutoff length. The quantity a has not been varied in the simulations and is only included for completeness in the calculations.

There is a removable degeneracy in the representation as it stands. One can restrict the parameterisation so that the tangent at the starting position is horizontal i.e. $\psi(0)=0$. One can impose this restriction by choosing A_0 s.t.

$$A_0=-\sum_{n=1}^{M} A_n \qquad (5.4.3;2)$$

Barker and Grimson (1987) pointed out that there is a further removable degeneracy in the representation as it stands. The origin of the degeneracy is reflective symmetry of the ensemble; every vesicle configuration has a reflectional conjugate. The degeneracy can be removed by fixing one of the amplitudes.

A vesicle is a closed loop. So far the parameterisation of the tangent function is not restricted to closed loops. The required constraints are

$$x_\psi(0)=x_\psi(L) \quad \text{and} \quad y_\psi(0)=y_\psi(L) \qquad (5.4.3;3)$$

Clearly there is no simple analytical restriction one can place upon $\{A_i,B_i\}$ to satisfy this constraint. However having chosen a set $\{A_i,B_i\}$ one can perform an iterative transformation to a new set, $\{\tilde{A}_i,\tilde{B}_i\}$ say, which do satisfy the constraint. In fact with two constraints one only needs to constrain two of the variables, i.e $\{A_1,B_1\}\rightarrow\{\tilde{A}_1,\tilde{B}_1\}$ say. Making this transformation to satisfy the closure constraint introduces a non-trivial transformation Jacobian, J say, into the partition function from the relation

$$dA_1 dB_1 = \frac{d\tilde{A}_1 d\tilde{B}_1}{J(A_1,B_1)} \qquad (5.4.3;4)$$

A discussion of the nature of the iterative transformation and the detailed form of the Jacobian arising is contained in section 5.4.4 following.

There is one further restriction not yet encompassed in the parameterisation as it stands; self-avoidance. Having constructed a smooth closed loop, one has to determine whether it crosses itself, since vesicles are self avoiding. This is accomplished by evaluating the approximate trajectory of the loop, by integration. The trajectory is approximated by a series of line segments. Crossovers are detected by intersections of the line segments. The self crossing vesicles are eliminated from the integral by means of the crossover function θ which is defined as

$$\theta = \begin{cases} 1 : \text{loop does not cross itself} \\ 0 : \text{loop does cross itself} \end{cases} \qquad (5.4.3;5)$$

At this stage the partition function can be written:

$$Z = \int_{\Psi} \Theta(\{A_i,B_i\})\, e^{-\frac{E(\{A_i,B_i\})}{k_B T}} \frac{d\tilde{A}_1 d\tilde{B}_1}{J(A_1,B_1)} \prod_{i=2}^{M} dA_i dB_i \qquad (5.4.3;6)$$

5.4.4. Iterative Closure Of A Configuration

It is convenient to introduce some new notation to describe the closure condition, which will illustrate the more general nature of the problem. Let

$$R_1 = x_\psi(L) \quad \text{and} \quad R_2 = x_\psi(L) \qquad (5.4.4;1)$$

so that in fact

$$R_1(A_1,B_1) = \int_0^L \cos\left(\frac{2\pi s}{L} + A_0 + \sum_{n=1}^{M} A_n \cos\left(\frac{2\pi n s}{L}\right) + B_n \sin\left(\frac{2\pi n s}{L}\right)\right) ds \qquad (5.4.4;2)$$

$$R_2(A_1,B_1) = \int_0^L \sin\left(\frac{2\pi s}{L} + A_0 + \sum_{n=1}^{M} A_n \cos\left(\frac{2\pi n s}{L}\right) + B_n \sin\left(\frac{2\pi n s}{L}\right)\right) ds \qquad (5.4.4;3)$$

Also let

$$\underline{R} = (R_1,R_2) \qquad (5.4.4;4)$$

$$\underline{A} = (A_1,B_1) \qquad (5.4.4;5)$$

Then the closure condition is just

$$\underline{R}(\underline{A}) = \underline{0} \tag{5.4.4;6}$$

From the closure condition (5.4.4;6) it is clear that closing the vesicle is equivalent to finding the roots of a two-dimensional system of non-linear (in $\{A_i,B_i\}$) equations. One standard method of solving this problem numerically is to use the Newton-Raphson method (see Press *et al* 1986). The method is iterative. That is one starts with an initial "guess" solution, $\underline{A}_0$ say, which is operated on to get an improved solution, $\underline{A}_1$ say. The improved solution is in turn operated on, and so on. The iteration is based on the formula

$$\underline{A}_n = \underline{A}_{n-1} - J^{-1}(\underline{A}_{n-1}).\underline{R}(\underline{A}_{n-1}) \tag{5.4.4;7}$$

where $J^{-1}(\underline{A}_{n-1})$ is the inverse of the Jacobian matrix defined by

$$J(\underline{A}) = \begin{bmatrix} \dfrac{\partial R_1}{\partial A_1} & \dfrac{\partial R_1}{\partial B_1} \\ \dfrac{\partial R_2}{\partial A_1} & \dfrac{\partial R_2}{\partial B_1} \end{bmatrix} \tag{5.4.4;8}$$

There are two methods of evaluating the elements of the Jacobian matrix. Perhaps the simplest is to use the numerical approximation

$$\frac{\partial R_i}{\partial A_j} \approx \frac{\delta R_i}{\delta A_j} = \frac{R_i(\underline{A}) - R_i(\underline{A}-\delta A_j.\hat{j})}{A_j - \delta A_j} \tag{5.4.4;9}$$

Alternatively one can differentiate (5.4.4;2) and (5.4.4;3) to obtain integral expressions for the elements, which can be evaluated numerically. For instance

$$\frac{\partial R_1}{\partial A_1} = \frac{L}{2\pi}\frac{\partial}{\partial A_1}\int_0^{2\pi} \cos\left(\tilde{s} + A_0 - A_1 + A_1\cos(\tilde{s}) + B_1\sin(\tilde{s}) + \sum_{n=2}^{M}\left(A_n\cos(n\tilde{s}) + B_n\sin(n\tilde{s}) - A_n\right)\right) d\tilde{s}$$

where I have introduced the transformation $\tilde{s} = 2\pi s/L$ for convenience and the degeneracy constraint (5.4.3;2) has been included explicitly. On diffentiation this yields

$$\frac{\partial R_1}{\partial A_1} = \frac{L}{2\pi}\int_0^{2\pi}(1-\cos(\tilde{s}))\sin(\psi(\tilde{s}))\,d\tilde{s} \tag{5.4.4;10}$$

In the following work I chose the latter method following the original authors; although a brief investigation showed the methods to be consistent. The iteration is repeated until

$$\underline{R}(\underline{A}_n)^2 < \epsilon \qquad (5.4.4;11)$$

where in the work presented I have, arbitrarily, taken $\epsilon = L/1000$.

Then the curve is approximately closed for the transformed parameters $(\tilde{A}_1,\tilde{B}_1)=\underline{A}_n$. The Jacobian required for the calculation of the partition function in (5.4.3;6) is the determinant of the Jacobian matrix, $\det(J(\underline{A}_n))$, defined in (5.4.4;8); the computation of which for this 2×2 system is straightforward.

5.4.5. Energy Of A Configuration

The energy of a vesicle configuration due to the curvature elasticity of the Helfrich Hamiltonian is just:

$$E_c = \frac{1}{2}\frac{\kappa(4\pi)^2}{Ma}\left(1 + \sum_{m=1}^{M}\left((mA_m)^2 + (mB_m)^2\right)\right) \qquad (5.4.5;1)$$

this can easily be shown by integration and using the orthogonality relations of sin/cos series.

The energy of a vesicle due to an osmotic pressure difference between the interior and exterior of the vesicle is just:

$$E_p = \Delta p.A \qquad (5.4.5;2)$$

where Δp is the osmotic pressure difference and A the area of the vesicle; for which there is no simple analytic expression, but which can be evaluated from θ using:

$$A = \int_0^{2\pi} \sin(\psi(s)) \int_0^{s} \cos(\psi(t))\, dt\, ds \qquad (5.4.5;3)$$

5.4.6. Choosing The Amplitudes

Now to evaluate the partition function (5.4.3;6) or any many other average parameter for the ensemble requires one to perform a multi-dimensional integral. Since in general the dimensions of the space are likely to be too numerous for the

complete space to be explored one has to adopt a technique that allows one to sample the space. The scheme adopted by Ostrowsky and Peyraud revolved around sampling the configurations in the transformed configuration space $\{iA_i, iB_i\}$ i=2..M. It can be shown that transforming from the original space, $\{A_i, B_i\}$ i=2..M, to the transformed space only introduces a constant Jacobian into the partition function. Consequently, the value of ensemble average parameters is not affected since average parameters only depend on ratios of the partition integral.

The advantage of sampling in the transformed space becomes apparent when one considers the bending energy of a configuration (5.4.5;1). The bending energy of a configuration is simply related to the norm of the sampling space. If one defines the sampling vector, $\vec{X}$, by

$$\vec{X} = (iA_i, iB_i) \qquad i=1..M \tag{5.4.6;1}$$

then it is clear that the bending energy of a configuration is simply

$$E_c = 1+X^2 \tag{5.4.6;2}$$

Now it becomes clear that for ensembles with a non-zero curvature elasticity then one can restrict oneself to sampling from a sphere of given radius, X_{max} say, since by choosing the sphere sufficiently large one can be sure that the exterior configurations are unimportant on energetic grounds. Ostrowsky and Peyraud developed a scheme for estimating how large the sphere, X_{max}, needed to be to guarantee an upper bound for errors. Then to evaluate the integral they sampled the enclosed space evenly. They noted that many of the configurations outside (and some inside) the sphere of integration were crossing contributions and so had no contribution to the integral (section 5.4.3). This acted to reduce the error incurred due to the restricted sampling.

In my work I have departed from this scheme for two reasons. Firstly as the curvature of the membrane is reduced, $\kappa \to 0$, the radius of the sphere tends to infinity, $X_{max} \to \infty$. Consequently ensembles with vanishing surface tension cannot be adequately sampled using the method of Ostrowsky and Peyraud. Secondly, as I suspected, the method proved to be somewhat inefficient of computational resources.

I have systematically investigated the configuration space. An important discovery was that the space was *star shaped.* By this I mean that choosing a

direction, $\hat{X}$, from the origin and moving outward along the direction from the origin one encounters at a distance, X_{cut}, a point beyond which all the configurations are self-crossing. Since self-crossing configurations do not contribute to the integrals then all configurations, $\vec{X}$, such that $X^2 > X_{cut}^2$ can be ignored. The star shaped property refers to the fact that the non-crossing configurations do not appear to re-enter the space beyond the cutoff value, X_{cut}, in any given direction.

The partition function can be manipulated into a form that can take advantage of this star shaped property. Consider the following

$$d\vec{X} \rightarrow X^{2M-1}\, dX d\alpha \qquad (5.4.6;3)$$

This relation is just a generalisation of the familiar two-dimensional cartesian to polar transformation ($dxdy = rdrd\theta$). In this relation the 2(M-1) dimensional integral is transformed into a one dimensional integral along a direction, $\vec{X}$, and over a 2M-1 dimensional angle. Incorporating this into the partition function one arrives at

$$Z = \int\int X^{2M-1}\, \Theta(\alpha,X)\, J(\alpha,X)^{-1}\, e^{-\frac{E(\alpha,X)}{k_B T}}\, dX d\alpha \qquad (5.4.6;4)$$

By using the star shaped property this transforms to

$$Z = \int_{X=0}^{X_{cut}(\alpha)} X^{2M-1}\, J(\alpha,X)^{-1}\, e^{-\frac{E(\alpha,X)}{k_B T}}\, dX d\alpha \qquad (5.4.6;5)$$

where $X_{cut}(\alpha)$ is the cutoff value function.

To evaluate this integral by a Monte Carlo Sampling technique (not to be confused with the Monte Carlo simulation algorithm of Metropolis *et al*) one chooses random directions ($\alpha = \hat{X}$) in the sampling space. For each direction one determines the value of the cutoff function, $X_{cut}(\alpha)$, by means of a binary search (Press *et al* 1986). In practice I found that $2.4 \leq X_{cut}(\alpha) < 2M$ was a suitable interval for the binary search. Having determined the value of the cutoff function the contribution of each direction to the integral is evaluated by performing the radial integration on $(0,X_{cut}(\alpha))$ as indicated by (5.4.6;5).

I found that a few thousand random directions in the configuration space were sufficient to yield parameters with sufficiently small errors. The precise number of directions depended on the value of the physical control parameters; κ, Δp, etc.

5.4.7. Vesicle Attributes Of Interest

It has already been stated that it is now possible to evaluate ensemble average attributes for vesicles. What attributes are interesting? Some obvious examples are the average area, $\langle A \rangle$, and radius of gyration $\langle R_G \rangle$. In fact there are some other equally interesting attributes which I shall be looking at.

5.5. Analysis Of Results From Ostrowsky-Peyraud Method

In this section I present results obtained using the Ostrowsky-Peyraud method, analyzed using the scaling analysis methods of Leibler *et al* (1987). The presentation is arranged so that the discussion of each different regime is separate.

5.5.1. The Floppy-Flaccid Regime

In this section we consider an isolated vesicle subject only to the entropic forces arising from the self-avoidance, fixed contour length and fixed microscopic bending length.

Now in chapter four I presented the well known scaling relation for a random self-avoiding walk. Leibler *et al* (1987) remarked that for a floppy vesicle with one would expect a similar relation to hold. In fact one might expect the same relation to hold, albeit with a different prefactor. In figure 5.6 $\log(\langle R_G^2 \rangle)$ is plotted against log(M). The graph is clearly linear on this scale and a linear regression analysis of the points plotted yields an estimate of the scaling exponent: $\nu=0.7510\pm16$ (c.f. Leibler *et al* 1987 0.760). This result is consistent with the hypothesis that $\nu=0.75$.

The next question arising is whether the enclosed area of the vesicle scales in the same way as the radius of gyration with the same exponent; i.e. does

$$\langle A \rangle = A_0 \cdot M^{2\nu_A} \qquad M \to \infty \tag{5.5.1;1}$$

with $\nu=\nu_A$. In figure 5.7 $\log(\langle A \rangle)$ is plotted against log(M). Again the graph is clearly linear on this scale and a linear regression analysis yields an estimate of the

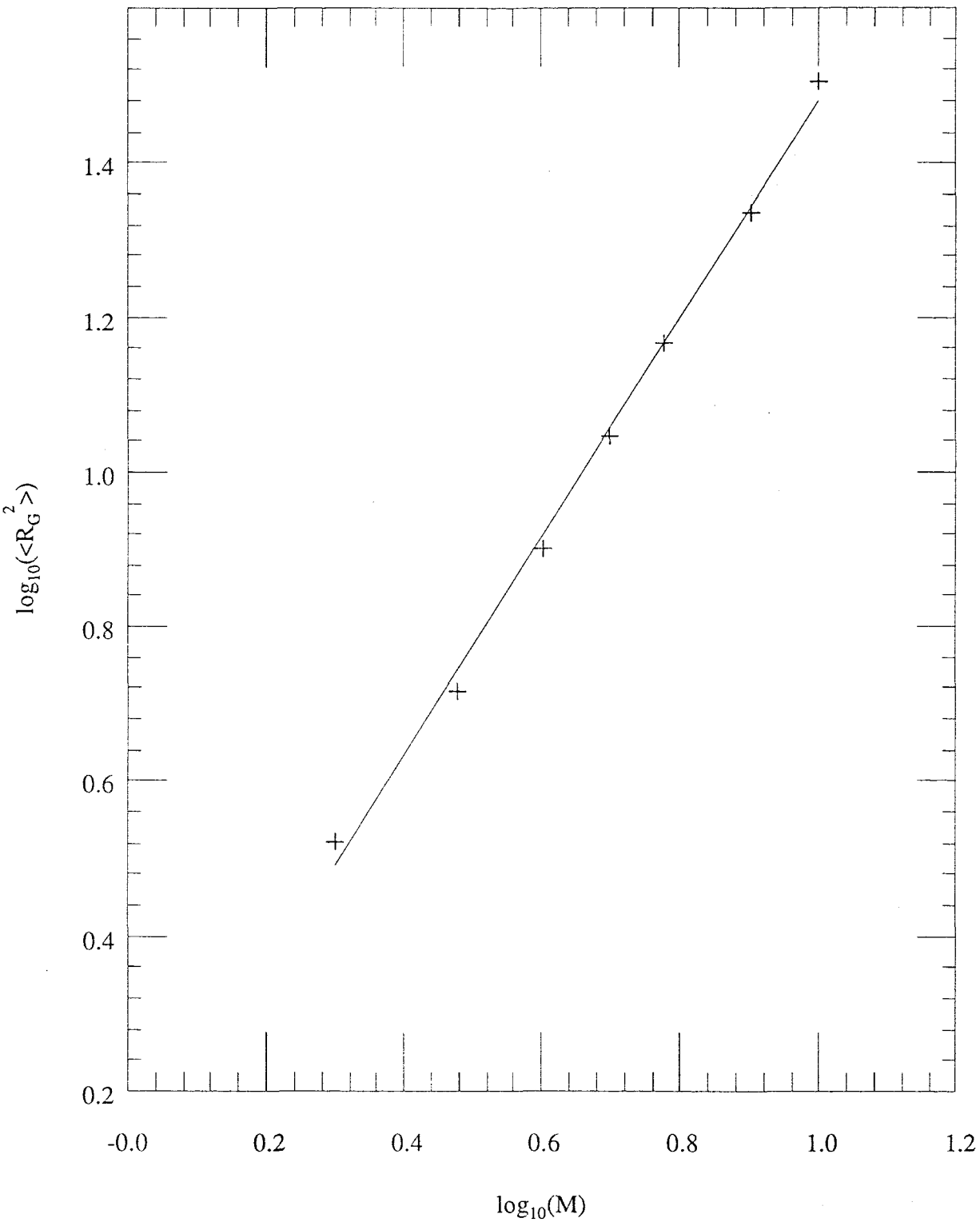

Figure 5.6

Graph of $\log_{10}(<R_G^2>)$ against $\log_{10}(M)$. The straight line is obtained from a linear regression analysis of the points.

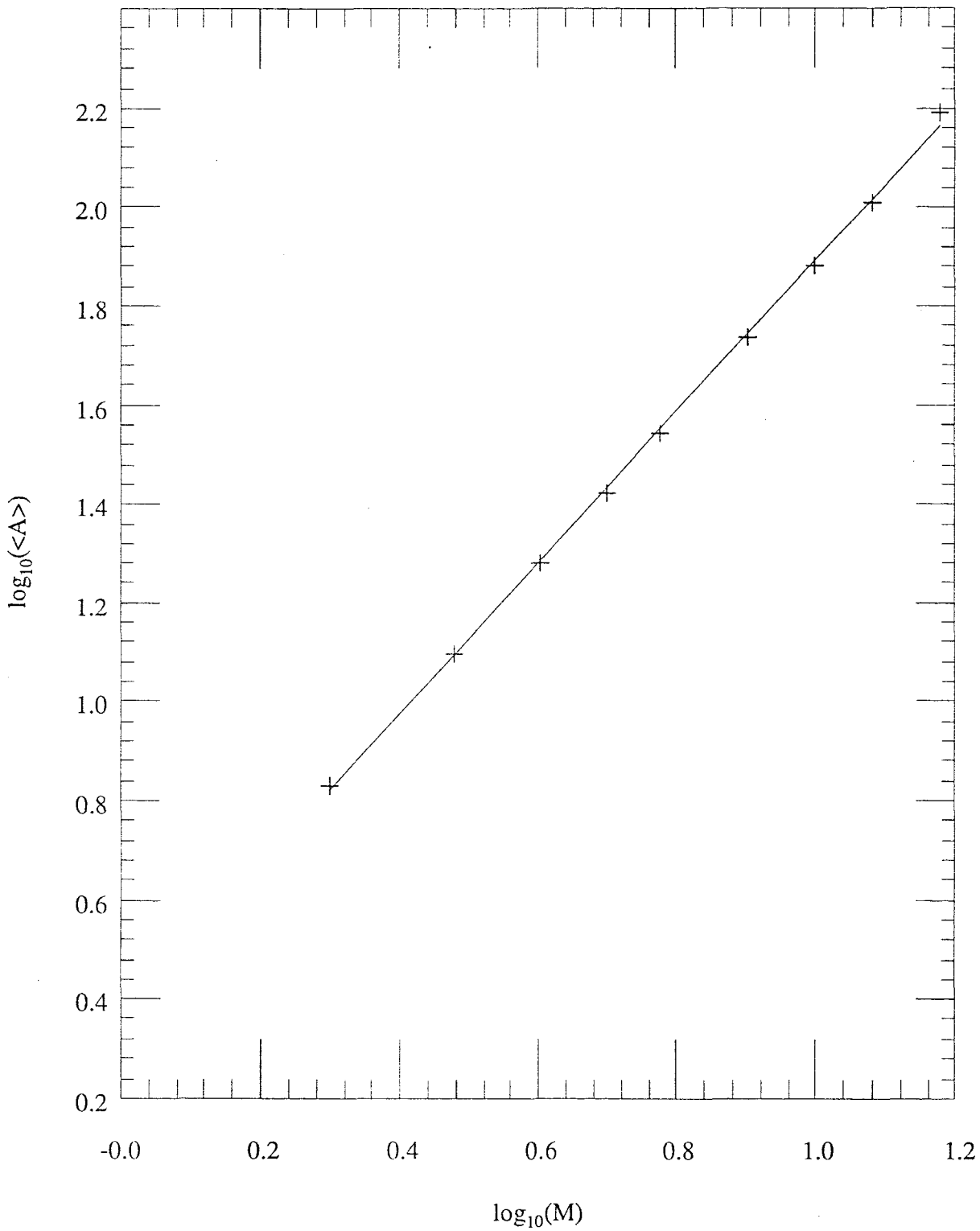

Figure 5.7

Graph of $\log_{10}(\langle A \rangle)$ against $\log_{10}(M)$. The straight line is obtained from a linear regression analysis of the points.

areal scaling exponent: ν_A=0.7514±20 (c.f. Leibler *et al* (1987) 0.755±0.018). Hence ν_A/ν=1.001±1 (c.f. Leibler *et al* (1987) ν/ν_A=1.007±0.013) confirming the hypothesis that $\nu=\nu_A$. In fact the result has now been proved analytically by Duplantier (1990).

Since the scaling exponents for the enclosed area and the radius of gyration are the same one should expect, as Leibler *et al* (1987) and Family *et al* (1985) anticipated, that the ratio of the radius of gyration to the enclosed area converges to some non-zero universal value, as $M\rightarrow\infty$.

The function Π is defined as the ratio of the ensemble average enclosed area to the ensemble average radius of gyration; i.e.

$$\Pi = \frac{\langle A \rangle}{\langle R_G^2 \rangle} \qquad (5.5.1;2)$$

So as $M\rightarrow\infty$,

$$\Pi \rightarrow \frac{A_0 M^{2\nu_A}}{R_0^2 M^{2\nu}} = \frac{A_0}{R_0^2} \qquad (5.5.1;2)$$

The value of this ratio is characteristic of the average shape of the ensemble. For instance if the ensemble were made of only circular vesicles of radius R_0; then one would obtain

$$\Pi = \frac{\pi R_0^2}{R_0^2} = \pi \qquad (5.5.1;3)$$

Similarly if the ensemble were rectangular of sides a,b; then one would obtain

$$\Pi = \frac{ab}{\frac{1}{2}ab^2 + \frac{1}{2}ba^2} = \frac{2}{(a+b)} \qquad (5.5.1;4)$$

which for the special case of a square ensemble is clearly 1/a.

In figure 5.8 I have plotted the function Π against M for κ=0. The figure shows a rapid convergence to a stable value, of around 2.393±2, which I take for an estimate of the asymptotic value (indicated by the horizontal line) followed by more erratically varying values. This value compares to the values obtained by Fisher (1989) using the model of Leibler *et al* (1987) in their bead simulations and by Family *et al* in their lattice animal model. The values of the function for larger vesicle ensembles (i.e.

larger M) are subject to a greater inaccuracy. This inaccuracy proved to be irremovable from the data, but see appendix I for further details.

Now rather than defining the function Π as in (5.5.1;2) we could have defined it in the following manner:

$$\tilde{\Pi} = \left\langle \frac{A}{R_G^2} \right\rangle \qquad (5.5.1;5)$$

which would seem to be a more natural definition of the average shape of an ensemble (Family *et al* 1985).

In figure 5.9 I have plotted the value of the function $\tilde{\Pi}$ for $\kappa=0$ is plotted against M, in the same manner as figure 5.8. Not surprisingly figure 5.8 mirrors the behaviour of figure 5.9. However the asymptotic value for figure 5.9 is 2.384±9. This compares to the values, 2.52±4 and 2.55±5 obtained by Camacho and Fisher (1990) using the models of Leibler *et al* (1987) and Family *et al* (1985), respectively.

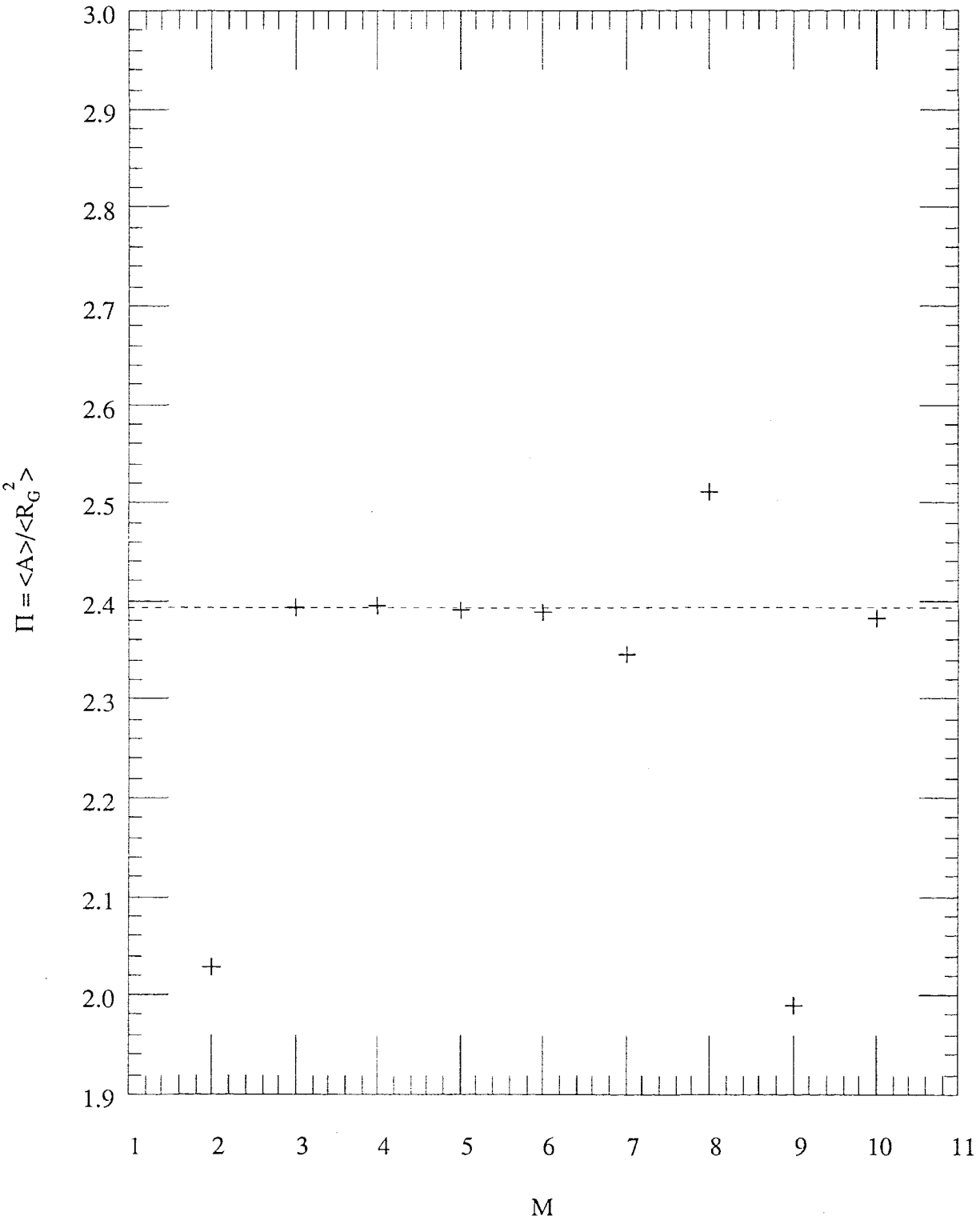

Figure 5.8

Graph of the shape parameter $\Pi = \langle A \rangle / \langle R_G^2 \rangle$ against M. The horizontal line represents the assymptotic value.

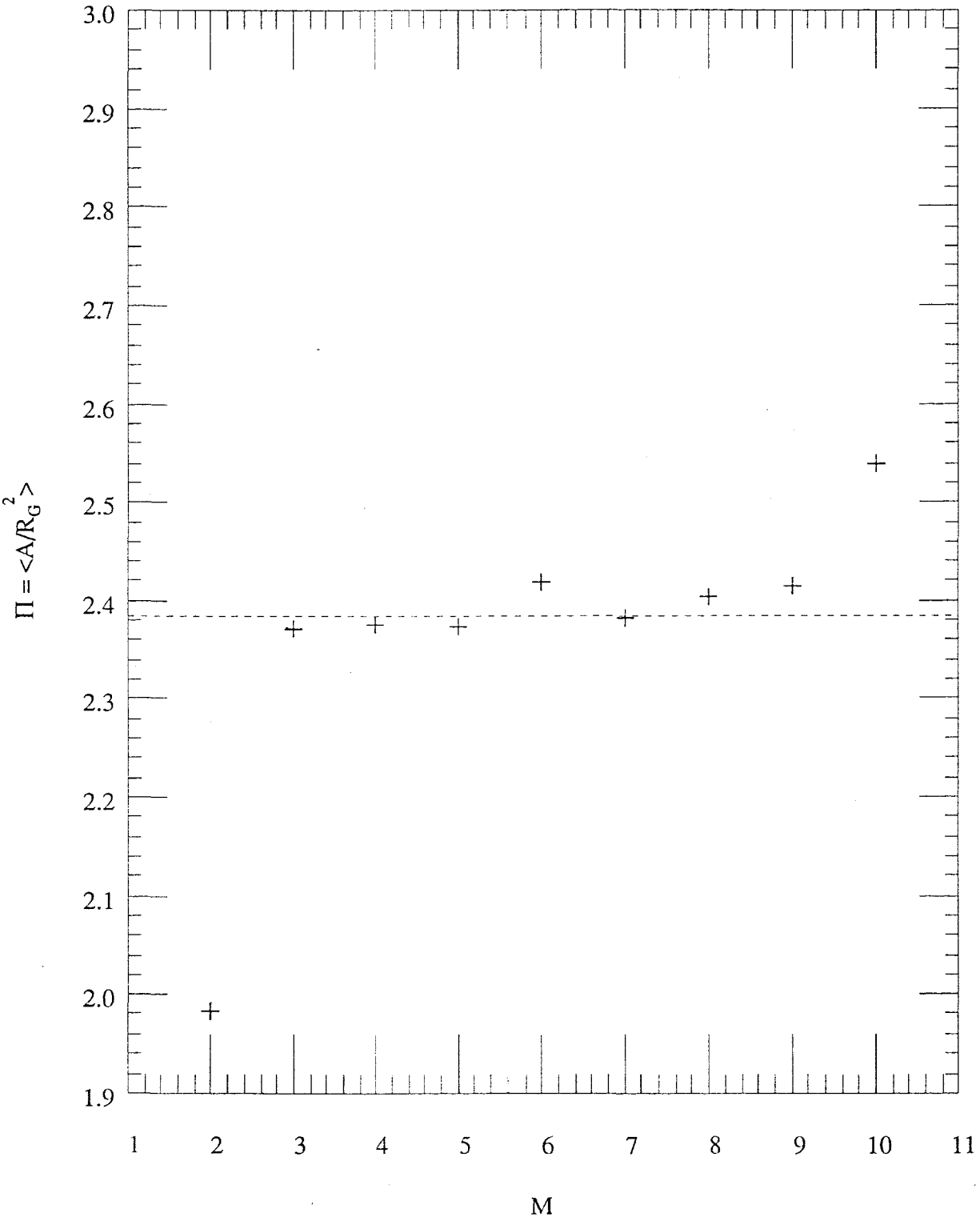

Figure 5.9

Graph of the shape parameter $\Pi = \langle A/R_G^2 \rangle$ against M. The horizontal line represents the assymptotic value.

Another, quite different, quantity that also reflects the nature of the average shape of the ensemble is the *anisotropy*, Σ, which is defined as follows:

$$\Sigma = \langle R_{G1}^2 \rangle / \langle R_{G2}^2 \rangle \qquad (5.5.1;6)$$

where R_{G1}^2 and R_{G2}^2 are the larger and smaller eigenvalues of the radius of gyration tensor, respectively.

For an ensemble of circles of radius R_0 then clearly $R_{G1}^2=R_{G2}^2=R_0^2$ and consequently $\Sigma=1$. For the more interesting case of an ensemble of ellipses of major axis a and minor axis b one finds that $R_{G1}^2 \propto a^2$ and $R_{G2}^2 \propto b^2$, so that consequently

$$\Sigma = \frac{a^2}{b^2} \qquad (5.5.1;7)$$

which is consistent with the result for an ensemble of circles (a=b).

Once again one expects a universal value for Σ when $\kappa=0$ in the limit as $M \to \infty$. So in figure 5.10 I have plotted the function Σ for $\kappa=0$ against M, in the same way that I plotted Π in figures 5.8 and 5.9. Although the numerical value of the asymptotic value is different, of course, the qualitative behaviour of the graph is, as one would hope, similar; the results rapidly converge to the asymptotic value, then vary somewhat erratically. The asymptotic value, indicated in the graph by the horizontal line, is 0.378±2, which compares with the result, 0.393±15, of Camacho and Fisher (1990) obtained using the LSF model and the result 0.405±9 obtained using the lattice animal model (Bishop and Saltiel 1989).

Of course on could have defined Σ in the following alternative way:

$$\tilde{\Sigma} = \langle R_{G1}^2 / R_{G2}^2 \rangle \qquad (5.5.1;8)$$

taking the average over the ratio rather than the ratio of the averages, just as we did for Π.

In figure 5.11 I have plotted the value of the function $\tilde{\Sigma}$ for $\kappa=0$ is plotted against M, in the same manner as figure 5.10. Not surprisingly figure 5.11 closely resembles figure 5.10. However the asymptotic value for figure 5.12 is 0.414±4. Camacho and Fisher (1990) have by comparison obtained the value 0.425±15 using the LSF model.

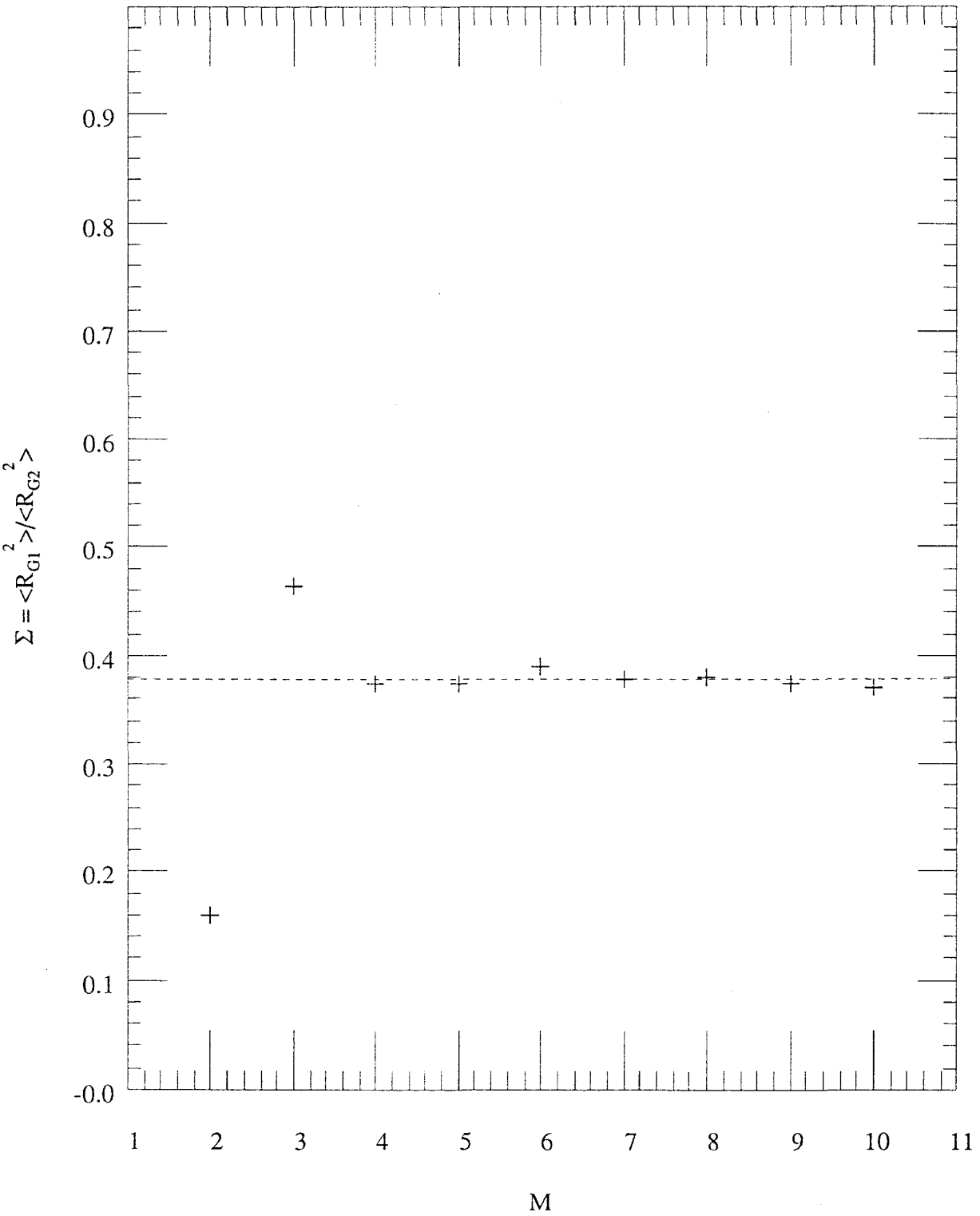

Figure 5.10

Graph of the shape parameter $\Sigma = \langle R_{G1}^2 \rangle / \langle R_{G2}^2 \rangle$ against M. The horizontal line represents the assymptotic value.

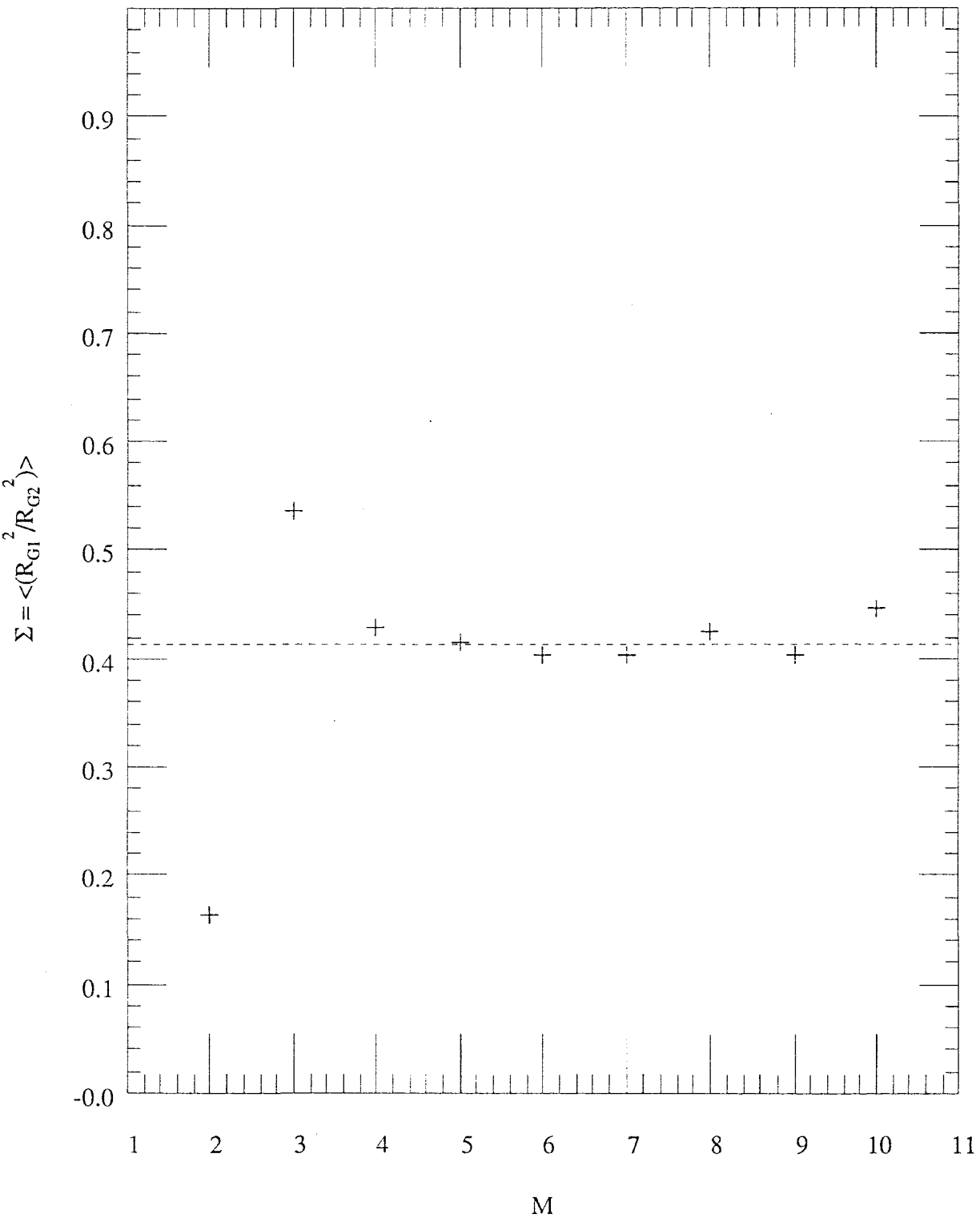

Figure 5.11

Graph of the shape parameter $\Sigma = <(R_{G1}^2/R_{G2}^2)>$ against M. The horizontal line represents the assymptotic value.

For completeness I have studied the behaviour of one further shape sensitive parameter, the so called *asphericity*, $\tilde{\Delta}$. It, like Σ and $\tilde{\Sigma}$, is defined in terms of the eigenvalues of the radius of gyration tensor:

$$\tilde{\Delta} = \left\langle \frac{\left(R_{G1}^{\ 2} - R_{G2}^{\ 2}\right)^2}{\left(R_{G1}^{\ 2} + R_{G2}^{\ 2}\right)^2} \right\rangle \qquad (5.5.1;9)$$

Once again expecting a universal value of Δ for $\kappa=0$ in the limit of $M\rightarrow\infty$, I have plotted the function Δ against M in figure 5.12. The graph would seem to indicate an asymptotic value of 0.269±6. The results for higher M seem to be consistent but I assume this to be an anomaly, since their accuracy is of the order 10% only, and so have ignored higher values in making this estimate. This compares with the result, 0.215±10 obtained by Camacho and Fisher (1990) using the LSF model.

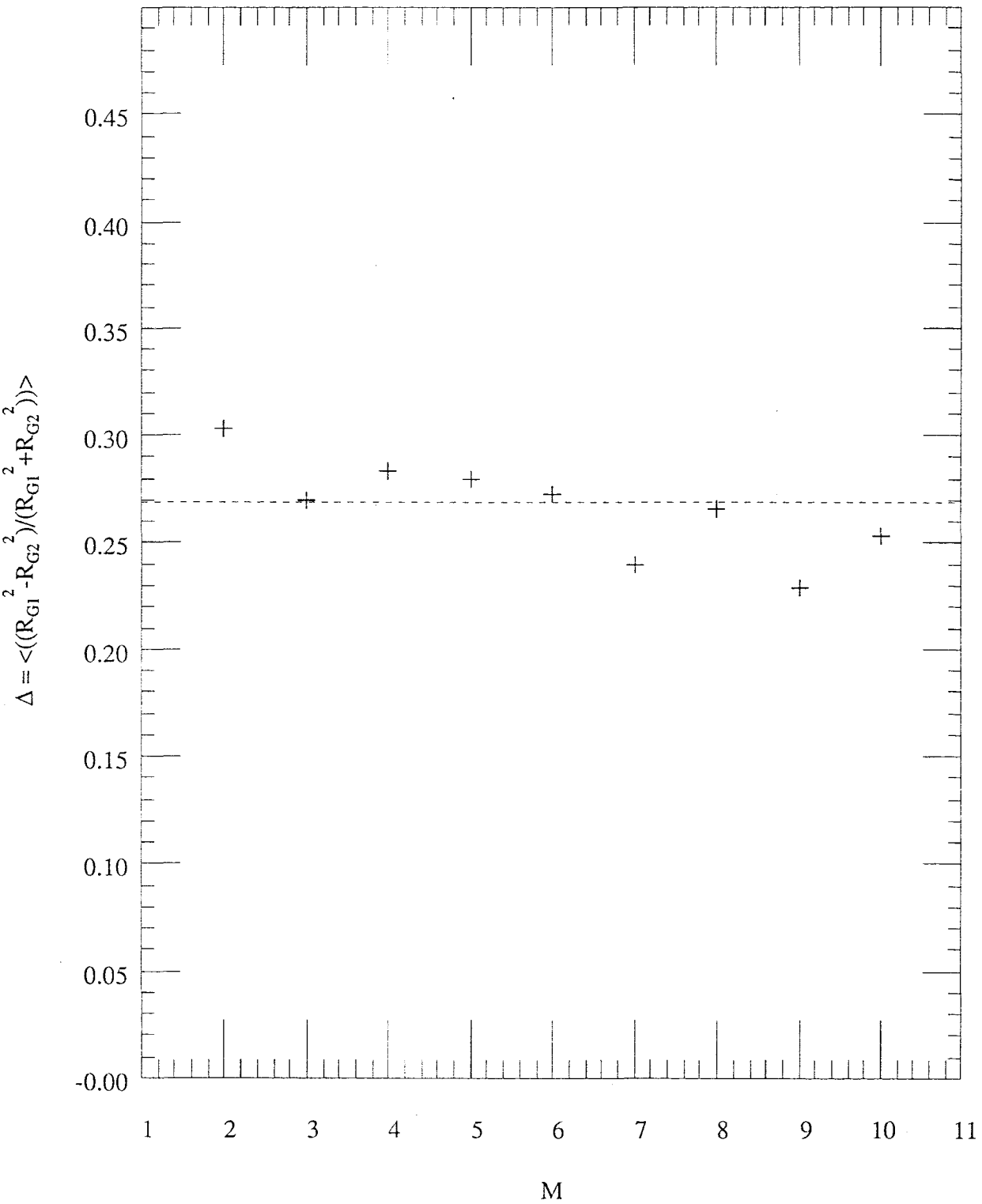

Figure 5.12

Graph of the shape parameter $\Delta = \langle((R_{G1}^2 - R_{G2}^2)/(R_{G1}^2 + R_{G2}^2))\rangle$ against M. The horizontal line represents the assymptotic value.

5.5.2. The Rigid Regime and the Rigid to Floppy Transition

In the preceding section we considered floppy-flaccid vesicles not subject to any internal or external forces, except the entropic forces due to self-avoidance, microscopic cutoff length and fixed contour length. In this section I subject the vesicle to an internal bending rigidity by introducing the Helfrich model Hamiltonian to the ensemble as outlined in section 5.4.5.

Clearly in the limit of $\kappa \to 0$ the loop is floppy; that is the bending rigidity is negligible and the floppy-flaccid behaviour is recovered. On the other hand for a loop of a given length (i.e. given M) then in the limit of $\kappa \to \infty$ then the loop is *rigid* and consequently circular. However for any fixed κ then as $M \to \infty$ we find that the loop crosses over from its rigid circular shape back to the floppy fractal shape; indicating that rigidity effects are *finite size effects.*

So there is a length, l_k, associated with the bending rigidity that characterises the nature of the vesicle, called the *rigidity length.* In fact $l_k = \kappa$.

Having defined the rigidity length one can describe the floppy and rigid regimes more clearly. For instance if the rigidity length, l_k, is less than the microscopic length, a, then clearly the rigidity effect will be negligible and the vesicles will floppy. On the other hand if the rigidity length, l_k is larger than the contour length, L, then clearly the rigidity effect will be dominant and vesicles will be rigid and circular, unable to support thermal fluctuations. i.e.

$$\begin{aligned} l_k &< a && : \text{floppy regime.} \\ l_k &> L && : \text{rigid regime.} \end{aligned} \qquad (5.5.2;1)$$

Alternatively, if one defines the dimensionless variable x by

$$y = \frac{L}{l_k} \qquad (5.5.2;2)$$

then one can rewrite the inequalities as:

$$\begin{aligned} y &> \frac{L}{a} && : \text{floppy regime} \\ y &< 1 && : \text{rigid regime} \end{aligned} \qquad (5.5.2;3)$$

Now the advantage of defining this scaling variable becomes evident if we plot the various ensemble quantities against y. For $y<1$ we are in the rigid regime where

vesicles are on average circular. We know that the area and radius of gyration of an ensemble of circles scales with scaling exponents $\nu=\nu_A=1$; i.e.

$$\langle A \rangle \cong M^2 \qquad (5.5.2;4)$$

$$\langle R_G^2 \rangle \cong M^2 \qquad (5.5.2;5)$$

So we should expect that if we plot $<A>/M^2$ and $<R_G^2>/M^2$ against y then for $y<1$, at least, the plots should be universal (Fisher 1989). On the other for $y>1$ then the universality should disappear gradually as y increases since for $y>L/a$ the vesicles are floppy and one expects the scaling exponent to be near 0.75, at least for the larger vesicles.

I have plotted $<A>/M^2$ and $<R_G^2>/M^2$ against y in the graphs in figures 5.13 and 5.14. The predicted behaviour is followed. In the graphs I have elected to distinguish between data points on the basis of which size vesicle they were obtained from. Smaller vesicles transform to floppy vesicles at lower values of y since the transition to floppiness occurs at about L/a which is, of course, lower for smaller vesicles. The graphs clearly show this behaviour with the smaller vesicle symbols breaking away from the main universal curve in sequence. Fisher (1989) predicted such behaviour and Camacho *et al* (1991) have recently published the analogous curves for the bead model.

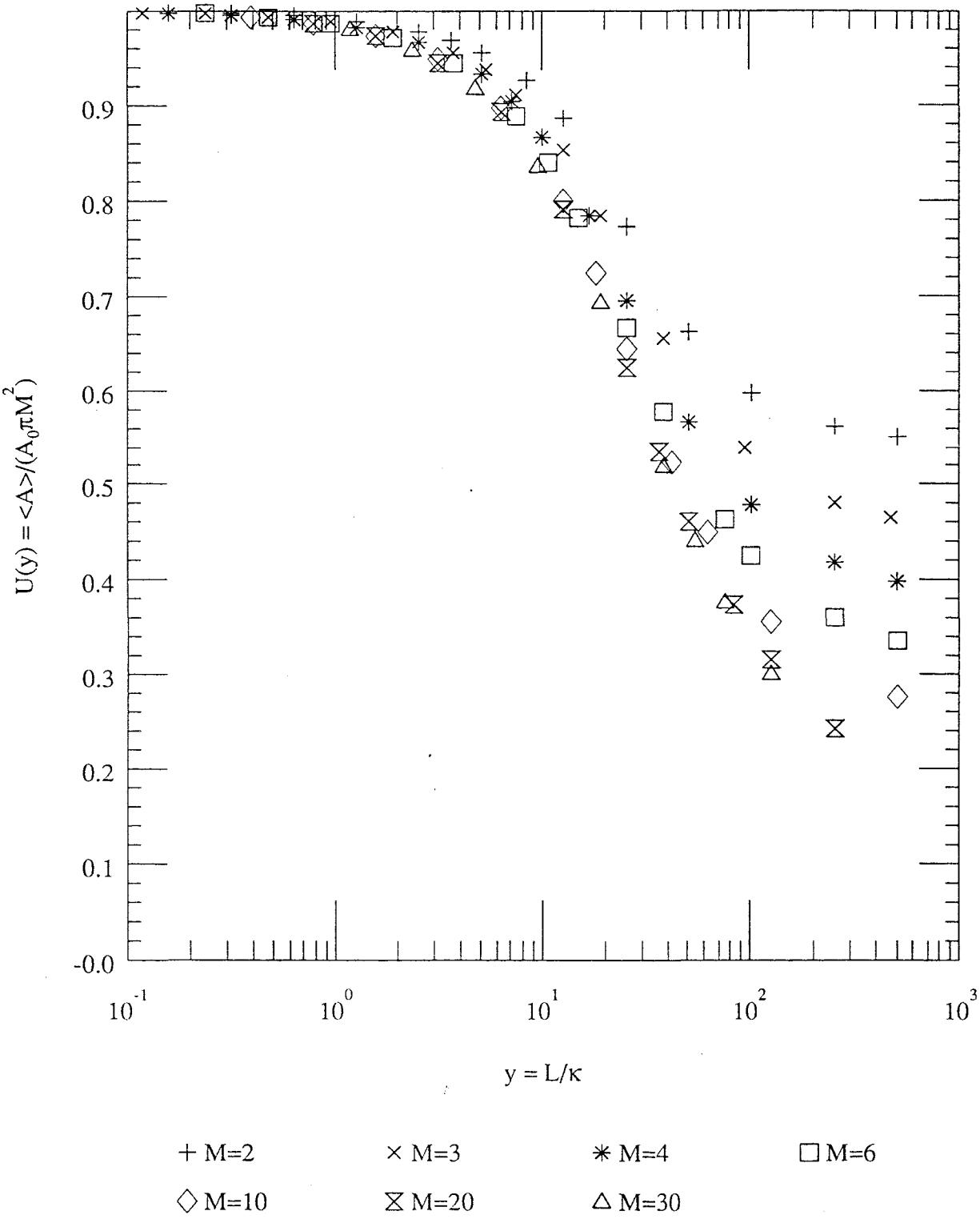

Figure 5.13

Graph of universal scaling function $U(y)=\langle A\rangle/A_0\pi M^2$ against $y=L/\kappa$.

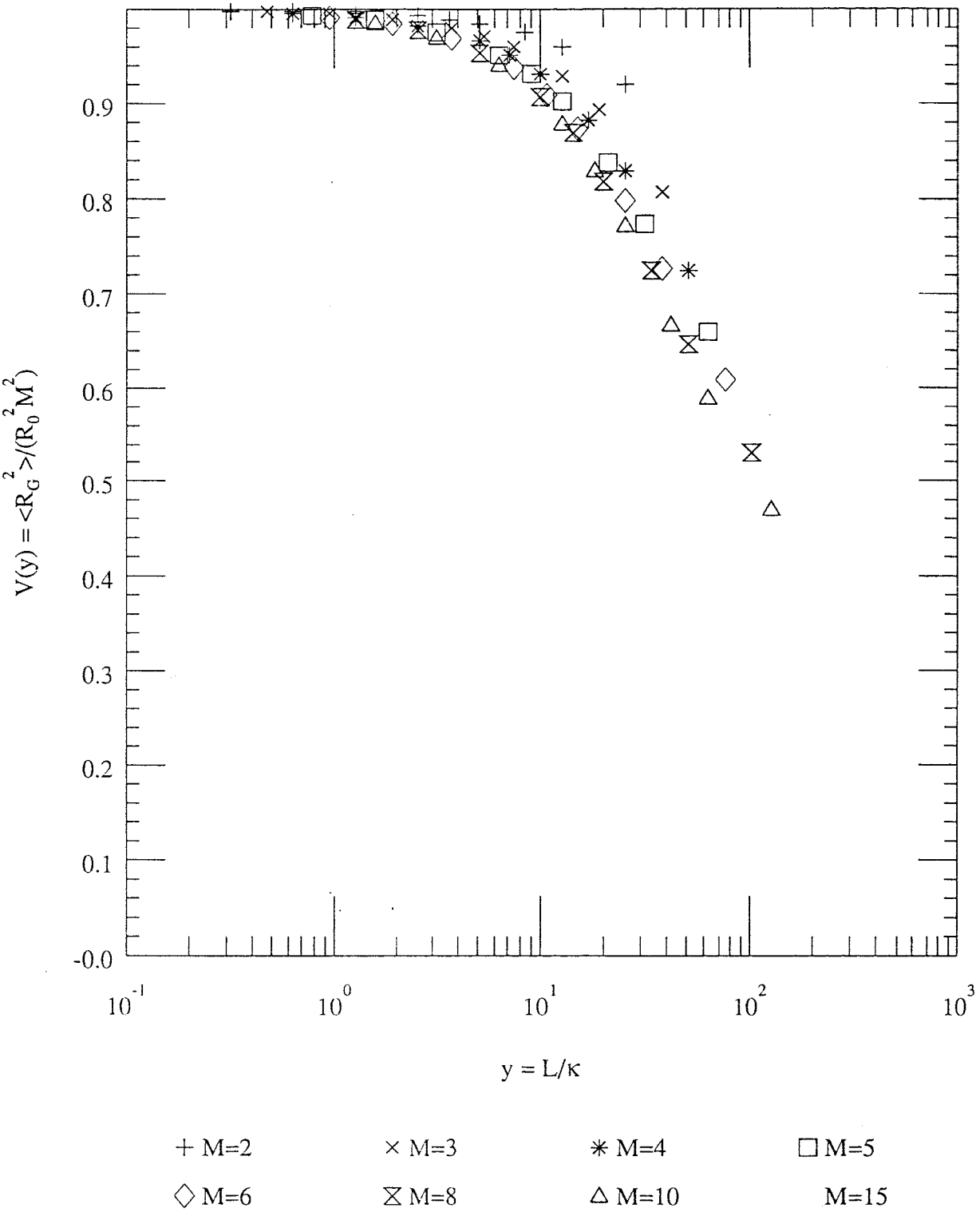

Figure 5.14

Graph of universal scaling function $V(y)=\langle R_G^2 \rangle / (R_0^2 M^2)$ against $y=L/\kappa$.

One can show more explicitly the transition from floppy to rigid vesicles if one plots what one could call the *running* or *effective* scaling exponents ν_{eff} and $\nu_{A,eff}$ defined by:

$$\nu_{eff} = \frac{1}{2}\frac{d\log\langle R_G^2\rangle}{d\log\langle y\rangle} \qquad (5.5.2;6)$$

$$\nu_{A,eff} = \frac{1}{2}\frac{d\log\langle A\rangle}{d\log\langle y\rangle} \qquad (5.5.2;7)$$

In the floppy regime, $y>L/a$ ($\to\infty$) then clearly these effective exponents will take on a value around 0.75, particularly for reasonably sized vesicles, where finite size effects are less important. On the other hand in the rigid regime, as $y<1$ ($\to 0$) then these effective exponents should approach the value 1.

In figures 5.15 and 5.16 I have plotted these effective scaling exponents against the scaling variable log(y). The graphs indicate that both scaling exponents do indeed $\to 1$ as $y\to 0$. Moreover the graph for the areal exponent seems to flatten at the high y region at a value of around 0.75. The graph of the radius of gyration on the other hand is less supportive in the high y region. However it would seem that the radius of gyration exponent descends somewhat later than that of the areal exponent, and since the enlarged y values are subject to greater error one can not properly infer anything about this.

One should note that in figures 5.15 and 5.16 the data are anomalously universal. That is, they are universal for anomalously large values of y. Why this is the case I cannot say.

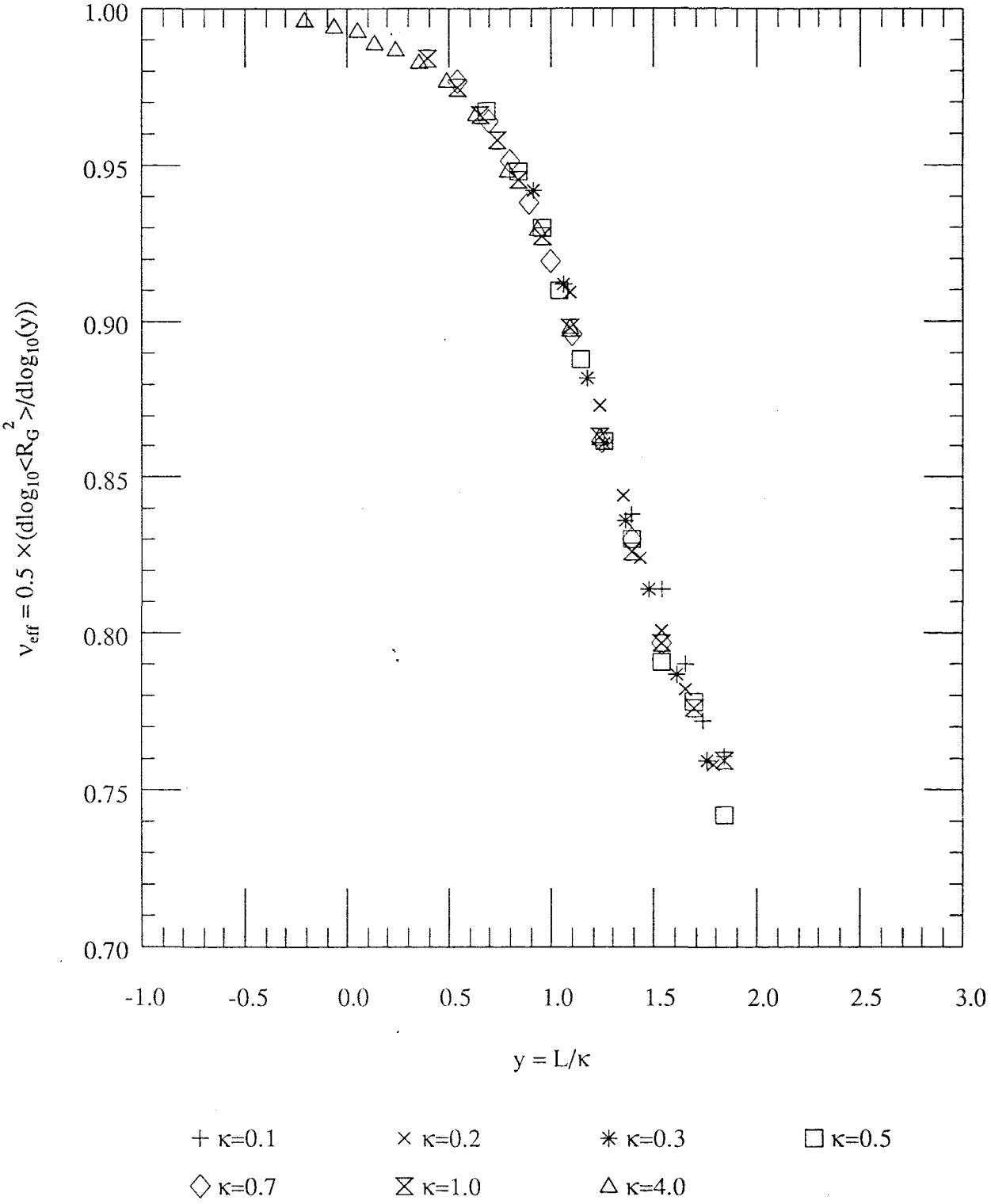

Figure 5.15

Graph of effective scaling exponent $\nu_{eff}=0.5 \times (d\log\langle R_G^2\rangle / d\log(y))$ against $y=L/\kappa$.

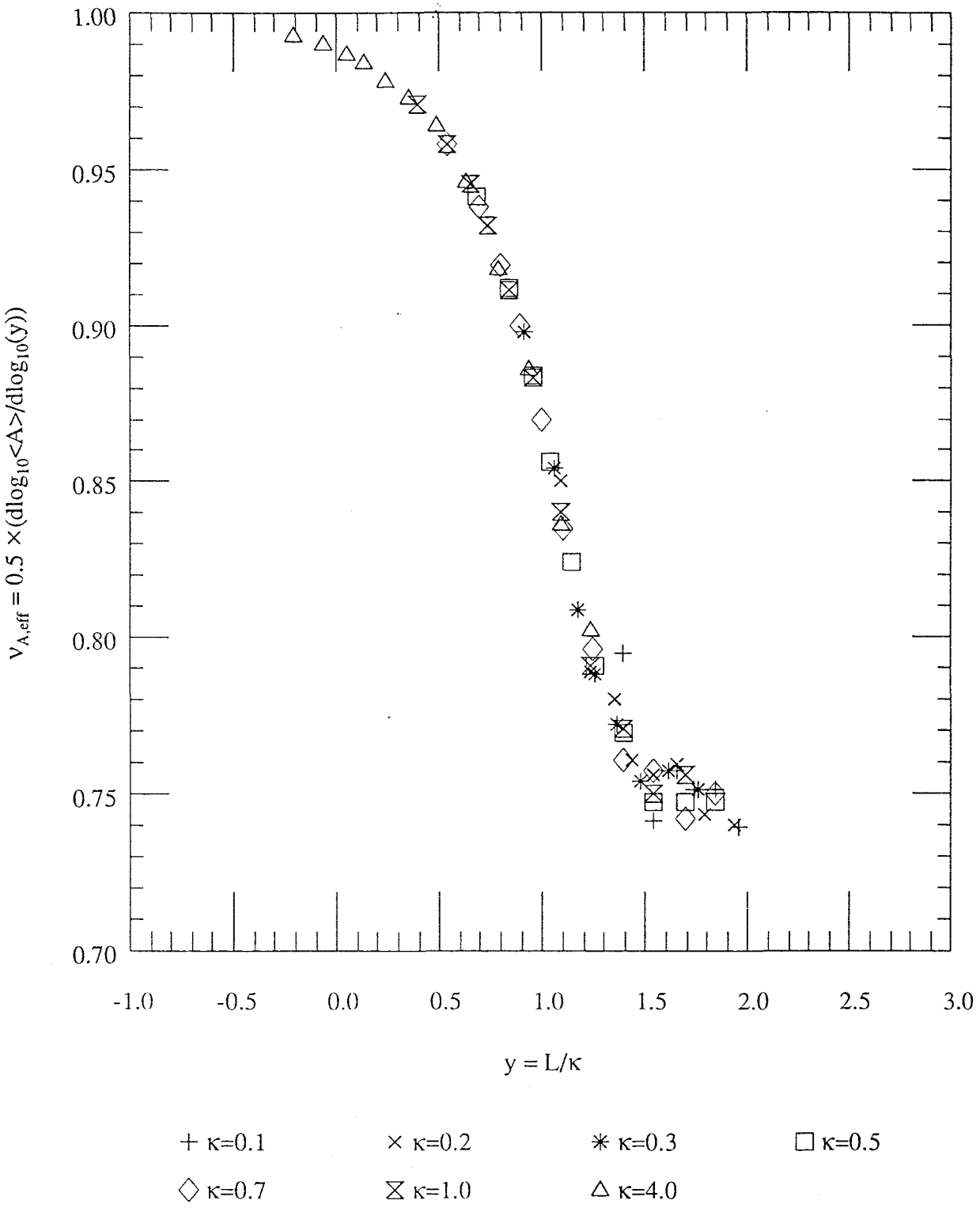

Figure 5.16

Graph of effective scaling exponent $\nu_{A,eff}$=0.5 ×(dlog<A>/dlog(y)) against y=L/κ.

One can also plot other vesicle properties to observe the transition from rigid to floppy regimes. These properties are more closely associated to the average geometrical shape of vesicles in the ensemble than the scaling exponents are.

In figures 5.17 and 5.18 I have plotted the shape functions Π and $\tilde{\Pi}$. Both curves are reasonably well behaved. Again the functions seem to be anomalously universal, like the effective scaling exponents.

In figures 5.19 and 5.20 I have plotted the anisotropy functions Σ and $\tilde{\Sigma}$. Both curves behave similarly. Unexpectedly both curves exhibit a minimum turning point. The results of Camacho *et al* (1991) also seem to exhibit this turning point, although the effect is apparently less marked in their data.

In figure 5.21 I have plotted for completeness the asphericity function $\tilde{\Delta}$. The curve clearly has a maximum turning point.

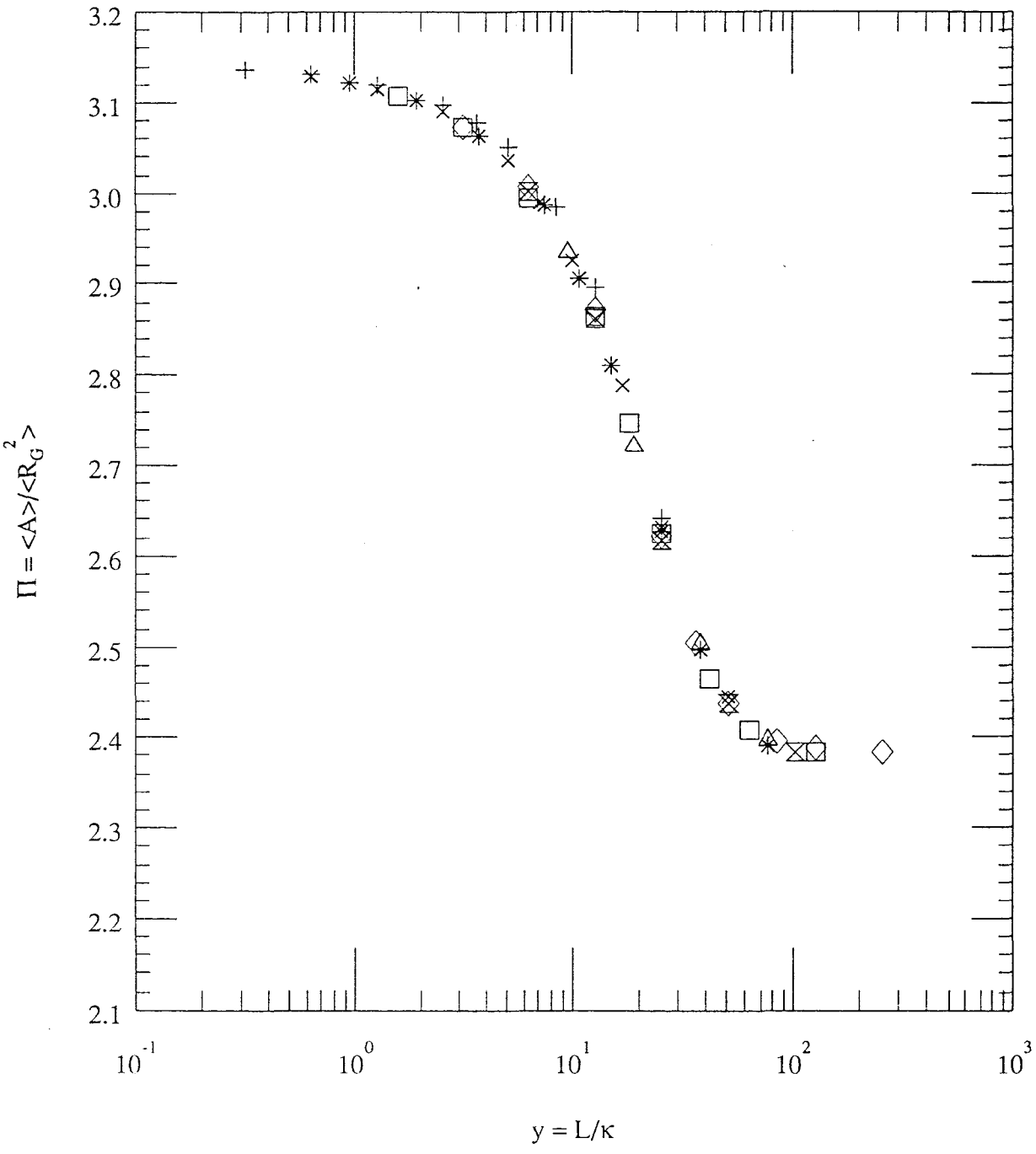

Figure 5.17

Graph of universal shape function $\Pi(y)=\langle A\rangle/\langle R_G^2\rangle$ against $y=L/\kappa$.

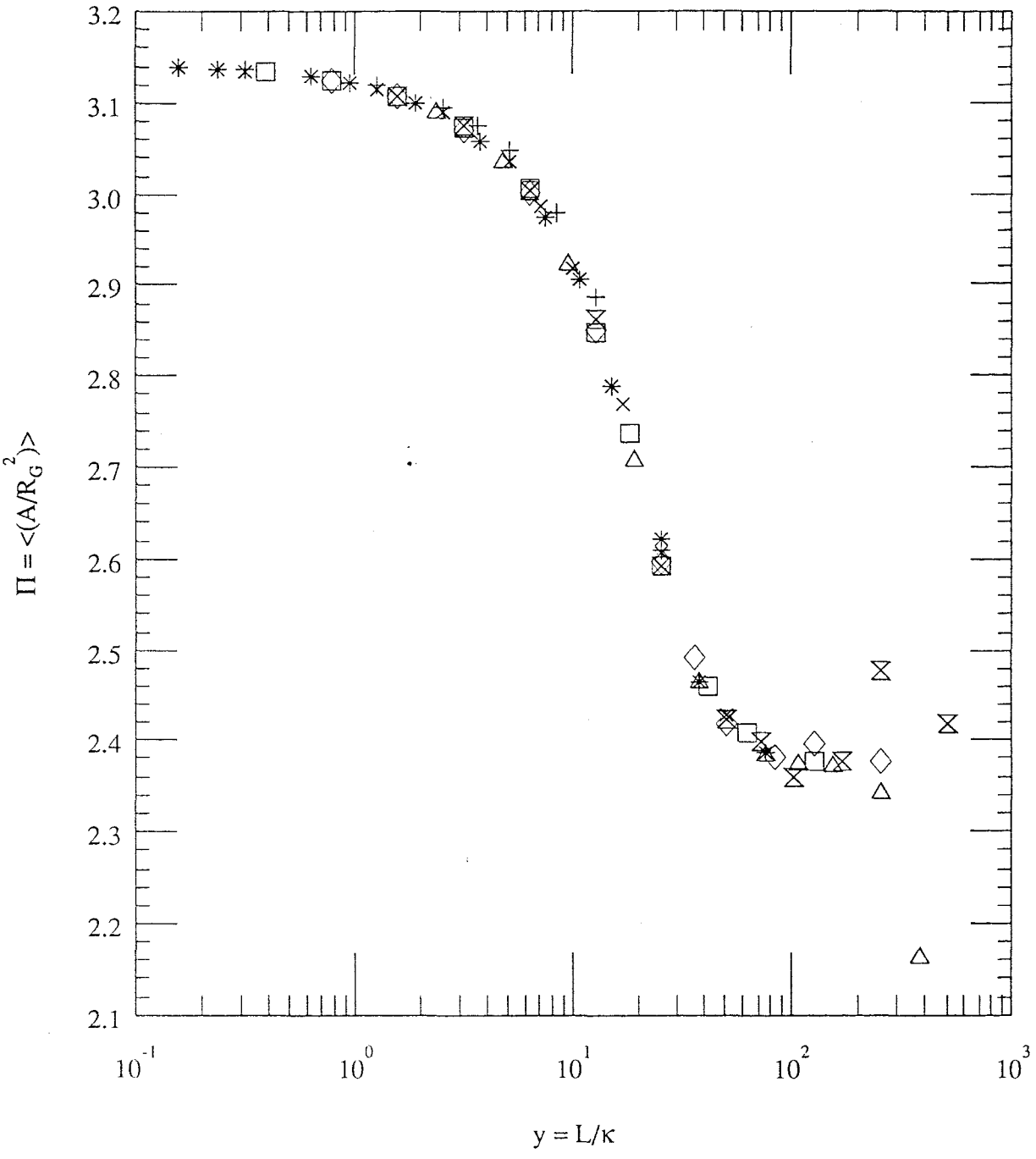

Figure 5.18

Graph of universal shape function $\Pi(y)=\langle(A/R_G^2)\rangle$ against $y=L/\kappa$.

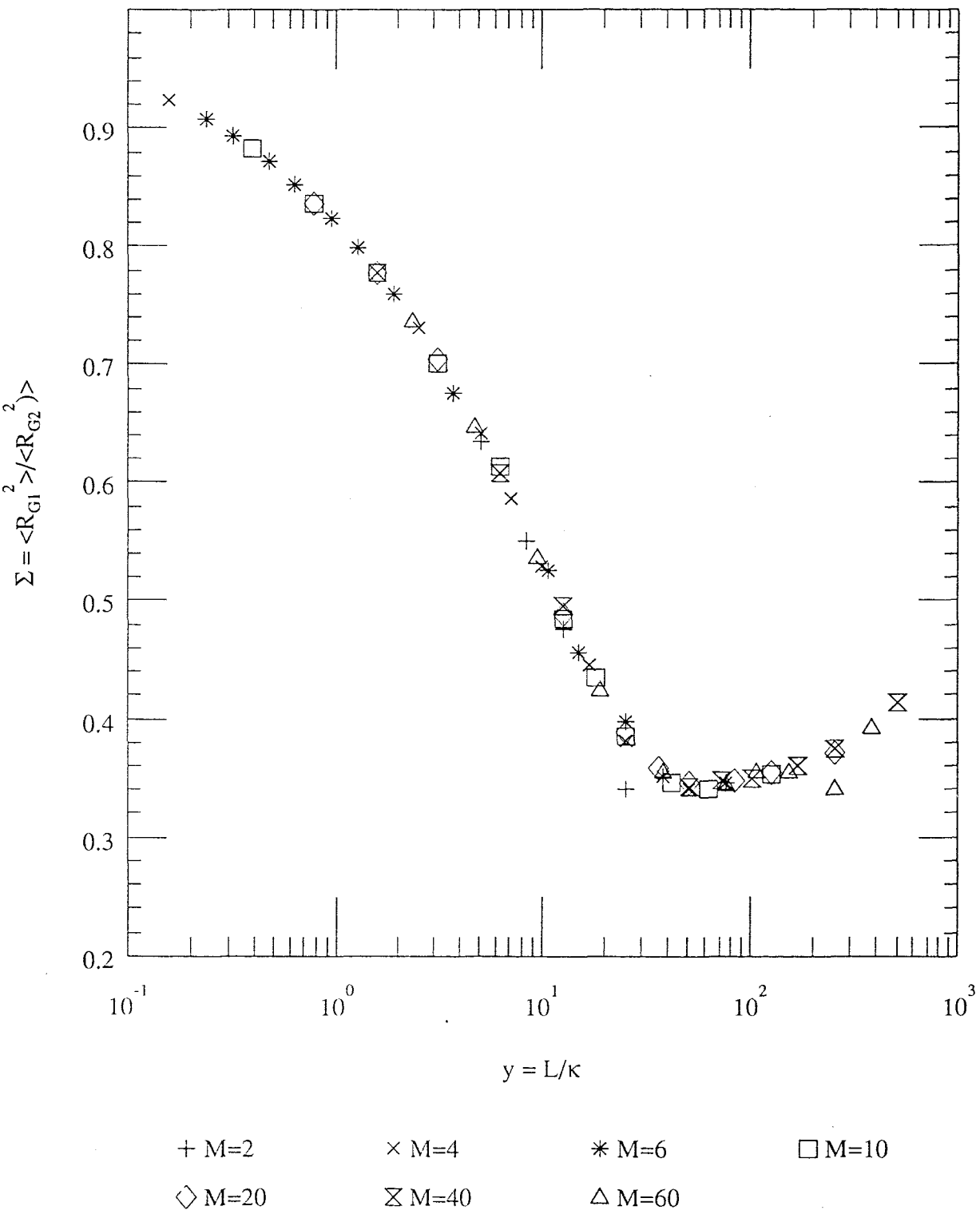

Figure 5.19

Graph of universal shape function $\Sigma(y)=\langle R_{G1}^2 \rangle / \langle R_{G2}^2 \rangle$ against $y=L/\kappa$.

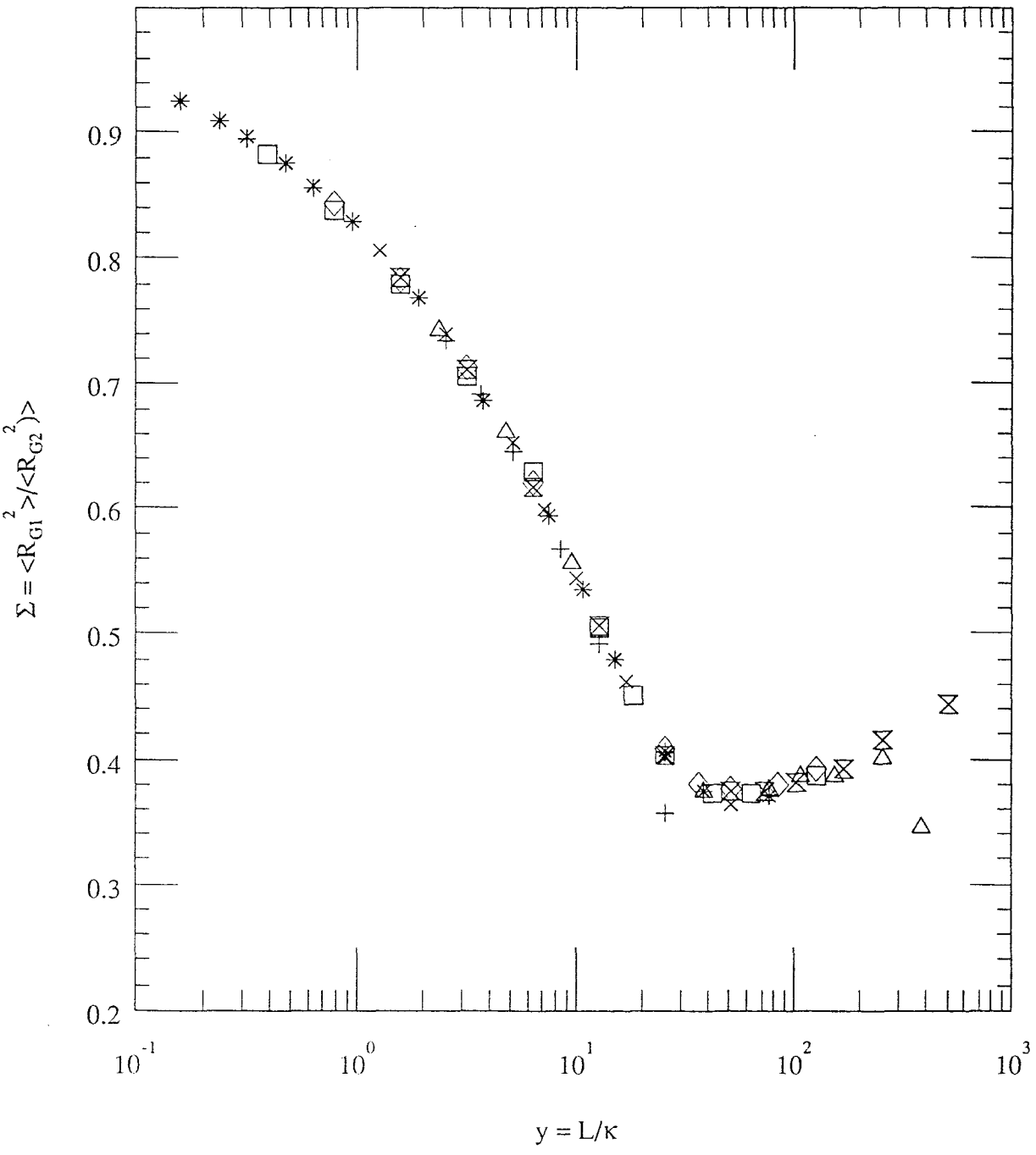

Figure 5.20

Graph of universal shape function $\Sigma(y)=\langle R_{G1}^2 \rangle / \langle R_{G2}^2 \rangle$ against $y=L/\kappa$.

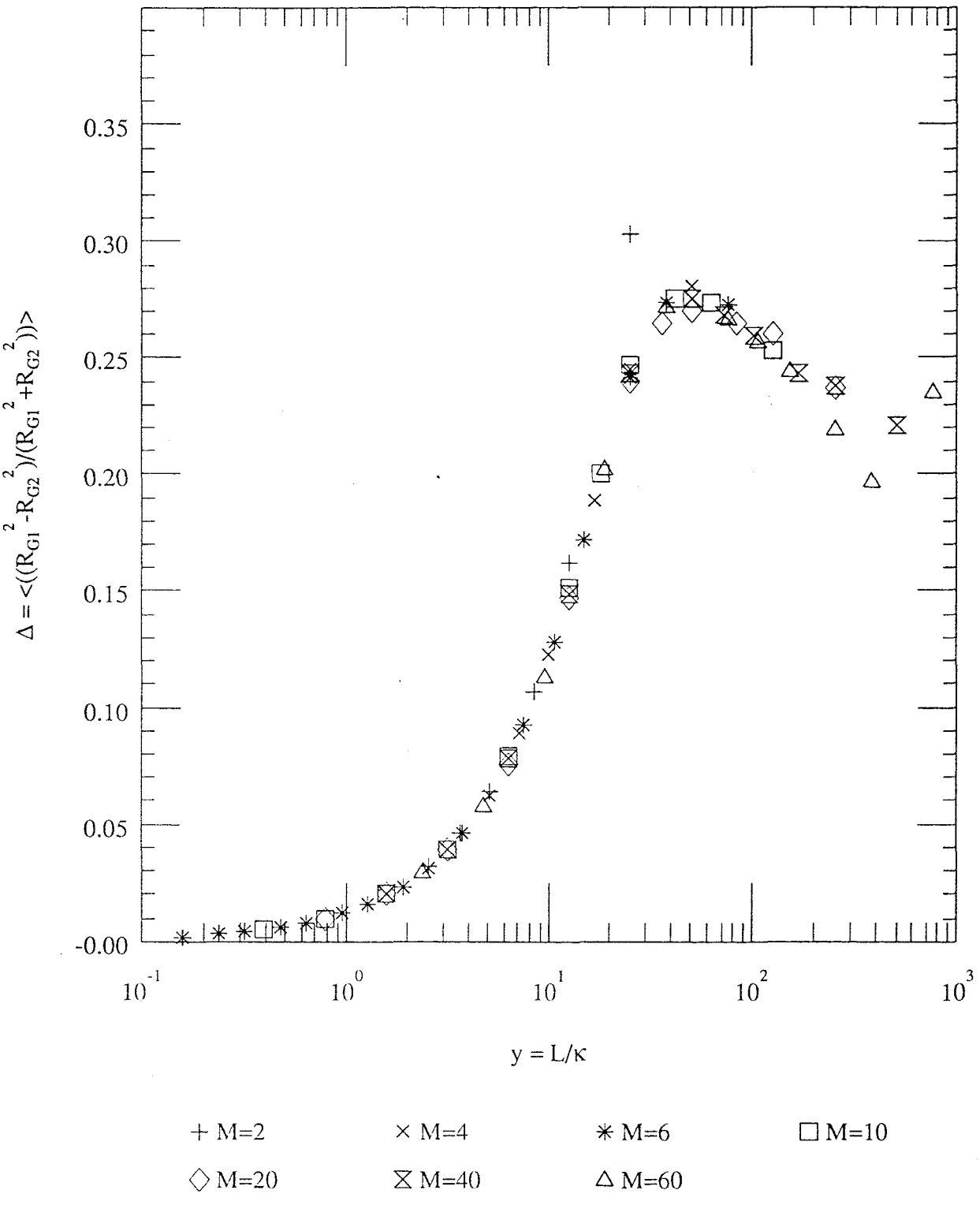

Figure 5.21

Graph of universal shape function $\Delta(y)=\langle((R_{G1}^2-R_{G2}^2)/(R_{G1}^2+R_{G2}^2))\rangle$ against $y=L/\kappa$.

5.5.3. The Deflated and Inflated Regimes

In section 5.5.1. I considered floppy-flaccid vesicles. Then in section 5.5.2, the previous section, I considered rigidity and the transition from floppy to rigid vesicles. One saw, as foretold by Leibler et al, that rigidity effects were finite size effects that could always be eliminated by sufficiently increasing the contour length, L, of the vesicles. In this section I apply an osmotic pressure difference to the vesicle by introducing the pressure term, detailed in section 5.4.5, to the Hamiltonian. It will become evident that the osmotic pressure effect unlike the rigidity effect is not a finite size effect.

Following the work of Leibler *et al* (1987) one would expect the floppy-flaccid scaling laws to be altered according to

$$\left\langle R_G^2 \right\rangle \approx M^{2\nu} X(\Delta \bar{p} M^{\phi\nu}) \tag{5.5.3;1}$$

$$\langle A \rangle \approx M^{2\nu} Y(\Delta p M^{\phi\nu}) \tag{5.5.3;2}$$

where one expects the *crossover exponent* ϕ=2. Writing $x=\Delta p M^{2\nu}$ then for the scaling functions one can write:

$$X(x) \approx \frac{\left\langle R_G^2 \right\rangle}{M^{2\nu}} \tag{5.5.3;3}$$

$$Y(x) \approx \frac{\langle A \rangle}{M^{2\nu}} \tag{5.5.3;4}$$

I have plotted the log of the scaling function X(x) against log(|x|) in figures 5.22. Comparison with the graphs presented by Leibler *et al* (1987) appears, at least, qualitatively good.

For values of log(|x|) greater than about 0.5 the graphs split into two branches; one rising, one falling. The falling branch is from vesicles being compressed under the action of a positive osmotic pressure difference, Δp, while conversely the rising branch is from vesicles being inflated by the action of a negative osmotic pressure difference, Δp. Both branches appear to be asymptotically linear, albeit with different gradients.

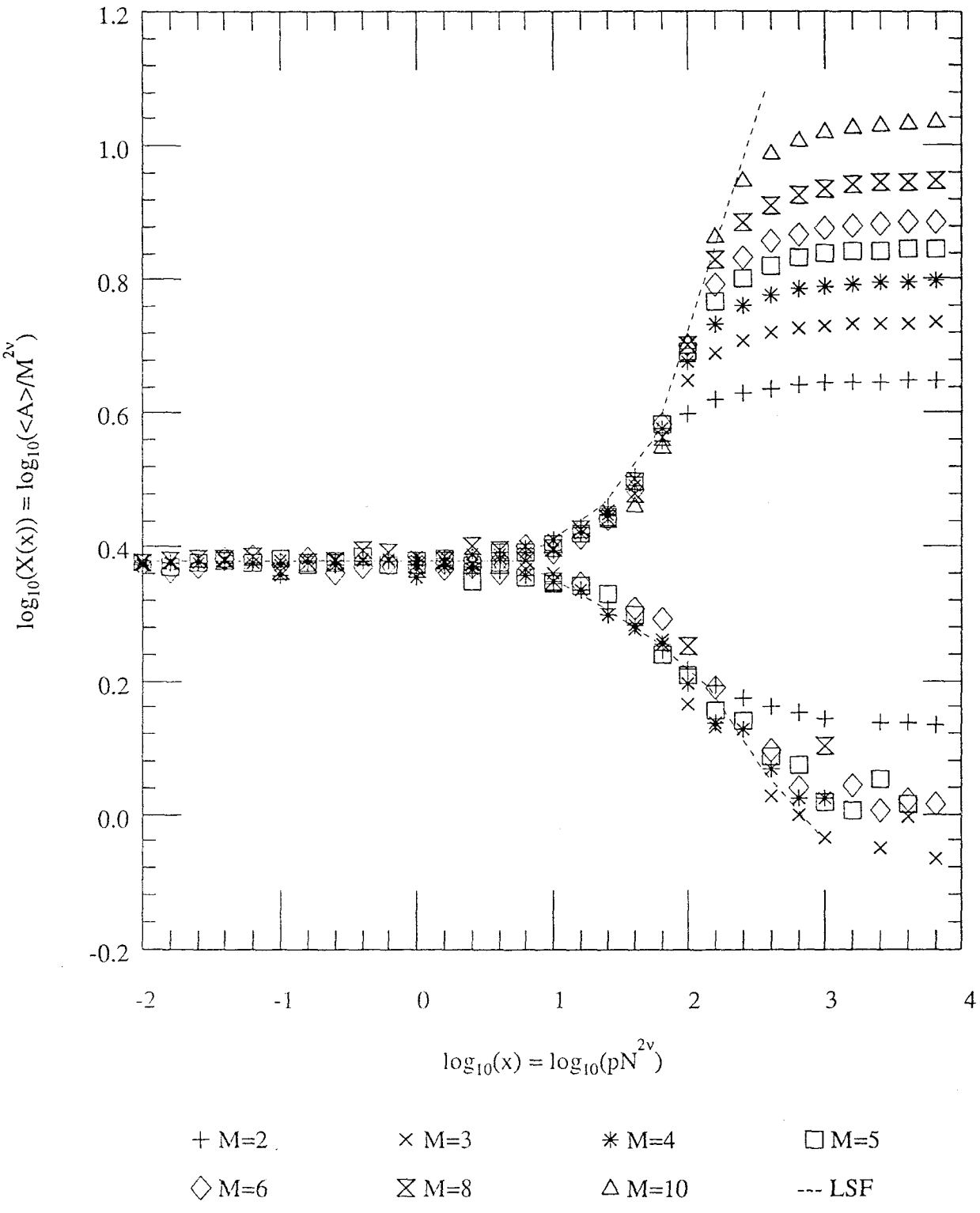

Figure 5.22

Graph of universal area scaling function $X(x)=<A>/M^{2\nu}$ against $x=pN^{2\nu}$.

5.5.4. The Nematic Ordering Field Regime

So far I have considered isolated vesicles in free, rigid and pressurised regimes. I now wish to consider the effect that a *nematic ordering field* induces; a nematic ordering field is a field that tends to align objects to point in a given direction. Although the nematic ordering potential that I introduce is itself only a hypothetical potential, it is expected that the effect of a shear flow on an isolated vesicle could be very similar. Since vesicular objects are often subject to shear flow regimes the interest is clear.

The actual form of the nematic ordering potential is

$$E_N = \int_0^{2\pi} \cos(2\psi(s))ds \qquad (5.5.4;1)$$

The magnitude of the field is controllable through the parameter V. The ordering nature of the field is embodied in the $\cos(2\psi(s))$ component.

A parameter that should vary interestingly according to the value of V is the *nematic anisotropy* (this is my own naming convention), Σ^*, defined by:

$$\Sigma^* = \frac{\langle R_{Gxx}^2 \rangle}{\langle R_{Gyy}^2 \rangle}. \qquad (5.5.4;2)$$

where R_{Gx}^2 and R_{Gy}^2 are the x and y axial components of the radius of gyration tensor.

In figure 5.25 I have plotted the nematic anisotropy against the nematic filed strength V for various vesicle sizes. The curves seem loosely universal, although the accuracy of the results makes a stringent assertion of universality impossible.

In the absence of the nematic ordering field the nematic anisotropy is approximately one. This is because in the absence of the nematic ordering field the vesicle configuration is isotropically ordered; that is it is equally likely to be displaced in any direction. In particular that means that the xx and yy components of the radius of gyration tensor are equal leading to a value of one for the nematic anisotropy.

As the nematic ordering field is applied the nematic anisotropy rapidly falls; indicating that the vesicles are ordering along the y-axis in preference to the x-axis. As the field is increased further the anisotropy begins to flatten out. The anisotropy does not continue to fall rapidly to zero, as one might expect *a priori*. The reason for

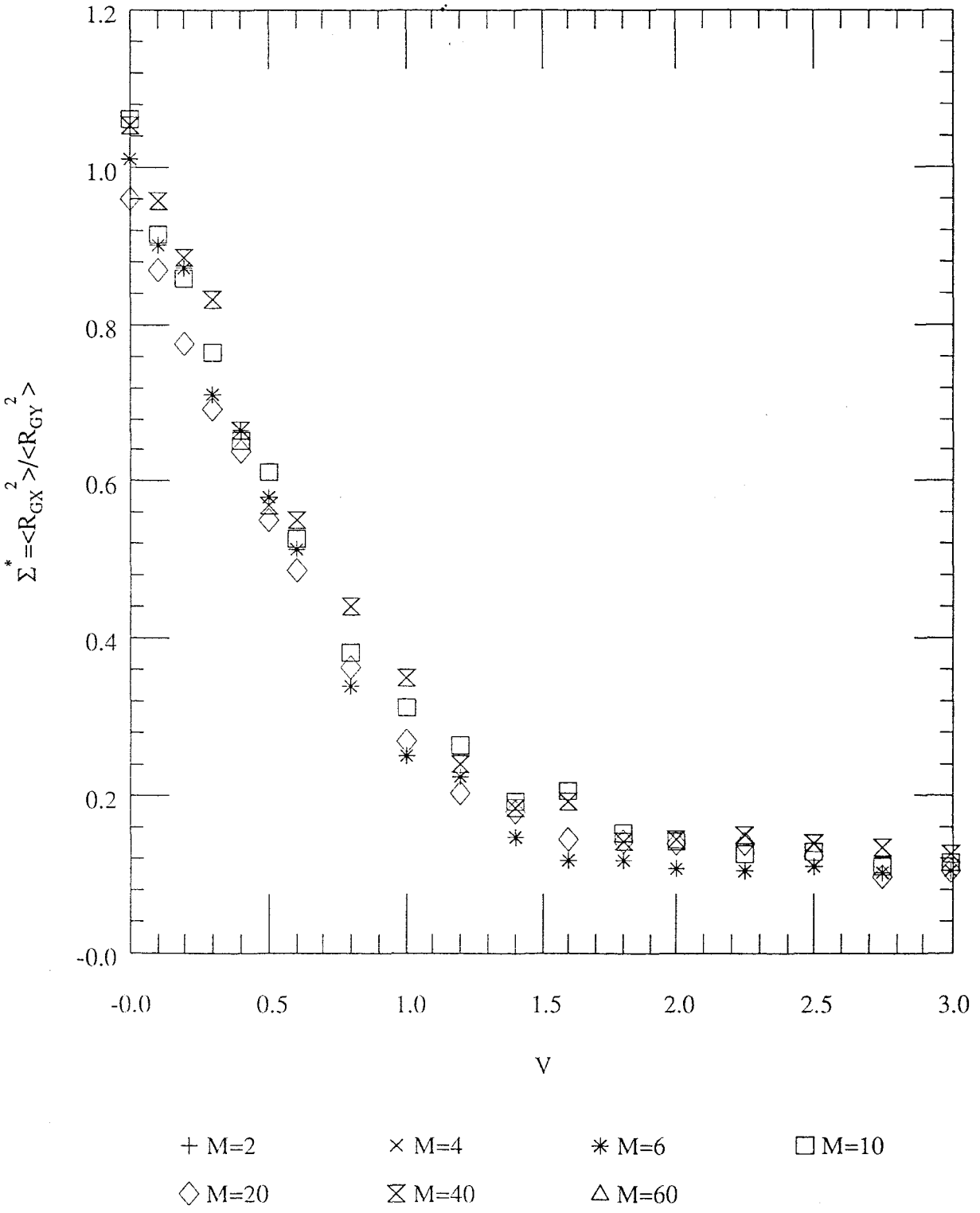

Figure 5.23

Graph of nematic anisotropy parameter $\Sigma^* = \langle R_{GX}^2 \rangle / \langle R_{GY}^2 \rangle$ against the nematic ordering field intensity V.

this unexpected behaviour is not clear. However, one plausible explanation is that the effect is due to the hard-core self-avoidance property of the vesicles. As the vesicle ensemble nematically orders initially the vesicles walls do not interfere apart from their intrinsic self-avoidance. Hence the initial fall in anisotropy is rapid. As the anisotropy continues to fall and the vesicles order along the y axis the vesicle walls are effectively drawn together. Neglecting the ends of the vesicle, it is as if one is forcing two undulating membranes on top of one another. The independent undulations of the membranes have to be overcome to continue to force the sides together. Thus membrane self avoidance could be the source of the flattening anisotropy. One way of testing this hypothesis would to be to consider ensembles where the self-avoidance property has been switched off. Such an experiment is well within the scope of this model, although I have not completed such an experiment at this stage.

5.6. Conclusions

I have investigated the properties of a model of two dimensional vesicles. The vesicle consists of a closed membrane subject to a bending rigidity modulus, and extra terms which couple to the area inside it and the orientation of the local curve perimeter. The model is the continuum version of a bead (Leibler *et al* 1987) model whose properties were investigated by other authors (Fisher 1989, Camacho *et al* 1990, 1991, Maggs and Leibler 1990, Maggs *et al* 1990) using the Metropolis Monte Carlo method. I have used a method essentially due to Ostrowsky and Peyraud (1985) in order to carry out the functional integrals necessary in order to obtain average quantities for the Helfrich model. I have found that the method is rather more versatile than the authors had originally anticipated; in particular I have been able to verify scaling laws, first found in the bead simulations, for the behaviour of the vesicle as a function of the various control parameters. I have extended this scaling analysis to look at the effect of the imposition of an external nematic orienting field. The work presented in this chapter forms the basis of a recent publication [Norman *et al* 1992].

Finally, despite the encouraging results obtained in this work I am not optimistic about using an analogue of this method to investigate vesicles embedded in three dimensional space. In two dimensions the differential geometry is trivial; in three dimensions, however, difficulties emerge which I am not able to overcome at this stage.

CHAPTER SIX

MEMBRANES AND INTERFACES CONFINED BETWEEN PARALLEL WALLS

6.1. Introduction

Up until this point in this thesis I have dealt with membrane structures. In this chapter I use a model originally used for investigating interfaces and adapt it for studying membranes as well. The differences between membranes and interfaces are sufficiently few to allow this; the similarity being that both membranes and interfaces in d dimensions are (d-1) dimensional objects.

In many physical situations it is of interest to study a membrane or interface in the gap between two walls (Parry 1992c, Gompper and Kroll 1991) or the physically similar problem of a membrane adsorbed onto a single wall by a binding potential (Parry 1992a-b, Maggs *et al* 1989, Maggs and Leibler 1990). The presence of the walls affects the statistical mechanics of the *surface* (I will use the term surface as a generic term to describe both interface and membrane in two, three or d-dimensional space), entropically, by eliminating many of the possible orientations through the exclusivity of the walls.

Initially I will discuss a model of interfaces called the *Solid on Solid (SOS)* model (Leamy *et al* 1975). We shall see that this model of interfaces restricts the available geometry of the interface somewhat. The *probability density functions (pdfs)* for an interface or membrane confined between a wall will be defined. I will discuss some analytical arguments which lead to a universal form for the pdf of confined two dimensional interfaces. A discussion of a more generic argument, that allows us to postulate a universal form for the pdf of two dimensional SOS membranes, follows.

Next I present an investigation of the two dimensional SOS interface by Monte Carlo Simulation. I will show that the results are consistent with the analytical work already discussed. This establishes, for us, the credentials of the Monte Carlo simulation method for investigating the universal behaviour of pdfs. I then present the results of a similar Monte Carlo investigation of the two dimensional SOS membrane.

I shall show that the results of the simulations affirm, with certain reservations, the universal form for the pdfs postulated in the earlier analytical work.

Having investigated these two dimensional interface and membrane models it would clearly be of interest if one could make similar progress with the analogous three dimensional models. Unfortunately, it has not proved possible to make any substantial progress analytically on three dimensional SOS problem. To make any progress in the literature authors have had to make very severe additional restrictions to the SOS model (Leamy *et al* 1975). Conversely the generalisation of the two dimensional simulations to three dimensions is not difficult conceptually. So following the two dimensional work I present the results of numerical simulations of the three dimensional SOS interface and membrane models. The absence of a clear theoretical framework for the three dimensional problems has dictated that I use the theoretical framework of the two dimensional problem to analyze the results. Unfortunately for three dimensions computational problems arise (namely that the number of computations required to obtain universality is too large) which limit the scope of this investigation. Nevertheless I was able to observe universal behaviour for the SOS model of a membrane in three dimensions. The corresponding interface showed no signs of universality.

The SOS model of interfaces and membranes is intrinsically restrictive of the membrane geometry only allowing certain types of fluctuations. It is not clear *a priori* whether these fluctuations are sufficient to model real systems adequately. Recall that a membrane in two dimensions can be considered isomorphic to a polymer in two dimensions (as pointed out in chapter 4). So naturally it is of interest to consider whether the results from a polymer type model for the membrane differ from the SOS model already investigated.

In order to investigate this problem more carefully I use a bead chain model based on the bead chain model of a polymer to investigate the membrane in two dimensions. The analogous model for vesicles has already been discussed in section 5.3. We shall see that the extra degrees of freedom of the membrane introduce an asymmetry to the membrane and consequently periodicity of the membrane is irretrievably lost. Despite the extra degrees of freedom in the problem and the lack of periodicity I have been able to observe universal behaviour in the pdf through a detailed scaling analysis.

Finally, I present a brief summary and comparison of the salient results obtained from the preceding work before concluding the chapter.

6.2 Parameterisation Of The Solid On Solid Model

The *Solid On Solid (SOS)* (Leamy *et al* 1975) model is a model of a "well behaved" interface. The parameterisation of the model is illustrated in figure 6.1.

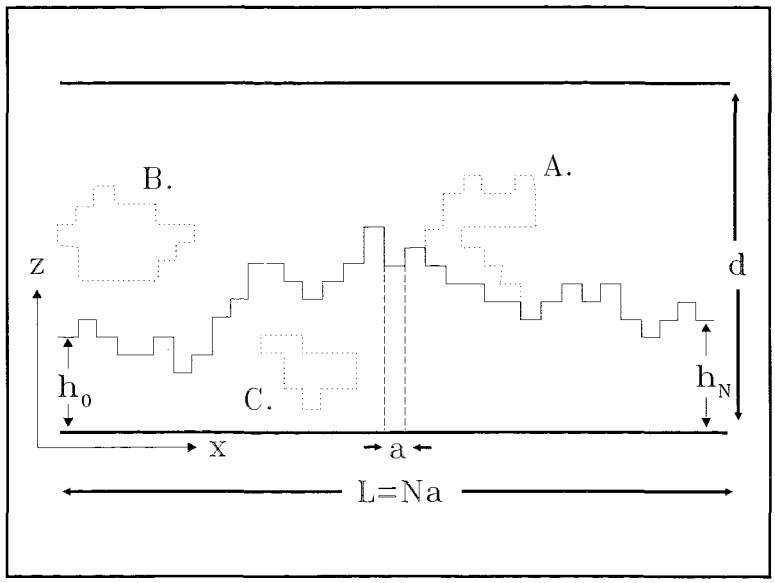

Figure 6.1
Parameterisation of the SOS model.

The surface is represented by a series of heights above one of the walls spaced equidistantly along the lengths of the walls as in the illustration. The model as presented is therefore inherently a lattice model in the plane of the walls. The heights however can be on or off lattice; in which case I shall call the model *lattice* or *continuum* respectively. Although, as already pointed out above, strictly speaking all SOS models are lattice models in the plane of the walls.

It should also be observed that for this model of surfaces that the height function is implicitly single valued; so that overhangs (dashed line), droplets (dotted line) and self-avoidance effects are implicitly ignored. These geometrical restrictions, which the model imposes on the surface ensemble, on the one hand permit progress on the analytical problem and on the other hand impair its applicability to real physical systems. Hence the model is inappropriate for vanishing surface tension and curvature elasticity regimes where overhangs, droplets and self-avoidance effects predominate.

It can be seen, particularly in the lattice model case, that the interface can be viewed as a special case of an *Ising Model* (Huang 1987). It partitions the model, according to the restrictions above, into two separate spin-up spin-down regions. In fact the SOS model represents a particular limit of the more general Ising Model problem tackled elsewhere (e.g. see Abrahams 1980, Beijeren 1977).

6.3 Classification of Interface and Membrane

In general interfaces have a Hamiltonian in which the surface tension (*line tension* for an interface in two dimensions) term is dominant whilst for membranes as we have seen it is the curvature term that dominates. Note that under this classification a bubble of soap is classified as an interface structure whilst a liposome is a membrane structure (Clearly under a different scheme of classification a bubble of soap might logically be regarded as a membrane structure rather the interface structure implied by this classification). The parameterisation of the SOS model presented in section 6.2 is the same for interface and membrane. To model the interface we use a surface tension Hamiltonian, only changing the Hamiltonian to a Helfrich curvature Hamiltonian to model a membrane.

The Hamiltonian of a continuous 2d interface can be written as

$$H_{int} = \frac{1}{2}\sigma\int_0^L \left(\frac{dh}{dx}\right)^2 dx \qquad (6.3;1)$$

where h(x) is the continuous height above the lower wall function and σ is the surface tension elasticity. We have already seen that the SOS model is inherently on lattice in the plane of the walls. In the discrete limit this reduces to

$$H_{int} = \frac{\sigma}{2a}\sum_{i=1}^{N}(h_i - h_{i+1})^2 \qquad (6.3;2)$$

where a is the lattice spacing in the x-direction.

In contrast we have seen in section 3.5.1 that the Hamiltonian for a continuous 2d membrane is the familiar Helfrich Hamiltonian. We can write this in its nearly flat nearly parallel (to x-axis) asymptotic form as

$$H_{mem} = \frac{1}{2}\kappa\int_0^L \left(\frac{d^2h}{dz^2}\right)^2 dz \qquad (6.3;3)$$

where κ is the Helfrich curvature elasticity. This reduces, in the discrete limit, to

$$H_{mem} = \frac{\kappa}{2a}\sum_{i=1}^{N}\left(h_{i-1} + h_{i+1} - 2h_i\right)^2 \qquad (6.3;4)$$

In addition these potentials were applied periodically so that

$$h_{N+1} = h_0 \qquad (6.3;5)$$

This periodicity ensures symmetry within the interface and is the standard procedure in simulations where one wants to look at long, length independent regimes.

6.4 The Probability Density Function (pdf)

Finally one can define more precisely the probability density function, P(z), for such systems to be the probability of finding the surface between z and z+dz. More formally, if $\tilde{P}(z)$ (the *probability distribution function*) is the probability of finding the surface in the vertical interval [0,z] then the pdf P(z) is that function which satisfies

$$\tilde{P}(z) = \int_0^z P(\tilde{z})d\tilde{z} \qquad (6.4;1)$$

Clearly this definition applies to the continuum model. For the lattice model the surface can only be found at a one of the lattice points. For this model the probability density function becomes a *probability vector (pv)*; i.e $P(z) \rightarrow P_i=P(z_i)$. The probability vector, P_i, is defined to be the probability of finding the surface at a lattice point of height z_i.

In practice when one wants to look at the pdf of the continuum model in numerical implementations one is forced to make the discrete approximation:

$$P(z) \rightarrow P_i = \frac{\tilde{P}(i.\delta z) - \tilde{P}((i+1).\delta z)}{\delta z} \qquad (6.4;2)$$

where $i=[z/\delta z]$ (the brackets [] represent the truncation integerisation operation). Like the probability vector for the lattice model this approximation of the pdf is a vector. Effectively a background lattice is created to approximate the pdf.

It approximates the pdf in the sense that

$$P(z) = \lim_{\delta z/d \rightarrow 0}\left(P_i\right) \qquad (6.4;3)$$

The value of δz is fixed by considerations of convergence and resolution of the model. Clearly if δz is too small in a particular simulation then the pdf approximation will take too long to equilibrate. Conversely if δz is chosen to be too large then the pdf approximation will equilibriate more quickly, but will represent a rather poor approximation to the continuous pdf. In practice for off-lattice model work that follows I have arbitrarily chosen $\delta z=1$, so that the off-lattice models should closely follow the on-lattice models where the lattice spacing is similarly fixed by $a=1$. Later in the chapter I shall, for convenience, use the term pdf collectively to describe both true probability density functions, approximate probability density functions and probability vectors.

6.5 Universality And Conformal Invariance: A Generic Argument For The Universal Form Of The Pdf

We have already covered some examples of universal behaviour in the discussion of polymers (section 4.6) and in the later work on vesicles (section 5.5). We have seen that often the properties of physical systems that initially seem to depend on a large set of control parameters can be shown to depend more simply on combinations of those parameters. The question arising here is whether universal regimes exist in the present context and if so what are they? I shall reproduce here an argument due to Parry (1992d) which uses *conformal invariance (CI)* to show that a universal regime does in fact exist for the two dimensional interface and membrane. Moreover, we shall see that, it is possible to obtain the universal form for the pdf in that regime (Parry 1992d).

The conformal invariance argument is based on intuitive ideas rooted in the renormalisation group theory (Ma 1985, Huang 1987). In the renormalisation group theory one makes successive global bulk transformations on the physical system - effectively magnifying or reducing the system. Systems that exhibit "true" fractality will seem qualitatively the same at all magnifications. Other physical systems will change there nature at a length scale characteristic of the system. If one can relate this characteristic length scale to the other control parameters then often the system can be

described more concisely in terms of this characteristic length scale; that is the length scale represents a universality of the regime.

The renormalisation group implies that if one makes small global scaling transformations of the system below the characteristic length scale then effectively one does not change physics of the system. One can imagine making small local scaling transformations and would not expect it to affect the physics either. In fact the CI argument goes one step further saying that if the physics of the system depends only on the local angles then one should be able to make a transformation to the system that preserves these local angles without affecting the physics. Transformations from the plane to the plane that preserve the local angle are called *conformal mappings* (Churchill and Brown 1989) and hence the term conformal invariance. The argument is intuitive in that it seems reasonable although it has not been rigorously proven.

The usefulness of CI in the context of confined interfaces and membranes stems from the fact that the physics of the membrane and interface is governed only by the local angles. So the physics of the membrane and interface should not be affected by a conformal mapping if the conformal invariance hypothesis is sound. The pdf case for the open plane can be arrived at by the principle of scale invariance. Conveniently there is a well known conformal mapping, the logarithmic map, that maps the open plane into a narrow strip (Churchill and Brown 1989). The logarithmic map from the (x,y) to the (u,v) plane is

$$W = \frac{d}{\pi} \ln(Z) \qquad (6.5;1)$$

where Z=x+iy and W=u+iv. The factor π/d ensures the strip has width d.

The pdf P(x,y) for the open plane interface and membrane is given by

$$P(x,y) = P(y) = y^{-\phi} \qquad (6.5;2)$$

where ϕ is a constant depending on the model (interface, membrane, polymer, ...). This form of the pdf has the required properties of analycity and symmetry. Note however that it cannot be properly normalised and is only a first order approximation of the pdf.

It can be shown using the fact that the pdf is an analytical function and the fact that the logarithmic map is a conformal map that the pdf in the confined strip is related to the pdf in the open plane by

$$P(u,v) = |W'(z)|^{\phi} P(x,y) = |W'(z)|^{\phi} y^{-\phi} \tag{6.5;3}$$

Expanding the mapping (6.5;1) into components one gets

$$u+iv = e^{\frac{\pi u}{d}}\left(\cos\left(\frac{\pi v}{d}\right) + i.\sin\left(\frac{\pi v}{d}\right)\right) \tag{6.5;4}$$

From which one can, by comparing imaginary parts, extract

$$y = e^{\frac{\pi v}{d}} \sin\left(\frac{\pi v}{d}\right) \tag{6.5;5}$$

Differentiating the mapping one gets

$$W' = \frac{d}{\pi \ln(Z)} \tag{6.5;6}$$

Expanding this

$$W' = \frac{d}{\pi} e^{-\frac{\pi u}{d}} e^{-i\frac{\pi v}{d}} \tag{6.5;7}$$

So that

$$|W'| = \frac{d}{\pi} e^{-\frac{\pi u}{d}} \tag{6.5;8}$$

Finally substituting (6.5;5) and (6.5;8) into (6.5;3) and tidying up one can write

$$P(u,v) = P(v) = \left(\frac{d}{\pi}\sin\left(\frac{\pi v}{d}\right)\right)^{\phi} \tag{6.5;9}$$

This is a remarkable result. It tells us that the pdfs of a whole class of two dimensional membrane and interface type models reduce to a single universal form independent of the physical control parameters σ, κ, etc. The pdf depends on the scale free relative height of the membrane y/d and a universal exponent ϕ characteristic of the particular model under consideration. It does not depend separately on the width of the strip. Moreover the functional form of the pdf is universal, which is a very strong form of universality.

6.6 Analytical Result For The 2d SOS Surface Tension Model pdf

The arguments presented in this section are due originally to Temperley (1951) although this discussion is based in particular on the discusions contained in Burkhardt (1981) and Chui and Weeks (1981). The arguments we shall see are based on transfer function and transfer matrix methods not uncommon in statistical physics (e.g. for some other examples of the application of transfer matrices see Huang 1987). Following these arguments, it is possible to proceed analytically to find the form of the pdf of the SOS interface in 2d. The partition function for the 2d SOS interface model is

$$Z = \int_{h(x)} \exp\left(-\sigma \int_0^L \left(\frac{dh}{dx} \right)^2 dx \right) Dh(x) \tag{6.6;1}$$

This functional integral becomes the following sum

$$Z = \sum_{\{h_i\}} \exp\left(-\sigma \sum_{i=0}^{N} (h_i - h_{i+1})^2 \right) \tag{6.6;2}$$

as the domain h(x) is replaced by its SOS representation $\{h_i\}$. It can be seen that this can be re-written in the following way

$$Z = \sum_{\{h_i\}} \prod_{i=0}^{N} \exp\left(-\sigma (h_i - h_{i+1})^2 \right) \tag{6.6;3}$$

Now if we define the transfer function T(h,h') by

$$T(h,h') = \exp\left(-\sigma (h - h')^2 \right) \tag{6.6;4}$$

then using (6.6;3) and the periodicity constraint

$$h_0 = h_{N+1} \tag{6.6;5}$$

it can be shown that the partition function can be written as the trace of the N'th power of the transfer function, i.e.

$$Z = \mathrm{Tr}\left(T^N \right) \tag{6.6;6}$$

The eigenvalues, λ, and eigenfunctions, ψ, of the transfer function T are defined by the equation

$$T(h,h') . \psi = \lambda \psi \tag{6.6;7}$$

Let the largest eigenvalue and the associated eigenfunction be denoted λ_m and ψ_m respectively. Then it can be shown that the free energy in the limit $N \to \infty$ is given by

$$A = -N \ln(\lambda_m) \tag{6.6;8}$$

Also it can be shown that the pdf, P(h), is related to the eigenfunction corresponding to the largest eigenvalue by

$$P(h) = c|\psi_m(h)|^2 \qquad (6.6;9)$$

where c is a normalising constant fixed by the requirement on P(h) that

$$\int_{-\infty}^{+\infty} P(h)\,dh = 1 \qquad (6.6;10)$$

which is the mathematical statement of the physical fact that the membrane has to lie somewhere between the walls.

So far in this section we have considered the height function, h(x), to be a continuous variable. If we consider h(x) to be restricted to a set of, say d, lattice positions between the walls then the discussion remains valid, albeit that the transfer function now becomes a transfer matrix and the eigenfunction becomes an eigenvector as a result of the discretisation. Strictly speaking the pdf now becomes a probability vector as it is now defined on the lattice points only. I shall continue the discussion using the lattice SOS model, as this model is conceptually easier to solve and the results can be shown to be valid in the continuum limit anyway.

To solve for the pv of the 2d SOS surface tension model analytically it is necessary to diagonalise the transfer matrix. From the definition of the transfer function, (6.6;4), it is evident that the matrix is a d×d matrix where d is the separation of the walls. In fact the transfer matrix T has the form

$$\begin{bmatrix}
1 & e^{-\sigma} & e^{-2\sigma} & e^{-3\sigma} & \cdot & \cdot & \cdot & e^{-(d-3)\sigma} & e^{-(d-2)\sigma} & e^{-(d-1)\sigma} \\
e^{-\sigma} & 1 & e^{-\sigma} & e^{-2\sigma} & & & & e^{-(d-4)\sigma} & e^{-(d-3)\sigma} & e^{-(d-2)\sigma} \\
e^{-2\sigma} & e^{-\sigma} & 1 & e^{-\sigma} & & & & e^{-(d-5)\sigma} & e^{-(d-4)\sigma} & e^{-(d-3)\sigma} \\
\cdot & \cdot & \cdot & \cdot & \cdot & & & & & \cdot \\
\cdot & & \cdot & \cdot & \cdot & \cdot & & & & \cdot \\
\cdot & & & \cdot & \cdot & \cdot & \cdot & \cdot & & \cdot \\
\cdot & & & & & \cdot & \cdot & \cdot & \cdot & \cdot \\
e^{-(d-3)\sigma} & e^{-(d-4)\sigma} & e^{-(d-5)\sigma} & & & & e^{-\sigma} & 1 & e^{-\sigma} & e^{-2\sigma} \\
e^{-(d-2)\sigma} & e^{-(d-3)\sigma} & e^{-(d-4)\sigma} & & & & e^{-2\sigma} & e^{-\sigma} & 1 & e^{-\sigma} \\
e^{-(d-1)\sigma} & e^{-(d-2)\sigma} & e^{(-d-3)\sigma} & \cdot & \cdot & \cdot & e^{-3\sigma} & e^{-2\sigma} & e^{-\sigma} & 1
\end{bmatrix} \qquad (6.6;11)$$

The diagonalisation of T as it stands is not a trivial matter. In order to simplify the analysis a further restriction is often made to the model at this stage, whereby it is considered that the difference in height between any two consecutive positions can be no more that one unit. In the large σ limit then clearly this does not affect the physics as then larger jumps become energetically inaccessible in the ensemble anyway. The model with this restriction is consequently called the *Restricted Solid On Solid (RSOS)* model.

The effect of the restriction imposed on the RSOS model is to render the transfer function tridiagonal. The transfer matrix for the RSOS model is

$$\begin{bmatrix} 1 & e^{-\sigma} & & & & & & \\ e^{-\sigma} & 1 & e^{-\sigma} & & & & & \\ & e^{-\sigma} & 1 & e^{-\sigma} & & & & \\ & & \cdot & \cdot & \cdot & & & \\ & & & \cdot & \cdot & \cdot & & \\ & & & & \cdot & \cdot & \cdot & \\ & & & & & e^{-\sigma} & 1 & e^{-\sigma} \\ & & & & & & e^{-\sigma} & 1 \end{bmatrix} \qquad (6.6;12)$$

The eigenfunction, ψ_m, can be found numerically by iteration (Press *et al* 1986). An initial guess eigenvector $\psi_{m,0}$ is normalised so that $\psi^2=1$ and then fed into the iteration

$$\psi_{m,i+1} = \frac{T.\psi_{m,i}}{\sqrt{|T.\psi_{m,i}|^2}} \qquad (6.6;13)$$

looking at $|\psi_{m,i+1} - \psi_{m,i}|^2$ to monitor the convergence of the result.

Once the eigenvector is found then the pv is easily obtained using (6.6;9). In figure 6.2 I have plotted the results obtained numerically for several matrix dimensions d. The dotted line is the graph of $\sin^2(\pi z/d)$. It is clear that all the results of the iteration lie upon this line. Consequently the pdf must have the latter form.

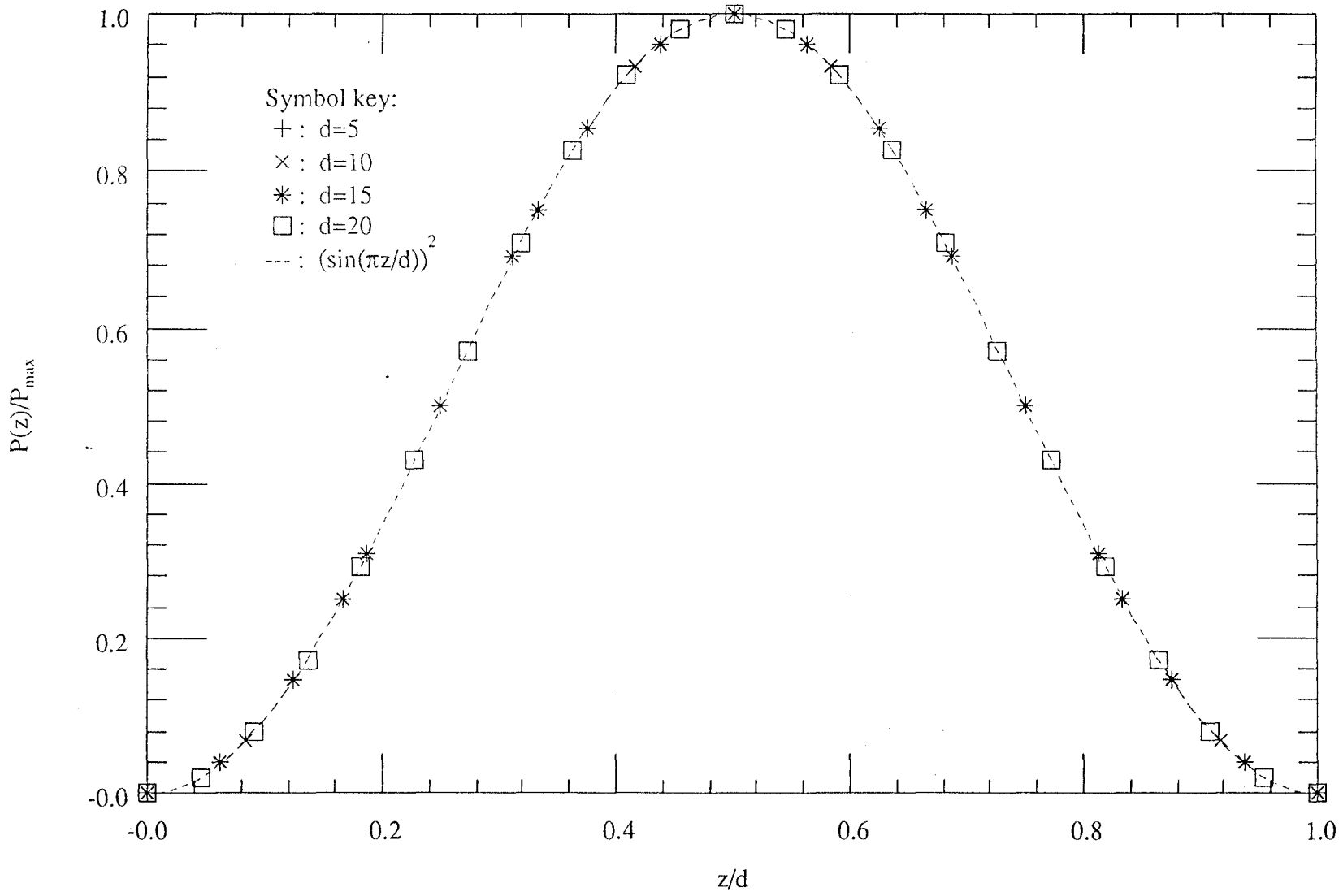

Figure 6.2

Probability distribution plot for 2-dimensional lattice model of a membrane solved by transfer matrix; varying d with κ=1.0
(Distributions normalised to have unit height)

In fact we shall see that it is possible to calculate the eigenvectors, and hence the pv (P_h), analytically. The analytical form of the eigenvector ψ_h is

$$\psi_h = \sin\left(\frac{h\pi}{d}\right) \tag{6.6;14}$$

In order to show that this is true then let $\alpha=e^{\sigma}$. Equation (6.6;7), the defining equation for the eigenvector, becomes

$$\begin{bmatrix} \alpha & 1 & & & & & & \\ 1 & \alpha & 1 & & & & & \\ & 1 & \alpha & 1 & & & & \\ & & \ddots & & & & & \\ & & & 1 & \alpha & 1 & & \\ & & & & \ddots & & & \\ & & & & & 1 & \alpha & 1 \\ & & & & & & 1 & \alpha \end{bmatrix} \begin{bmatrix} \sin(\pi/d) \\ \sin(2\pi/d) \\ \sin(3\pi/d) \\ \vdots \\ \sin(i\pi/d) \\ \vdots \\ \sin((d-3)\pi/d) \\ \sin((d-2)\pi/d) \\ \sin((d-1)\pi/d) \end{bmatrix} = \frac{\lambda_m}{\alpha} \begin{bmatrix} \sin(\pi/d) \\ \sin(2\pi/d) \\ \sin(3\pi/d) \\ \vdots \\ \sin(i\pi/d) \\ \vdots \\ \sin((d-3)\pi/d) \\ \sin((d-2)\pi/d) \\ \sin((d-1)\pi/d) \end{bmatrix} \tag{6.6;15}$$

Expanding for the i'th term on the LHS

$$\sin\left(\frac{(h-1)\pi}{d}\right) + \alpha\sin\left(\frac{h\pi}{d}\right) + \sin\left(\frac{(h+1)\pi}{d}\right) \tag{6.6;16}$$

Using trigonometric sum and difference identities to expand the sin terms

$$\left(2\cos\left(\frac{\pi}{d}\right) + \alpha\right)\sin\left(\frac{h\pi}{d}\right) \tag{6.6;17}$$

Now one can identify λm with

$$\lambda_m = \alpha\left(2\cos\left(\frac{\pi}{d}\right) + \alpha\right) \tag{6.6;18}$$

whereupon the consistency of LHS and RHS becomes self-evident proving (6.6;14) to be the correct form for the pv.

Hence we arrive at the following expression for the probability vector for the two dimensional interface

$$P_h = c\left(\sin\left(\frac{h\pi}{d}\right)\right)^2 \tag{6.6;19}$$

A crucial feature of this result is that the profile of the probability vector is only dependent on the scaling combination h/d, as opposed to depending on h and d

separately. This means that the probability of finding the membrane at a given point depends only on the relative distance of the point from the walls. Moreover the results is independent of the surface tension, $\sigma>0$. This is what universality means in this context. Note also that the result is consistent with the universal form (6.5;9) motivated by the CI argument. So this well established result lends some weight to the less formal CI argument. The associated universal scaling exponent $\phi=2$.

6.7 Analytical Result For The 2d SOS Helfrich Model pdf

In the preceding section I have discussed in detail an analytical argument which yields the universal form of the pdf of the SOS interface in 2d. In this section I write down the result of an analytical argument for the form of the SOS membrane in 2d (Parry 1992d). The argument requires an intimate knowledge of the *Theory of Wetting* which is rather tangential to the current investigation. Hence I make no attempt to present or justify the analytical argument by which the result is obtained. At any rate the argument (Parry 1992d) is to be published together with the results obtained later in this chapter.

The analytical result for the universal form of the pdf of the SOS membrane in 2d is

$$P(z) \propto \sin^{\frac{2}{3}}\left(\frac{\pi z}{d}\right) \qquad (6.7;1)$$

The argument implies that the universal exponent, ϕ, takes the value of 2/3 in the case of the SOS membrane model in 2d. The argument for this exponent is not able to support the CI argument presented in section 6.5, since the current argument relies on the latter argument for its validity. In section 6.9 I will be looking at the SOS membrane in 2d by Monte-Carlo simulation in an effort to determine, amongst other things, the value of the universal exponent, if indeed one exists.

6.8 Results Of MC Simulation Of The 2d SOS Surface Tension Model

In section 6.6 we saw an analytical solution of the 2d SOS interface model and obtained the pdf for the universal regime $N\to\infty$, $\sigma \gg 0$. In this section I present results from Monte Carlo Simulations of the SOS ensemble and compare them with the analytical results to establish the veracity of the method.

Recall that the Hamiltonian for this system is

$$H_{int} = \frac{1}{2}\sigma\int_0^L \left(\frac{dh}{dx}\right)^2 dx \qquad (6.8;1)$$

6.8.1 Approach To Universality

In order to investigate the pdf for the universal regime one must first establish if one is in the universal regime or not. Firstly we know that we will be interested in the large N limit, but how large does N need to be? Also we know that $\sigma>0$ and for realistic analysis of the functional form of the pdf d should be large (but not too large), at least for the lattice model.

To answer these important questions I initially performed a number of pilot simulations, which led to the following more systematic analysis of the approach to universality.

In the simulations I used the mean height, <h>, of the interface above the lower wall to gauge the approach to equilibrium since it is known that <h>=0 in equilibrium and since this parameter appeared in practice to equilibrate more slowly than the mean energy of the ensemble <E>.

The square width of the pdf, W^2, defined by

$$W^2 = \langle h^2 \rangle - \langle h \rangle^2 \qquad (6.8.1;1)$$

proved to be a suitable parameter for observing the approach to universality since it encapsulates most of the important information of the pdf rather concisely.

In figure 6.3 the square width is plotted against, L, the length parameter. The other control parameters: the wall separation, d, and the surface tension, σ, are at fixed values for this analysis. Subsequent analysis will show the wall separation, d=20, and the surface tension, σ=0.5, as suitable for obtaining universality. The figure indicates that the square width rapidly falls from its maximum value, at L=1, as the length of the

membrane, L, is increased. The L=1 value for the square width represents the square width for an independent oscillator. An independent oscillator has an equal probability of being found anywhere between the two walls and as such has a square shaped pdf. This explains why the square width is maximum at L=1. By L=100 the figure indicates that the square width has stopped falling. From L=200 to L=1000 (and presumably above) the square width is essentially constant and invariant of N; a clear sign of universality.

In figure 6.4 the square width is plotted against, σ, the surface tension control parameter. The other control parameters: the wall separation, d, and length parameter, L, are at fixed values. I have shown that the length parameter, L=1000, should be sufficiently large for universality and subsequent analysis will show the wall separation, d=20, is also suitable. The figure indicates that the square width falls rapidly from its maximum value, at σ=0, as the surface tension, σ, is increased. The σ=0 value for the square width represents the square width of a set of N (N=L/a) independent oscillators. The pdf of an interface of independent oscillators is, of course, the same a the pdf of a single independent oscillator. So this explains why the square width is maximum at σ=0. The figure indicates that the square width flattens out stops falling at around σ=0.5. Above σ=0.5 the square width is essentially constant; once again a clear sign of universality.

Finally, in figure 6.5 the square width is plotted against, d, the wall separation distance parameter. The other control parameters: the surface tension, σ, and the length, L, are at fixed values for this analysis. The previous analysis indicates that the length, L=1000, and the surface tension, σ=1.0, should be suitable for obtaining universality. The graph is flat and essentially featureless except from an initial dip at the d=2 value, which is possibly a finite size anomaly. The figure indicates therefore that the square width is essentially independent of the wall separation, $d \leq 20$, for these particular choices of L and σ; a clear indication of universality.

From this analysis it is apparent that a universal regime exists for the pdf. Appropriate values for the control parameters are $d \leq 20$, $\sigma \geq 0.5$, $L \geq 1000$. Clearly one could fine tune these parameters further and there is a degree of interdependence, but the work above shows that values in these regions are suitably universal.

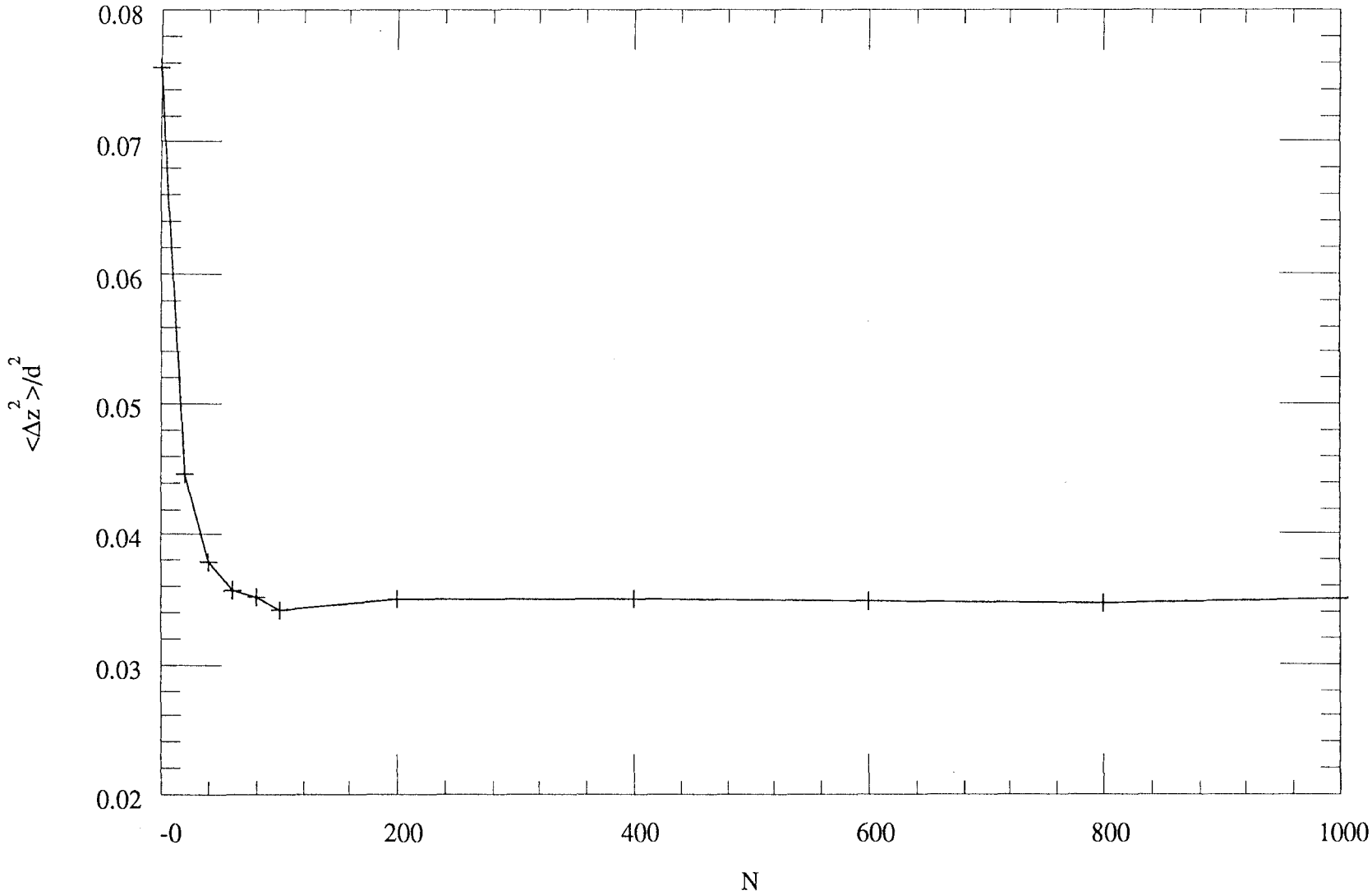

Figure 6.3
Variation of square width, W^2, of 2-dimensional interface.
(Varying N with σ=0.25 and d=20.0 (a_0=1.0))

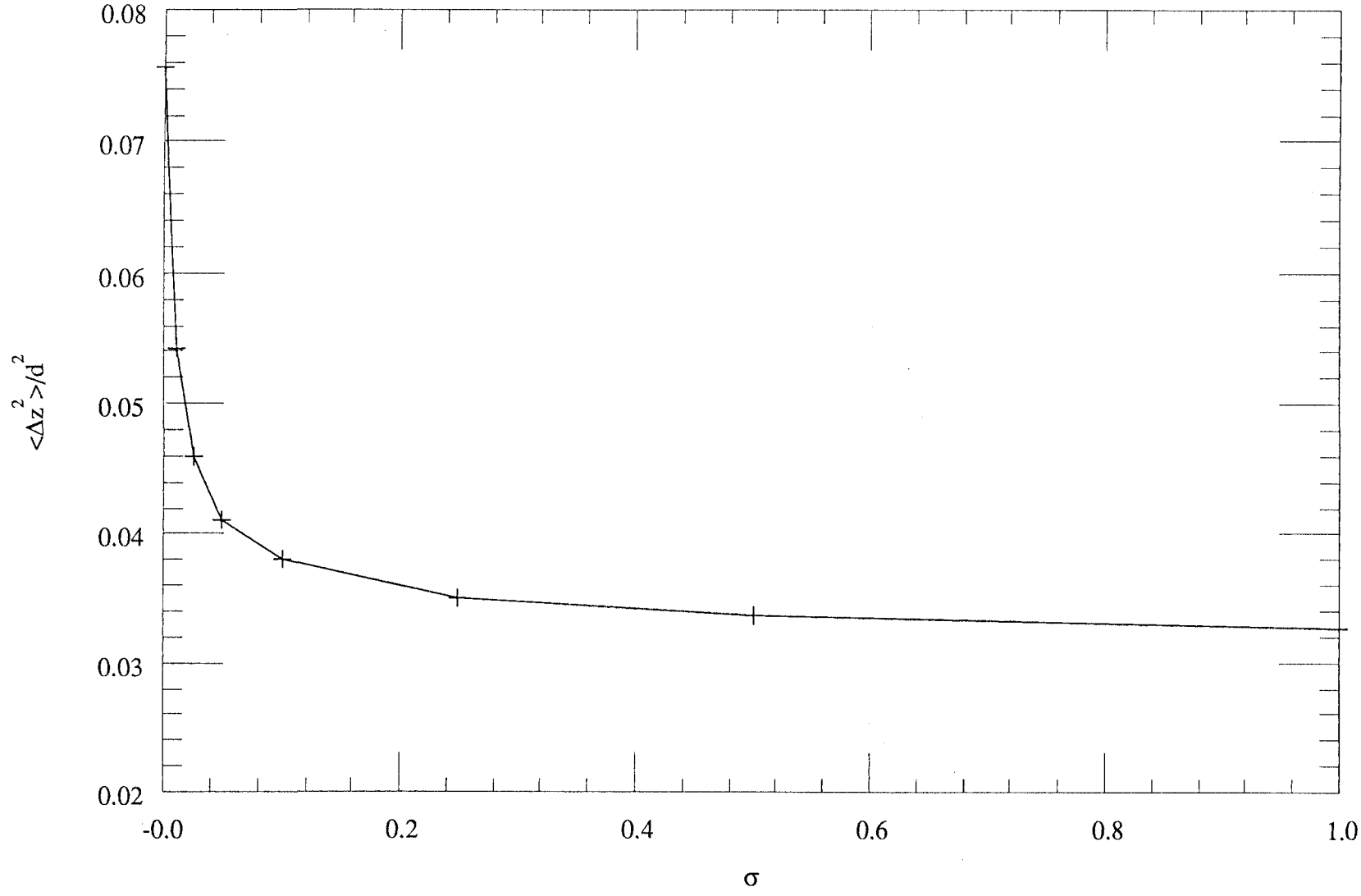

Figure 6.4
Variation of square width, W^2, of 2-dimensional interface.
(Varying σ with d=20.0 and N=1000 (a_0=1.0))

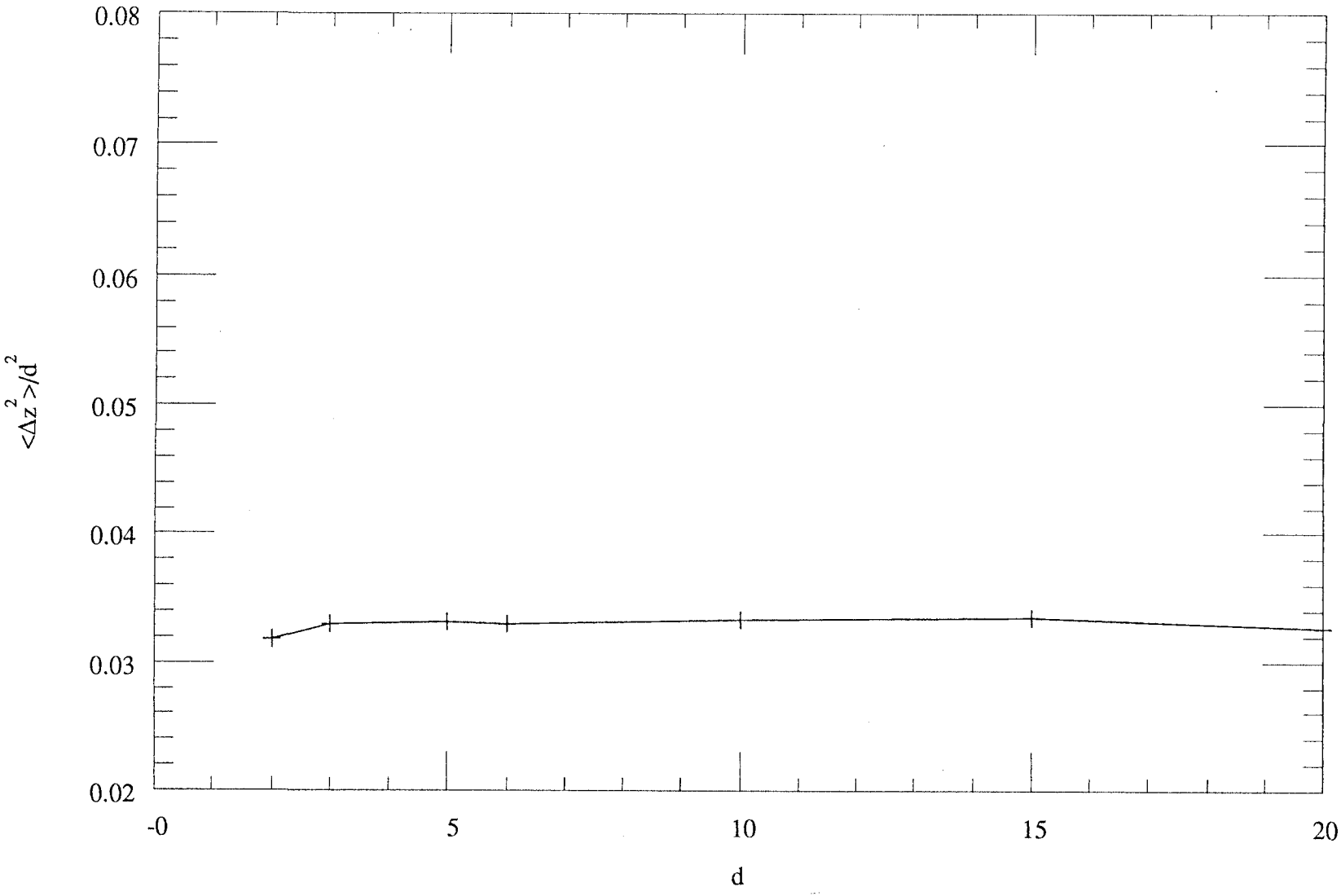

Figure 6.5
Variation of square width, W^2, of 2-dimensional interface.
(Varying d with σ=1.0 and N=1000 (a_0=1.0))

6.8.2 Short Distance Expansion For Universal pdf Near Wall

Having determined suitable values of the control parameters (N,σ,d) for analyzing the universal regime it is now necessary to analyze the results. Clearly one could analyze the results in a variety of ways; some more interesting than others. One rather simple, but interesting, method of analysis is to ask what the analytical form of the pdf is close to the wall. The method is called a *short distance expansion (SDE)* analysis because it yields an analytical form of the pdf valid at short distances from the wall.

Consider what one knows about the pdf from the experimental results. One has a set of data, $\{P_i\}$, that gives one empirically the probability of finding the interface at given regularly spaced heights from the wall. For a reasonable SDE analysis one must have several results close to the wall. Since in my simulations I decided to fix the lattice size, a=1, then this means that the wall separation, d, needs to large enough for the SDE approximation to be valid.

Now consider how to interpolate the pdf results near the walls. Consider the value of the pdf at the three lattice points nearest the wall. Figure 6.6 illustrates the scenario.

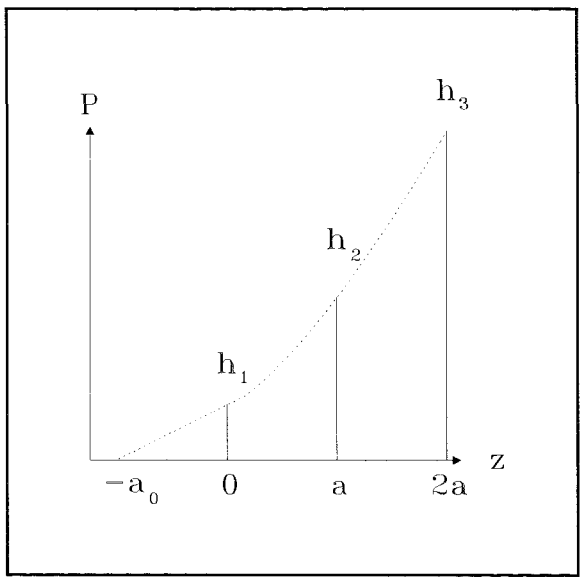

Figure 6.6
Interpolation of lattice model pdf for short distance expansion.

Each of the probabilty values are non-zero. In fact the precise position at which the pdf becomes zero is not known *a priori*. We do know however that the pdf becomes zero beyond the last lattice point. In a sense therefore, for the lattice model, the wall separation, d, is in fact only the "notional" separation of the walls. The "bare width" of the strip to which the membrane is confined is the width of the pdf $d+2a_0$; where a_0 is the distance of the extrapolated zeros of the pdf beyond the notional position of the walls.

To determine a_0 one could take the two points nearest the wall and use a linear extrapolation. However, using three points allows one to extrapolate using the following interpolation of the points.

$$P(z) = c(z + a_0)^{\phi} \tag{6.8.2;1}$$

One can show that the exponent, ϕ, corresponds to the universal exponent covered in the preceding analytical work, albeit, in the SDE limit. The parameter c is a constant of proportionality required for fitting the form to three data points, and is related to the normalisation of the pdf.

Solving (6.8.2;1) so that one obtains an interpolation of the observed probability values requires some consideration. We have three equations for the three unknowns (a_0,ϕ,c)

$$\begin{aligned} P(0) &= h_1 = c a_0^{\phi} \\ P(a) &= h_2 = c(a + a_0)^{\phi} \\ P(2a) &= h_3 = c(2a + a_0)^{\phi} \end{aligned} \tag{6.8.2;2}$$

where (h_1,h_2,h_3) are known from the simulation experiments. Solving these equations for ϕ one gets the following transcendental equation

$$\left(\frac{h_3}{h_1}\right)^{\frac{1}{\phi}} - 2\left(\frac{h_2}{h_1}\right)^{\frac{1}{\phi}} = -1 \tag{6.8.2;3}$$

which in general has to be solved numerically. Since we have an idea of the value of the universal exponent, ϕ, then the method of bisection (see Press *et al* 1986) around that value is the simplest approach to solving the equation. We make the association

$$B(\phi) = 2\left(\frac{h_2}{h_1}\right)^{\frac{1}{\phi}} - \left(\frac{h_3}{h_1}\right)^{\frac{1}{\phi}} - 1 \tag{6.8.2;4}$$

then we want the root (there should only be one) of $B(\phi)$.

Having determined a value for the exponent ϕ, by finding the root of $B(\phi)$, it is possible to procede analytically to evaluate the remaining unknowns. It can be shown that

$$a_0 = \frac{a}{(h_2/h_1)^{1/\phi} - 1} \qquad (6.8.2;5)$$

which can now be evaluated directly. Moreover it is possible to show that

$$c = \frac{h_1}{a_0^{\phi}} \qquad (6.8.2;6)$$

which, having determined ϕ and a_0, can also be evaluated directly.

Now from simulation experiments I have obtained the values for h_1, h_2 and h_3 displayed table 6.1.

z	$P(z)/P_{max}$
0	0.0211
a	0.0807
2a	0.1726

Table 6.1

Note that the probability values in table 6.1 have been averaged so that the pdf which they represent is correctly symmetrical. This averaging acts so as to improve the quality of the results. Also the results above are normalised so that the pdf has unit height rather than unit area (the usual normalisation).

Following the analysis described above and using the data in table 6.1 I obtained $\phi=1.806\pm1$ from the bisection. The error band represents the accuracy of the bisection in determining the root rather than the accuracy of the universal exponent due to imperfect source data. In fact the difference of the SDE result for the universal scaling exponent, ϕ, from the analytical exponent consists of two components. One component is the accuracy of the data in table 6.1 the other is the systematic error that arises from the short distance approximation of the result.

Further evaluating (6.8.2;5) yields the value 0.91 (approx 1) for, a_0, the root of the pdf. So the root of the pdf lies approximately one lattice unit beyond the nominal wall position. In retrospect, we can see that this is consistent with the result of the transfer matrix calculations and the analytical results, presented in section 6.6. In the transfer matrix argument the zero point of the pdf was implicitly assumed to be exactly one unit beyond the possibly sites occupied by the interface.

The value of the normalising constant, c, could now be determined. However I shall refrain since it is of little interest and is of no further use.

Having determined the location of the roots of the pdf, a_0 it is now possible to plot out the universal pdfs with the roots included. Several pdfs in the universal regime have been plotted in figure 6.7. The graphs have been normalised to have unit height and are plotted against $z^*=(z+a_0)/(2a_0+d)$. The universality is evident from the way in which the pdfs coincide with one another.

It should also be noted that the effective widening of the confining strip for the lattice model affects the evaluation of the square width, W^2, of the interface. Note that this effect has been taken into consideration and close inspection of the preceding figures of the interface square width, W^2, will reveal that they have been handled appropriately.

6.8.3 Global Form Analysis Of Universal pdf

Having established the location of the zeros of the pdf using the SDE analysis it is now possible to perform the global form analysis of the universal regime. We already know suitable values for the control parameters: length, L, surface tension, σ and wall separation, d, for universality.

To establish the functional form of these pdfs I have plotted in figure 6.6 $\log(P(z^*)/P_{max})$ against $\log(\sin(\pi z^*))$. The significance of this plot is that a straight line implies that

$$P(z^*) \propto (\sin(\pi z^*))^{\phi} \qquad (6.8.3;1)$$

and moreover the slope of the line is ϕ.

Figure 6.8 is clearly linear verifying (6.8.3;1) and the slope is consistent with $\phi=2$, as shown by the analytical arguments in section 6.6.

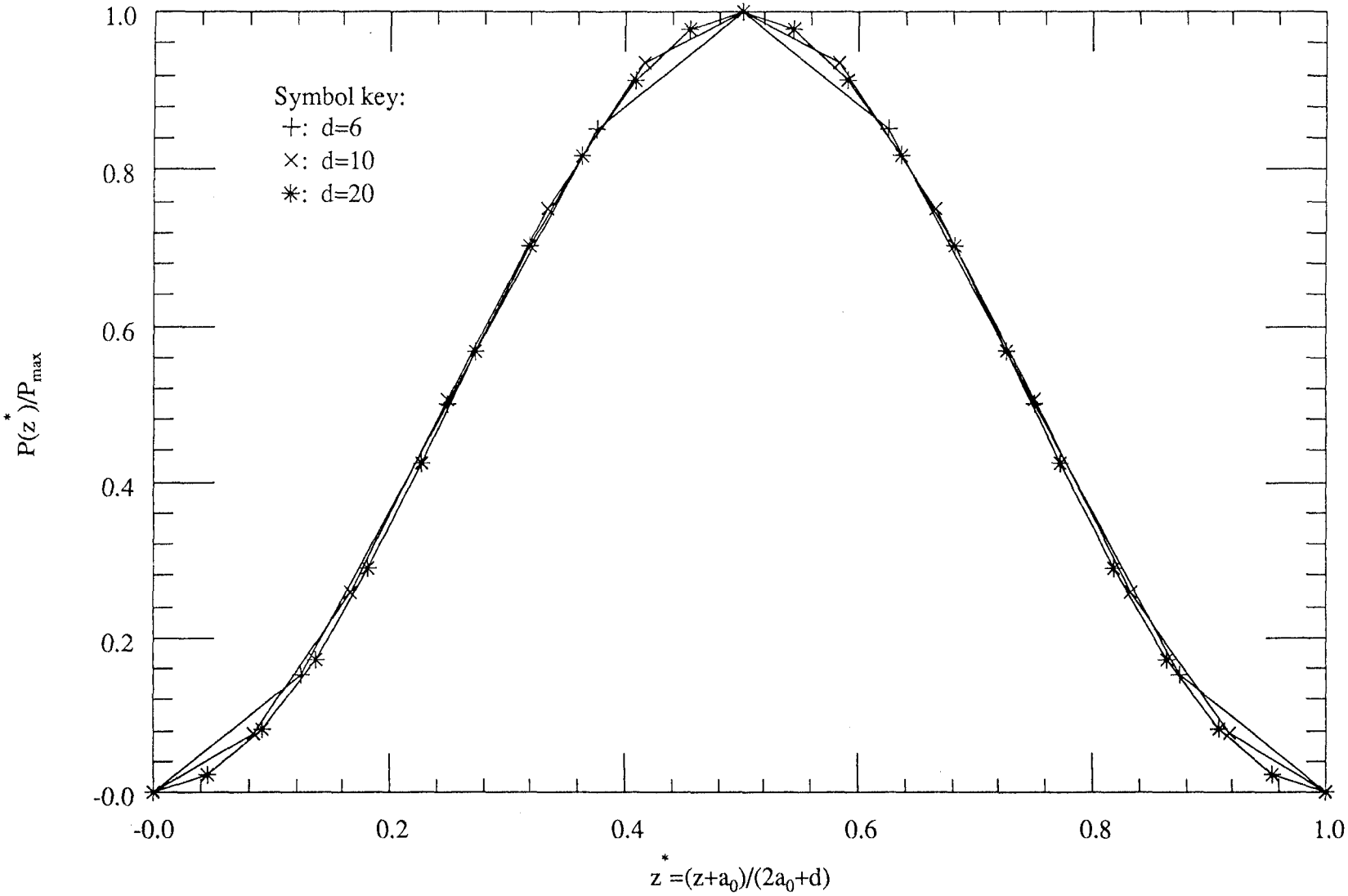

Figure 6.7

Probability distribution plot for 2-dimensional lattice model of an interface; varying d with σ=1.0 and N=1000. (Distributions normalised to have unit height and a_0=1.0)

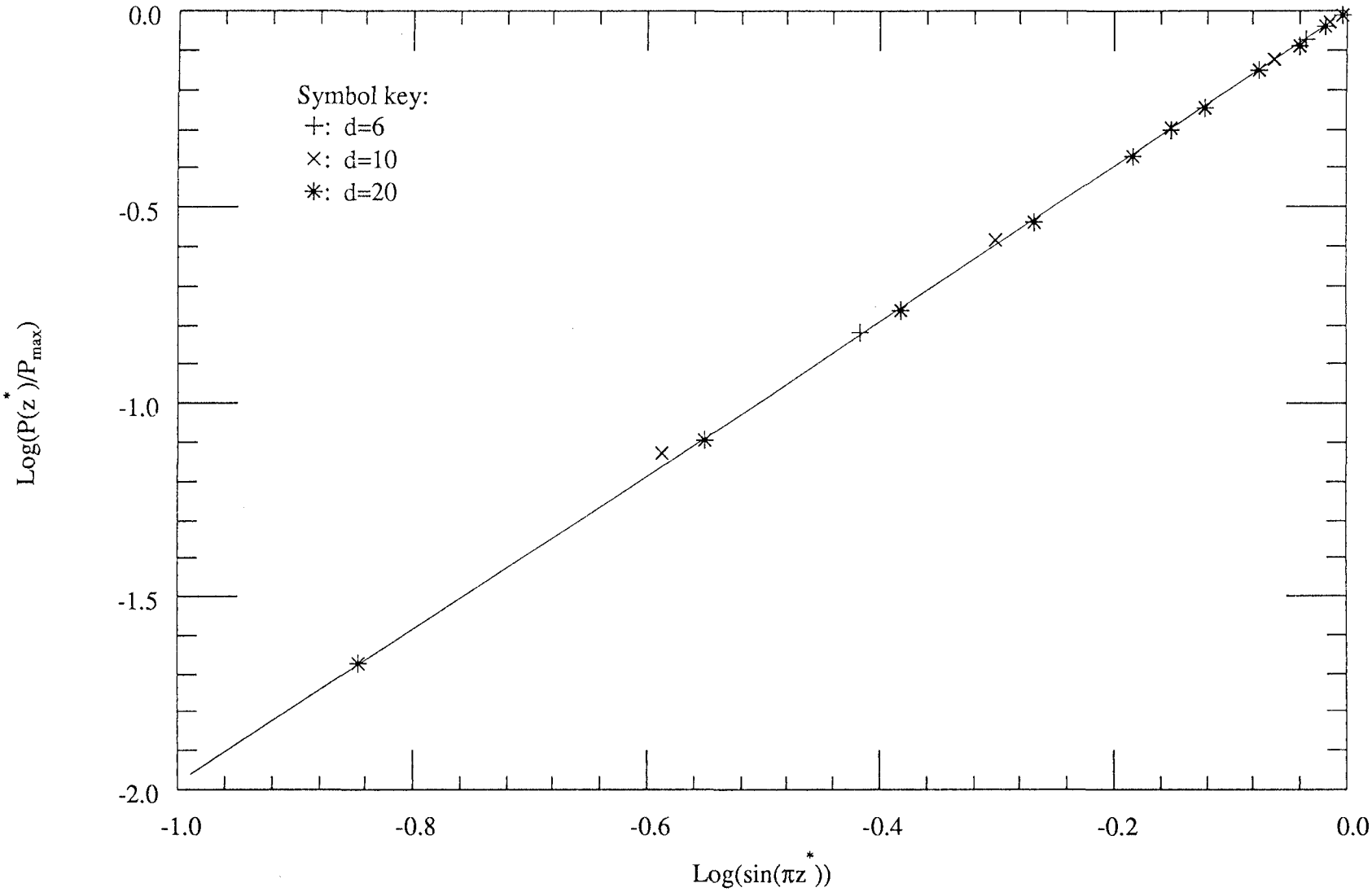

Figure 6.8

Log(sin(πz^*)) plot for 2-dimensional lattice model of an interface; $z^*=(z+a_0)/(2a_0+d)$.
(Varying d with σ=1.0 and N=1000)

6.9 Results Of MC Simulation Of The 2d SOS Helfrich Model

In section 6.4 we saw some tentative analytical arguments which suggested a form for the pdf in the universal regime $N\to\infty$, $\kappa\gg 0$. I present here the results from Monte Carlo simulations of the Helfrich ensemble and compare them with the analytical results.

Recall that the Hamiltonian for this system is

$$H_{mem} = \frac{1}{2}\kappa\int_0^L\left(\frac{d^2h}{dz^2}\right)^2 dz \qquad (6.9;1)$$

6.9.1 Approach to Universality

As in section 6.8.1. one again has to determine suitable values of the control parameters for investigating the universal regime. I adopt the same step by step analysis of the parameter space to find the universal regime.

Once again, I found it was useful to use the mean height of the membrane, $\langle h\rangle$, to observe the equilibration of the simulations. Further I used the square width, W^2, of the pdf (6.8.1;1) in order to indicate the approach of the pdfs to universality.

In figure 6.9 the square width is plotted against, L, the length parameter (c.f. figure 6.3). The other control parameters: the wall separation, d, and the curvature elasticity, κ, are at fixed values for this analysis. Subsequent analysis will show the wall separation, d=20, and the curvature elasticity, κ=0.5, as suitable for obtaining universality. The figure indicates that the square width has its maximum value, at L=1. The L=1 value for the square width represents the square width for an independent oscillator. In fact, rather surprisingly, the square width of the pdf appears to be independent of N over the range of simulated lengths, $50\le L\le 1000$. However for sufficiently short lengths there is, presumably, a crossover to the independent oscillator value. Comparison with the interface (figure 6.3) indicates that the membrane approaches universality rather faster than the interface. One should be quite safe in expecting universality for $L\ge 1000$.

In figure 6.10 the square width is plotted against, κ, the curvature elasticity control parameter (c.f. figure 6.4). The other control parameters: the wall separation, d, and length parameter, L, are at fixed values. I have shown that the length parameter,

L=1000, should be sufficiently large for universality and subsequent analysis will show the wall separation, d=20, is also suitable. The figure indicates that the square width falls rapidly from its maximum value, at $\kappa=0$, as the curvature elasticity parameter, κ, is increased. The $\kappa=0$ value for the square width represents the square width of a set of N (N=L/a) independent oscillators. This explains why the square width is maximum at $\kappa=0$. The figure indicates that the square width flattens out stops falling at around $\kappa=0.05$. Above $\kappa=0.05$ the square width is essentially constant; once again a clear sign of universality. Direct comparison with the interface (figure 6.4) is not quite meaningful in the sense that the control parameters do not represent the same quantity. However a direct comparison indicates that membrane approaches universality at a lower value of the elasticity constant than the interface.

Finally, in figure 6.11 the square width is plotted against, d, the wall separation distance parameter. The other control parameters: the curvature elasticity, κ, and the length, L, are at fixed values for this analysis. The previous analysis indicates that the length, L=1000, and the surface tension, $\kappa=0.25$, should be suitable for obtaining universality. The figure indicates that the square width drops steadily and flattens out as the wall separation, d, is increased. For wall separations of $d\geq15$ the square width would seem close to the asymptotic value. The figure therefore indicates that one should expect to be able to observe universality for $d\geq15$. Comparison with the interface (figure 6.5) indicates that the membrane is rather more strongly affected by the separation of the walls, d, in its approach to universality.

From this analysis it is apparent that a universal regime exists for the pdf. Appropriate values for the control parameters are $d\geq15$, $\kappa\geq0.05$, $L\geq1000$. Clearly one could fine tune these parameters further and there is a degree of interdependence, but the work above shows that values in these regions are suitably universal.

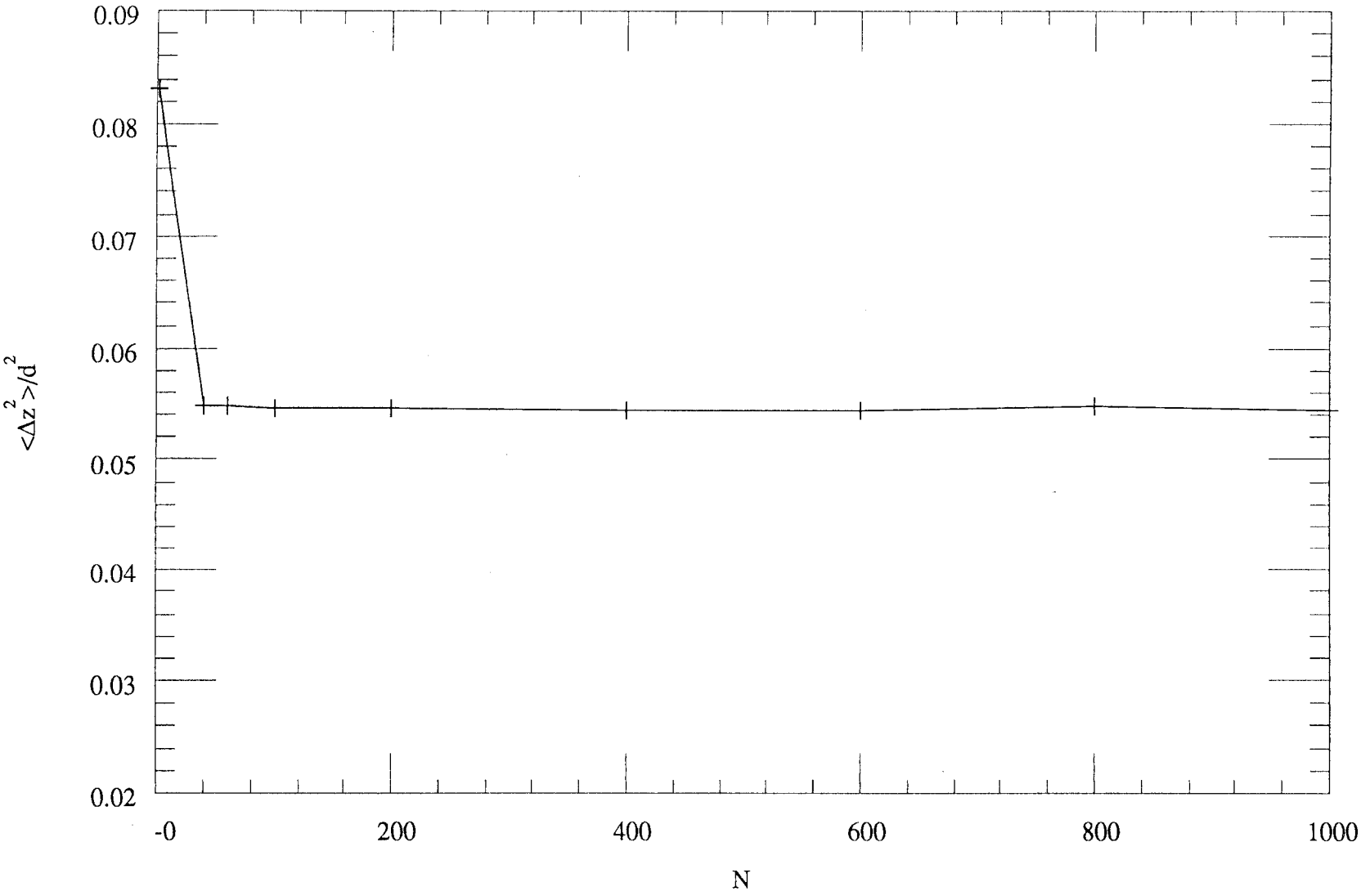

Figure 6.9
Variation of square width, W^2, of 2-dimensional membrane.
(Varying N with κ=0.5 and d=20.0 (a_0=0.5))

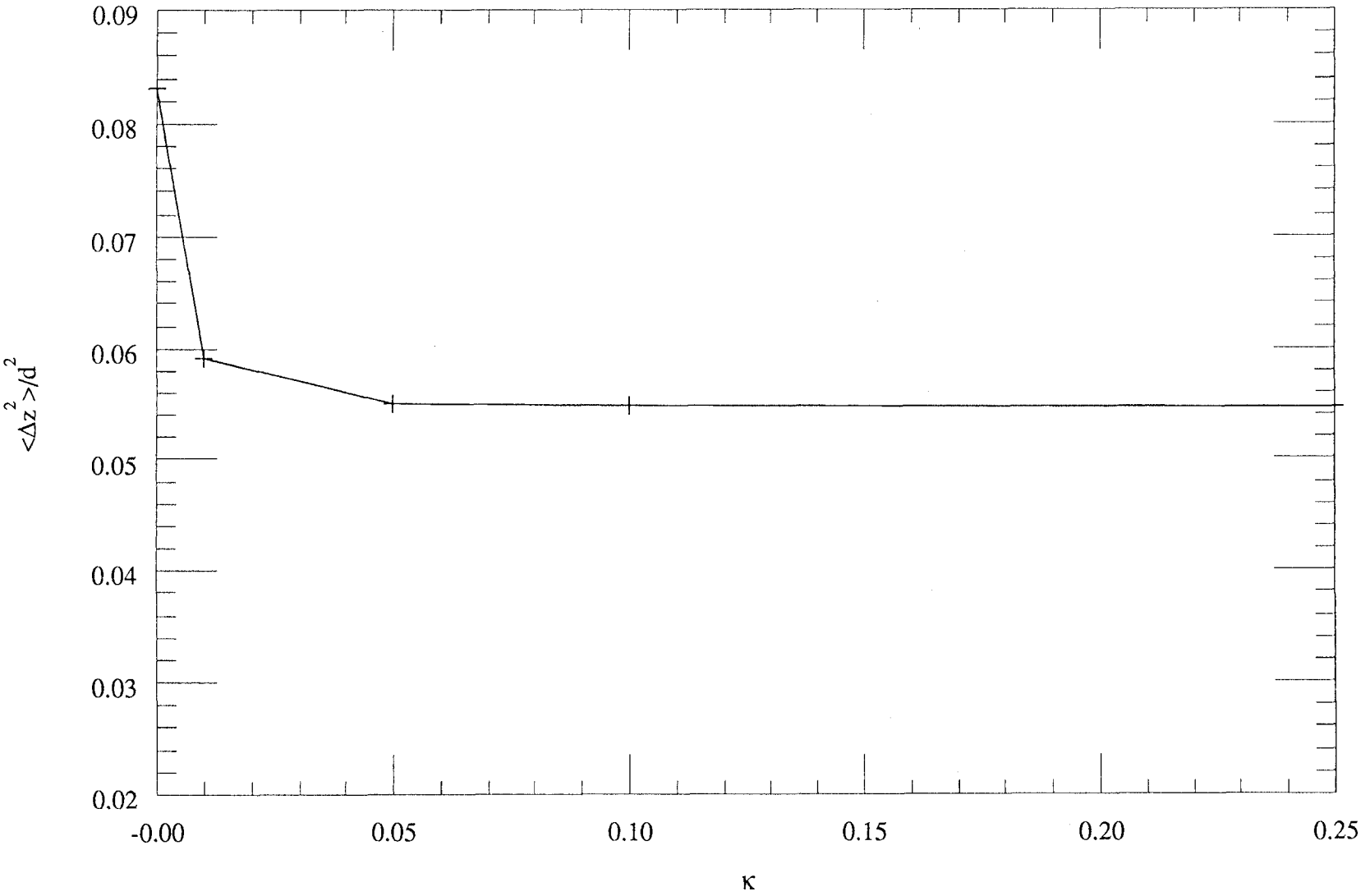

Figure 6.10
Variation of square width, W^2, of 2-dimensional membrane.
(Varying κ with d=20.0 and N=1000 (a_0=0.5))

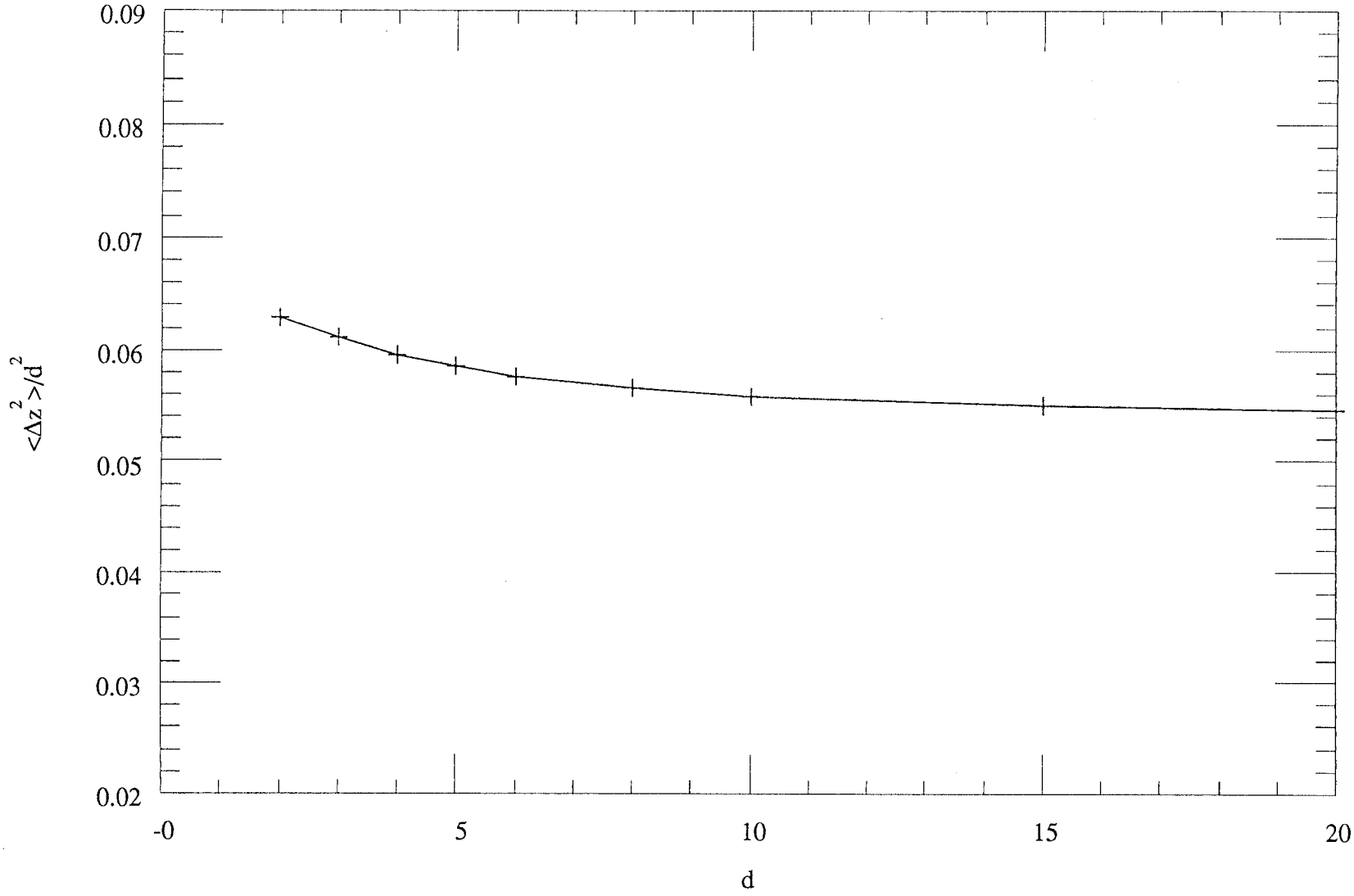

Figure 6.11
Variation of square width, W^2, of 2-dimensional membrane.
(Varying d with κ=0.25 and N=1000 (a_0=0.5))

6.9.2 Short Distance Expansion For Universal pdf Near Wall

Once again having determined suitable values of the control parameters (N,κ,d) for analyzing the universal regime it is now necessary to analyze the results. The analysis proceeds in much the same way as for the interface.

Recall that a short distance approximation of the postulated universal form of the pdf is

$$P(z) = c(z + a_0)^{\phi} \qquad (6.9.2;1)$$

where $z=-a_0$ is the zero that we require for our non-local analysis and c is a constant of proportionality corresponding to the normalisation constant of the non-local pdf.

Now from the simulation experiments I have obtained values for h_1, h_2 and h_3 displayed in table 6.2.

z	$P(z)/P_{max}$
0	0.171
a	0.337
2a	0.478

Table 6.2

Following the analysis described in section 6.8.2 and using the data in table 6.2 I obtained $\phi=0.748\pm1$ from the bisection. Again the error band represents the accuracy of the bisection in determining the root rather than the accuracy of the universal exponent due to imperfect source data. As before the difference of the SDE result for the universal scaling exponent, ϕ, from the analytical exponent consists of two components. One component is the accuracy of the data in table 6.1 the other is the systematic error that arises from the short distance approximation of the result.

Further evaluating (6.8.2;5) yields the value 0.67 (approx ½) for, a_0, the root of the pdf. So the root of the pdf lies approximately half a lattice unit beyond the nominal wall position.

The value of the normalising constant, c, could now be determined. However I shall refrain since it is of little interest and is of no further use.

Having determined the location of the roots of the pdf, a_0 it is now possible to plot out the universal pdfs with the roots included. Several pdfs in the universal regime have been plotted in figure 6.12. The graphs have been normalised to have unit height and are plotted against $z^*=(z+a_0)/(2a_0+d)$. The universality is evident from the way in which the pdfs coincide with one another.

It should also be noted that the effective widening of the confining strip for the lattice model affects the evaluation of the square width, W^2, of the interface. Note that this effect has been taken into consideration and close inspection of the preceding figures of the membrane square width, W^2, will reveal that they have been handled appropriately.

6.9.3 Global Form Analysis Of Universal pdf

Having established suitable values for the control parameters: length, L, curvature elasticity, κ, and wall separation, d, for the universal regime and with the extra information about the location of the zeros of the pdf it is now possible to present and analyze the universal regime consistently.

As in section 6.8.3, in order to establish the functional form of these pdfs I have plotted in figure 6.13 $\log(P(z^*)/P_{max})$ against $\log(\sin(\pi z^*))$. The significance of this plot is that a straight line implies that

$$P(z^*) \propto (\sin(\pi z^*))^{\phi} \qquad (6.9.3;1)$$

and moreover the slope of the line yields the universal exponent ϕ.

Figure 6.13 is clearly linear verifying the universal form (6.9.3;1). Moreover the slope indicates that the universal index, $\phi=0.72\pm0.05$. This value is not inconsistent with the value predicted by the analytical arguments discussed in section 6.7 although, at 2/3, the analytical results represents the lower bound of the 'experimental' value obtained here.

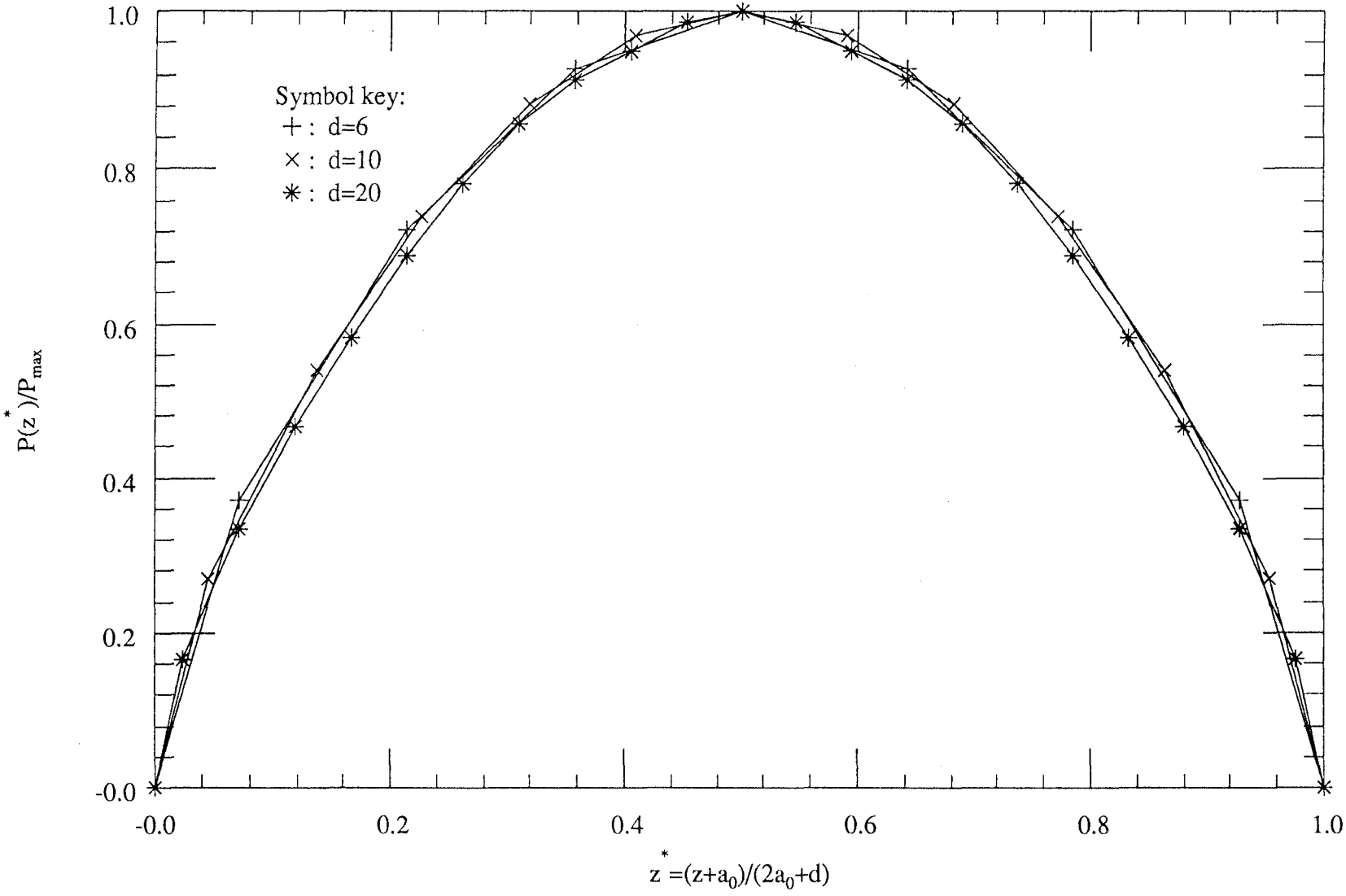

Figure 6.12

Probability distribution plot for 2-dimensional lattice model of a membrane; varying d with κ=1.0 and N=1000
(Distributions normalised to have unit height and a_0=0.5)

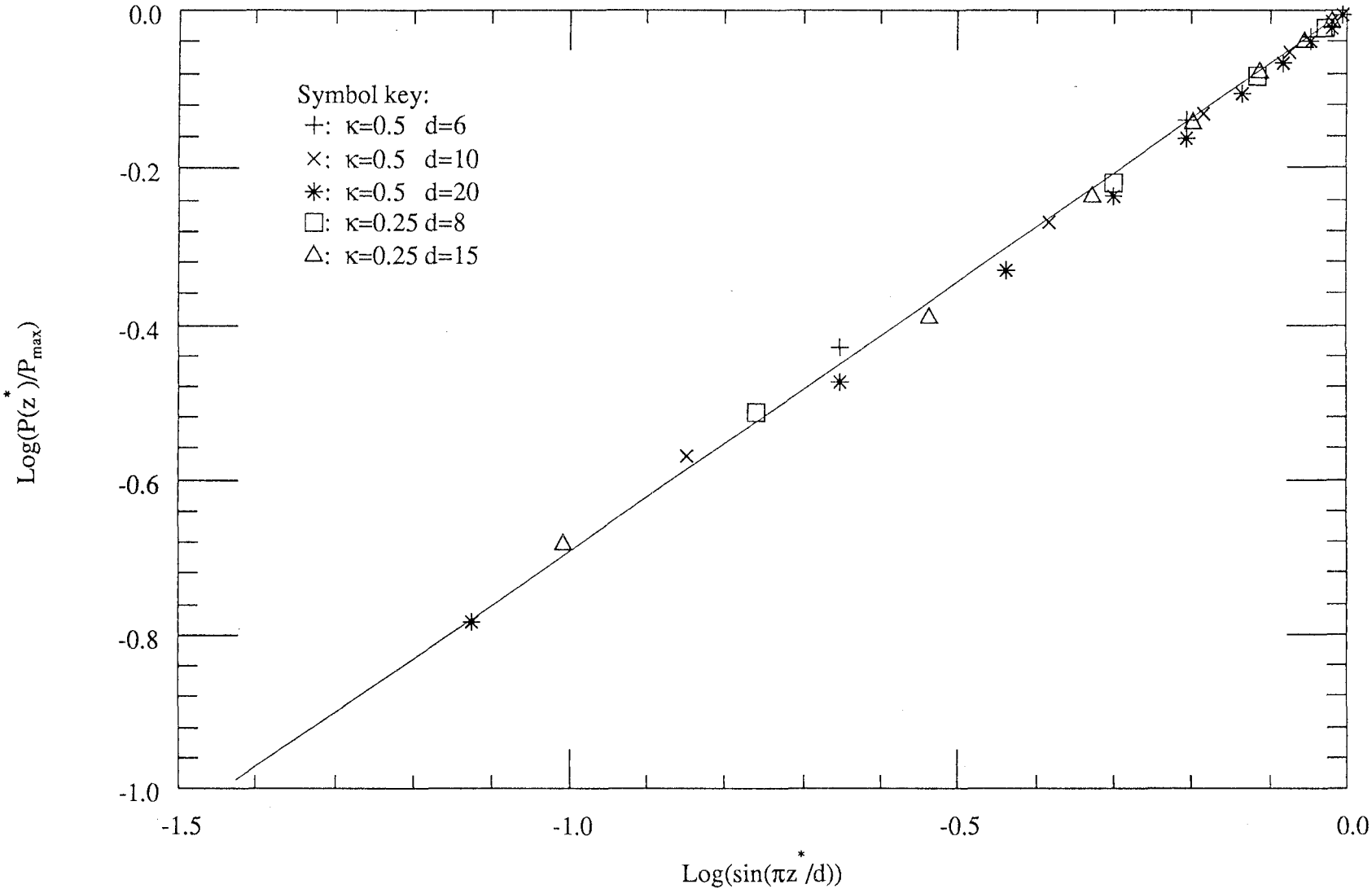

Figure 6.13

Log(sin(πz/d)) plot for 2-dimensional lattice model of a membrane;$z^{*}=(z+a_0)/(2a_0+d)$.
(Varying κ and d with N=1000)

6.10 Results Of MC Simulation Of The 3d SOS Surface Tension Model

I have not presented any analytical arguments so far that can predict the functional form for the SOS model of an interface in three dimensions as the analysis turns out to be far too involved to make any significant progress on the problem. However the simulation problem in three dimensions is not significantly more difficult conceptually than in two. Hence I am able to present results of an investigation into the three dimensional model here.

The Hamiltonian for the two dimensional system was discussed in section 6.3; see (6.3;2). The analogous Hamiltonian for the three dimensional system is

$$H_{int} = \frac{\sigma}{2a^3} \sum_{(i,j)=1}^{N} \left((h_{(i,j)} - h_{(i+1,j)})^2 + (h_{(i,j)} - h_{(i,j+1)})^2 \right) \qquad (6.10;1)$$

Additionally the Hamiltonian is applied periodically so that

$$h_{(N+1,j)} = h_{(0,j)} \qquad \text{and} \qquad h_{(i,N+1)} = h_{(i,0)} \qquad (6.10;2)$$

6.10.1 Approach to Universality

As in the previous investigations the first task is to establish where, or indeed if a universal regime exists. The physical control parameters are basically the same as for the 2d model; (L,σ,d). However the parameter L now represents the length of a square shaped interface region and so the number of interface points under observation is L^2 rather than L.

An important consequence of this is that doubling the length of the membrane involves quadrupling the number of interface points. Since one wants to look for universality as $L \to \infty$ this has a significant effect on the computational workload. In fact the number of Monte Carlo timesteps per interface point required for equilibration is significantly larger in three dimensions than two. This, together with the former problem, conspires to limit the range of observable L so that effectively $L \leq 20$ (with more computational power this could be increased somewhat but the problem is still fundamentally non-linear).

As in the two dimensional models I have used the mean height, $\langle h \rangle$, of the interface to observe the equilibration of the interface. Further I used the square width, W^2, of the interface to investigate the approach to universality of the interface.

In figure 6.15 the square width is plotted against, d, the wall separation distance parameter. The length control parameter, L, is at a fixed value; L=20. This represents the largest system realisable, computationally. Several curves have been plotted each corresponding to a different value of the surface tension constant, σ. The curves are therefore curves of "iso-elasticity". The figure reveals that at low surface tensions ($\sigma \leq 0.05$) the square width slowly falls as the separation distance of the walls, d, is increased. At sufficiently large surface tensions ($\sigma \geq 0.025$) however it is apparent that the behaviour of the square width changes. After initially falling as the walls are drawn apart the square width then appears to rise as the walls are separated further. For none of the results is the square width entirely independent of the wall separation. Thus it cannot be said that these results display any degree of universal behaviour for the wall separation, d. The probable reason for this is that the size of the interface, L=20, is too small; i.e. the non-universality is a finite-size (FS) effect.

Finally, in figure 6.16 the square width is plotted against, σ, the surface tension control parameter. The length control parameter, L, is at a fixed value; L=20. Again this represents the largest system realisable, computationally. Several curves have been plotted each corresponding to a different value of the wall separation distance, d. The results indicate that for narrow wall separations, $d \leq 8$, the square width initially falls quite rapidly as the surface tension parameter, σ, is increased. As the surface tension is further increased the square width falls more slowly and the curves begin to flatten, an indication perhaps of a degree of universality. However for systems whose walls are wider, $d \geq 10$, and at sufficiently large surface tensions the square width stops falling and begins to rise. Thus the initial indications of a fragile universality prove to be unfounded. Again, the probable reason for the non-universality of the results is that the size of the interface, L=20, is too small; i.e. the non-universality is a finite-size (FS) effect.

From this analysis it is evident that a universal regime, if one exists, is not achievable for computationally realisable sizes of membrane, $L \leq 20$. All the non-universal behaviour of the results could be due to FS effects. If one could garner enough computational power to tackle large systems it is possible that a universal regime may be achievable.

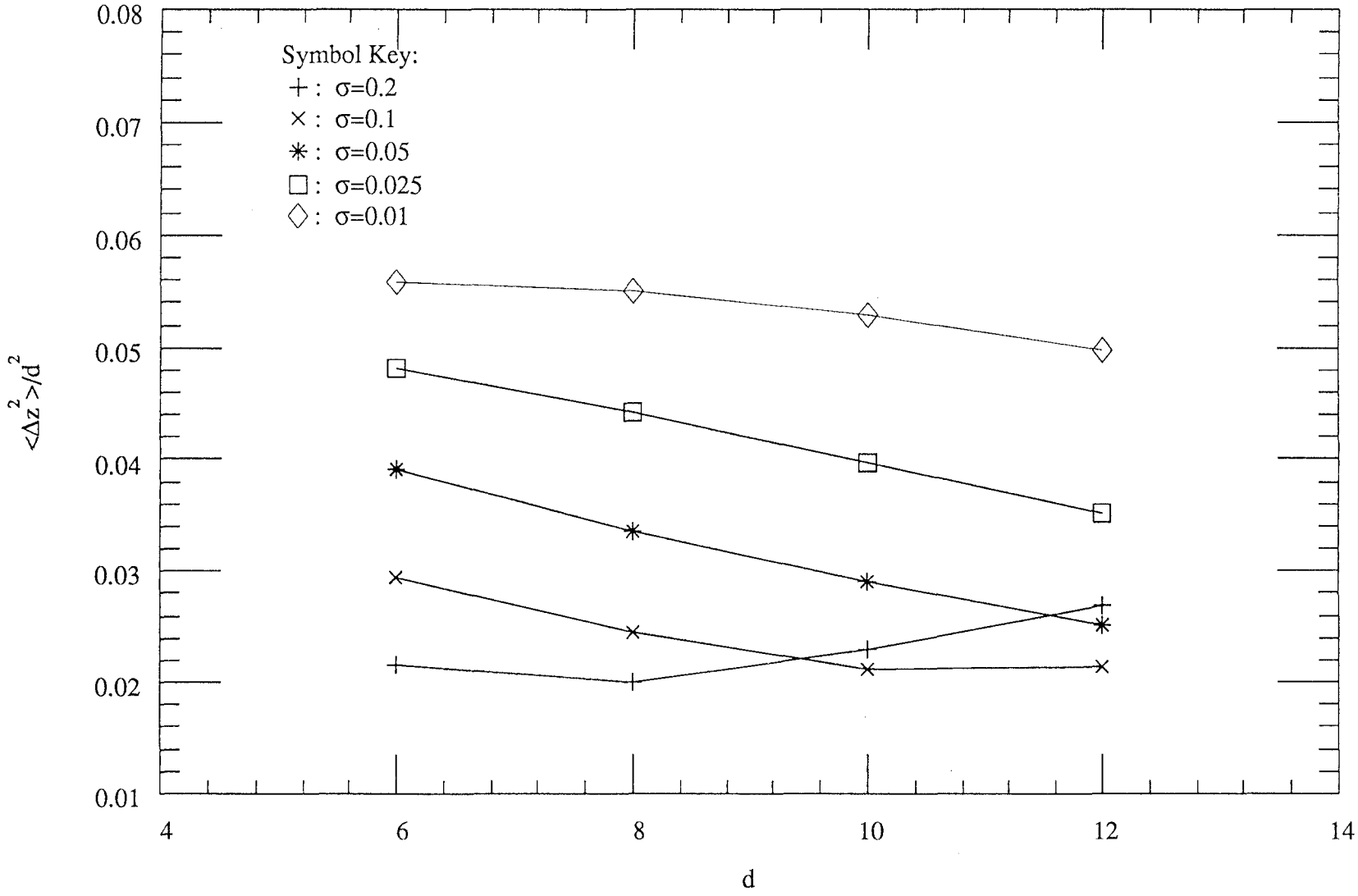

Figure 6.14
Variation of square width, W^2, of 3-dimensional interface.
(Varying d and σ with N=20 (a_0=1.0))

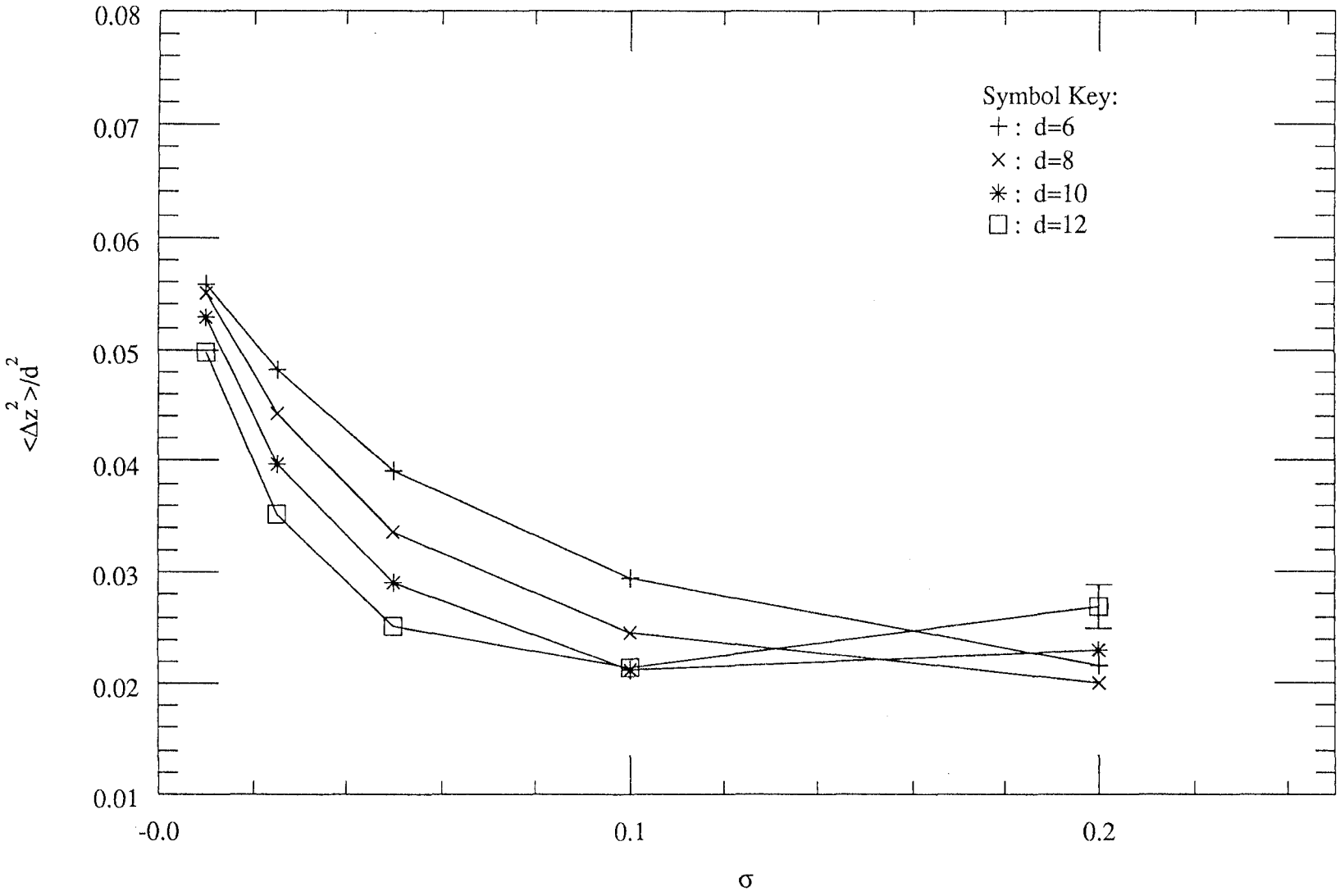

Figure 6.15
Variation of square width, W^2, of 3-dimensional interface.
(Varying d and σ with N=20 (a_0=1.0))

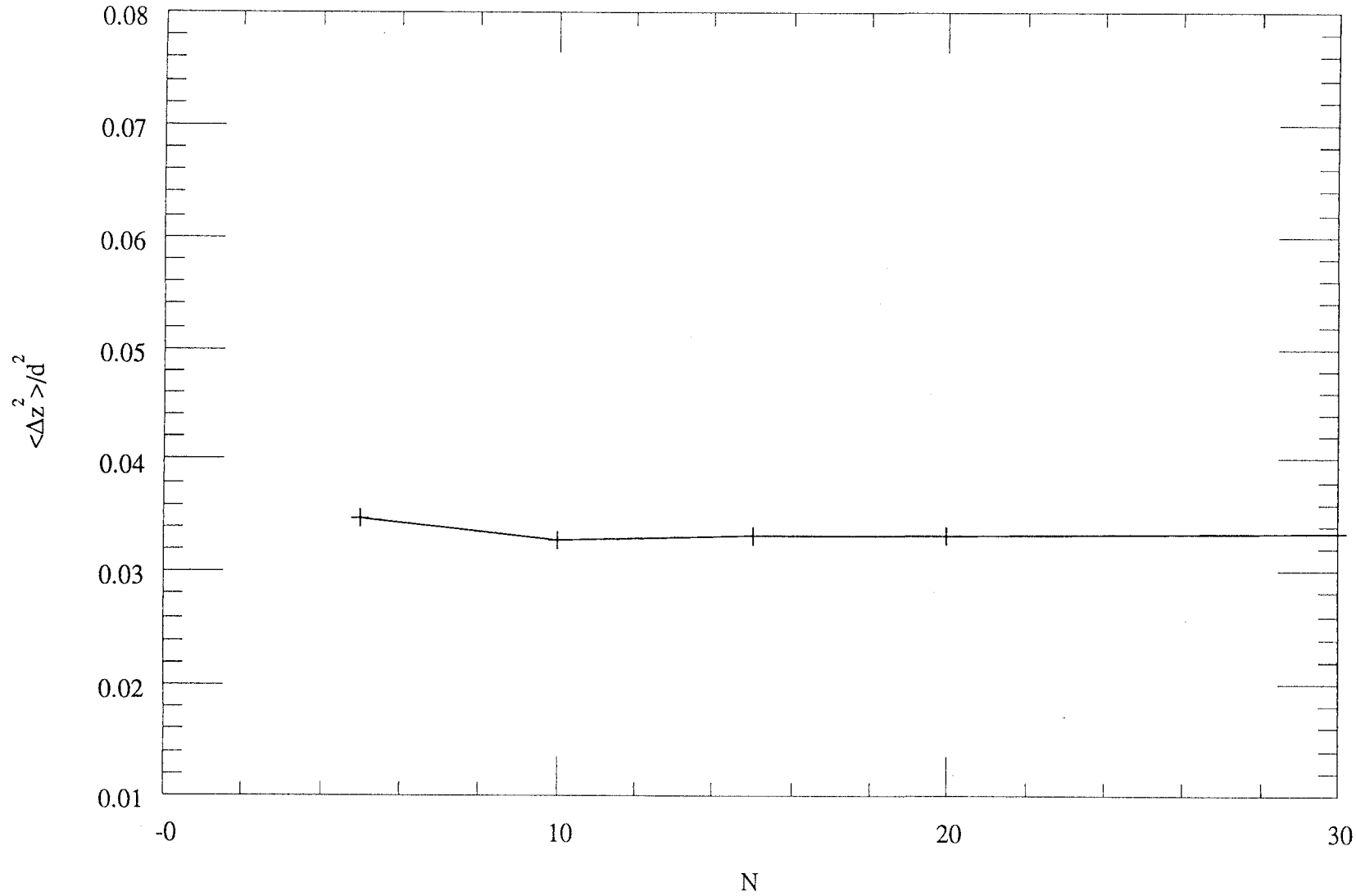

Figure 6.16
Variation of square width, W^2, of 3-dimensional interface.
(Varying N with d=12.0 and σ=0.025 (a_0=1.0))

6.11 Results Of MC Simulation Of The 3d SOS Helfrich Model

I have not presented any analytical arguments that can predict the functional form for the SOS model of a membrane in three dimensions. In fact the analysis is far too involved for any significant progress on the problem. In contrast to the problems encountered with the analytical work the simulation problem is no more difficulty conceptually in three dimensions than in two. In this chapter I present the results of an investigation of the three dimensional model. I shall show that there is good evidence for a universal regime. I shall show however that the universal regime does not appear to have the same functional form as the two dimensional systems.

The Hamiltonian for the three dimensional system is

$$H_{mem} = \frac{\kappa}{2a^3} \sum_{(i,j)=1}^{N} \left(\left(h_{(i-1,j)} + h_{(i+1,j)} - 2h_{(i,j)} \right)^2 + \left(h_{(i,j-1)} + h_{(i,j+1)} - 2h_{(i,j)} \right)^2 \right) \qquad (6.11;1)$$

Additionally the Hamiltonians are again applied periodically so that

$$h_{(N+1,j)} = h_{(0,j)} \qquad \text{and} \qquad h_{(i,N+1)} = h_{(i,0)} \qquad (6.11;2)$$

6.11.1 Approach to Universality

Once again the first problem one encounters investigating the universal form of the pdf is to establish where and indeed whether a universal form exists. The physical control parameters are essentially the same as for the 2d membrane model; (L,κ,d). However, as for the 3d interface, the length parameter, L, now represents the length of a square shaped membrane region. So the number of membrane points in the simulation is L^2 as opposed to L.

Clearly this has important consequences for the computational workload considerations as for the interface (section 6.1). The number of Monte-Carlo timesteps per membrane point required for equilibration is also significantly larger in three dimensions than two. This together with the former problem limits the range of attainable lengths for the membrane so that effectively $L \leq 20$.

As in the two dimensional models I have used the mean height, <h>, of the membrane, <h>, to monitor the equilibration of the membrane. Further I have used the square width, W^2, of the membrane to investigate the approach to universality of the membrane.

In figure 6.17 the square width is plotted against, L, the length parameter of the membrane. The other control parameters: the separation distance of the walls, d, and the curvature elasticity, κ, are at fixed values for this analysis. Subsequent analysis will indicate that the wall separation distance, d=10, and the curvature elasticity, κ=0.2, are suitable for observing universality. The figure indicates that the square width falls quite rapidly from a maximum value at L=1. At L=1 the membrane is an independent oscillator which explains the maximum. By L=10 the square width has ceased falling and remains constant as the length is increased further; a clear sign of universality. N.B. the universal behaviour appears to set in at a surprisingly low length of membrane (compared to the separation of the walls).

Next in figure 6.18 the square width is plotted against, d, the separation distance of the walls. The length control parameter, L, is at a fixed value; L=20. This represents the largest computationally realisable system. Several curves have been plotted each corresponding to a different value of the curvature elasticity constant, κ. The curves are therefore curves of "iso-elasticity". The figure shows that at low curvature elasticities ($\kappa \leq 0.025$) the square width falls slowly as d is increased. At higher curvature elasticities ($\kappa \geq 0.05$) the figure indicates that the square width is essentially constant, independent of d, within the bounds of experimental error. Clearly this universal behaviour is a good indication of a universal regime.

Finally in figure 6.19 the square width is plotted against, κ, the curvature elasticity control parameter. The length control parameter, L, is at a fixed value; L=20. Again this represents the largest computationally realisable system. Several curves have been plotted each corresponding to a different value of the wall separation distance, d. The results indicate that the square width falls quite rapidly from its maximum value at κ=0. When κ=0 the membrane is effectively a set of L^2 independent oscillators which explains why the square width is maximum at κ=0. The square width flattens as the curvature elasticity, κ, is increased further. For $\kappa \geq 0.1$ the square width is effectively constant and independent of the curvature elasticity, κ; a clear sign of universality. There is some spread of the data for the different curves indicating that perhaps one could do better with a longer system.

The evidence for universality would seem to be strong. The figures indicate that the square width is almost independent of the control parameters for $L>10, d \geq 6, \kappa > 0.1$.

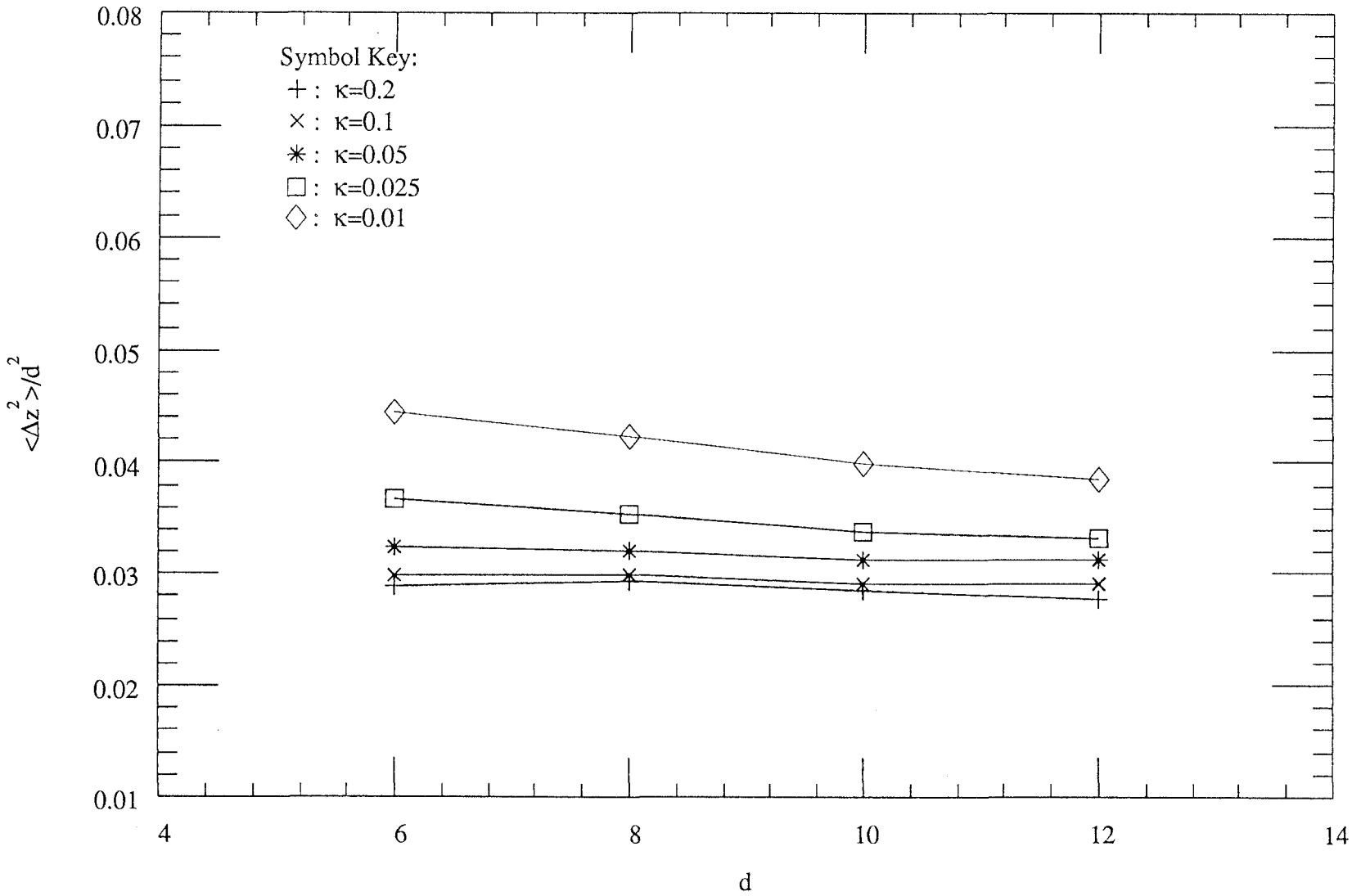

Figure 6.17
Variation of square width, W^2, of 3-dimensional membrane.
(Varying d and κ with n=20 (a_0=1.0))

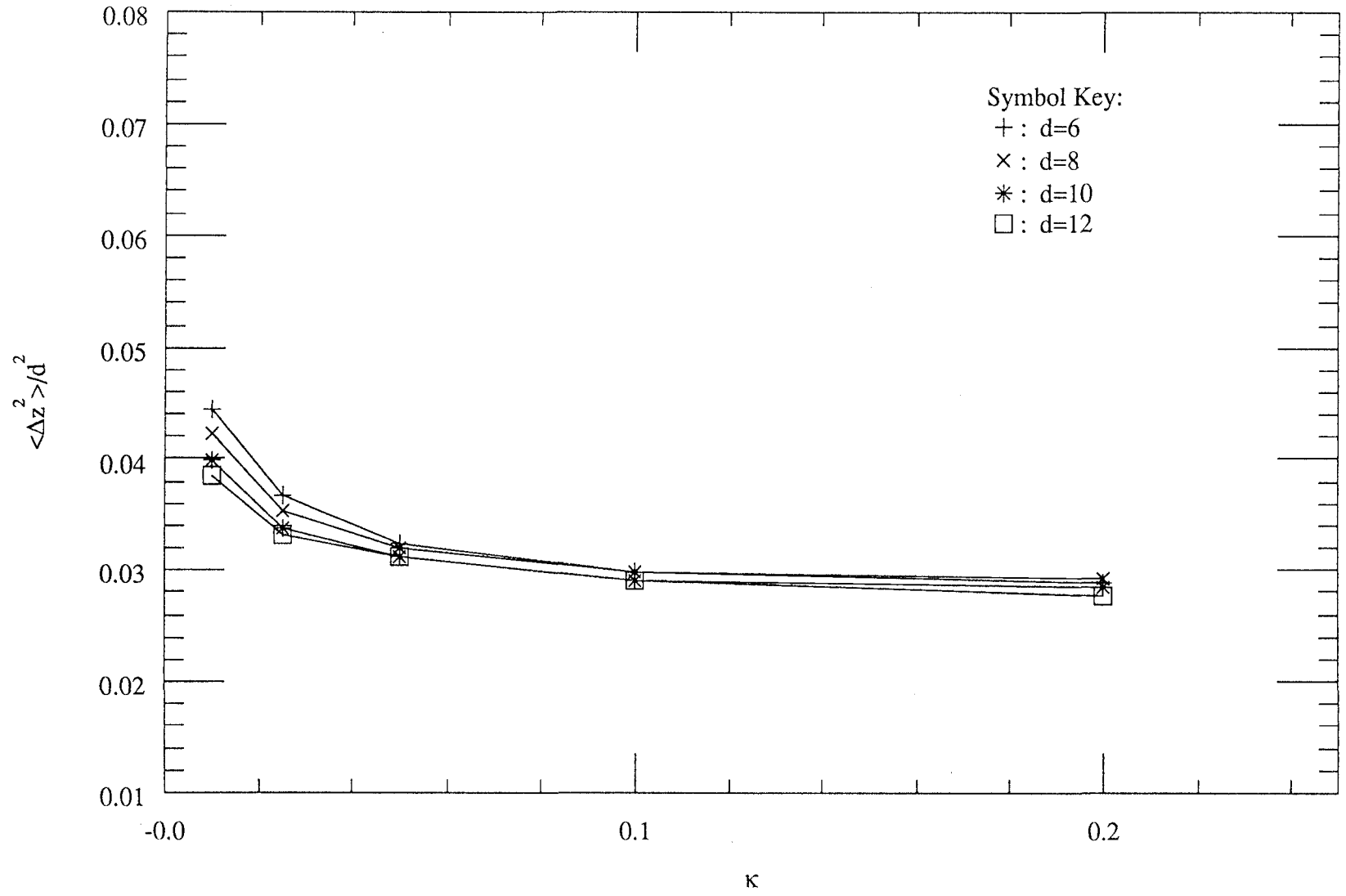

Figure 6.18

Variation of square width, W^2, of 3-dimensional membrane.

(Varying d and κ with N=20 (a_0=1.0))

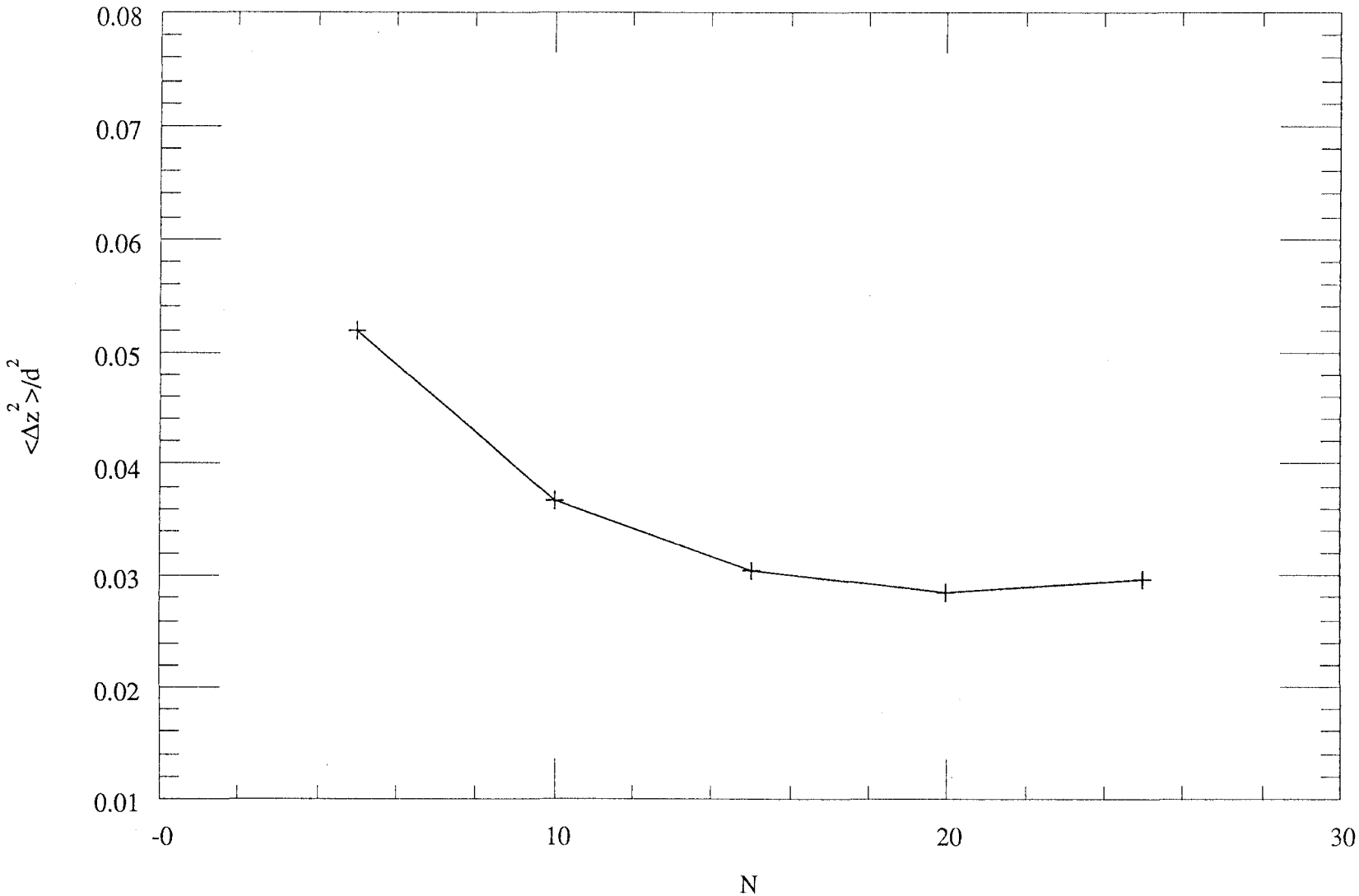

Figure 6.19
Variation of square width, W^2, of 3-dimensional membrane.
(Varying N with d=10.0 and κ=0.2 (α=1.0))

6.11.2 Short Distance Expansion Analysis Of Universal pdf

In the preceding section I presented strong evidence pointing to existence of a universal regime for the 3d SOS Helfrich model. In this section I present and analyze the universal data in an attempt to classify the nature of the universal regime. The SDE analysis used in the analysis of the 2d models is equally valid for the analysis of the 3d model.

Recall that a short distance approximation of the postulated universal form of the pdf is

$$P(z) = c(z + a_0)^{\phi} \qquad (6.11.2;1)$$

where $z=-a_0$ is the zero that we require for our non-local analysis and c is a constant of proportionality corresponding to the normalisation constant of the non-local pdf.

Now from simulation experiments I have obtained values for h_1, h_2 and h_3 displayed in table 6.3.

z	$P(z)/P_{max}$
0	0.025
a	0.118
2a	0.293

Table 6.3

Following the analysis described in section 6.8.2 and using the data in table 6.3 I obtained $\phi=2.208\pm1$ from the bisection. Again the error band represents the accuracy of the bisection in determining the root rather than the accuracy of the universal exponent due to imperfect source data. As before the difference of the SDE result for the universal scaling exponent, ϕ, from the analytical exponent consists of two components. One component is the accuracy of the data in table 6.3 the other is the systematic error that arises from the short distance approximation of the result.

Further evaluating (6.8.2;5) yields the value 0.97 (approx 1) for, a_0, the root of the pdf. So the root of the pdf lies approximately one lattice unit beyond the nominal wall position.

The value of the normalising constant, c, could now be determined. However I shall refrain since it is of little interest and is of no further use.

Having determined the location of the roots of the pdf, a_0 it is now possible to plot out the universal pdfs with the roots included. Several pdfs in the universal regime have been plotted in figure 6.20. The graphs have been normalised to have unit height and are plotted against $z^*=(z+a_0)/(2a_0+d)$. The universality is evident from the way in which the pdfs coincide with one another.

It should also be noted that the effective widening of the confining strip for the lattice model affects the evaluation of the square width, W^2, of the interface. Note that this effect has been taken into consideration and close inspection of the preceding figures of the membrane square width, W^2, will reveal that they have been handled appropriately.

6.11.3 Global Form Analysis of Universal pdf

In the preceding section I analyzed the universal pdf data using the SDE technique. In this section I use the global analysis method which enabled us to successfully classify the global form of the universal pdf for the two dimensional models. Recall that the analysis is designed to test whether the universal pdf has the following analytical form.

$$P(z^*) \propto (\sin(\pi z^*))^{\phi} \qquad (6.11.3;1)$$

If the pdf is of the latter form then the analysis allows one to extract the value of the universal exponent, ϕ. On the other hand, it is meaningless to ascribe the universal form a universal exponent, ϕ, if is not of the latter form.

A selection of pdfs in the universal regime are plotted for analysis in figure 6.21. The results appear linear although there may be a small deviation from linearity at short distances from the wall. At any rate the results are as linear as any of the preceding results. Hence (6.11.3;1) is in the very least a good parameterisation of the results. The slope of the graph indicates that the universal exponent, $\phi=2.44\pm0.05$.

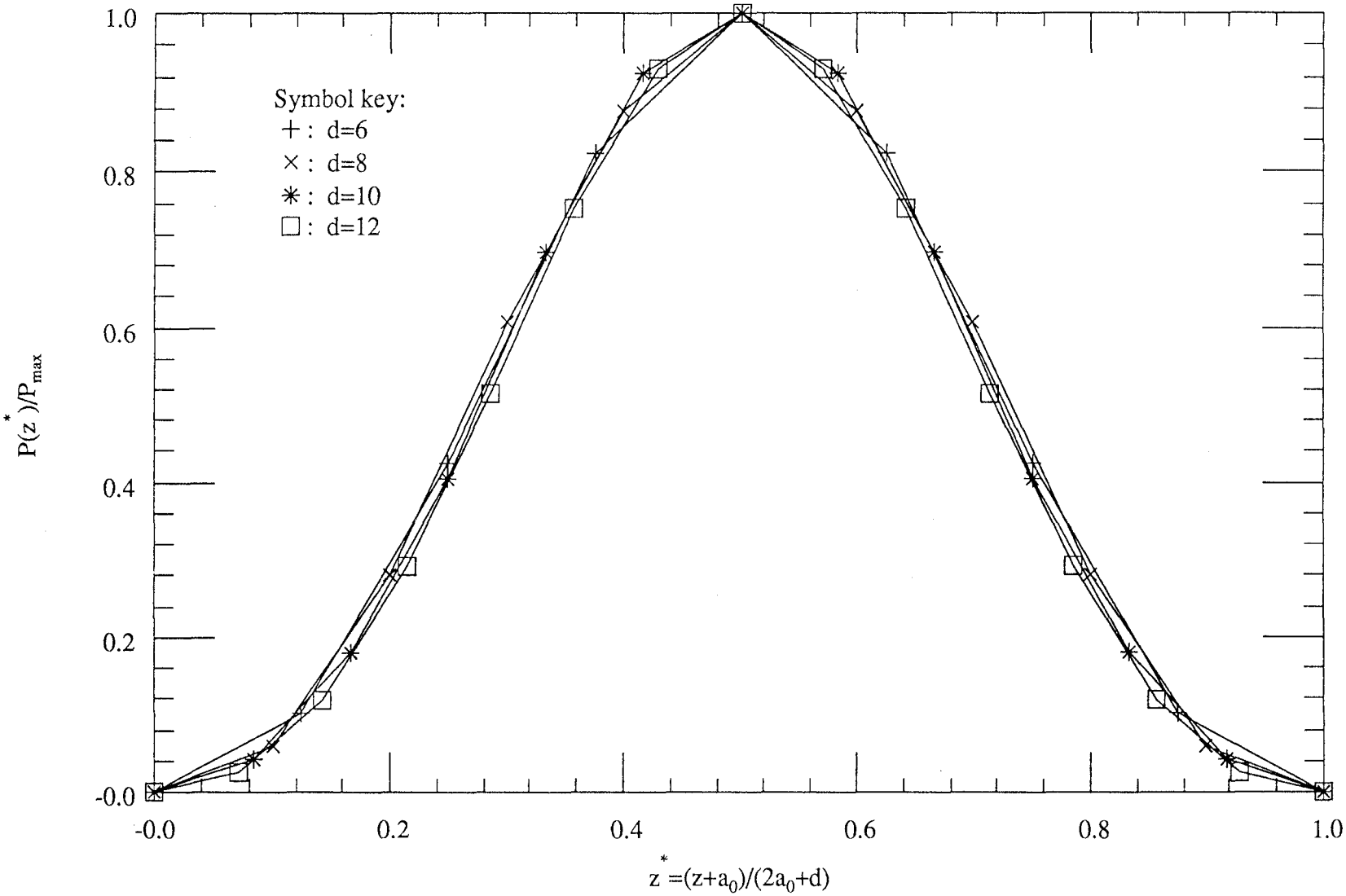

Figure 6.20

Probability distribution plot for 3-dimensional lattice model of a membrane; varying d with κ=1.0 and N=1000
(Distributions normalised to have unit height and a_0=1.0)

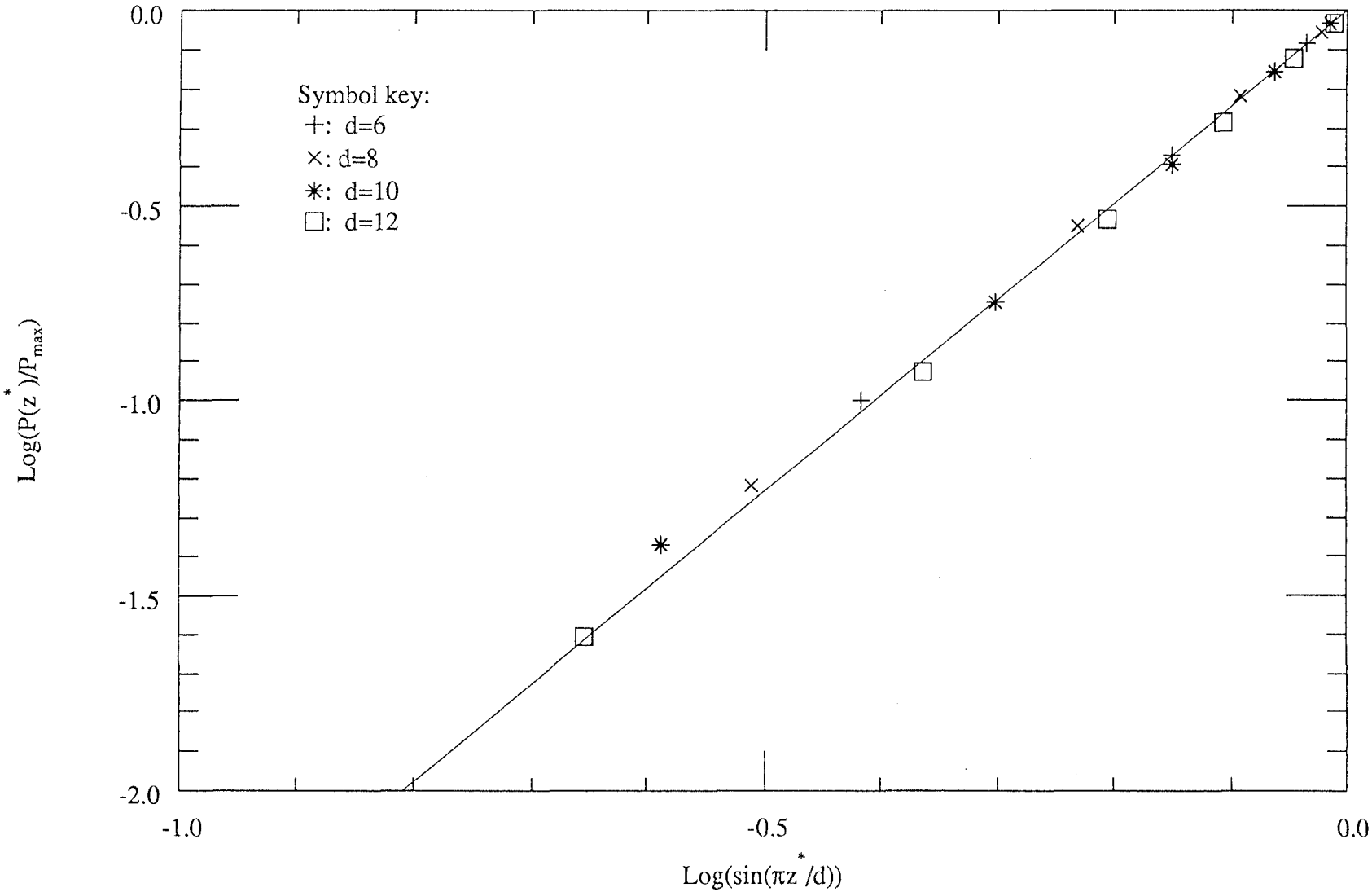

Figure 6.21

Log(sin(πz/d)) plot for 3-dimensional lattice model of a membrane; $z^{*}=(z+a_0)/(2a_0+d)$.
(Varying d with $\kappa=0.2$ and $N=1000$ ($a_0=1.0$))

6.12 The Bead Chain Model Of A 2d Membrane

In sections 6.9 and 6.11 somewhat restrictive models of a membranes were analyzed by Monte Carlo simulation. It was noted that substantial progress was possible analytically on these restrictive models (at least in the case of the 2d model). The principal simplification of the models stemmed from disallowing overhangs (hence SOS), and so avoiding membrane self-avoidance features which can sometimes be crucial to the understanding of real physical systems.

In this section I introduce a less restricted model of a two dimensional membrane based on the bead chain type models for polymers and vesicles (Remember that a polymer and a membrane can be considered the same in two dimensions and that a vesicle can be considered as a closed or cyclic polymer). No progress has been made on the associated analytical problem for this model due principally to the extra complexity involved in the inclusion of self-avoidance features.

6.12.1 Description of the Model

The model is based on the familiar bead chain models of polymers adapted by LSF to study vesicles and discussed briefly in section 5.3. The membrane is considered to consist of a set of n-hard beads, of diameter a, linked sequentially by flexible tethers, of length L=9/5a.

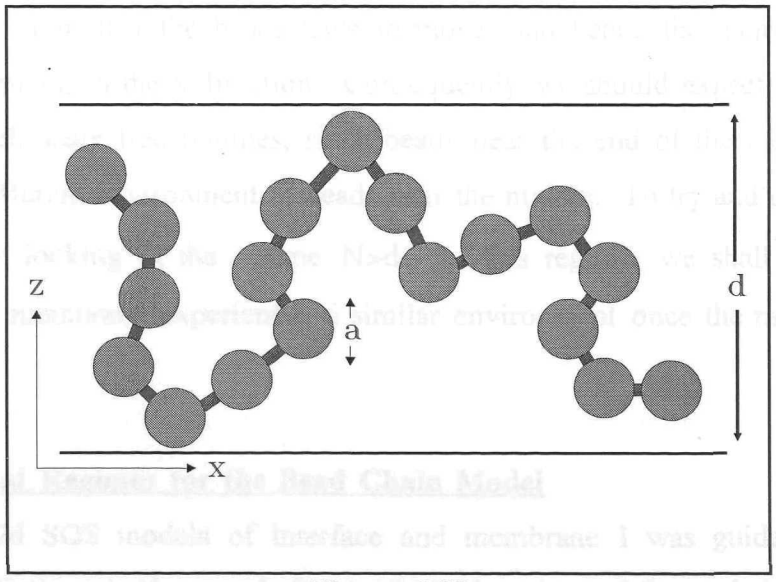

Figure 6.22
Bead chain model of a membrane in 2d.

The simulation is initiated with the chain lying flat in the centre of the walls. The beads are then jiggled about using the algorithm of Metropolis *et al.* Membrane self-avoidance is maintained by the mechanism described in section 5.3, based on the impenetrability of the beads and the tether length L<2a. The implementation of the self-avoidance property is time critical to the simulation. In appendix A the details of an efficient algorithm are presented. Use of a less efficient algorithm would have precluded some of the work presented in this section due to computational limitations.

Figure 6.22 indicates a possible configuration of the bead chain after it has relaxed from its initial position.

6.12.2 Hamiltonian and Aperiodicity of the Membrane

The Hamiltonian for the membrane is precisely the same as that discussed earlier in section 5.3, i.e.

$$H = \frac{\kappa}{2a} \sum_{i=1}^{N} (1 - \cos \beta_i) \qquad (6.10.2;1)$$

where β_i is defined as before to be the angle between the i-1,i and i,i+1 pairs. Recall that this can be shown to be the familiar Helfrich Hamiltonian in the continuum limit.

It should be noted that it is not possible to consistently apply periodic boundary conditions to this model in the way that we did for the SOS models. This is because of the extra freedom that the beads have to move, and hence the membrane has to expand and contract, in the x-direction. Consequently we should expect it to be more difficult to reach scale free regimes, since beads near the end of the membrane will experience a different environment to beads near the middle. To try and eliminate this effect I will be looking in the regime $N \gg d$. In this regime, we shall see that the majority of the membrane experiences a similar environment once the membrane has relaxed.

6.12.3 Universal Regimes for the Bead Chain Model

In the 2d SOS models of interface and membrane I was guided by strong theoretical predictions in the search for a universal regime of the probability density. There is in particular one specific difference between the latter models and the current model which makes the search for universality more interesting. In the current model

setting the curvature elasticity constant, κ, to zero does not lead to an uninteresting unphysical step function for the pdf. This is because, like a real membrane with vanishing surface tension and curvature elasticity, the beads do not become independent oscillators as in the SOS model. Rather they are bound together the fluctuation of one bead implicitly affecting that of the others through this linkage and the self avoidance property.

In the previous simulations universality was achieved by looking in the regime $N>>d>>\kappa,\sigma>0$. Clearly for a meaningful and interesting universality of the pdf it is still going to be necessary to maintain $N>>d$ and $N>>\kappa$. As I have stated it is now possible to set the curvature elasticity, κ, to zero. Therefore an interesting question is whether the purely *self-avoiding membrane (SAM)* ($\kappa=0$) exhibits a universal regime; and if so what are the characteristics of that regime.

The many extra degrees of freedom of this model of a membrane as compared to the previous SOS models leads one to expect that the equilibration of the system should take significantly more time steps. Indeed this is what I have observed. Whereas I used the mean height of the membrane as a guide to equilibration in the previous SOS models, I use the mean horizontal length of the membrane in this model. This approach has the virtue that the horizontal length relaxes significantly more slowly than the mean height (see figure 6.23), thus helping to ensure true equilibration. Moreover this value is useful to observe for analyzing the approach to universality, since the number of beads per unit horizontal length should approach a characteristic universal value.

6.12.4 Approach to Universality

As in the previous simulations it is possible to observe the approach to universality using the membrane width. Setting the curvature elasticity, κ, to zero means that there are only two remaining control parameters the number of beads, N, and the width of the gap between the walls d.

In figure 6.24 the membrane width of a SAM confined between walls of fixed separation d=20 is plotted against the length of the membrane L=Na. In figure 6.25 the membrane width of a SAM of fixed length, L=400a, is plotted against the separation of the walls, d.

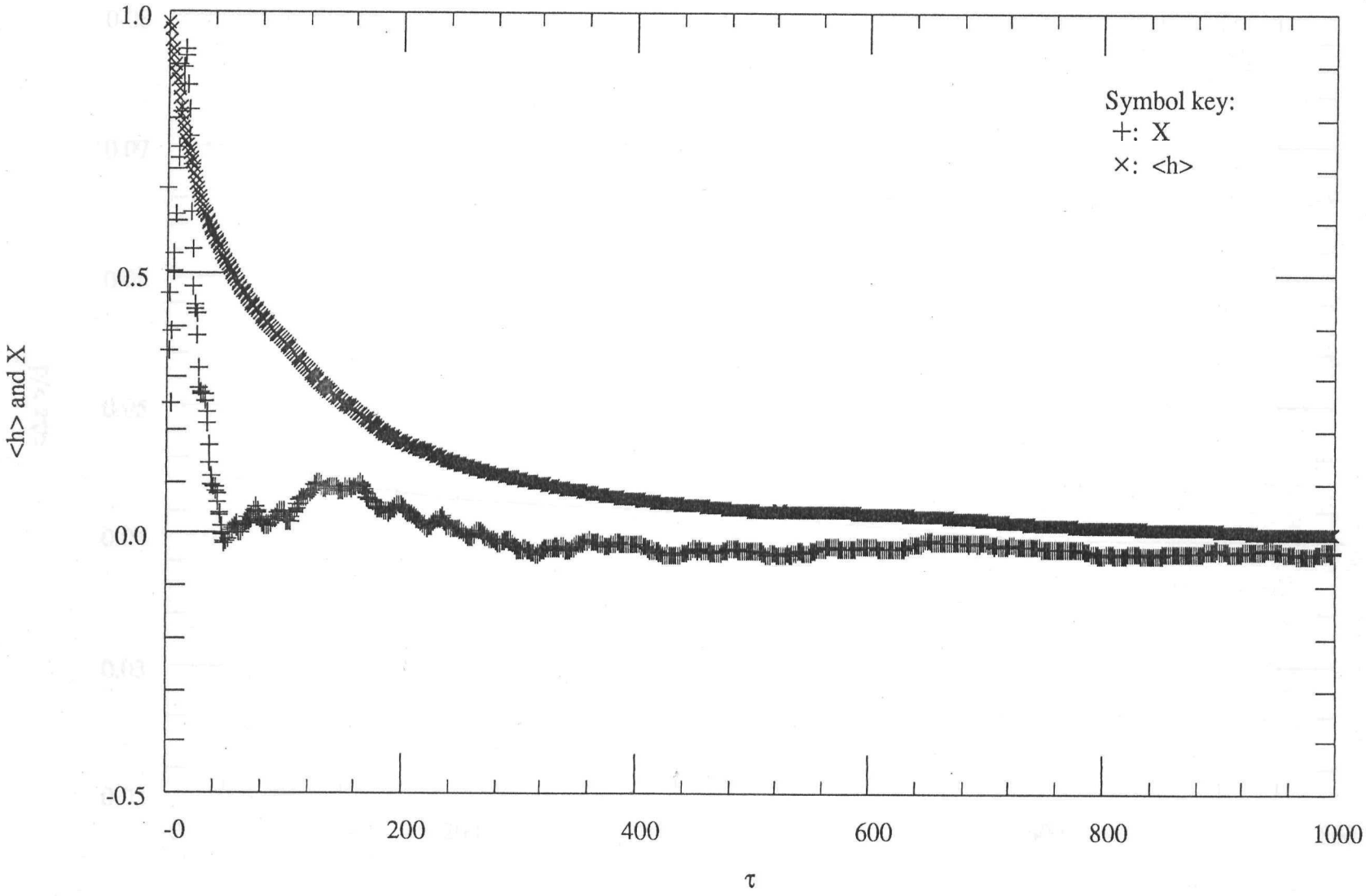

Figure 6.23

Comparison of relaxation of mean membrane height, <h>, and x-projection of membrane end-to-end length, X. (κ=0.0 d=20.0 N=400)

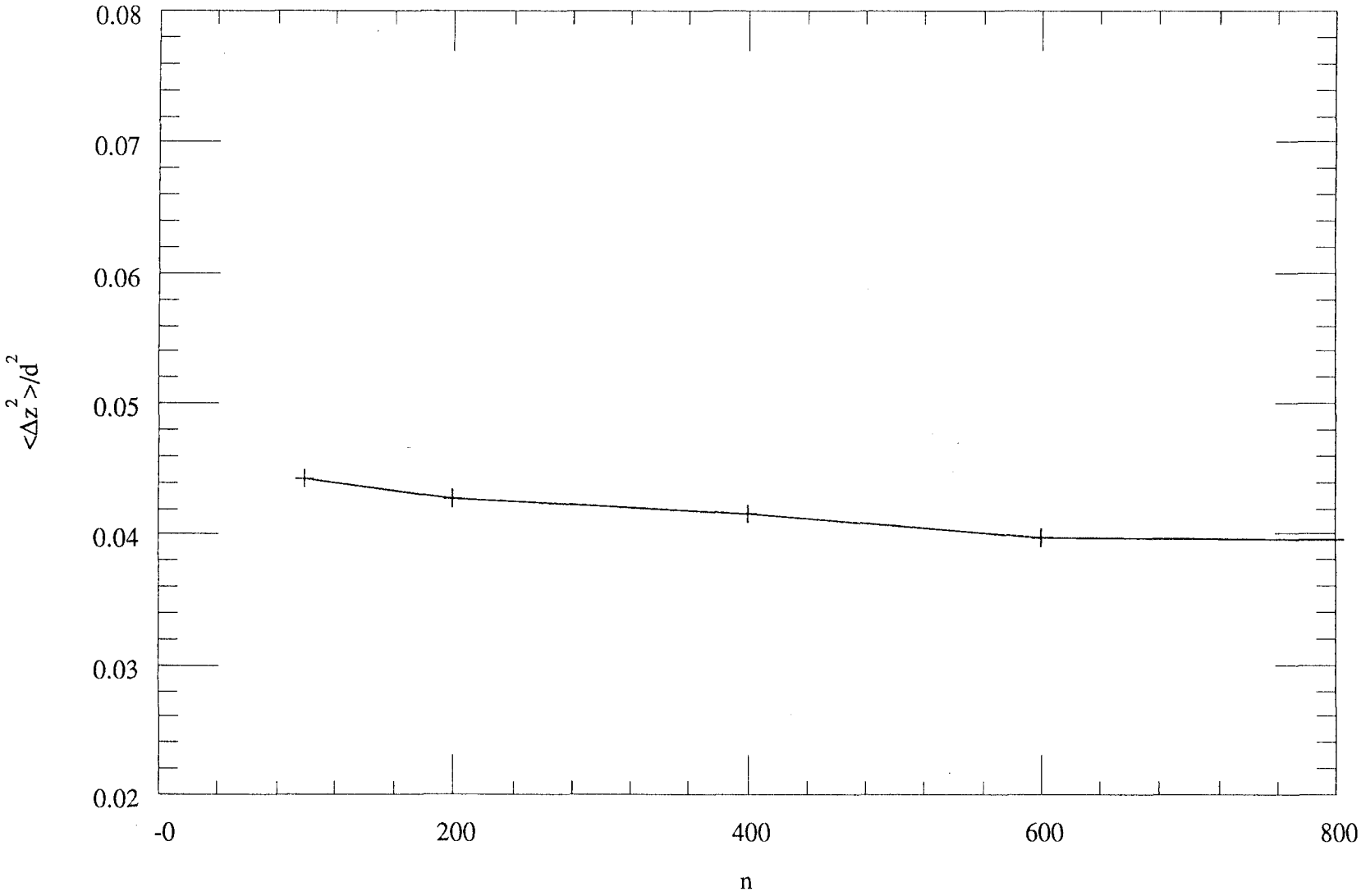

Figure 6.24

Variation of square width, W^2, of 2-dimensional bead chain membrane.

(Varying N with κ=0.0 and d=20.0 (a_0=0.5))

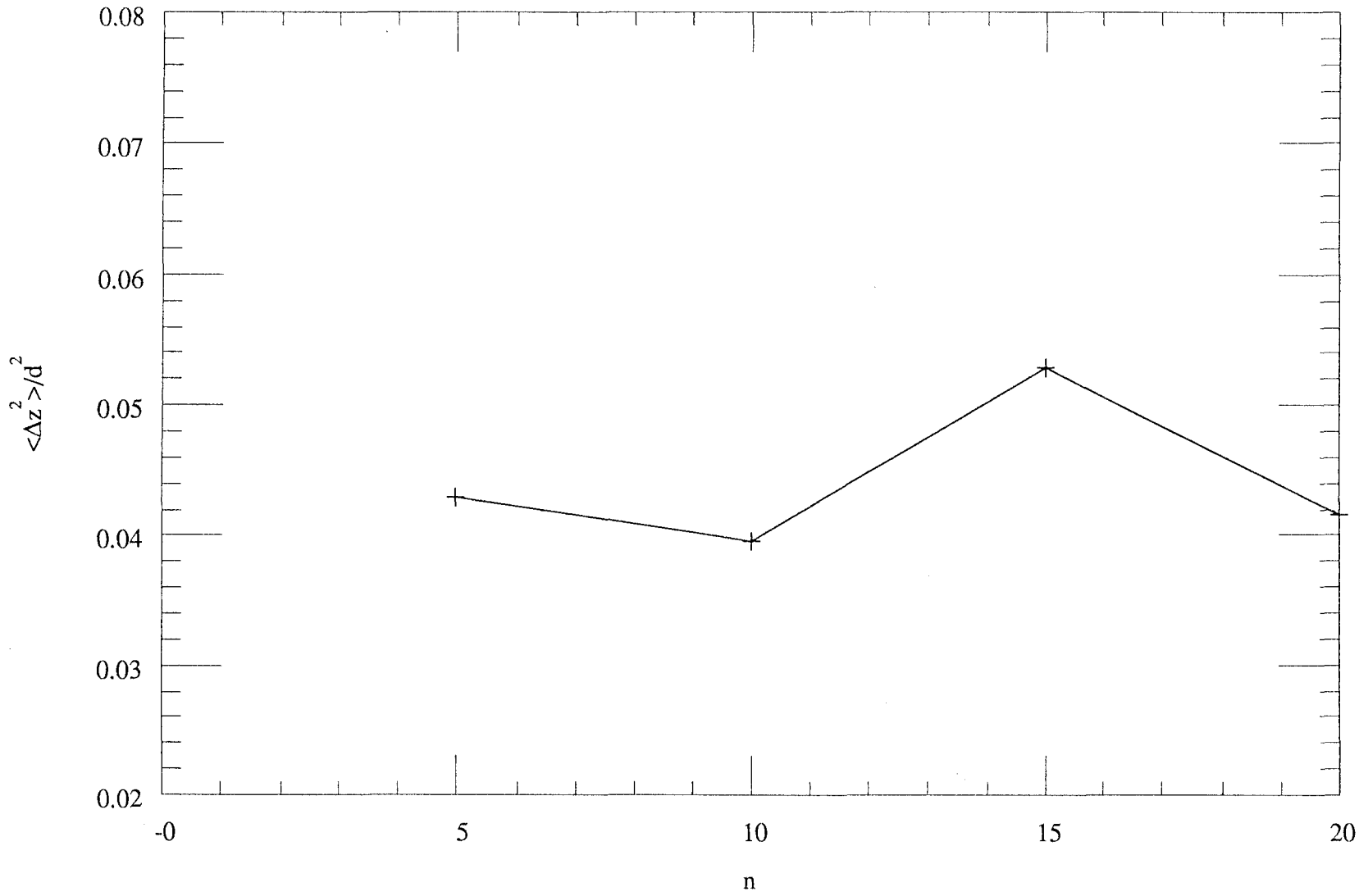

Figure 6.25

Variation of square width, W^2, of 2-dimensional bead chain membrane.
(Varying d with κ=0.0 and N=400 (a_0=0.5))

The figures indicate that any universality in the results is fragile in these results. Unfortunately it has not proved possible to extend the range of the control parameters looked at here due to computational limitations. (Simulations for an 800 bead membrane with d=20 takes 5 days on a SUN*IPX* Workstation. For an N=1000 membrane with d=20 would take about 20 days; an unacceptable time period).

6.12.5 Short Distance Expansion Analysis Of pdfs Near Wall

We have seen that the universality of the results appears to be rather fragile. Hence it is rather difficult to select appropriate values of the control parameters (N and d) (κ has already been set to zero) for which the pdfs are universal. However for a SDE analysis we need to know the form of the pdf near to the wall. Recall in section 6.4 I defined the width of the sampling intervals for an off-lattice pdf approximation to be $\delta z=1$. For a SDE analysis to be appropriate we require $\delta z/d = 1/d \ll 1$. Hence we are rather impelled to take the largest width confining strip in the search for universality. So I have taken the largest strip width of the simulations, d=20.

Now for the simulations with $\kappa=0$, d=20 and varying number of beads I have performed a series of short distance expansions. The results of the short distance expansions are to be plotted against the number of beads in the chain N. For universality the results should converge to a universal value as N is increased.

The short distance expansion analysis for this inherently off-lattice model is somewhat different from the on-lattice models already investigated. The source of this difference is that for this off lattice models the positions of the walls is known. That is the locations of the zeros of the pdf are known exactly. There is however some degree of uncertainty over the position the probabilty values should take with respect to their probability intervals. Although in principal one could determine the position each probability value should take exactly, as a first approximation it seems reasonable to locate them at the centre of the probability intervals.

In general, this approximation works well when considering global properties of the pdf. When considering an SDE analysis however one should note that the location of the probability values is critical. Fortunately we are able to circumvent any problems we have by considering a short distance expansion of the probability

distribution function rather than the probability density function. In figure 6.26 the details of the probabilty distribution function are illustrated.

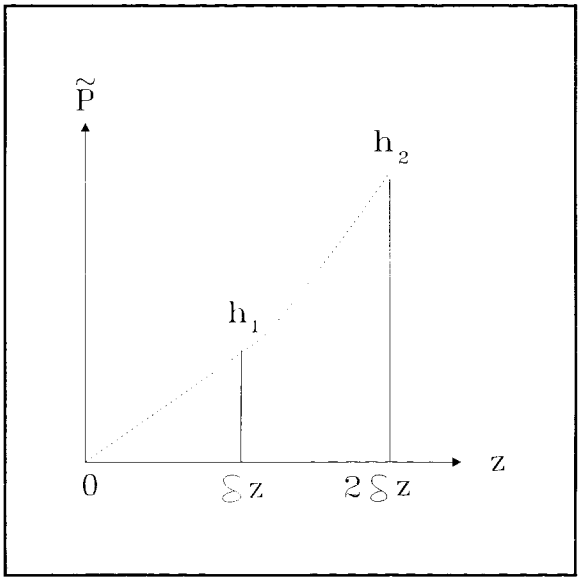

Figure 6.26
Interpolation of bead-chain model prob. distribution. fn. for SDE analysis.

As with the on-lattice SDE analysis in order to obtain a SDE approximation of the universal exponent, ϕ, it is neccessary to look at three points of the pdf near the wall. In fact we can use the value of the pdf at the wall now, which means that effectively only two values are required from the simulation. It can be shown that the three points (including the wall point) can be interpolated by

$$P(z) = cz^{\phi} \qquad (6.12.5;1)$$

Note that there are only two interpolation parameters in this interpolation formula since the zero of the pdf at the wall is intrinsically satified. As in the on-lattice analysis one can show that the interpolation parameter, ϕ, corresponds to the universal scaling exponent for the pdf, albeit in the SDE limit. Also the interpolation parameter, c, as before is related to the normalisation of the pdf and is of little interest.

Now as remarked above this formula for the pdf, P(z), as remarked above is not useful directly. However on integration we get

$$\tilde{P}(z) = c\phi z^{(\phi-1)} \qquad (6.12.5;2)$$

where $\tilde{P}(z)$ is the probability distribution function defined in (6.4;1). Now one can solve (6.12.5;2) directly, without recourse to numerical techniques. We have two equations for the two unknowns (ϕ,c)

$$\begin{aligned} \tilde{P}(\delta z) &= h_1 = \phi c(\delta z)^{(\phi-1)} \\ \tilde{P}(2\delta z) &= h_1+h_2 = \phi c(2\delta z)^{(\phi-1)} \end{aligned} \qquad (6.12.5;3)$$

where (h_1,h_2) are known from the simulation experiments. Solving these equations for ϕ one gets

$$\phi = \frac{\log(h_1+h_2) - \log(h_1)}{\log(2)} - 1 \qquad (6.12.5;4)$$

and finally, knowing ϕ, one can now solve for c using

$$c = \frac{h_1}{\phi}\left(\frac{1}{\delta z}\right)^{(\phi-1)} \qquad (6.12.5;5)$$

Now from simulation experiments I have obtained the values for h_1 and h_2 displayed in table 6.4.

	N=100	N=200	N=400	N=600	N=800
h_1	0.0400	0.0339	0.0302	0.0260	0.0255
h_2	0.178	0.157	0.144	0.122	0.119

Table 6.4

Note as always the probability values in table 6.4 come from symmetrised pdfs. The symmetrisation impoves the quality of the results. Also the results come form pdfs normalised to have unit height rather than unit area.

Following the analysis method described above and using the data in table 6.4 I obtained values for the effective scaling exponent, $\phi_{eff}(N)$, displayed in table 6.5. The results are also plotted against number of beads in figure 6.27. The dotted line represents the universal value of the scaling exponent, ϕ.

	N=100	N=200	N=400	N=600	N=800
$\phi_{eff}(N)$	1.45	1.49	1.53	1.51	1.50

Table 6.5

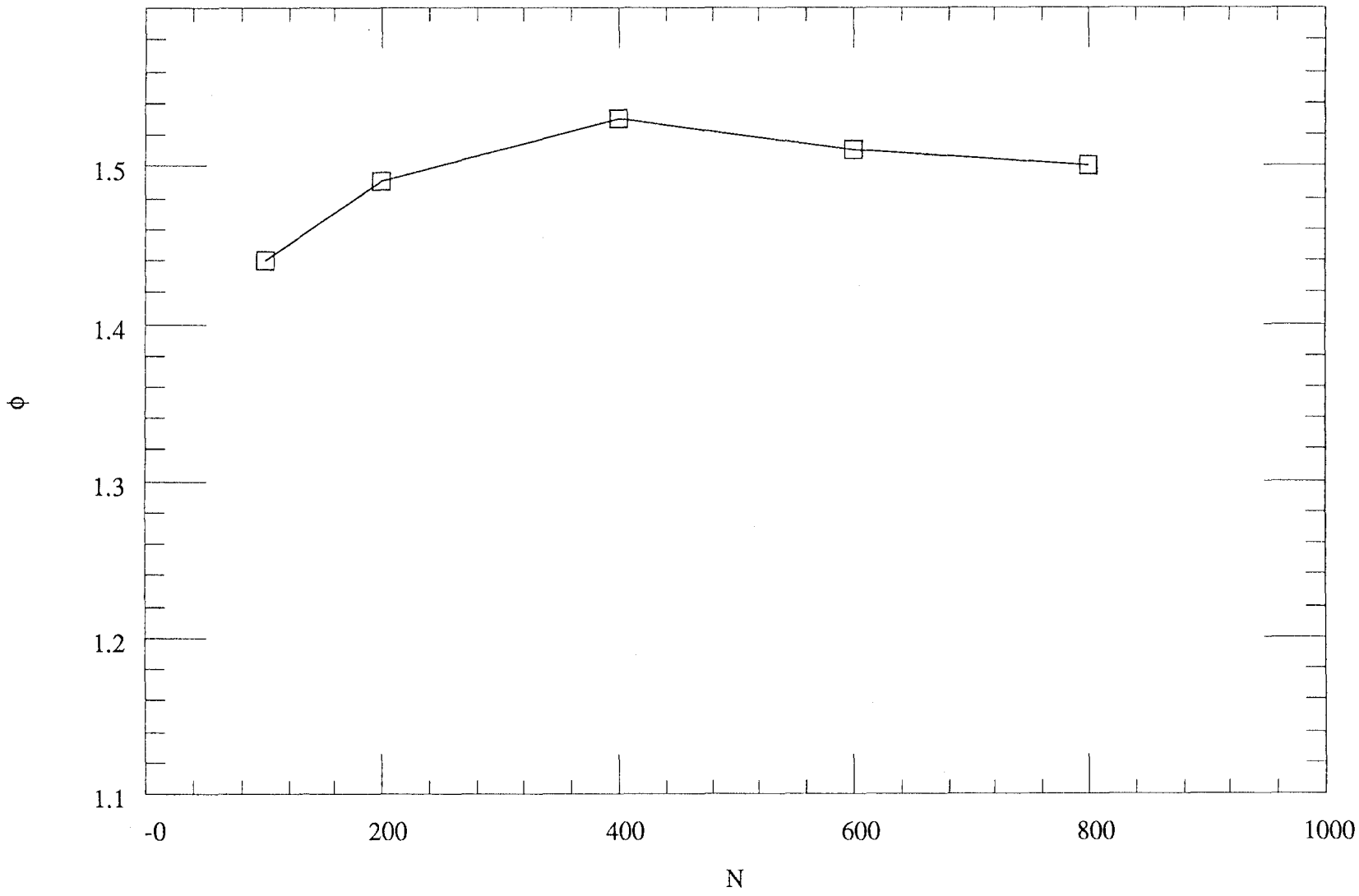

Figure 6.27

Variation of ϕ_{eff} (determined by short distance expansion) against n.

6.13 Summary and Comparison of Results

In table 6.6 I summarise the main results obtained in the preceding sections:

Model	ϕ Analysis	ϕ SDE	ϕ Global	W^2 Expt	W^2 Analysis
SOS Interface 2d	2.0	1.8	2.0	0.0352±3	0.0327
SOS Membrane 2d	2/3	0.749	0.72	0.0546±1	0.0544
SAM 2d	-	1.50	-	0.0395±5	-
SOS Interface 3d	-	-	-	-	-
SOS Membrane 3d	-	2.2	2.4	0.0285±10	-

Table 6.6

Also in figure 6.28 a direct comparison of the pdfs in the observed universal regimes have been plotted including the roots of the pdfs. The figure clearly illustrates the differences between the universal regime pdf profiles for the different models.

Further in figure 6.29 the pdfs are plotted using the global form analysis method. The linearity of the graphs suggest that the postulated universal form is, in the very least, a good parameterisation of the results. Moreover the figure indicates that the differing models clearly have differing universal exponents as indicated by the differing slopes of the lines.

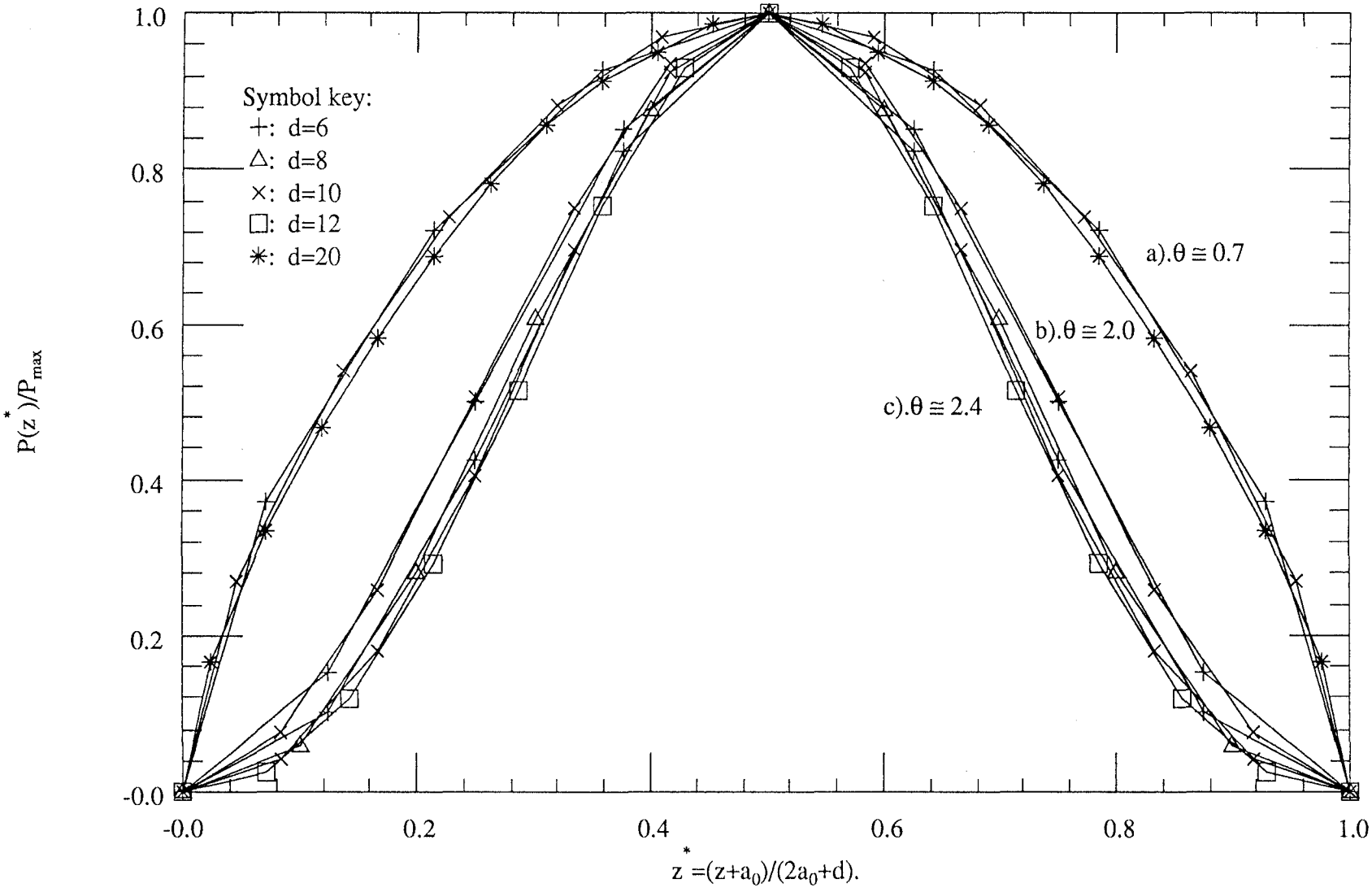

Figure 6.28

Comparison of pdfs for a). SOS model of a membrane in 2d, b). SOS model of an interface in 2d and c). SOS model of a membrane in 3d. Pdfs normalised to have unit height and domain. Varying d with a). κ=0.5, b). σ=1.0, c). κ=0.2 and n=1000.

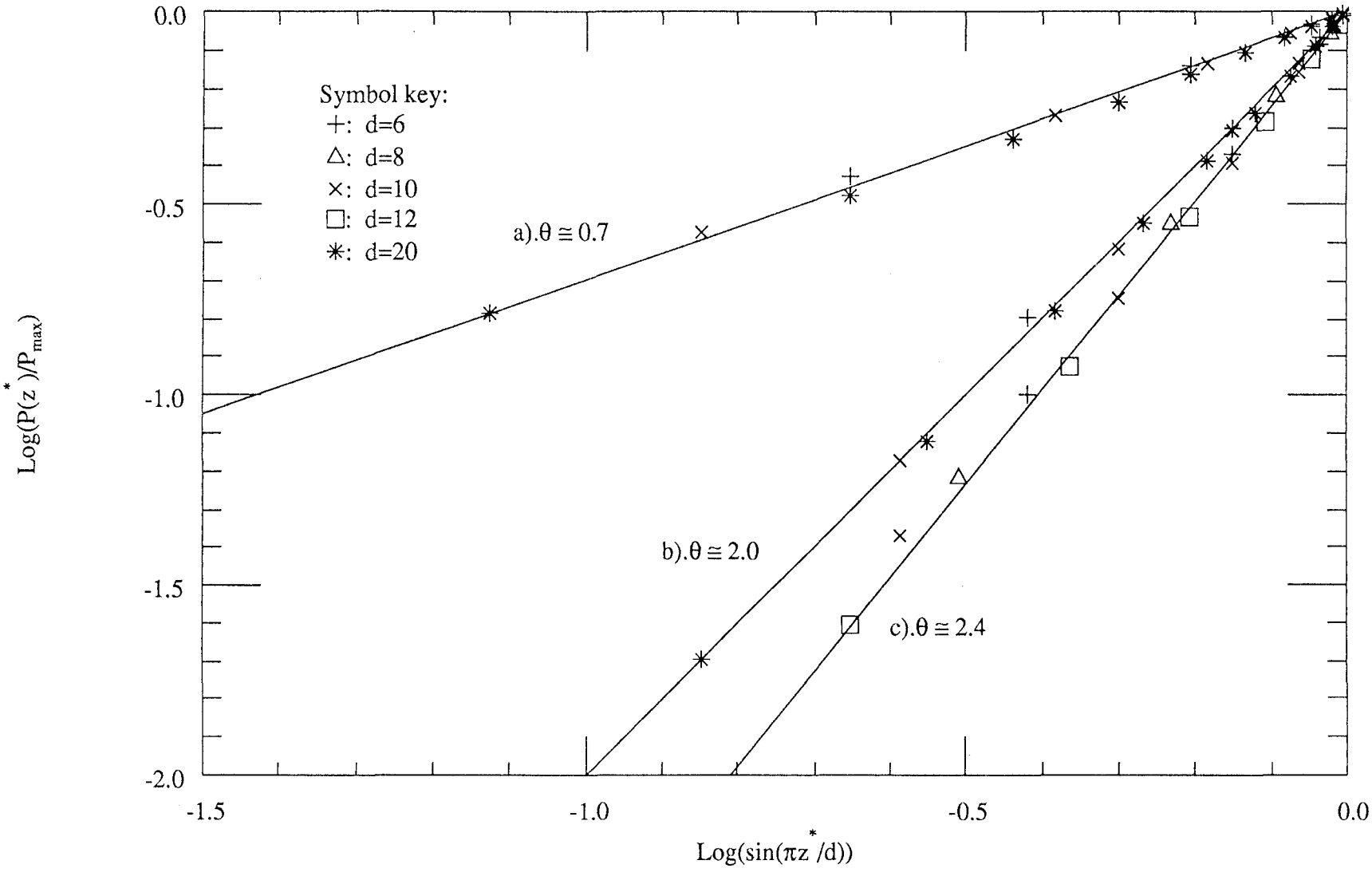

Figure 6.29

Log(sin(πz/d)) plot for a). SOS model of a membrane in 2d, b). SOS model of an interface in 2d and c). SOS model of a membrane in 3d. Varying d with a). κ=0.5, b). σ=1.0, c). κ=0.2 and n=1000; $z^* = (z+a_0)/(2a_0+d)$.

6.14 Conclusions and Further Work

I have demonstrated that the Monte Carlo Simulation method applied to a variety of confined interface and membrane models is a powerful tool for investigation of those models. I have been able to achieve universality for a number of the models. The analysis of the results has indicated that, at the very least, the generic universal form, motivated by a neat analytical argument based on conformal invariance, is a very good parameterisation of the results. In the case of the confined interface in 2d the hypothetical is form is known to be correct by an analytical argument.

The qualitative form of the pdf for the confined membrane in 2d seems to accord with a tentative analytical argument. A universal regime for the SOS membrane in 3d has been achieved for surprisingly, perhaps anomalously, short length scales. It appears qualitatively similar to the confined SOS interface in 2d although with a larger universal exponent. Further work could be done to improve the accuracy of the result.

Universality also appeared to have been be achieved for the 2d bead-chain model of a membrane in the SDE analysis. Work in the literature (Gompper and Kroll 1991) indicates that the universal regime for the SAM in 3d is currently inaccessible due to computational limitations. With the continual improvement of computing performance future work could involve obtaining and characterising the universal regimes for these models.

The work in the final sections of this chapter form the basis of a paper to be submitted for publication (Norman *et al* 1993). Further work on advancing the analysis of the models would prove useful, although the simulation work performed here is largely due to the difficulty of furthering the analytical work.

The confined SOS membrane in 2d is currently being investigated using a Fokker-Plank method (Parry 1992d). Preliminary results from that study indicate are not inconsistent with the results I have presented here. Any experimental analysis using alternative methods are useful as independent confirmation the work presented here.

CHAPTER SEVEN

A BEAD NET MODEL FOR TILTED CHIRAL LIPID BILAYERS

7.1. Introduction

Recent experimental observation of *tilted chiral lipid bilayers* (TCLBs) (Nakashima *et al* 1984, Yamada *et al* 1984, Nakashima *et al* 1985, Yager and Schoen 1984, Yager *et al* 1985) have revealed the existence of several new exotic bilayer structures. The experimental observations indicate that the chirality of the lipid molecules is an important factor in the formation of these exotic structures. Some progress has been made in understanding the structural *raison d'être* of these new structures (Helfrich 1986, de Gennes 1987, Helfrich and Prost 1988, Zhong-can and Jixing 1991) through mean field analytical arguments. These models though successful in explaining the form of the observed structures are unable to answer, by their very nature, important questions concerning statistical mechanics of these structures.

The purpose of the work in this chapter has been to develop a model of the lipid bilayer that can answer some of these questions. The very complexity of the statistical mechanics of self-avoiding surfaces, that has precluded analytical solutions of simpler problems than this, forces one to proceed numerically. In the next section I shall describe the *bead net model* (also called the *tethered* or *polymerised membrane model*) of a membrane (Kantor *et al* 1986, 1987, Kantor and Nelson 1987). I shall go on to explain how this model can be adapted to model the tilted chiral lipid bilayer (TCLB).

Having adapted the bead net model to TCLBs I go on to present the results of simulations of the model. Initially I investigate "long thin" membranes for which experimental observations and the analytical arguments have definite predictions to make. I present a systematic analysis of the results. Actual configurations of "observed" membrane structures are also presented.

Having investigated a particulary simple shape of membrane I proceed to look at the less simple case of diamond shaped regions. Since the experimentally observed

structures were thread-like comparison with experiment is difficult. Moreover the analytical arguments of the mean field models cannot be used since membrane self avoidance is almost certainly an important consideration for these membranes. The results are again analyzed systematically and a selection actual "observed" membranes are presented.

7.2 The Bead Net model

The field of membrane simulation is currently the subject of intense investigative effort. There are several models being studied, but most models are abstracted from the so called *bead net* or *tethered membrane model*. This model is closely related to the bead chain model of polymers discussed in sections 5.3 and 6.12. A bead net description of a surface is illustrated in figure 7.1.

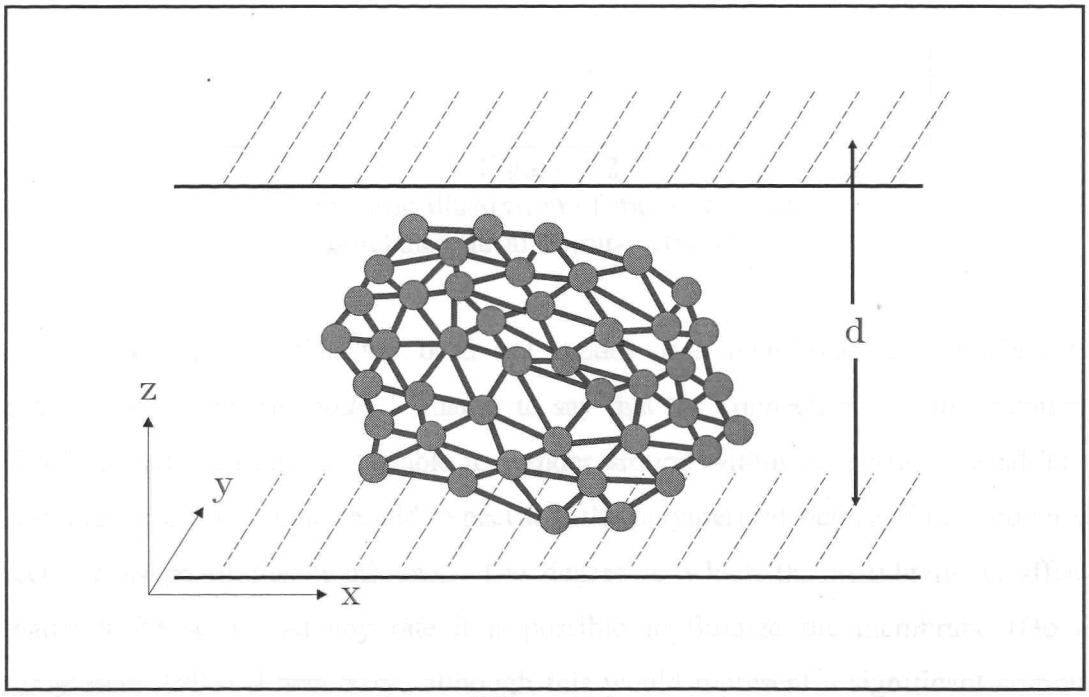

Figure 7.1
Schematic illustration of bead net model
of a lipid bilayer.

The surface consists of a set of N hard beads linked, by short flexible tethers, to neighbouring beads, into a hexagonal net structure. Self-avoidance of the net is achieved by restricting tether length, so beads cannot stray far from their neighbours. The maximum tether length is sufficiently short so that taken together with the fact that the beads are hard, and so exclude one another, the result is to render the net

impenetrable. This is because the net is sufficiently dense of beads that the remaining gaps between the beads are too narrow for non-neighbouring bead to pass through. The implementation of the hard, or self-avoiding, bead property is time critical to the simulation and an efficient algorithm for its implementation is discussed in detail in appendix A. This impenetrable arrangement of the beads is featured in the schematic illustration figure 7.2.

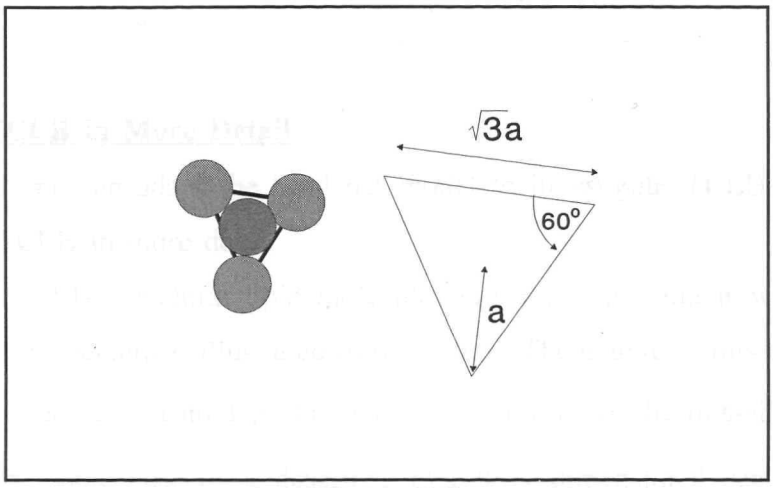

Figure 7.2
Schematic illustration of membrane self-avoidance through impenetrability.

It can be seen that the bead net model of a membrane as described is a *polymerised membrane model.* That is to say that the connectivity of the membrane is fixed so that the beads are unable to wander around within the surface. Real TLCB membranes are fluid. One should expect that the polymerised nature of this model will affect the shape of the membrane. The degree to which the membrane is affected remains to be seen. At any rate it is possible to fluidize the membrane (Ho and Baumgartner 1990) if necessary; although this would represent a significant computational complication of the problem. Constructing a consistent TCLB model for a fluid membrane also would also require some careful consideration and reappraisal of the modelling details.

In an attempt to identify the shape characteristics dependent on the self-avoidance property of the membrane I have briefly considered *Phantom* or *Ghost membranes* (Kantor *et al* 1987). Ghost membranes do not self-avoid globally. The membrane area is preserved by only keeping the beads hard with respect to their

neighbouring beads. It should be possible to predict analytically the behaviour of fluid ghost membranes under the chiral action. Comparison of the polymerised ghost membrane with the analytical result for the fluid membrane should help one to understand effects due to the polymerisation of the membrane. Unfortunately, the mean field result for the diamond shaped membrane is not available to me. Nevertheless one hopes that this comparison will become possible as the analytical result is made available.

7.3 The TCLB in More Detail

Before one can adapt the bead net model to investigate TCLBs one needs to consider the TCLB in more detail.

In the TCLB the chiral lipid molecules are out of alignment with the surface normal. The arrangement is illustrated in figure 7.3. The degree of mis-alignment with the surface normal is measured by the angle θ_0. Ordinarily the mis-alignment of the lipid molecules would need to be described by a three dimensional vector field on the membrane surface. However, it has been observed experimentally that this angle tends to be fairly constant throughout the membrane in TCLBs. This means that the misalignment of the lipid molecules can be described by a two dimensional vector field in the surface, corresponding to the projection of the three dimensional field onto the surface.

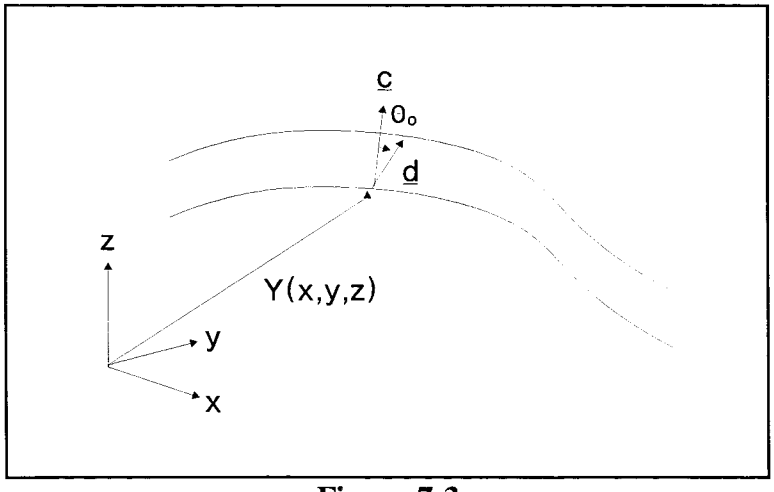

Figure 7.3
Diagrammatic representation of internal structure of TCLB.

It should be apparent from figure 7.3 that the theory of *smectic liquid crystals* (c.f lyotropic phases in section 2.3.4) should be a useful tool in this work. Indeed the associated Frank theory of elasticity (Oseen 1933, Zocher 1933, Frank 1958) already contains an energy term encapsulating the chiral effect (Helfrich and Prost 1988). The energy density due to the chiral effect can be written (Zhong-can and Jixing 1991) as

$$g_{chiral} = -\kappa_2 d.(\nabla \times d) \qquad (7.3;1)$$

where κ_2 is the associated Frank elastic constant and d is the tilt director illustrated in figure 7.3.

The chiral energy density in this form is not very amenable for use in the bead net model of TCLBs which I shall describe next. Fortunately a more useful form has been obtained (Zhong-can and Jixing 1991).

7.4 Adaptation of Bead Net Model to Study TCLB

Having introduced the bead net model and considered the essential features of the TCLB one is now in a position to adapt the bead net model to study TCLBs.

7.4.1 Definition Of a Surface Field for The Bead Net Model

The bead net model as originally formulated makes no provision for the definition of a surface field, so one has to define one. Clearly the definition of a vector field on the surface representing the internal structure of the membrane complicates the model somewhat. The simplest vector field that one can define is a uniform one. In an effort to keep the model as simple as possible I have elected to consider surfaces with only a fixed and uniform surface field. Obviously in reality the interaction between the membrane geometry and the internal lipid geometry may well be important. Nevertheless one would hope that even with a fixed and uniform internal geometry the model will still exhibit important new physical features.

I have defined a vector field that is uniform with respect to the bead net surface on which is defined as follows. Imagine the bead net without the beads. The net is a triangular mesh. Consider the mesh when it is flat and the triangles are all equilateral. Now construct lines from the centre of each triangle to the vertices. All of these construction lines lie in one of three possible (six if you count the sense) directions. Choose one of the directions. Obliterate all the construction lines not

parallel to the chosen direction. Now one is left with a set of triangles each containing a vector. For half the triangles the vector is from the centre to the vertex, for the other half the reverse is the case. It can be seen that the vector field in this regular geometry of the net is uniform with respect to the membrane and real space. As the beads are moved during a MC simulation the vector field is updated so that the new vectors run from the centre to the selected vertex, or vice versa. Obviously as the surface develops the vector field becomes non uniform in space. It can however be considered uniform with respect to the surface. This arrangement is illustrated in figure 7.4

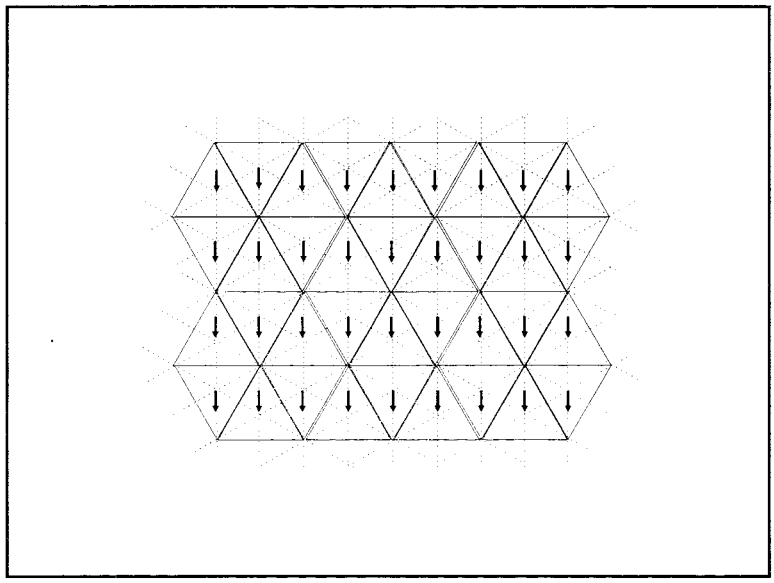

Figure 7.4
Construction of uniform TCLB surface field.

7.4.2 Definition of a Hamiltonian For TCLB Model

The application of the bead net model to physical systems is achieved by imposing a Hamiltonian representative of the physics. For instance a study of the explicit curvature of the surface (the membrane has intrinsic curvature properties also worthy of interest) involves the imposition of a Helfrich curvature Hamiltonian of the form

$$H_{helf} = \frac{\kappa}{2}\sum_{\langle\alpha,\beta\rangle}\left(1 - \hat{c}_\alpha.\hat{c}_\beta\right) \qquad (7.4.2;1)$$

where $\hat{c}_\alpha$ represents the unit normal formed from the plane of three neighbouring beads, denoted α. The summation, $\langle\alpha,\beta\rangle$, is over adjacent *plaquettes* or bead triangles. Clearly one can write this in the form

$$H_{helf} = \frac{\kappa}{2}\sum_{\langle\alpha,\beta\rangle} g_{\alpha\beta} \qquad (7.4.2;2)$$

where one defines

$$g_{\alpha\beta} = 1 - \hat{c}_\alpha.\hat{c}_\beta \qquad (7.4.2;3)$$

as the curvature energy density for the surface.

The task of applying the bead net model to the TCLB problem is now reduced to the task of choosing a Hamiltonian. Fortunately the task of formulating a Hamiltonian representative of the physics of TCLBs is made easier, due to the precursory mean field studies (Helfrich and Prost 1987, Zhong-can and Jixing). However, since we are not dealing with a continuum model here then some manipulation is required. In particular the Frank form of the chiral energy density (7.3;1) is not particularly easy to interpret. Fortunately the Frank form can be put into the following form (Zhong-can.and Jixing 1991)

$$g_{chiral} = -\kappa_\chi \tau_g \qquad (7.4.2;4)$$

where

$$\kappa_\chi = -2k_2 \sin^2\theta_0 \cos\theta_0 \qquad (7.4.2;5)$$

is the chiral elastic constant or *chirality* (the author's own naming convention) and τ_g is the so called *geodesic torsion* (Spivac 1979). Alsos θ_0 is the lipid tilt angle, as illustrated in figure 7.3. For the geodesic torsion one can write

$$\tau_g = \dot{c}.(Y\times c) \qquad (7.4.2;6)$$

where Y and c are described in section 7.3. The derivative is with respect to the surface field. For the full derivation see Zhong-can and Jixing 1991.

The essential nature of the chiral Hamiltonian is to drive *torsion* into the surface, hence the resulting twisted and helical structures. To understand the chiral field let us compare it with the curvature field. Imagine moving along the surface field generated by the TCLB. In figure 7.5 a set of curve trajectories are drawn to illustrate the concept of torsion. In figure 7.5a the trajectory curves with no torsion, whilst in

figure 7.5c the trajectory twists with no curvature. In figure 7.5b the trajectory both curves and twists.

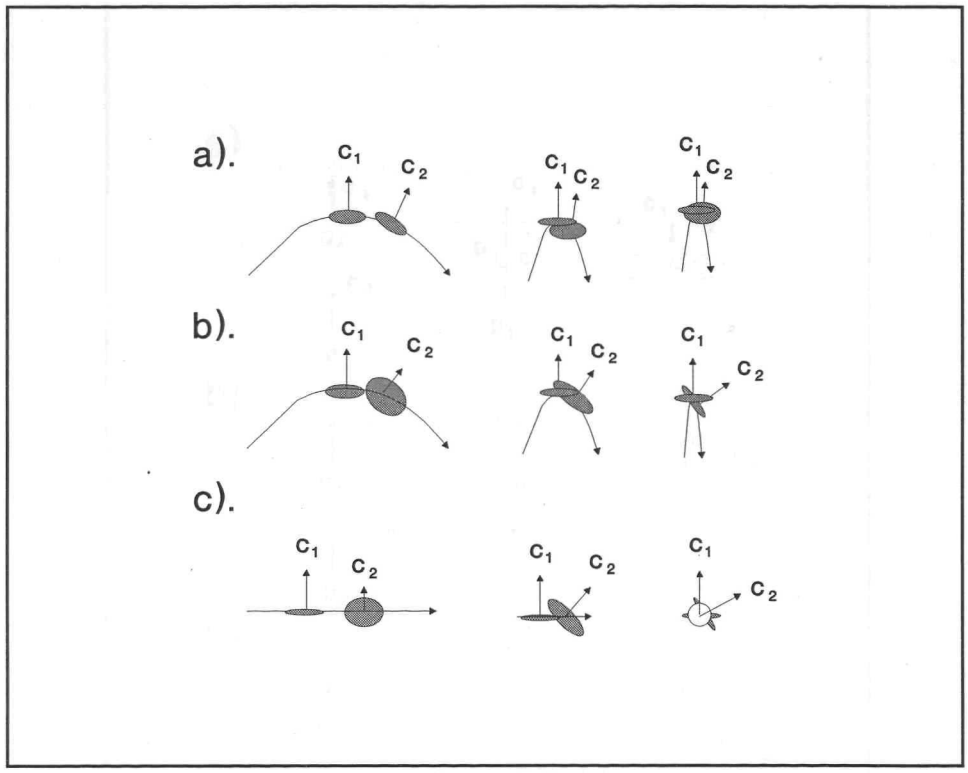

Figure 7.5
Torsional and curved paths along a path on a membrane.

If one moves along the chiral field of a TCLB the effect of the chirality of the molecules is to twist the surface with respect to the trajectory. One needs to construct a Hamiltonian that mimics this effect.

Now consider adjacent triangles in the bead net. It is easy to see that there is ample freedom to curve the surface represented by the triangles. It is not clear however whether the surface can be twisted. In fact it can be seen the opportunity for twist type deformations between adjacent triangles is severely restricted by their very adjacency. In order to obtain a reasonable freedom to twist, and hence satisfy a torsion driving potential, one has to look at neighbouring triangles that share at most one corner. In figure 7.6 several orientations of such triangles are illustrated.

In figure 7.6a the triangles are untwisted, whilst in figure 7.6b the triangles have been twisted through 90°. In figure 7.6b the triangles are twisted by 45°. The

deformations of the triangles illustrated are a simplification of real triangle deformations since in each of the deformations the chiral field vectors, p_1 and p_2, are co-linear.

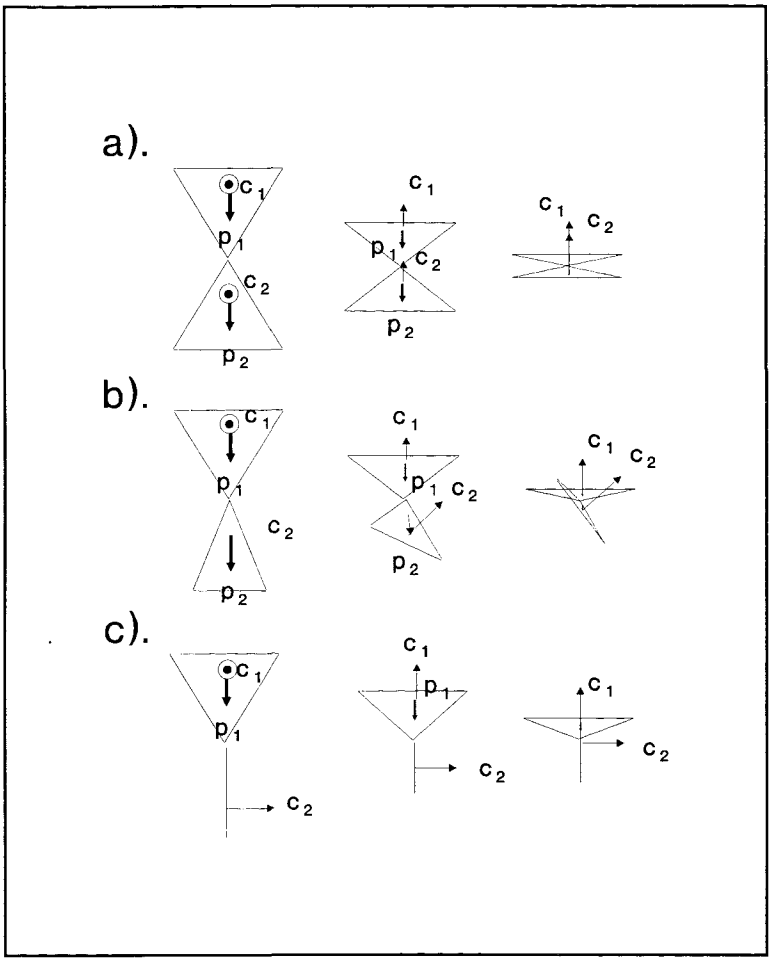

Figure 7.6
Illustration of twist deformations of triangles sharing a common vertex.

Nevertheless the figure illustrates well the degree of torsion deformation possible between triangles sharing a common vertex. Moreover a natural measure of the torsion becomes apparent - the degree of twist of the triangles. One needs a more rigorous definition of this quantity.

Careful consideration of this problem has led one to consider the following measure to be an appropriate measure for the twist between the triangles

$$\chi_{12} = \hat{p}_1\cdot(\hat{c}_1\times\hat{c}_2)+\hat{p}_2\cdot(\hat{c}_1\times\hat{c}_2) = (\hat{p}_1+\hat{p}_2)\cdot(\hat{c}_1\times\hat{c}_2) \qquad (7.4.2;7)$$

This quantity has the correct symmetry properties and for deformations such as those in illustrated in figure 7.6 (deformations with co-linear chiral fields) it corresponds to the intuitively apparent value of the twist of the triangles.

One expects that the twist between a plaquette α and its twist neighbour β, $\chi_{\alpha\beta}$, as defined above should become equivalent to the geodesic torsion, τ_g, in the continuum limit.

Now this quantity can be classed as a strain type quantity. One forms the corresponding stress quantity in the usual way, by making the elastic approximation. One arrives at the following Hamiltonian for the membrane

$$H_{chiral} = \frac{\kappa_\chi}{2} \sum_{\langle\alpha,\beta\rangle} \chi_{\alpha\beta} \qquad (7.4.2;8)$$

where k_χ is the chirality for the model and should correspond to the chirality of the continuum model defined in (7.4.2;5).

7.5 Results Of MC Simulation Of TCLB Model

Having constructed a model and Hamiltonian for the study of TCLBs, in this section I present the results of Monte-Carlo (Metropolis *et al*) simulations of the model. Figure 7.7 illustrates the general form of membrane geometry that I intend to investigate. For long thin membranes one has $l_x \gg l_y$ whilst conversely for diamond shaped regions one has $lx \ll ly$.

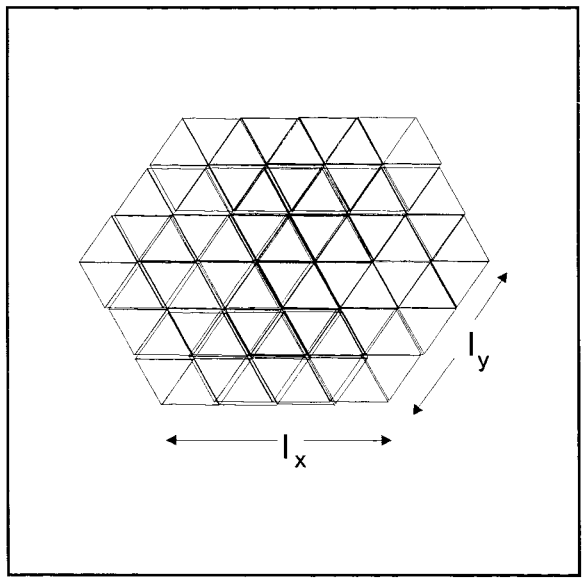

Figure 7.7
General membrane geometry to be considered.

Initially I investigate long-thin membrane geometries, as something of the behaviour of these geometries is known from experimental and mean field studies. Moreover long-thin geometries are less computationally demanding than the alternatives. Next I consider diamond shape geometries. Diamond shaped geometries represent a significant increase in complexity, for the analytical problem. Membrane self avoidance and the competing stresses within the membrane are the source of this extra complexity.

7.5.1 Results For Long-Thin Membranes

The particular long-thin membrane geometry that I have considered is illustrated in figure 7.8.

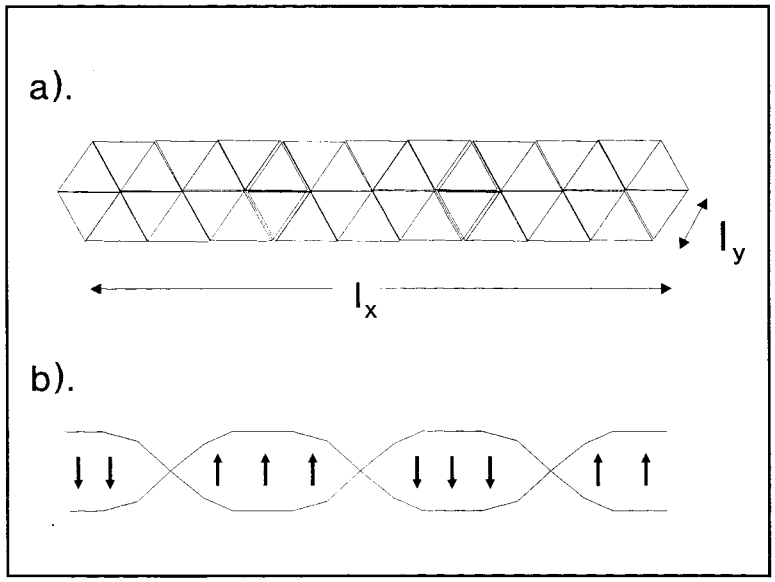

Figure 7.8
Long thin membrane geometry under consideration, (a.), with mean field result (b.).

The mean field models (Helfrich and Prost 1987, Zhong-can and Jixing 1991) predict that this geometry should form the twisted strip configuration, also illustrated in figure 7.8, in order to minimise the chiral energy. In figure 7.9 I have plotted the *twist*, χ, of the membrane in response to the chiral Hamiltonian defined by

$$\chi = \frac{1}{N_\chi} \sum_{\langle \alpha,\beta \rangle} \chi_{\alpha\beta} \qquad (7.5.1;1)$$

where N_χ is the number of triangle pairs over which the pair twist $\chi_{\alpha\beta}$ is summed. It can be seen that the twist is a measure of the torsion of the membrane as a whole. It has a maximum value of one and as such can be regarded as an order parameter for chirality.

Several length membranes are considered. Each membrane has the minimum possible width of unity. The figure indicates that for these long thin membranes the response is almost independent of the length. Initially the membrane is equally likely to twist in one direction as the other. Hence initially the twist of the membrane is on average zero. As the chiral elastic constant is increased the membrane energetically prefers to twist in one direction in preference to the other. Consequently the twist increases. The twist continues to rise with the chiral elasticity but the rate of increase is reduced as the maximum value of one is approached. In fact the twist appears to approach the maximum value only very slowly.

In figure 7.10 and figure 7.11 membrane configurations from the Monte Carlo simulations are displayed. In figure 7.10 the membrane is free of the chiral effect whilst in figure 7.11 the chiral effect is strong. One can see from the membrane configurations the effect of the chiral Hamiltonian is indeed to twist the membrane. I have attempted to quantify the observed twisting by evaluating the *inverse pitch / wavelength* of the twisting defined by

$$\lambda = \frac{1}{L}\sum_{i=1}^{N} \hat{L}.(\tilde{p}_i \times \tilde{p}_{i+1}) \qquad (7.5.1;2)$$

where

$$\tilde{p}_i = p_i - p_i.\hat{L} \qquad (7.5.1;3)$$

and $\underline{L}$ is defined as the end to end displacement of the membrane.

The response of the inverse pitch of the twist to the chiral elasticity is plotted in figure 7.12. As with the twist the inverse pitch of the membrane is initially zero. As the chiral elasticity is increased the inverse pitch rise rapidly. As the chiral elasticity is increased still further the inverse pitch of the membrane begins to flatten out. The results for the inverse pitch for different membrane lengths do not appear to lie on the same curves, although the asymptotic value is arguably the same. It is also interesting to note that the inverse pitch appears to reach asymptotia somewhat earlier than the results for the twist.

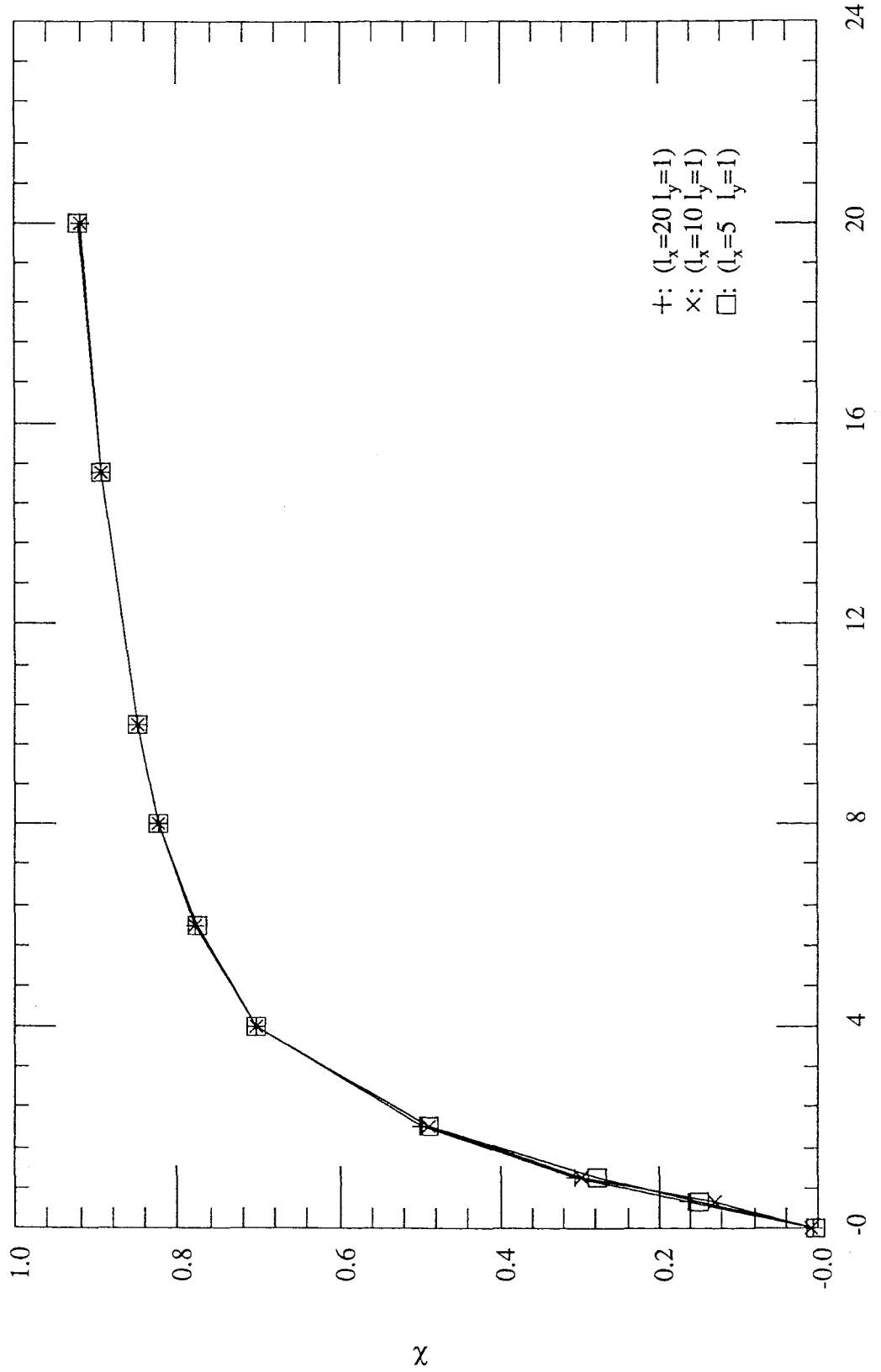

Figure 7.9

Plot of twist parameter, χ, against chirality, κ_χ for long thin membranes.

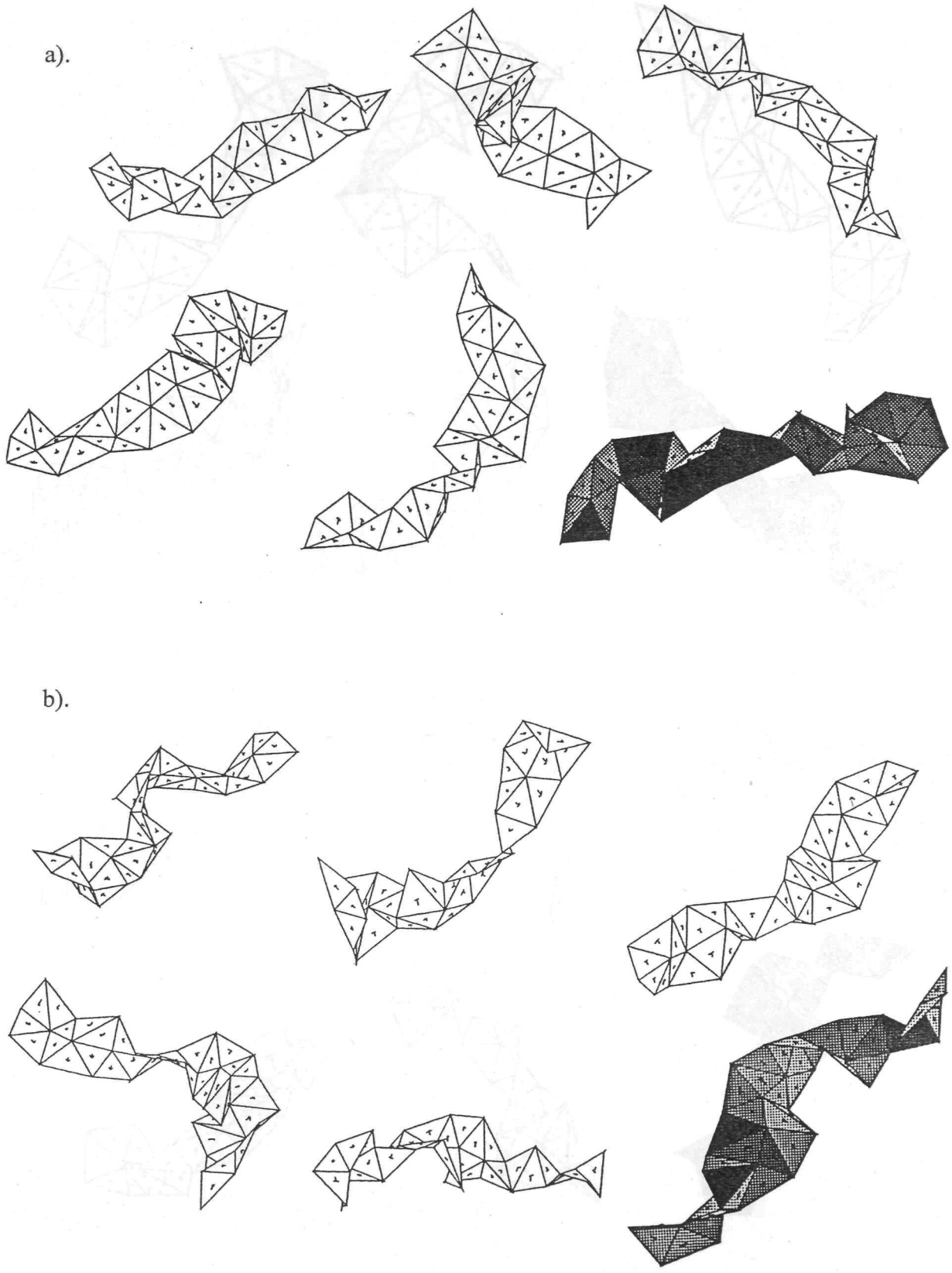

Figure 7.10

Membrane conformations observed during simulation for long thin geometry (l_x=10,l_y=1) with a). κ_χ = 0.0 and b). κ_χ = 2.0.

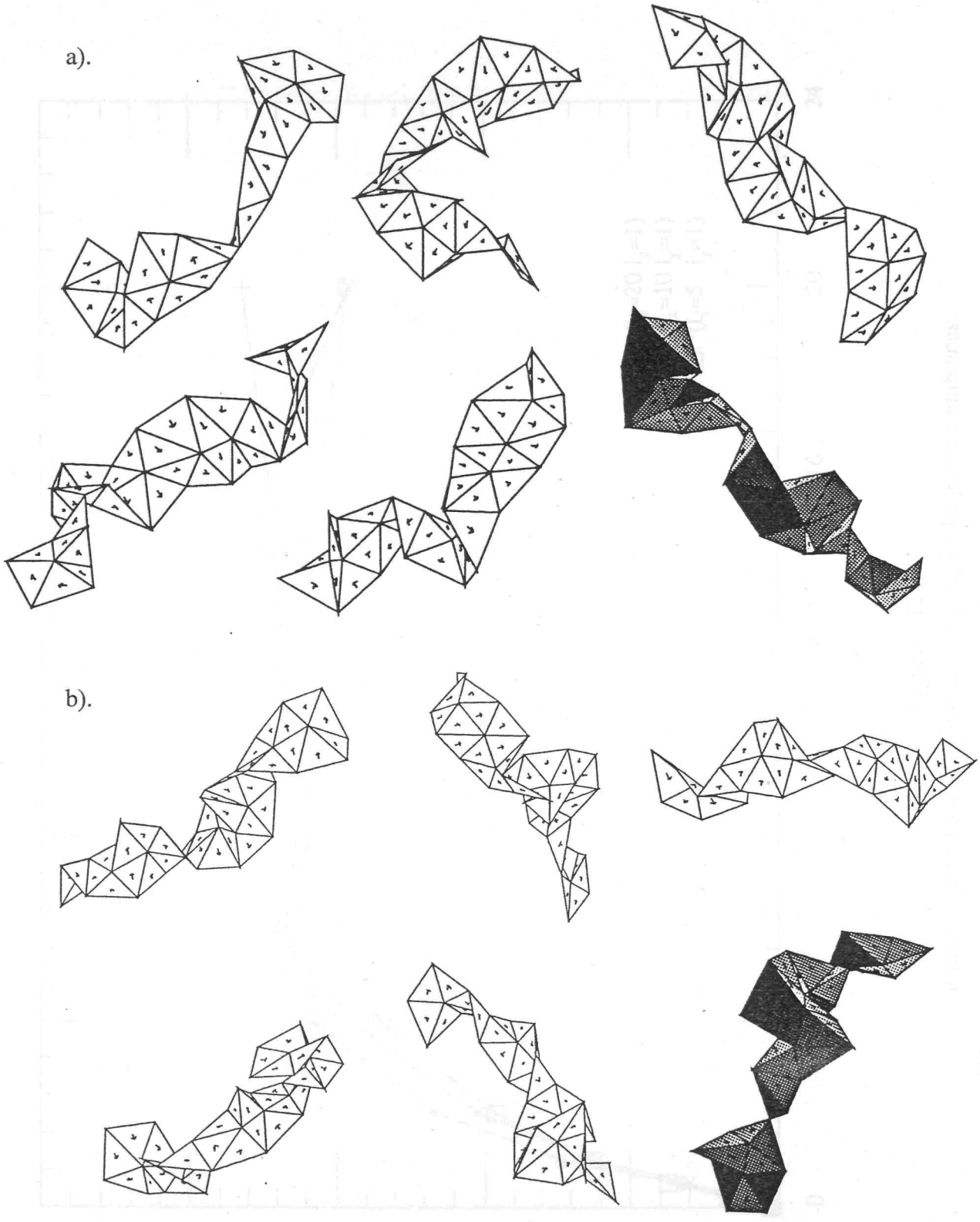

Figure 7.11

Membrane conformations observed during simulation for long thin geometry (l_x=10,l_y=1) with a). κ_χ = 4.0 and b). κ_χ = 15.0.

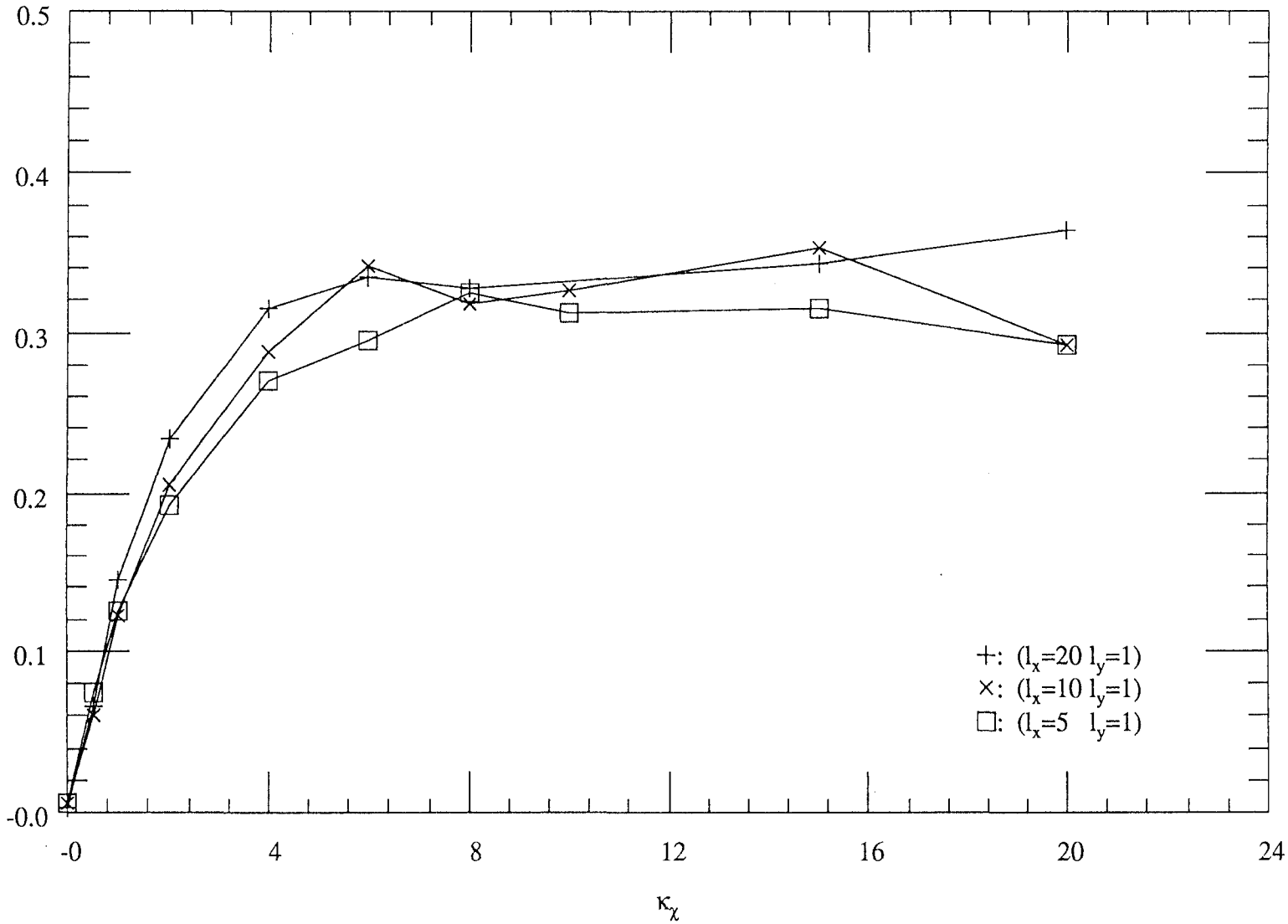

Figure 7.12

Plot of inverse pitch, λ, against chirality, κ_χ for long thin membranes.

7.5.2 Results For Diamond Shaped Geometries With Self-Avoidance

The particular diamond shaped geometry that I shall study is illustrated in figure 7.13.

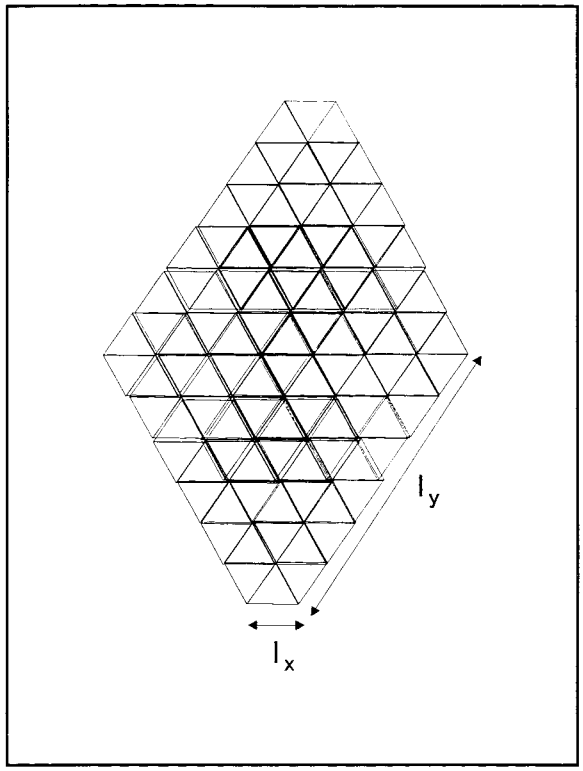

Figure 7.13
"Diamond" shaped geometries.

One can see that the region is in fact not quite a diamond. Two points of the diamond have been shaved. There is no particular physical significance in this, it merely aided the implementation of the software.

Mean field models are unable to predict what the effect of the chirality will be on such an object. This is because if one attempts to minimise the chiral energy of such an object one is bound to arrive at a configuration that intersects itself, and, this is of course in reality, forbidden.

I have considered several sizes of membrane. In figure 7.14 I have plotted the twist (7.5.1;1) response of the membrane against the chirality. As before the twist of the membranes is zero when the chirality is zero because then the membrane has no preferred direction to twist in. Again as the chirality is increased the twist of the membranes rapidly increase. In contrast to the long thin geometry, the different size membranes appear to have different twist response profiles. The larger the membrane

the lower the apparent response to the chirality is. As the chirality is increased further the twist of the membranes begin to flatten. The apparent asymptotic values appears to depend on the size of the membrane and is clearly no the maximum value of unity. Hence it would appear that self-avoidance effects or some other consideration prevents the membrane from achieving the maximum twist value required for minimisation of the chiral energy. This in itself is interesting.

In figure 7.15 and figure 7.16 membrane configurations from the Monte Carlo simulations are displayed. In figure 7.15 the membrane is free of the chiral effect whilst in figure 7.16 the chirality is strong. The free membrane is rather "flat" as expected (free polymerised membranes are widely recognised to be "flat"). The effect of the chirality on the other membrane is immediately apparent. The chiral membrane is "rolled" up. The roll appears to be "sheared" somewhat along the axis of the roll. Further, increasing the chirality appears to cause the membrane to roll up more tightly. See the figures for a better explanation.

For completeness, I have plotted the inverse pitch parameter for the diamond shaped membranes in figure 7.17. The parameter was strictly not designed to be sensible for rolled up diamond shaped membranes. In particular the definition of $\underline{L}$ is questionable value in this context.

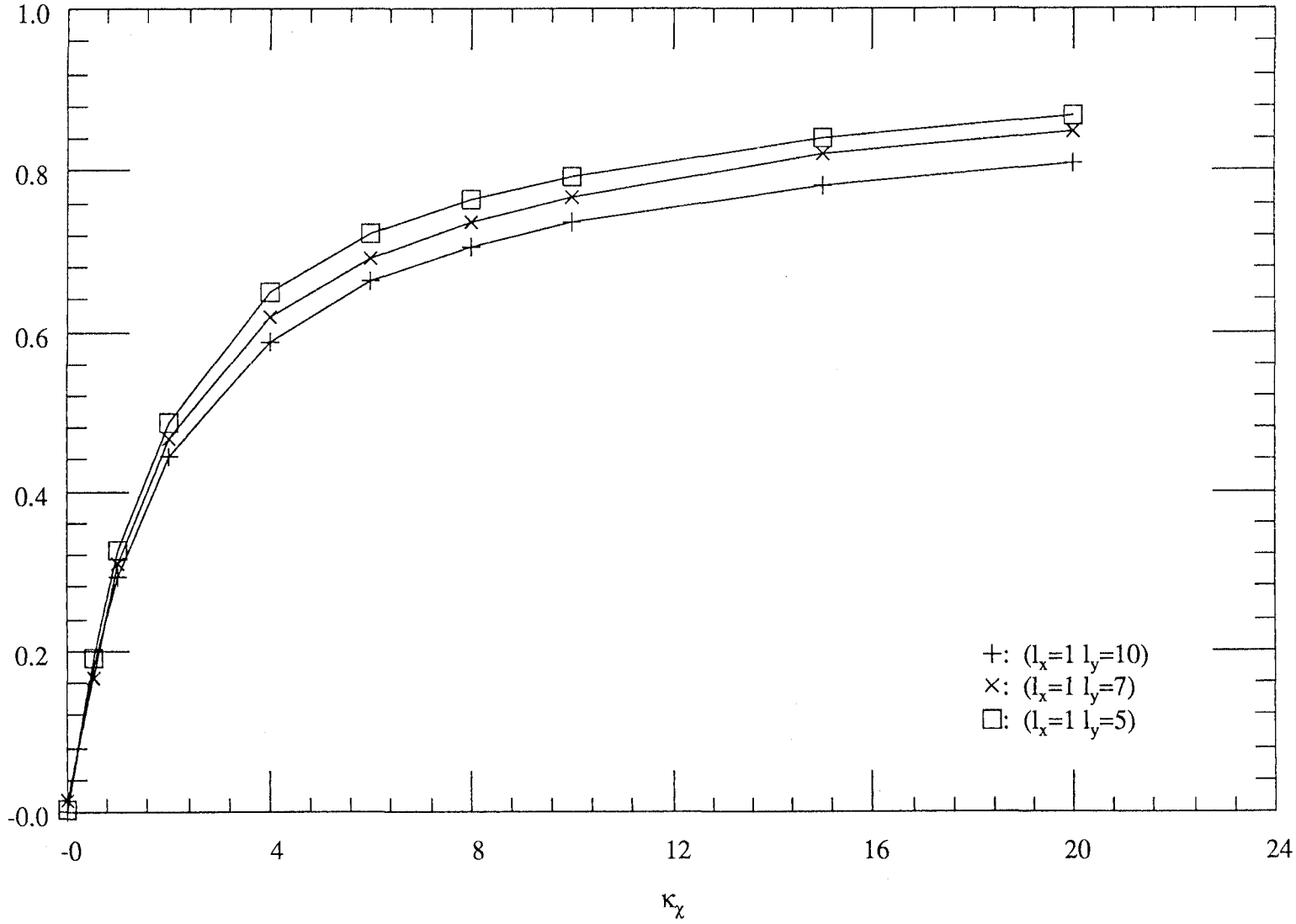

Figure 7.14

Plot of twist parameter, χ, against chirality, κ_χ for diamond shaped membranes.

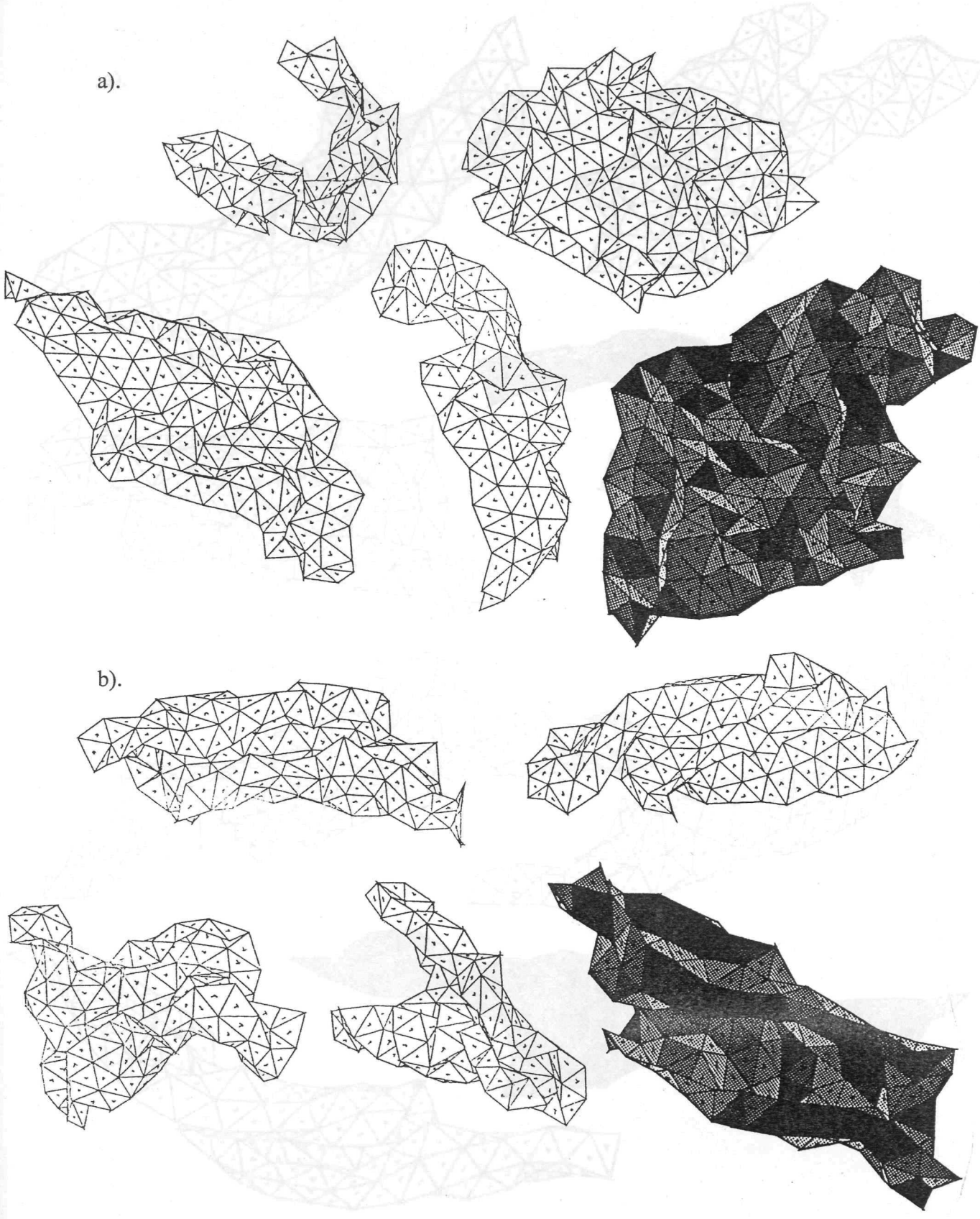

Figure 7.15

Membrane conformations observed during simulation for diamond shaped geometry (l_x=1,l_y=10) with self-avoidance for a). κ_χ = 0.0 and b). κ_χ = 2.0.

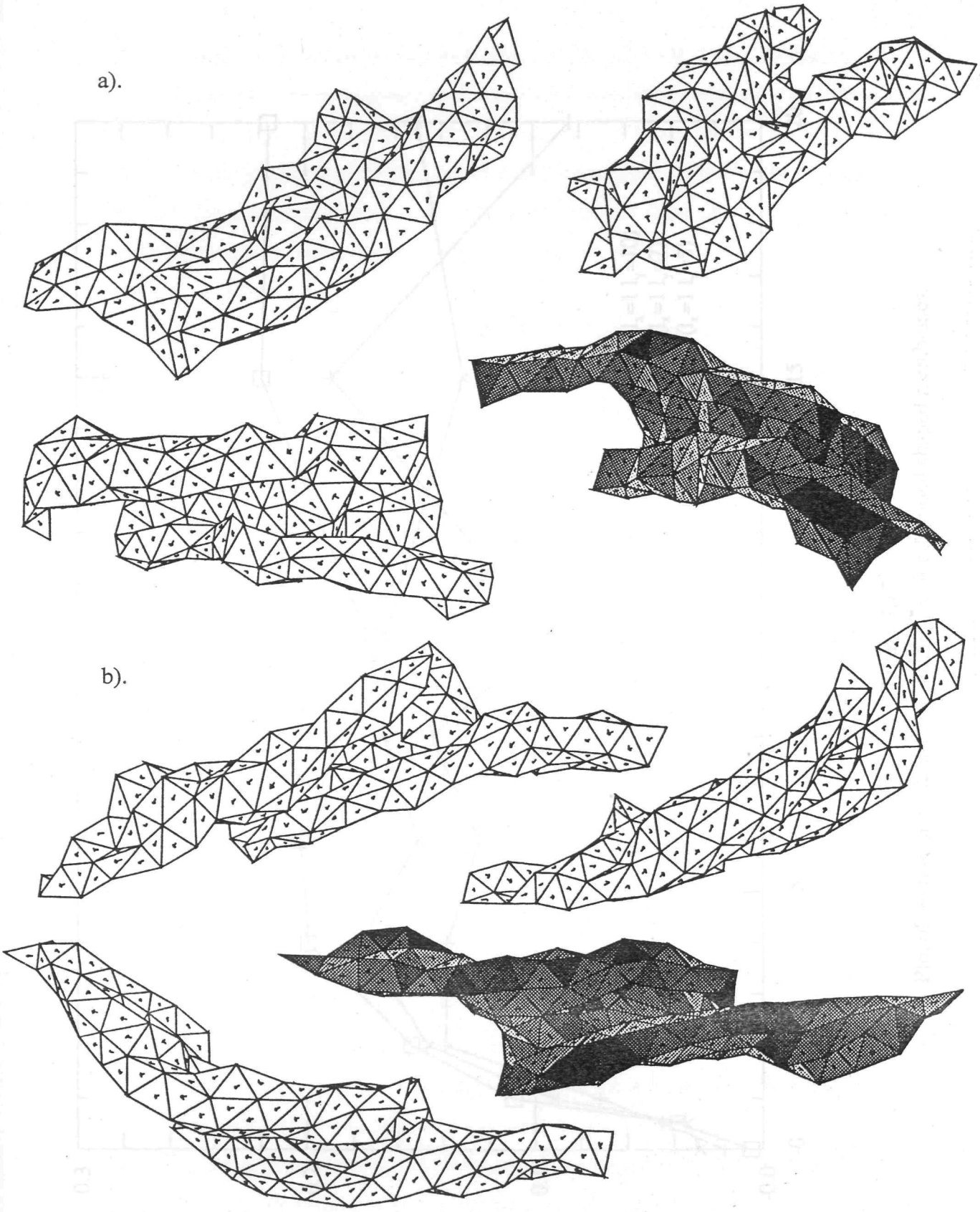

Figure 7.16

Membrane conformations observed during simulation for diamond shaped geometry (l_x=1,l_y=10) with self avoidance for a). κ_χ = 4.0 and b). κ_χ = 20.0.

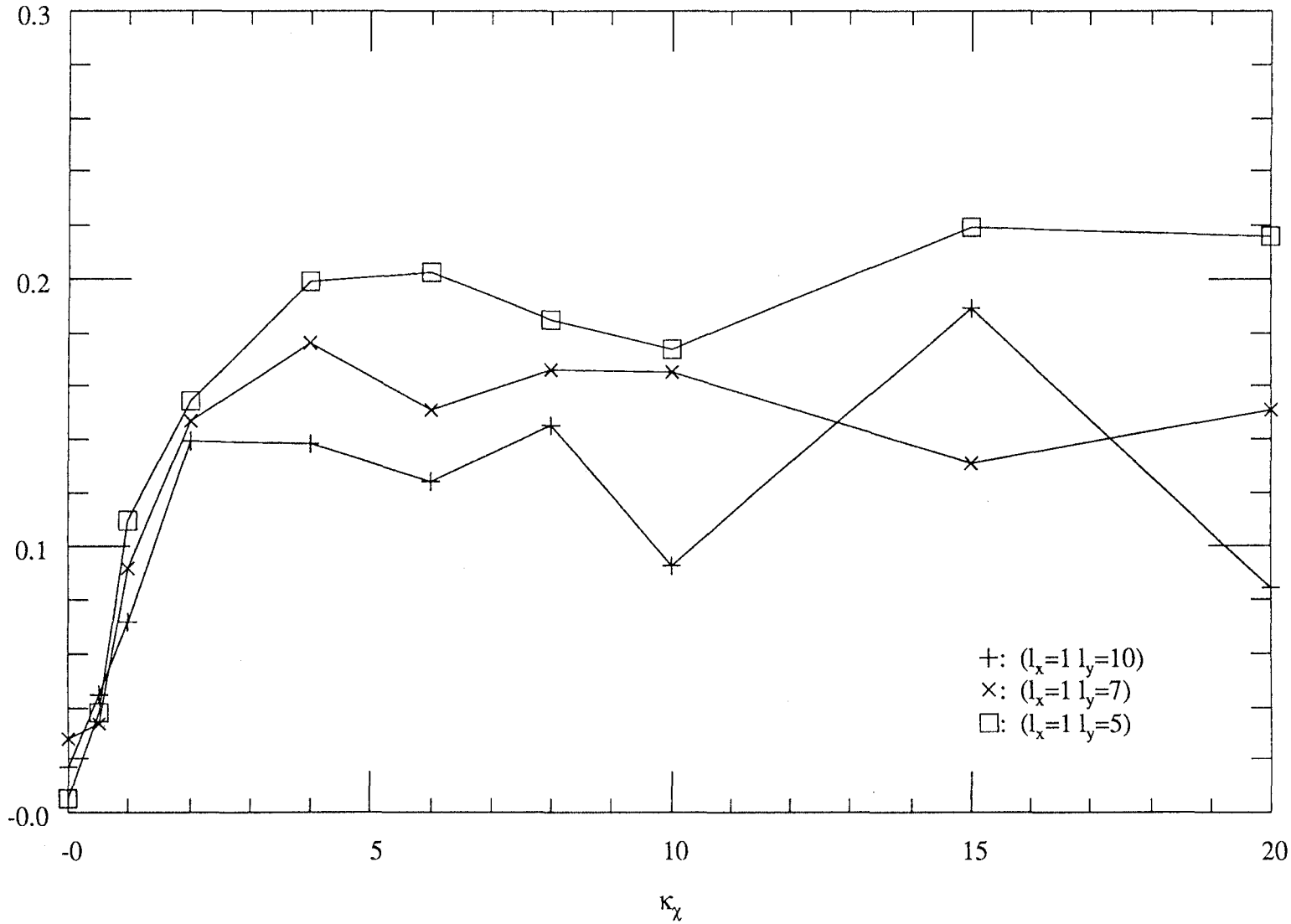

Figure 7.17

Plot of inverse pitch, λ, against chirality, κ_χ for diamond shaped membranes.

7.5.3 Results For Diamond Shaped Geometries Without Self-Avoidance

For completeness I present some results for simulations where the self-avoidance property of real physical membranes is not enforced. These results can be compared with the analogous results for the self-avoiding membrane. Ideally one would like to compare the results with the mean field result for the fluid ghost membrane. This would allow one to easily pinpoint the effect that the polymerisation of the membrane has on its conformation.

In figure 7.18 I have plotted the twist (7.5.1;1) response against the chirality. I have plotted the analogous result for the self-avoiding membrane for easy comparison. Initially the twist of the ghost membrane rises somewhat more slowly than for the corresponding self-avoiding surface. This can be understood by considering the fact that the ghost membrane with zero chirality has a much larger range of accessible conformations. This is reflected by the way that the membrane is initially in a somewhat crumpled state. As the chirality is switched on the membranes can no longer access all the previously accessible states on energetic grounds. The ghost membrane has to gain significantly more entropy to satisfy the same energetic constraints. Consequently, initially it responds more slowly to the Hamiltonian.

As the chirality is increased further the twist of the ghost membrane eventually exceeds that of the self-avoiding membrane. This too can easily be understood. As the chirality is increased the membrane rolls up. The self-avoiding membrane is unable to roll up as tightly as the ghost membrane because many of the rolled up configurations are disallowed due to steric hindrance. Hence the self-avoiding membrane now has to gain more entropy to balance the same chiral driving Hamiltonian.

As a consequence the ghost membrane's response curve contains a point of inflection whereas, interestingly, the self-avoiding membrane's does not.

The difference in the twist between the ghost and the self-avoiding membrane is a measure of the degree to which the self-avoidance affects the conformation of the membrane. Similarly the difference in twist between the ghost membrane and the theoretical maximum twist, 1, is a measure of the degree to which the polymerisation affects the conformation of the membrane. Using this criterion the non-zero shear property of this model of membranes appears to be at least as important as the self-avoidance property in affecting the conformation of the membrane.

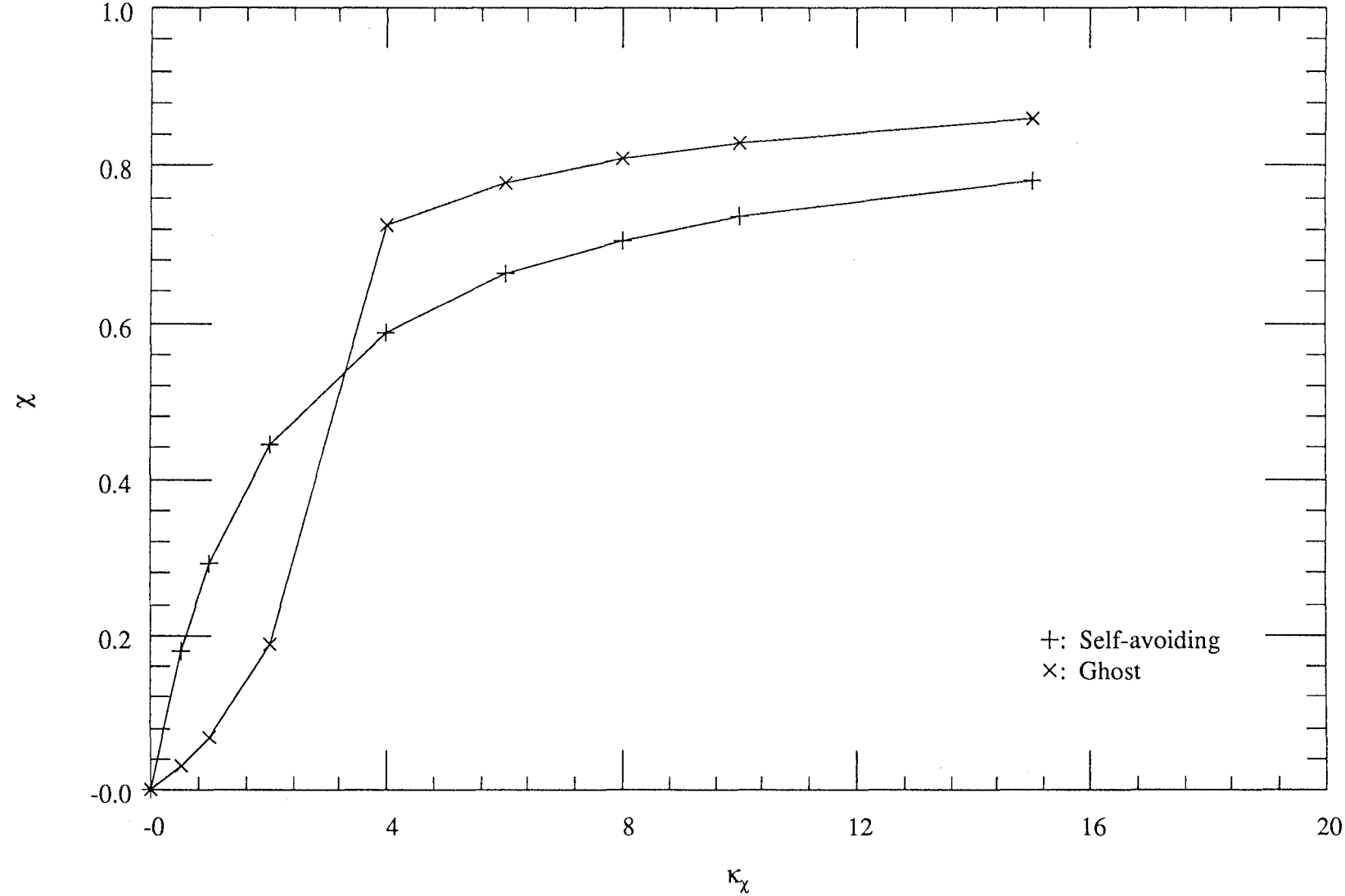

Figure 7.18

Plot of twist parameter, χ, against chirality, κ_χ for diamond shaped ghost membrane compared with. analogous self-avoiding membrane. (l_x=1 l_y=10)

In figures 7.19 and 7.20 I have plotted actual membrane conformations typically obtained from the simulations. The effect of removing the self-avoidance of the membrane is immediately apparent. The membranes with zero chirality are no longer flat; rather they are somewhat collapsed. The highly chiral membranes are not collapsed. Rather they are essentially the same "rolled up" and sheared shape as the self-avoiding membrane. In this case however the membrane can "roll up" even more tightly since the membrane can now pass through itself.

The delayed onset of the membrane twist as evidenced by figure 7.18 can be seen visually in the figures. Comparison with the conformations for the self-avoiding membrane in figures 7.15 and 7.16 confirm this. Also at high chiralities it is also clear from comparison with the self-avoiding membranes that the ghost membrane are more able to twist.

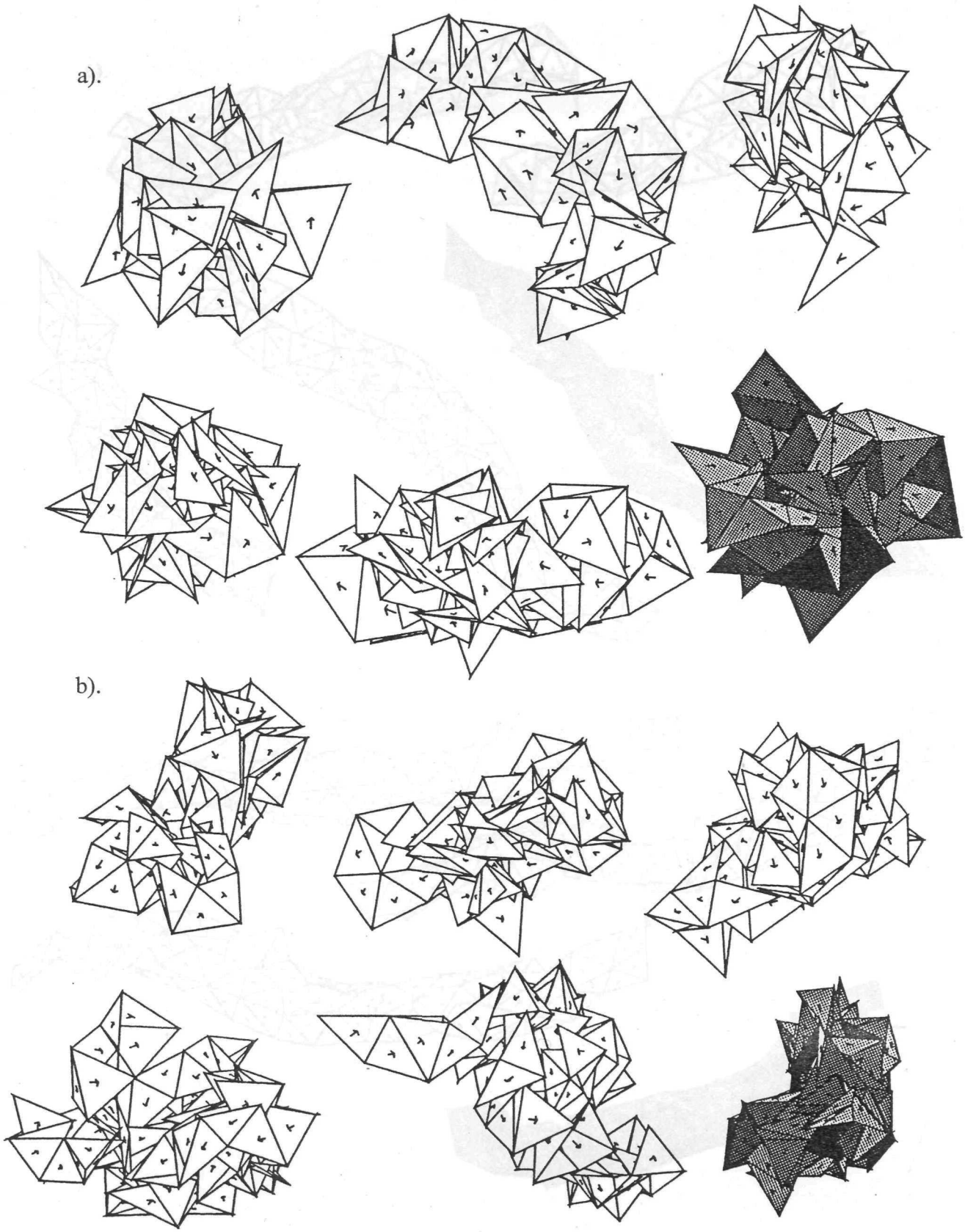

Figure 7.19

Membrane conformations observed during simulation for diamond shaped geometry (l_x=1,l_y=10) without self-avoidance for a). κ_χ = 0.0 and b). κ_χ = 2.0.

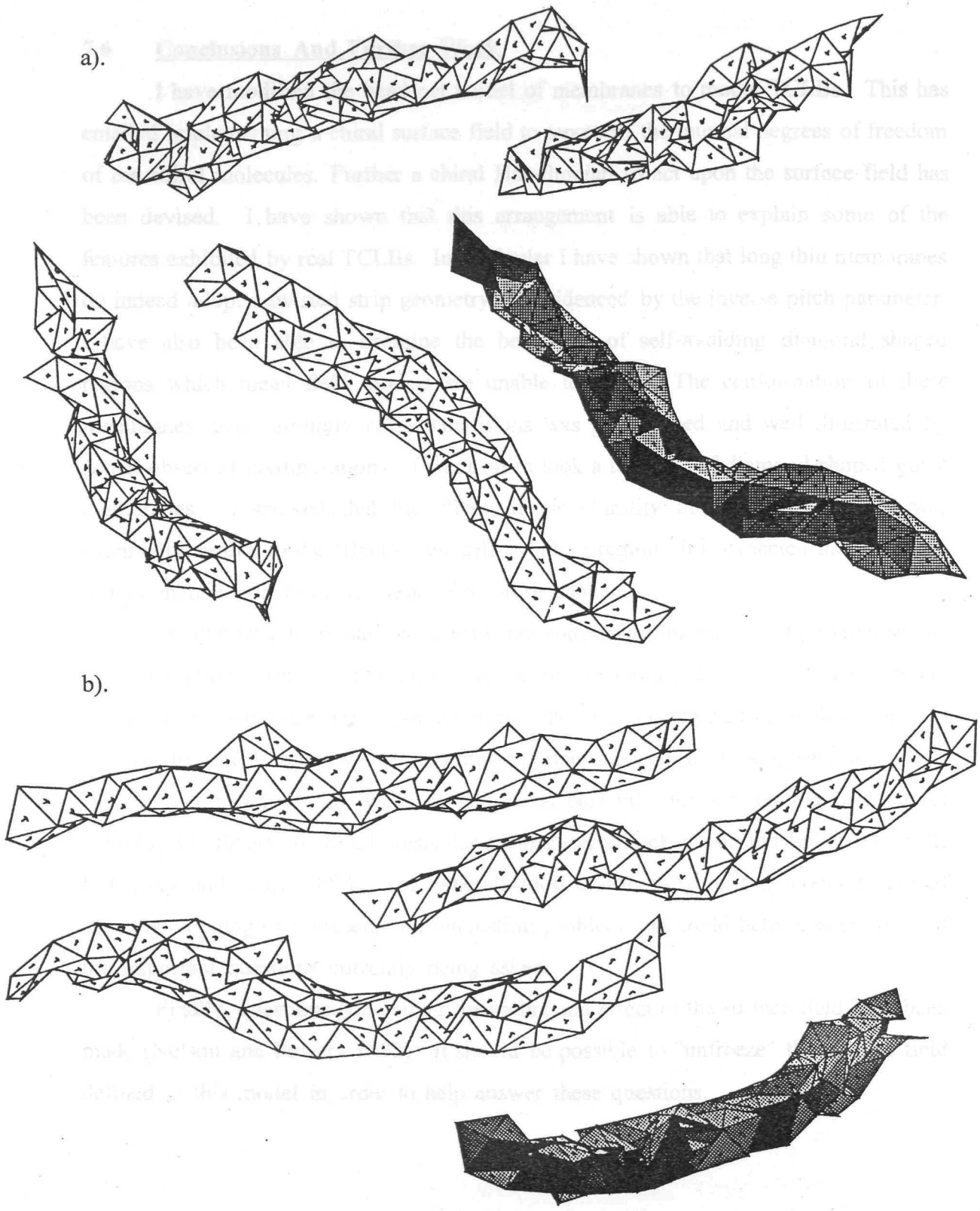

Figure 7.20

Membrane conformations observed during simulation for diamond shaped geometry (l_x=1,l_y=10) without self avoidance for a). κ_χ = 4.0 and b). κ_χ = 10.0.

7.6 Conclusions And Further Work

I have modified the bead net model of membranes to model TCLBs. This has entailed implementing a chiral surface field to represent the internal degrees of freedom of the chiral molecules. Further a chiral Hamiltonian to act upon the surface field has been devised. I have shown that this arrangement is able to explain some of the features exhibited by real TCLBs. In particular I have shown that long thin membranes do indeed adopt a twisted strip geometry, as evidenced by the inverse pitch parameter. I have also been able to examine the behaviour of self-avoiding diamond shaped regions which mean field models are unable to solve. The conformation of these membranes under strongly chiral conditions was pronounced and well illustrated by actual observed configurations. I went on to look a the case of diamond shaped ghost membranes. I showed that the effect of the chirality on the ghost regions was essentially similar to the effect on the self-avoiding region. It is expected that the work in this chapter will form the basis of a future publication.

Many questions remain to be answered concerning the effect that polymerisation of the membrane has on the conformation of the membrane. Since real TCLBs are not polymerised then these are important questions. The generalisation of this model to case of fluid membranes would provide important answers to these questions.

Also much of the work on TCLBs is currently focused on the problem of applying the theory to closed, vesicular membranes (MacKintosh and Lubensky 1991, Lubensky and Prost 1992). The generalisation of this polymerised model to closed vesicular topologies represents an interesting problem and could help answer some of the important questions currently being asked.

Finally, questions concerning the nature and effect of the surface field have been made (Nelson and Powers 1992). It should be possible to "unfreeze" the surface field defined in this model in order to help answer these questions.

CHAPTER EIGHT

FINAL REMARKS AND FURTHER WORK

8.1. Conclusions

In this final chapter I shall make some concluding remarks and re-iterate some points concerning further work.

In this thesis I have tried to gently introduce the reader to some of the ideas, methods and concepts currently in use in statistical physics today. In particular, these ideas have been used to study the complex statistical mechanical properties of exotic liquid crystalline structures.

In this light I have first familiarised the reader with many of the complex liquid crystalline structures. Then using simple models of the bilayer I explained the origin of many of the terms in the bilayer Hamiltonian. In particular I showed the importance of curvature in the bilayer Hamiltonian and motivated the Helfrich curvature Hamiltonian, which is ubiquitous in the later chapters.

Then I introduced the reader to some of the important ideas and concepts used to model and analyze the statistical mechanics, indeed the physics, of polydisperse systems. In particular I introduced universality, fractality and the renormalisation group in the context of free-flight chains and self-avoiding walks.

Having introduced many of the necessary analytical tools required to investigate and model statistical systems I proceeded to look at a particular system. I showed that there were several ways in which one could model two dimensional vesicles. I briefly discussed a particularly successful mean field model due to Helfrich and a statistical mechanical model due to LSF. Then I made a detailed examination of a statistical mechanical model proposed by Ostrowsky and Peyraud. I was able to extend the model far beyond the initial expectations of the originators. In fact the model was able to compete successfully with the alternative model of Leibler, Singh and Fisher. Heartening agreement was found in comparisons of the results, even to the point of reproducing a suspected anomaly in some of the results. This was really quite

remarkable considering the radically different nature of the models. The methods introduced earlier proved invaluable in the analysis of the results. In particular the importance and power of ideas of universality were clearly demonstrated. Moreover the renormalisation group was shown to be an invaluable tool in the explanation and motivation for the observed universality. Generalisation of the model to three dimensional vesicles has, so far, proved impossible. Consequently further development of the model is only of restricted interest.

Having discussed a two dimensional model of vesicles I went on to look at a model of interfaces that could be generalised to membranes; the so called solid on solid model. The model of the interface consisted of an interface confined between hard parallel walls, and subject to a surface/line tension Hamiltonian. The membrane was modelled by subjecting the membrane to a Helfrich curvature Hamiltonian. A novel argument motivating a generic universal form for the probability density function of confined surface objects was discussed. I discussed the transfer matrix solution of the interface model in two dimensions. We saw that the analytical result for the interface in two dimensions accorded with the generic universal form. It was noted that a novel a solution for the membrane in two dimensions indicates that it too accords with the generic universal form, albeit with a different and characteristic universal exponent to the interface.

In order to investigate the validity of the generic universal form for the pdf and the novel solution of the pdf of the membrane in two dimension, I performed an extensive set of Monte Carlo simulations on the model. I showed that the method of simulation concurred with the well established transfer matrix result for the interface in two dimensions, indicating the veracity of the method. The membrane in two dimensions was indeed shown to have a universal regime. Moreover the universal form did indeed concur with the generic universal form, indicating that at the very least the generic form is a good parameterisation of the results. The value of the universal exponent was not inconsistent with the value obtained from the novel analytical argument reported to us.

I considered the analogues of the interface and membrane in three dimensions. I was unable to obtain a universal regime for the interface in three dimensions. However, I did achieve a universal regime for the membrane in three dimensions and

I determined the universal exponent. Again the generic universal form represented a good parameterisation of the result, although the argument strictly only applies to the two dimensional models.

I investigated a polymer type model of the two dimensional membrane. A scaling analysis of SDE results indicated that a universal regime had been achieved. I was unable to obtain an analytical argument to supplement this experimental result. I did not investigate the three dimensional generalisation of this model (the bead-net membrane model) as I decided that I was unlikely to be able to obtain the universal regime due to computational limitations.

In the next chapter I introduced a statistical mechanical model of tilted chiral lipid membranes. I discussed the fact that to study tilted chiral lipid bilayers one has to consider the internal structure of the membrane. I modified the bead-net membrane (tethered surface) model to take account of the internal structure of the membrane. I proposed a Hamiltonian to model the effect of the chirality of the constituent molecules of the membrane, motivated by the geodesic torsion form of the chiral term obtained from the Frank theory of elasticity. Results for long thin membranes indicated that the effect of the chirality was indeed to cause the membrane to twist, as evidenced by a non-zero inverse pitch. The case of parallelogram or diamond regions was investigated. Membrane conformations observed during the simulations were presented. In this geometry it was expected that membrane self-avoidance and the polymerised nature of the membrane would affect its conformation. The ghost membrane was studied. The effect of the chirality on the ghost membrane allowed one to understand the effect the self-avoidance was having on the conformation of the self avoiding membrane. The ghost membrane was not able to achieve the maximum order parameter, the twist, even for large chiralities. Nevertheless at high chiralities the ghost membrane was more twisted than the self-avoiding membrane. I concluded that this effect was due to the polymerisation of the membrane and that one should expect the conformation of the fluid self-avoiding membrane to be as different from the self-avoiding membrane as was the ghost membrane.

8.2 Further Work

Scope for further work on the two dimensional vesicle model of Ostrowsky and Peyraud as it stands is somewhat limited. The method is rather involved and having confirmed the equivalence of the results of this model and the LSF model then there is no advantage to be conferred in using it. In contrast the LSF model is rather easy to study. However, if the model could be generalised to three dimensions then the results would surely arouse interest. Unfortunately, I am not confident that the model can be successfully generalised to three dimensions.

In contrast there is some scope for further work on the confined interfaces and membranes. This work could focus on achieving universality for the confined polymer model or the interface in three dimensions. Also the universal regime for the membrane in three dimensions could be improved. Moreover one could model the confined tethered membrane with interesting results. However this work will have to await significant improvements in computational power. After all, that is why I have not accomplished the work in this thesis. One does not doubt that this improvement in computing resources will arrive. Also other approaches to the problem are possible, and, I am aware that, an investigation of the model using the Fokker-Planck method has been undertaken elsewhere.

The outlook for the final topic concerning the simulation of tilted chiral bilayers is brightest of all. There remain many unanswered questions. An important question concerns the effect of fluidising the membrane. A mean field study of a bulk membrane to characterise the conformation of the fluid ghost membrane should be possible and would undoubtedly be of use in predicting the conformation of the fluid self-avoiding membrane. The fluidisation of the current model should be possible to answer these questions directly. The effect of chirality on vesicular membrane structures is currently the focus of much of the mean field work. It should be relatively easy to form such a structure. One would expect the investigation to reveal some interesting effects. The fluidisation of the internal chiral field of the membrane should also be possible and would undoubtedly yield interesting results too.

APPENDIX A

BEAD SELF-AVOIDANCE ALGORITHMS

A.1. Introduction

In this appendix I briefly describe an efficient algorithm for the implementation of bead self-avoidance. Recall bead self-avoidance is important in that bead-chain and bead-net membrane models require bead self-avoidance in order to achieve membrane self-avoidance. First I shall describe the simplest algorithm for implementing bead self-avoidance, and variations. Then I shall discuss a more efficient algorithm. I shall compare timings for the two algorithms to illustrate the importance of the bead self-avoidance to the overall efficiency of the model.

A.2. The Simple Bead Self-Avoidance Algorithm

The problem we are faced with is, given a number of beads, say N, of equal diameter, say a, how can we detect whether a randomly moved bead impinges upon any other bead? The simplest answer to this question is that we check the position of the moved bead against the position of each of the other, N-1, beads in turn. If the distance between the bead centres is less than the bead diameters then the beads have impinged (and consequently in the Monte Carlo simulation the bead move must be rejected).

In this algorithm as it stands the average number of position comparisons required to detect an impingement is (N-1)/2. To determine that a bead does not impinge on any other bead takes (N-1) position comparisons. Therefore the number of position comparisons required per trial bead move is less than (N-1) and on average in excess of (N-1)/2. If on average half the trial bead moves were found to impinge then the number of position comparisons per trial bead move would be 3(N-1)/4.

In fact the computational complexity of requiring the bead self-avoidance is said to be of order 1 since the number of position comparisons depends linearly on the control variable N.

There are several ways to speed up the implementation of this algorithm. The basis of one method is to speed up the position comparison method. To compare whether a bead impinges a relatively quick preliminary test is carried out (the *extents* of the beads are compared to see if they overlap) which can often determine if a bead does not impinge. If the preliminary test cannot determine that the beads do not impinge then the more time consuming test is required. On average the number of time consuming tests, N_C say, is related to the spatial density of the beads. If, as often is the case, this is independent of the number of beads, N, then the number of preliminary tests, N_P say, will depend linearly on N through $N_P=N-N_C$. Then if on average half the trial bead moves were found to impinge then the number of preliminary position comparisons per trial bead move would be $3(N_P-1)/4$.

So performing quick preliminary tests does not improve the computational complexity of the algorithm since the number of position comparisons, albeit relatively fast preliminary position comparisons is still linear in N. Note that this does not mean that implementing the preliminary test method is not worthwhile, only that it is of limited use as N increases.

Another technique for speeding up this method requires some additional information from the membrane models. In the membrane models each bead is attached to, n, neighbouring beads by short tethers. Now when a bead moves it is more likely, on average, to impinge upon its, n, neighbouring beads than the remaining beads, since the bead can only make small moves and the neighbouring beads are always in the vicinity. By initially checking for impingement with the neighbouring beads one is able to reduce, on average, the average number of tests required to detect impinging beads.

Again it can be shown that this improvement does not affect the computational complexity of the problem. Nevertheless the improvement is still worthwhile.

A.3. The More Efficient Bead Self-Avoidance Algorithm

The improvements to the simple algorithm described above did not alter the computational complexity of the method. That is the time taken to ensure self-avoidance of N beads although reduced still depended linearly upon N. Here I discuss an algorithm which ensures self-avoidance of the beads, and whose computational

complexity is of order 0. That is the time taken to detect a whether a trial bead move causes an impingement is independent of the number of beads, N.

The method is based on the principal that a bead is only able to impinge on beads near to it. This truth of this statement is clear. The problem we have however is how we determine whether a bead is near or not. In the second improvement to the simple method I noted that the method could be improved by testing the neighbouring beads for impingement first. That was possible because the additional information of which of the beads was a neighbouring bead was available to us. Unfortunately having tested the neighbouring, n, beads and found them not to have been impinged then the remaining N-n beads had to be tested. For that reason the improvement did not alter the computational complexity and so was of limited value. One needs a way of determining all of the local beads.

To determine the local beads space is divided up by a "background" or "shadow" lattice. Ideally the lattice spacing should be a single bead diameter, a, but may be larger if necessary because of computer memory constraints. Initially each lattice site contains a list of the beads located within it. To maintain the lattice site bead lists they are updated every time a bead move is accepted. When a trial bead move is made the lists are temporarily updated; they will be reset if the bead move is rejected. In fact an update of the lists is only necessary if the bead changes its lattice site during the move. The update consists of removing the bead from the initial lattice site bead list and appending it to the destination lattice site bead list.

Now one can check whether the moved bead impinges with any other by checking that it does not impinge with any bead in the destination lattice site or the surrounding lattice sites. No other checks are necessary. Now consider the situation for the 2d bead ensemble with a square lattice, illustrated in figure A.1.

In the ideal case where the lattice spacing is a single bead diameter it can be seen that the maximum number of beads a single lattice site can contain is two. The destination lattice site has eight neighbours. Therefore the maximum number of position comparisons necessary is 17 ($1+8\times2$). In fact the maximum number of beads that can be packed into the destination lattice site and its neighbours is 14 (in a hexagonal arrangement). Consequently the maximum number of position comparisons is actually 13. In practice the beads are most unlikely to be packed so densely and the

average number of position comparisons required is unlikely to exceed 5 or so (every other lattice site occupied).

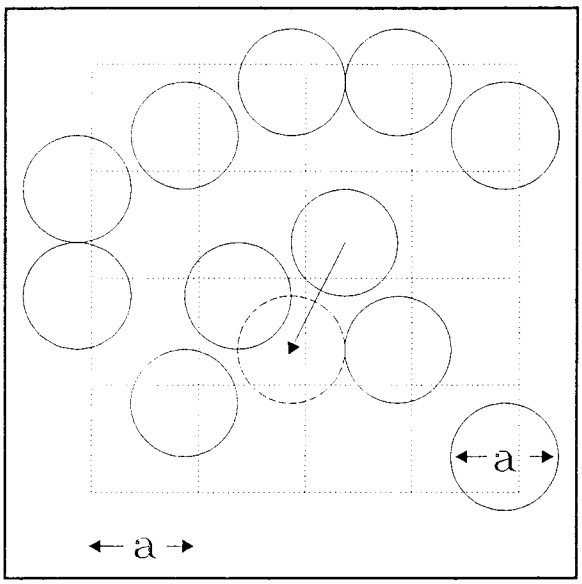

Figure A.1.
Shadow lattice for a 2d bead ensemble.

So it can now be seen that the number of bead comparisons depends on the lattice site geometry and the density of beads in the lattice but not the number of beads. Consequently the computational complexity is now order 0 since the time taken to determine an impingement is independent of the control parameter N. So despite the (minimal) time overhead of building, maintaining and traversing lattice site bead lists this method will be more efficient, at least in the limit of large N, than the simple method.

Note that in practice for the 2d simulations of a bead-chain membrane confined to a strip (section 6.12), of width d, I used a 1d shadow lattice so that the lattice sites were rectangular strips perpendicular to the wall. This has two advantages over the square lattice arrangement. Firstly, each lattice site has only two neighbouring lattice sites and consequently there are only three lattice site bead lists to be checked for each bead move rather than the nine of a square lattice. Secondly the amount of computer memory required for implementing the shadow lattice is significantly reduced as the number of lattice sites is far less (~N as opposed to ~Nd). The main disadvantage of this scheme is that the number of position checks per bead could be large if the bead-

chain were to align itself along a particular lattice site. If the bead chain is long with respect to the separation of the walls, as is the case in the simulations considered, then it can be seen that this is not an important consideration.

Similarly in practice for the simulations of the bead net membrane in 3d (chapter 7) I used a 2d square lattice extended infinitely in the out of plane direction. The same advantages and disadvantages apply. However memory considerations are likely to be even more important since the number of lattice sites $\sim L^3$ for a cube lattice and $\sim L^2$ for the 2d lattice; where L is the length of the membrane.

A.4. A Comparison Of The Simple And Efficient Bead Self-Avoidance Algorithms In Practice

Now in order to demonstrate computational the improvement of the latter algorithm I have plotted in figure A.1 a comparative plot of the time taken to simulate a bead-net model of a membrane in 3d using the simple and more efficient algorithm of self avoidance. I plot also the time taken to simulate a ghost membrane so that the overhead for implementing self-avoidance can be seen. The simple algorithm implemented includes the two improvements discussed in the previous section. The more efficient algorithm timing includes the time overhead of initialising and maintaining the shadow lattice. From the plots it is clear that the for the efficient algorithm the time taken per bead to maintain self-avoidance is independent of the number of beads, as claimed. It is also evident that for the simple algorithm the time taken per bead to maintain self-avoidance depends linearly on the number of beads, as claimed. Moreover it can be seen that a timing saving factor in excess of 20 can easily be achieved using the efficient algorithm for moderately sized simulations.

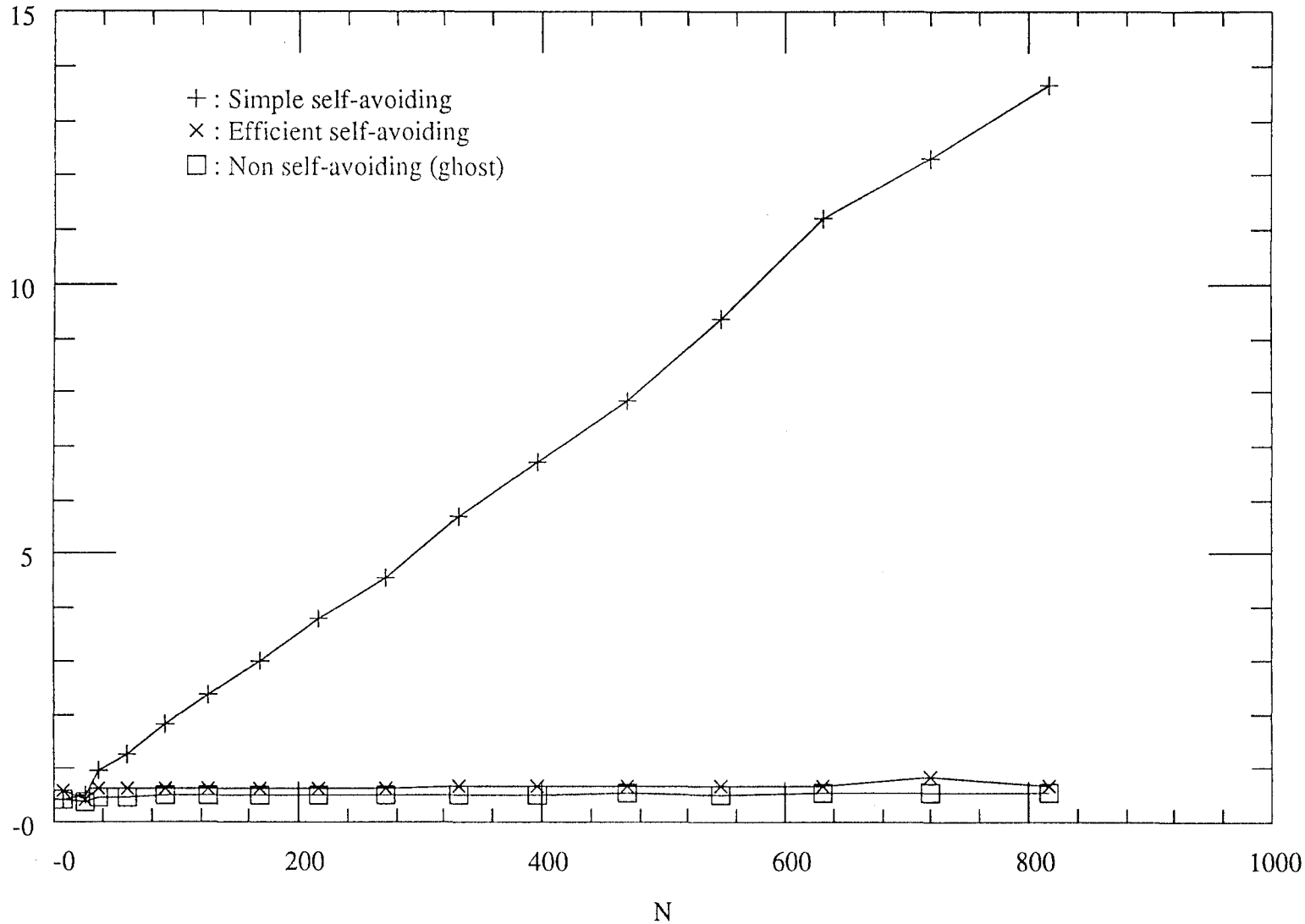

Figure A.1

Comparison of time per bead move, τ, for simple self-avoiding, efficient self-avoiding and non self-avoiding algorithms. (Varying N with d=5.0)

APPENDIX B

INCLUDED SOFTWARE

B.1. Introduction

In this appendix I detail the software on the included disk. The disk is a high density disk and is in sun tar format. To extract the software from the disk log on to a sun terminal or workstation. Place the disk into the workstation floppy disk drive and type the following command:

tar -xvf /dev/rfd0

whereupon the software will promptly extracted from the disk. Details of how to use the software are included on the disk.

B.2 Structure of the included software.

The software on the included disk is divided into three toplevel directories (*ch5*, *ch6* and *ch7*) corresponding to chapters 5, 6 and 7 of this thesis. Details of how to compile and run each of the programs are contained in the *readme* files on the disk. Following is a brief description of the disk contents:

- *ch5*: contains a fortran implementation of the Ostrowsky-Peyraud model of vesicles.
- *ch6*: is divided into a set of sub-directories. The sub directories con tain the following:
    - *2d_lattice_sos*: contains a C implementation of the 2d lattice sos model. The program can be compiled for the interface or membrane by setting appropriate switches.
    - *2d_continuum_sos*: code analogous to the the continuum sos model albeit that in this model the membrane heights h_i are off-lattice.

- *bead_chain*: contains a C implementaion of the bead-chain model of a membrane confined between a wall. The program uses the efficient algorithm for bead self-avoidance described in Appendix A.
- *bead_chain_viewer*: contains a program, written in C and using the Sunview graphics library, that can be used in conjunction with the preceding three programs to view the surface configuration. Pictures can be viewed as the simulation progresses or they can be viewed at a later date.
- *3d_lattice_sos*: contains code analogous to the 2d lattice sos model albeit that the model is three dimensional.
- *3d_continuum_sos*: contains code analogous to the 2d continuum sos model albeit that the model is three dimensional.
- *transfer_matrix*: contains a C implementation of the transfer matrix formulation 2d SOS interface model. The program solves the model by iteration.
- *support*: contains a variety of programs useful for investigating the results from the previous programs

- *ch7*: is divided into two sub-directories.
  - *bead_net*: contains a C implementation of the bead_net model of tilted chiral lipid bilayers. The program uses the efficent algorithm for bead self-avoidance described in Appendix A.
  - *bead_net_viewer*: contains a viewing program, written in C using the Sunview graphics libraries, which can be used in conjunction with the bead_net program to view the membrane as it evolves. It also allows one to print out pictures of the membrane on the printer. Pictures can be viewed as the simulation progresses or they can be viewed at a later date.

REFERENCES

Abrahams D.B. 1980. "Solvable model with a roughening transition for a planar Ising ferromagnet", *Phys. Rev. Lett.*, **44**, 1165.

Arfken G. 1985. "Mathematical methods for physicists", 3rd ed., Academic Press Inc., New York, Tokyo, London.

Ashcroft N.W. and Mermin N.D. 1976. "Solid state physics", Holt, Reinhart and Winston, New York.

Atkins P.W. 1982. "Physical chemistry", 2nd ed., chapter 10, Oxford University press.

Bansal V.K. and Shah D.O. 1976. "Micellar solutions for improved oil recovery" in "Micellization, solubilization and micro-emulsions", Volume 1, p87, ed K.L. Mittal; Plenum press, New York-London.

Barker G.C. and Grimson M.J. 1987. "The structure of deformable particles in applied external fields"; *J. Physique*, **48**, 465.

Beijeren H.V. 1977. "Exactly solvable model for the roughening transition of a crystal surface", *Phys. Rev. Lett.*, **38**, 993.

Berndl K., Kas J., Lipowsky R., Sackmann E. and Seifert U. 1990. "Shape transformations of giant vesicles: extreme sensitivity to bilayer asymmetry", *Europhys. lett.*, **13**, 659.

Bishop M. and Saltiel C.J. 1989. *J. Phys. A*, **22**, L87.

Burkhardt T.W. 1981. "Localisation-delocalisation transition in a solid-on-solid model with a pinninig potential", *J. Phys. A : Math. Gen.*, **14**, L63-L68.

Camacho J., Fisher M.E. and Singh R.R.P. 1991. "Semiflexible planar polymeric loops", *J. Chem. Phys.*, **94**, 5693.

Camacho C.J. and Fisher M.E. 1990. "Tunable fractal shapes in self-avoiding polygons and planar vesicles", *Phys. Rev. Lett.*, **65**, 9.

Cevc G. and Marsh D. 1987. "Phospholipid bilayers, physical principles and models", Wiley, New York-Chichester-Brisbane-Toronto-Singapore.

Chandrasekhar S. 1943. "Stocastic problems in physics and astronomy", *Rev. of Mod. Phys.*, **15**, 1.

Chui S.T. and Weeks D. 1981. "Pinning and roughening of one-dimensional models of interfaces and steps", *Phys. Rev. B.*, **23**, 2438.

Churchill R.V. and Brown J.W. 1989. "Complex variables and applications", eds Corrigan J.J., Devine P.R. and Bradley J.W. (McGraw-Hill, London) 4'th ed.

Dake L.P. 1982. "Fundamentals of reservoir engineering", p128, Elsevier, Oxford.

de Gennes P.G. 1979. "Scaling concepts in polymer physics", Cornell Univ. press, Ithaca, New York.

de Gennes P.G. 1987. *C. R. Acad. Sci (Paris)*, **304**, 259.

Deuling H.J. and Helfrich W. 1976. *J. Physique*, **37**, 1335.

Dickinson E. 1984. "Statistical model of a suspension of deformable particles", *Phys. Rev. Lett.*, **53**, 728.

Dickinson E. (ed) 1987. "Food emulsions and foams", special publication no. 58, Royal Soc. Chem., London.

Dickinson E. (ed) 1991, "Food polymers, gels and colloids", special publication no. 82, Royal Soc. Chem., Cambridge.

Duplantier B. 1990. *Phys. Rev. Lett.*, **64**, 493.

Family F., Vicsek T. and Meakin P. 1985. "Are random fractal clusters isotropic?", *Phys. Rev. Leit.*, **55**, 641.

Fisher M.E. 1989. "Fractal and nonfractal shapes in two-dimensional vesicles", *Physica D*, **38**, 112.

Fisher M.E., "Walks, walls, wetting and melting".

Flory P.J. 1969. "The statistical mechanics of chain molecules", Interscience, New York.

Frank F.C. 1958. *Discuss. Faraday Soc.*, **25**, 19.

Gasiorowicz S. 1966. "Quantum physics", Wiley, New York-Chichester-Brisbane-Toronto-Singapore.

Golden S. 1964. "Elements of the theory of gases", Addison Wesley, Reading-Massachusetts-Palo Alto-London.

Gompper and Kroll D.M. 1991, "Fluctuations of a polymerised membrane between walls", *J. Phys. I. France*, 1411.

Hall T.S. 1969. "Ideas of life and matter", Volume 1, University of Chicago press, Chicago London.

Harbich W., Deuling H.J. and Helfich W. 1977. *J. Physique*, **38**, 727.

Helfrich W. 1973. *Z. Naturforsch*, **28c**, 693.

Helfrich W. 1974. *Z. Naturforsch*, **29c**, 510.

Helfrich W. 1986. *J. Chem. Phys.*, **85**, 1085.

Helfrich W. 1990. "Elasticity and thermal undulations of fluid films of amphiphiles", in Liquids at interfaces ed. Charvolin J., Joanny J.F. and Zinn-Justin J. (Les Houches XLVIII, North Holland, Amsterdam) p209.

Helfrich W. and Prost J. 1988. "Intrinsic bending force in anisotropic membranes made of chiral molecules", *Phys. Rev. A*, **38**, 3065.

Hemmer P.C. and Lund B. 1988. "Correlations at a liquid-gas interface: asymptotic analysis for weak gravity", *J. Phys. A : Math. Gen.*, **21**, 3463.

Ho J.-S. and Baumgartner A. 1990. "Simulation of fluid self-avoiding membranes", *Europhys. Lett.*, **12**, 295.

Hoar T.P. and Schulman J.H. 1943. *Nature*, **152**, 102.

Huang K. 1987. "Statistical mechanics", 2nd ed., Wiley, New York.

Israelachvilli J.N., Mitchell D.J. and Ninham B.W. 1976. "Assemblies of hydrocarbon amphiphiles", *J. Chem. Soc. Faraday Trans.*, **72**, 1525.

Israelachvilli J.N., Mitchell D.J. and Ninham B.W. 1977. *Biochim. Biophys. Acta.*, **470**, 185.

Kahlweit M. 1988. "Microemulsions", Science, **240**, 617.

Kahn F.J. 1982. "The molecular physics of liquid crystal devices", *Physics Today*, 66.

Kantor Y. and Nelson D.,R. 1987. *Phys. Rev. A*, **48**, 1085.

Kantor Y. Mehran K. and Nelson D.R. 1986. "Statistical mechanics of tethered surfaces", *Phys Rev Lett*, **57**, 791.

Kantor Y., Kardar M. and Nelson D.R. 1987. "Tethered surfaces: statics and dynamics", *Phys. Rev. A*, **35**, 3056.

Kittel C. 1986. "Introduction to solid state physics", 6th ed., Wiley, New York-Chichester-Brisbane-Toronto-Singapore.

Kreyszig E. 1983. "Advanced engineering mathematics", 5th ed., Wiley, New York-Chichester-Brisbane-Toronto-Singapore.

Langevin D., Meunier J. and Cazablat A.M. 1985. "Les microemulsions", *La Recherche*, **167**, 720.

Leamy H.J., G.H. Gilmer, and K.A. Jackson 1975, "Statistical thermodynamics of clean surfaces", in "Surface physics of materials", volume 1, ed Blakely J.M. (New York, London : Academic) pp121-88.

Leibler S., Singh R.R.P. amd Fisher M.E. 1987. "Thermodynamic behaviour of two-dimensional vesicles", *Phys. Rev. Lett.*, **99**, 1989.

Lipowsky R. 1991. "The conformation of membranes", *Nature*, **349**, 475.

Lubensky T.C. and Prost P. 1992. "Orientational order and vesicle shape", *J. Phys. II. France II*, **2**, 271.

Ma S.K. 1985. "Modern theory of critical phenomena", World Scientific, Singapore.

Maggs A.C., Huse D.A. and Leibler S. 1989. "Unbinding transitions of semi-flexible polymers", *Europhys. Lett.*, **8**, 615.

Maggs A.C., Leibler S., Fisher M.E. and Camacho C.J. 1990. "The size of an inflated vesicle in two dimensions", *Phys. Rev. A*, **4**, 691.

Maggs A.C. and Leibler S. 1990. "Adsoption and fluctuations of two-dimensional vesicles", *Europhys. Lett.*, **12**, 19.

MacKintosh F.C. and Lubensky T.C. 1991. "Orientatinal order, topology, and vesicle shapes.", *Phys. Rev. Lett.*, **67**, 1169.

Mandelbrot B. 1983. "The fractal geometry of nature", Freeman and Co., San Francisco.

Metropolis N., Rosenbluth A.W., Rosenbluth M.N., Teller A.H. and Teller E. 1953. "Equations of state calculations by fast computing machines", *J. Chem. Phys.*, **21**, 1087.

Meier G., Sackmann E. and Grabmaier J.G. 1975. "Applications of liquid crystals", Springer Verlag, Berlin-Heidelberg-New York.

Meunier J., Langevin D. and Boccara N. (eds.) "Physiscs of amphiphilic layers", Volume 21, Springer Proceedings in Physics, Springer Verlag, Berlin.

Mittal K.L. and P.Mukerjee 1976. "The wide world of micelles" in "Micellization, solubilization and micro-emulsions", Volume 1, p87, ed K.L. Mittal; Plenum press, New York-London.

Nakashima N., Asakuma S. , Kim J.M. and Kunitake T. 1984. *Chem. Lett.*, 1709.

Nakashima N., Akasuma S. and Kunitake 1985. *J. Am. Chem. Soc.*, **107**, 509.

Needham J. 1956. "Science and civilisation in China", Volume 2, Section 13, University Press Cambridge.

Nelson P. and Powers T. 1992. "Rigid chiral membranes", *Phys Rev Lett*, **69**, 3409.

Norman R.E., Barker G.C. and Sluckin T.J. 1992. "Statistical mechanics of two dimesional vesicles"; *J. Phys. II France*, 1363.

Norman R.E., Parry A.O. and Sluckin T.J. 1993. "Universality for confined interfaces and membranes", to be published.

Ostrowsky N. and Peyraud J. 1982. "Monte Carlo study of two-dimensional vesicle shapes", *J. Chem. Phys.*, **77**, 2081.

Oseen C.W. 1933. *Trans Faraday Soc.*, **29**, 883.

Parry A.O. 1992a. " A universal parameterization of finite-size effects for interfaces in two dimensions, conformal mappings and local scale invariance", *J. Phys. A : Math. Gen.*, **25**, L685-L691.

Parry A.O. 1992b. "Universal amplitude-exponent relations for interfaces and conformal mappings", *J. Phys. A : Math. Gen.*, **25**, L1015-L1021.

Parry A.O. 1992c. "Scaling and local scale invariance for wetting transitions and confined interfaces", *J. Phys. A : Math. Gen.*, **25**, 257.

Parry A.O. 1992d. Private Communication.

Poste G. and Papahadjopolous D. 1979. "Uses of liposomes in biology and medicine", p101, Gregoriadis G. and Allison A. (Eds.), Wiley, New York.

Press W.H., Flannery B.P., Teukolsky S.A. and Vetterling W.T. 1986. "The art of scientific computing", Cambridge University Press.

Prince L.M. (ed.) 1977. "Microemulsions", Academic Press.

Pryde J.A. 1966. "The liquid state", ed G. Jones, Hutchinson and Co., London.

Schadt M. 1989. "The history of the liquid crystal display and liquid crystal material technology", *Liq. Cryst. 1*, **57**.

Seddon J. and Templar R. 1991. "Liquid crystals and the living cell",*New Scientist*, 45.

Seifert U. 1991. "Adhesion of vesicles in two dimensions", *Phys. Rev. A.*, **43**, 6803.

Seifert U., Berndl K. and Lipowsky R. 1991. "Shape transformations of vesicles: Phase diagram for spontaneous curvature and bilayer-coupling models", *Phys Rev A*, **44**, 1182.

Shah D.O. (Ed.) 1981. "Surface phenomena in enhanced oil recovery", Plenum, New York.

Shanks I.A. 1982. "The physics and display applications of liquid crystals", *Contemp. Phys*, **23**, 65.

Singer S.J. and Nicolson G.L. 1972. "The fluid mosaic model of cell membranes", *Science*, **175**, 720.

Svetina S. and Zeks B. 1983. *Biomed. Biochim. Acta*, **42**, 86.

Svetina S. and Zeks B. 1989. *Eur. Biophys. J.*, **127**, 257.

Spivak M. 1979. "A comprehensive introduction to differential geometry", Publish or Perish, Berkeley.

Temperely H.N.V. 1952. *Proc. Camb. Phil. Soc.*, **48**, 683.

Wright D.C. and Mermin N.D. 1989. "Crystalline liquids: The blue phases", *Rev. of Modern Phys.*, **61**, 385.

Yager P. and Schoen P. 1984. *Mol. Cryst. Liq. Cryst.*, **106**, 371.

Yager P., Schoen P., Davies C., Price R., and Singh A. 1985. *Biophys. J.*, **48**, 899.

Yamada K., Ihara H., Ide T., Fukumoto T. and Hirayama C. 1984. *Chem. Lett.*, 1713.

Zhong-can O.-Y. and Jixing L. 1991. "Theory of helical structures of tilted chiral lipid bilayers", *Phys Rev A*, **43**, 6826.

Zocher H. 1933. *Trans. Faraday Soc.*, **29**, 945.